NEI-NO--1055

Design of Multiphase Flow Experiments

Hege Urkedal

A dissertation submitted to the Department of Physics at the University of Bergen
in the partial fulfillment of the requirements for the degree doctor scientiarum.
Bergen, Norway, May 1998

Printed at
Bergen Print Service

ISBN 82-994679-1-8
Bergen, Norway
1998

Acknowledgement

First of all, I have to express my gratitude to Dr. Jan-Erik Nordtvedt who has been my advisor during this work. He has been available for discussions and always encouraging. Further thankfulness goes to Prof. Kristofer Kolltveit at the University of Bergen and Prof. Ted Watson at Texas A&M University. I specially thank Prof. Ted Watson and his family for arranging my stay at Texas A&M University in College Station, spring 1995. Further, I want to thank the staff and the other students I got in touch with at the Department of Chemical Engineering and who made my stay memorable.

I will also express thanks to the students I have been working with at the University of Bergen. During the doctoral work I have been at RF–Rogaland Research. I thank my colleagues for interesting discussions and a relaxed social atmosphere.

Financial support of this work is gratefully acknowledged from the Strategic Institute Program on Inverse Problems at RF–Rogaland Research sponsored by the Norwegian Research Council.

Finally, I will thank my family and friends for supporting me and for always being there when I needed you.

Preface

This dissertation consists of six papers and a summary comprised of the background, methodology and results from the papers. The work comprises the development of an experimental design procedure of two- and three-phase displacement experiments. Technical contribution such as implementation of analytical sensitivity coefficients has been performed. The purpose of the experimental design is to determine the number and type of experiments, the data and accuracy of the data necessary for estimate multiphase flow functions with an acceptable accuracy. The work presents two- and three phase relative permeability and capillary pressure functions that have been estimated simultaneously from a multiple set of data from several experiments.

Paper III (submitted for publication) presents the estimation of two-phase relative permeability and capillary functions and the statistical criteria for accepting a solution. Paper VI (published) compares different experimental designs and including additional data for determination of two-phase flow functions. Paper I and II (proceeding papers) present the experimental design procedure and methodology for determination of three-phase relative permeability and capillary pressure functions. In Paper IV (published) is this methodology verified on experimental data. In Paper V (to be submitted) the development of analytical sensitivity coefficients using the direct method for two- and three-phase flow is proposed.

This work has been performed at RF–Rogaland Research. I have also visited the Department of Chemical Engineering at Texas A&M University in College Station for a period of six months. The other contributors to this work have mainly been Dr. Jan-Erik Nordtvedt who wrote Paper II and IV. Paper VI is written in cooperation with the research group at Texas A&M University. I also want to mention Einar Ebeltoft and his contribution as a link between the theoretical work and the core analysis laboratory at RF–Rogaland Research in Stavanger. André Sylte has contributed in the estimation process to determine the three-phase relative permeability and capillary pressure functions. Finally, Prof. Ted Watson has contributed with valuable comments to all the papers.

Contents

List of Papers

This dissertation comprises the following six papers.

Paper I: Urkedal, H., Langaas, K., Nordtvedt, J.E., Watson, A.T.: "Design of Three-Phase Relative Permeability Experiments," in Proceedings of the 1995 International Symposium of the Society of Core Analysts, San Francisco, California, Sept. 12-14, 1995, pp. 1-15.

Paper II: Nordtvedt, J.E., Langaas, K., Sylte, A., Urkedal, H., Watson, A.T.: "Estimation of Three-Phase Relative Permeability and Capillary Pressure Functions," in Proceedings of the 5th European Conference on the Mathematics of Oil Recovery, Leoben, Austria, Sept. 3-6. 1996, pp. 1-10.

Paper III: Urkedal, H., Ebeltoft, E., Nordtvedt, J.E., Watson, A.T.: "A New Design of Steady-State Type Experiments for Simultaneous Estimation of Two-Phase Flow Functions," submitted for publication in *SPE Formation Evaluation*, March 1997.

Paper IV: Nordtvedt, J.E., Ebeltoft, E., Iversen, J.E., Sylte, A., Urkedal, H., Vatne, K.O., Watson, A.T.: "Determination of Three-Phase Relative Permeabilities From Displacement Experiments," *SPE Formation Evaluation*, December 1997, pp. 221-226.

Paper V: Urkedal, H., Nordtvedt, J.E., Watson, A.T.: "Development of Analytical Sensitivity Coefficients for Determination of Porous Media Properties," to be submitted for publication in *Computational Geosciences*.

Paper VI: Watson, A.T., Kulkarni, R., Nordtvedt, J.E., Sylte, A., Urkedal, H.: "Estimation of Porous Media Flow Functions," *Measurement Science and Technology*, Vol. 9, No 6, June 1998, pp. 898-950.

1 Scope of Work

Reliable predictions of reservoir behavior are essential for effective design of exploitation strategies. Examples of such strategies, especial in late production phases, are water-altering-gas (WAG) injection, gas injection, thermial oil recovery or surfactant flooding. Specification of the multiphase flow properties is necessary for simulation of these production processes. Hence, relative permeabilities and capillary pressure (i.e. multiphase flow properties) are to be specified at all locations throughout the reservoir. Consequently, accurate determination of these flow properties is an issue of great concern. However, the relative permeabilities can not be measure directly. Therefore, displacement experiments are conducted on core samples and various data sets such as pressure drop, production and *in situ* saturation and pressure (see Figure 1.1) are measured. These data are then used to get an estimate of the relative permeabilities by calculation from an appropriate mathematical model of the experiment. This calculation procedure is referred to as the inverse problem.

The displacement experiments can be conducted under various conditions. If the capillary pressure is neglected, the experiments can be represented by a set of partial differential equations that can be solved analytically. The inverse problem is then solved in an explicit way and the relative permeabilities are determined using the JBN-method, proposed by Johnson, Bossler and Nauman [1959], based on the Buckley-Leverett theory [Buckley and Leverett, 1942] and Welge [1952]. The experiments are conducted with high flow rates to minimize capillary end effects according to the assumptions made. However, this approach leads to several numerical problems such as calculation of derivatives of the data witch can lead to substantial estimation errors [Tao and Watson, 1984] and estimates of the relative permeability at only discrete set of saturation values [Richmond and Watson, 1990]. Another explicit method for determination of the relative permeabilities is to interpret data form steady state experiments [Dullien, 1992]. Here, two phases are injected simultaneously into the core at constant total rate until equilibrium (or steady state) and the saturation is assumed to be uniform in the core. Since the fluid rates are known and the pressure drop is measured, Darcy's law can be used directly to compute the phase relative permeabilities. This method is very time consuming since the equilibrium must be achieved [Marle, 1981, Honarpour et al., 1994], and only relative permeability *points* are computed for each rate fraction. The capillary pressure is typically determined directly utilizing the centrifuge technique [Hassler and Brunner, 1945; Slobod et al., 1951; Forbes, 1991], the micro-membran technique [Hammervold, 1994], the diaphragm technique or mercury injection [Dullien, 1992]. These techniques for determination of relative permeability and capillary pressure are typically conducted under flow conditions different from the reservoir conditions and possibly on different core samples or on core samples with reestablished initial saturation and wetting conditions.

A fundamentally different manner to solve the inverse problem, is the implicit method. In this method the properties are estimated as *functions* as opposed to *points* obtained through the explicit approach. Corey [1956] proposed an functional relationship

between the relative permeability and saturation using only few parameters. However, few parameters give little flexibility in the functions and bias error is introduced. No experimental data has been reconciled using this type of functional representation. Watson et al. [1980] introduced B-splines as a functional representation of relative permeability and capillary pressure due to its flexibility. Later Watson et al. [1988] extended this method and introduced a regression based method for determination of the flow function coefficients. B-splines are used to represent the two-phase relative permeabilities and capillary pressure because they can represent any function arbitrary accurately and bias error can be minimized. In the inverse approach, the effects of capillary pressure can be included in the analysis; capillary pressure can be specified independently, or it can be estimated simultaneously with the relative permeability. Hence, the flow functions are determined from experimental data on the same core sample and under the same flow processes. The utility of this method has been demonstrated by analyzing dynamic displacement experiments such as pressure drop and production data [Richmond et al., 1990], *in situ* saturation measurement [Mejia et al., 1995], centrifuge experiments [Nordtvedt et al., 1993], and its extension to steady-state-type displacement experiments as shown in Paper III.

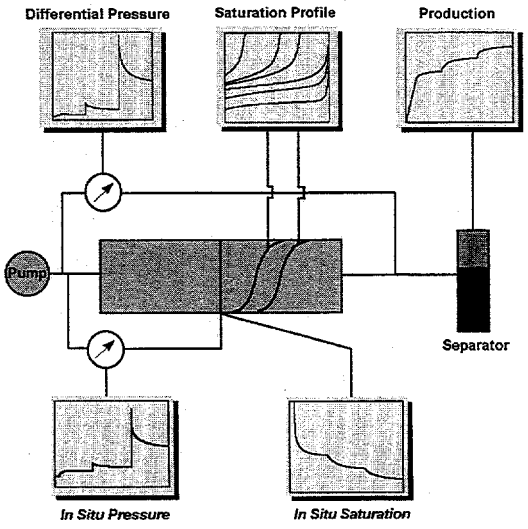

Figure 1.1 Different types of data gathered from displacement experiments (figure from Paper III).

In two-phase flow, the relative permeability and capillary pressure were taken to be univariate functions of saturation. When there are three fluids present, each of the relative permeability and capillary pressure functions can be represented as bivariate functions of two independent saturations. There are three methods for determination of three-phase relative permeabilities. One approach is to calculate them using already measured two-phase relative permeabilities in predictive methods [Manjnath and

Honarpour, 1984; Baker, 1988]. Another approach is to estimate the flow functions on the basis of laboratory data collected during displacement experiments either in an explicit approach [Virnovsky, 1984; Helseth, 1996] or an implicit approach [Mejia et al., 1996].

Historically, three-phase relative permeabilities are found from correlation and interpolation of two-phase relative permeability data, see review by Manjnath and Honarpour [1984]. Some of these methods were reviewed by Baker [1988] using all published three-phase relative permeability data, and compared with two interpolation methods he proposed. Baker concluded that the reviewed methods were not very good predictors of experimental data. The interpolation methods he proposed provided a better match with the experimental data than the reviewed theoretically based methods. He also concluded that more accurate three-phase experimental data would be necessary for properly testing and developing of correlation models. Robinson and Slattery [1994] presented a model for computation of relative permeability of the intermediate phase. They found that only a portion of the data [Oak et al., 1990] was suitable for comparison with available models.

There are some explicit methods for determination of three-phase relative permeabilities. The JBN method [Johnson et al., 1959] has been extended to three phases by Virnovsky [1984]. However, this method gives relative permeability data only for a limited saturation interval, i.e., after the shock wave. In more recent theoretical work on three-phase relative permeability [Helset et al., 1996], *in situ* saturation and pressure data can be used to estimate the relative permeability over a larger scale than the JBN method and the method proposed by Virnovsky [1984]. However, dynamic *in situ* saturation and pressure drop data are very expensive (if possible) to measure and might not be measured with acceptable accuracy.

Mejia et al. [1996] was the first to report estimation of three-phase flow functions depending on two saturations from a set of synthetic data in an implicit approach. The regression based method [Watson et al., 1988] was extended so that three-phase flow functions could be estimated. In this method the relative permeabilities are represented by tensor products of univariat B-splines [Schumaker, 1981] which is an extension of B-splines representation of two-phase flow properties. Hence, the dependency on two saturations is taken care of. In this approach, capillary effects are also addressed since capillary pressure and relative permeabilities can be estimated simultaneously from the experimental data.

Since experimental data and the combination of these are essential for accurate determination of two- and three-phase flow properties, an experimental design procedure for multiphase experiments is proposed in this work. The two-phase flow functions can be determined using data from a single experiment, while the three-phase relative permeabilities must be determined using data from multiple experiments since the entire saturation region must be spanned with data. Hence, an experimental design will be essential for the success of estimation of (two- and) three-phase flow properties from experimental data. There are a large variety of experimental designs that can be used for estimating two- and three-phase flow functions. For design of three-phase experiments, one can start experiments at saturations for which one, two, or three fluid

phases are mobile, and inject, at any fraction, one, two, or three fluid phases. In this work average saturation paths similar to those expected for the reservoir flow processes have been used. In Paper I and Paper II different three-phase experimental designs have been investigated and the accuracy with which the flow functions may be determined using the corresponding data have been computed. In that study, a linearized covariance analysis was utilized. In the different experimental designs, various experiments (e.g., unsteady state, steady state, centrifuge), experimental data sets (differential pressure, production, *in situ* saturation and pressure and saturation profiles as illustrated in Figure 1.1), injection strategies (high-rate, low-rate, multi-rate) and accuracy of these data are evaluated. The information in these data for estimation of multiphase flow functions can be used to design the two- and three-phase experiments. The data sets are measured with different cost, time and accuracy; *in situ* measurements (by NMR [Chen, 1993; Chen 1994], X-ray [Oak, 1988; Oak, 1990; Ebeltoft, 1998]) are much more complicated and expensive than pressure drop and production data (Ebeltoft [1998] has presented an experimental apparatus for two- and three-phase experiments where differential pressure and production data are measured with high accuracy). Hence, the experimental design procedure can be used to evaluate the experiments, or the combination of such, in order to optimize the accuracy of the estimated flow functions, or to arrange the necessary data and accuracy of these in order to get estimates of the flow properties within a certain accuracy. Then, the flow functions can be estimated with high accuracy in the saturation region of interest with a limited number of experiments and data sets. The accuracy of the flow functions can be computed in a linearized covariance analysis [Kerig, 1986; Paper III]. Since the accuracy of the flow functions can be analyzed before the experiments take place, guidelines for the experiments can be given to improve the information content in the data.

The experimental design has been further developed in Paper V. In this paper analytical sensitivity coefficients were developed from two-phase to three-phase flow. Sensitivity coefficients are the derivative of the model output (differential pressure, production) with respect to the model parameters (coefficients in the functional representation of flow functions). Analytical sensitivity coefficients are derived using the direct method [Tortorelli, 1994]. The sensitivity coefficients are essential in both parameter estimation and in assessing accuracy of flow functions. For correctly evaluation of data and experimental designs, accurate sensitivity coefficients are essential. The analytical sensitivity coefficients for three-phase flow developed in this work are an extension of a method proposed by Anterion [1989] and Vignes [1993] for two-phase relative permeabilities. The direct method takes advantage of that the model equations are solved using the Newton-Raphson method, and some of the results from this solution can be used directly when solving the sensitivity equation. In Paper V it is shown how the accuracy of the computations are improved since numerical derivatives are avoided. The numerical sensitivity coefficients tend to introduce "false" sensitivity in saturation regions with little information content in the data and the accuracy of the estimates are over-predicted, i.e., they give too narrow confidence intervals. With the implementation of analytical sensitivity coefficients, the "trial and error" when choosing parameter increment and the numerical error introduced by "false" sensitivity is avoided. Hence, the computation of parameter estimates and assessment of accuracy becomes faster, more stable and more accurate. The experimental design procedure has been further

developed in Paper V where also the contribution of observations is computed and the identifiability of the parameters with the current design is investigated.

In this work, the inverse approach is used for determination of three-phase relative permeability and two-phase capillary pressure functions from several sets of experimental data, in Paper IV. The pressure drop and production data from three experiments (one two-phase experiment, and two three-phase experiments) were reconciled simultaneously. Ebeltoft et al. [1998] has presented an apparatus for displacement experiments at reservoir conditions, with emphasis on getting three-phase differential pressure and production data with high accuracy. These data were used to get an accurate estimate of the three-phase flow functions in Paper IV. In this paper the results obtained using the inverse approach were compared with results using Stone [1970] predictive model. Two-phase relative permeabilities estimated using the inverse approach were used as input to the Stone model. The Stone three-phase relative permeabilities were then used to predict pressure drop and production data and these were compared to the experimental data. For this case, Stone predictive model over-predicted the oil production and differential pressure. This agrees with the conclusions from Baker's [1988] work.

In this work, the inverse methodology for determination of two- and three-phase relative permeability and capillary pressure functions is further developed (Paper I, II, III, IV and VI). The main work has been development of analytical sensitivity coefficients for two- and three-phase flow (Paper V). This technical contribution has improved the accuracy both in parameter estimation and accuracy assessment of the estimates and reduced the computer time requirements. The proposed experimental design is also dependent on accurate sensitivity coefficients to give the right guidelines for how two- and three-phase experiments should be conducted. The experimental design has been developed in several papers (mainly Paper I and Paper V). Following the proposed experimental design, three-phase relative permeability and capillary pressure functions have been estimated when multiple sets of experimental data have been reconciled by simulations.

2 Background

Accurate information of the properties describing fluid flow in porous medium is important in reservoir forecasting and exploration. These properties are typically found from experimental data measured in experiments on core samples from the reservoir. The fluid flow in porous media is simulated by a mathematical model. In this chapter, the mathematical model describing multiphase flow will be described in section 2.1. The assumptions made will also be discussed. However, some of the flow properties can not be determined directly, and they have to be inferred from the experimental data in an inverse approach. The methods used for deriving these properties will be discussed in section 2.2. The accuracy of estimates and measures of non-linearity in the model are discussed in section 2.3.

2.1 Mathematical Model

2.1.1 Problem Formulation

When describing the fluid flow in porous media, we use a macroscopic model where we assume the different size in pores and channels will vary randomly with a well-defined mean. Therefore, we can introduce mean properties such as velocity and pressure in a sufficient reference volume. The continuity equation for single phase flow is given as [Aziz and Settari, 1979]:

$$\nabla \cdot \rho \boldsymbol{u} + q = -\frac{\partial \varphi \rho}{\partial t}, \tag{2.1}$$

with q negative for injection and positive for production.

For horizontal, one-dimensional processes the fluid movement is caused by pressure differences. Let k denote the permeability of the rock and μ the viscosity of the fluid. Darcy [1856] showed experimentally that the velocity u at a point would be proportional to the pressure gradient, $-\partial p/\partial x$. Darcy's law is given as

$$u = -\frac{k}{\mu}\frac{dp}{dx}. \tag{2.2}$$

Darcy's law assumes that there is no reaction between fluid and rock and that there is only one fluid present. Further, the flow must be laminar. For a three dimensional medium, the permeability is given as a tensor, $[k]$, giving different permeability for different directions. Permeability will be reduced if there is a reaction between fluid and rock. There is also a reduction in permeability for each phase when several fluids are

present. Relative permeability, for generality dependent on two independent phases, is introduced for multiphase flow, and when gravity is taken into account, Darcy's law for three-phase flow (here considering water, oil and gas phases) is given as:

$$\boldsymbol{u}_f = -\frac{[k]k_{rf}}{\mu_f}(\nabla p_f - \rho_f \mathbf{g}\nabla z), \qquad f = w,o,g. \tag{2.3}$$

Substituting Darcy's law and the continuity equation, and replace the densities by volume factors gives the mass conservation equations for water, oil, and gas [Aziz and Settari, 1979]. This is called the black oil model:

$$R_w = \nabla\cdot\left[T_w(\nabla p_w - \gamma_w \nabla z)\right] + Q_w - \frac{\partial}{\partial t}\left(\varphi\frac{S_w}{B_w}\right) = 0 \tag{2.4}$$

$$R_o = \nabla\cdot\left[T_o(\nabla p_o - \gamma_o \nabla z)\right] + Q_o - \frac{\partial}{\partial t}\left(\varphi\frac{S_o}{B_o}\right) = 0 \tag{2.5}$$

$$R_g = \nabla\cdot\left[T_g(\nabla p_g - \gamma_g \nabla z)\right] + \nabla\cdot\left[R_s T_o(\nabla p_o - \gamma_o \nabla z)\right] + Q_g - \frac{\partial}{\partial t}\left(\varphi\frac{S_g}{B_g} + \varphi\frac{S_o R_s}{B_o}\right) = 0 \tag{2.6}$$

where the gravity term, volume factor, volumetric flow term and transmissibility is given as:

$$\gamma_f = \rho_{f,RC} g$$

$$B_f = \frac{\rho_{f,SC}}{\rho_{f,RC}}$$

$$Q_f = -\frac{q_f}{\rho_{f,SC}}$$

$$T_f = \frac{[k]k_{rf}}{\mu_f B_f}.$$

The saturations will sum up to unity, giving the relation

$$S_w + S_o + S_g = 1, \tag{2.7}$$

and the capillary pressure relations are given as

$$P_{c,ow} = P_{c,ow}(S_w, S_o) = p_o - p_w$$
$$P_{c,og} = P_{c,og}(S_o, S_g) = p_g - p_o. \tag{2.8}$$

The other equations of state are

$$\rho_f = \rho_f(p_o)$$
$$\mu_f = \mu_f(p_o)$$
$$\varphi = \varphi(p_o).$$

However, these relations are weak functions of pressure.

Darcy's law for three phases in three dimensions, the continuity equations, the saturation relation and the capillary pressure relations give 9 equations. In this system we have the following unknowns: p_w, p_g, p_o, S_w, S_g, S_o, u_w, u_g, u_o, and we have a complete set of equations. From these unknowns, S_w, S_g, and p_o are usually chosen as the unknown state variables:

$$\mathbf{u} = \{p_o, S_w, S_g\}^T.$$

The unknown parameters may include porosity, permeability, or flow properties as relative permeability and capillary pressure. In this work determination of the flow properties is addressed, and parameters in the representation of relative permeability and capillary pressure functions are assembled in the parameter vector:

$$\mathbf{p} = \{p_1, p_2, \ldots, p_{N_p}\}^T.$$

2.1.2 Initial and Boundary Conditions

In reservoir simulation, flow in and out of the system occurs only at the boundaries, such as the external boundaries of the reservoir and at the boundaries of the wells. It is customary in reservoir simulation to represent flow across all boundaries by source/sink terms and replace the actual boundary conditions by homogeneous Neumann (no-flow) boundary conditions on the entire boundary [Aziz and Settari, 1979].

For multiphase flow, flow rates of all phases must be specified, although they are not necessarily independent. There are two basic types of boundaries:

1. *Closed boundary* (Γ_2 in Figure 2.1)

There is no flow of any phase across a closed boundary; the product of Darcy velocity and the normal vector **n** vanishes:

$$q_f = T_f(\nabla p_f - \gamma_f \nabla z)\cdot \mathbf{n} = 0, \quad f = w, o, g,$$

where **n** is the normal to the boundary and T_f is the transmissibility in the direction of the normal.

2. *Boundaries open to flow* (Γ_1 and Γ_3 in Figure 2.1)

In this case, the flow rates q_f across the boundary are specified. The flow in reservoir units is

$$T_f\left(\nabla p_f - \gamma_f \nabla z\right)\cdot \mathbf{n} = q_f(\Gamma), \quad \Gamma = \Gamma_1, \Gamma_3.$$

On the boundary Γ_3 where fluids are injected, the flow rates for each phase are controlled and therefore known. Figure 2.1 shows typical boundary conditions for single-well models.

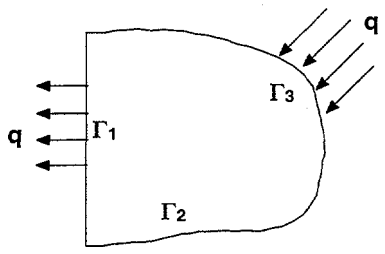

Figure 2.1 Boundaries for single-well model [Aziz and Settari, 1979].

The saturation $S_w(x,y,z,t=0)=f_1$, $S_g(x,y,z,t=0)=f_2$, and pressure $p_o(x,y,z,t=0)=f_3$ at the beginning of an experiment, or production, are used as the initial condition. The initial conditions must be given in accordance with the equilibrium of the reservoir, otherwise, unstable solutions can be achieved [Aziz and Settari, 1979].

Examples of initial and boundary conditions in a oil-water steady-state-type experiment can be:

- Injection of one or two fluid phases at constant total rate.
- Production at constant well pressure.
- Initial conditions: Irreducible water saturation and pressure given as: S_{wi}, $P_o = P_c + P_w$.

2.1.3 Direct Problems in Multiphase Flow

The non-linear partial differential equations (2.4)-(2.6) must be approximated and then solved numerically. In this work, the model equations are approximated by the corresponding finite difference equations and then solved numerically. Spatial finite difference approximations to the expressions for flow terms have been applied together with time discretization of the accumulation terms, and we have

$$
\begin{aligned}
R_o(\mathbf{u},\mathbf{p}) = {} & T_{o,i+\frac{1}{2}}(p_{o,i+1} - p_{o,i} - G_o)^{n+1} - T_{o,i-\frac{1}{2}}(p_{o,i} - p_{o,i-1} - G_o)^{n+1} \\
& + T_{o,i}(p_{well} - p_{o,i} - G_o)^{n+1} \\
& - \frac{V_b}{\Delta t}\left[\left(\varphi b_o(1 - S_w - S_g)\right)^{n+1} - \left(\varphi b_o(1 - S_w - S_g)\right)^{n}\right] = 0
\end{aligned}
\tag{2.9}
$$

$$
\begin{aligned}
R_w(\mathbf{u},\mathbf{p}) = {} & T_{w,i+\frac{1}{2}}(p_{w,i+1} - p_{w,i} - G_w)^{n+1} - T_{w,i-\frac{1}{2}}(p_{w,i} - p_{w,i-1} - G_w)^{n+1} \\
& + T_{w,i}(p_{well} - p_{w,i} - G_w)^{n+1} \\
& - \frac{V_b}{\Delta t}\left[\left(\varphi b_w S_w\right)^{n+1} - \left(\varphi b_w S_w\right)^{n}\right] = 0
\end{aligned}
\tag{2.10}
$$

$$
\begin{aligned}
R_g(\mathbf{u},\mathbf{p}) = {} & R_{s,i+\frac{1}{2}} T_{o,i+\frac{1}{2}}(p_{o,i+1} - p_{o,i} - G_o)^{n+1} - R_{s,i-\frac{1}{2}} T_{o,i-\frac{1}{2}}(p_{o,i} - p_{o,i-1} - G_o)^{n+1} \\
& + T_{g,i+\frac{1}{2}}(p_{g,i+1} - p_{g,i} - G_g)^{n+1} - T_{g,i-\frac{1}{2}}(p_{g,i} - p_{g,i-1} - G_g)^{n+1} \\
& + R_{s,i} T_{o,i}(p_{well} - p_{o,i} - G_o)^{n+1} + T_{g,i}(p_{well} - p_{g,i} - G_g)^{n+1} \\
& - \frac{V_b}{\Delta t}\left[\left(R_s \varphi b_o S_o + \varphi b_g S_g\right)^{n+1} - \left(R_s \varphi b_o S_o + \varphi b_g S_g\right)^{n}\right] = 0
\end{aligned}
\tag{2.11}
$$

Here, we define the vertical downward direction as the z-axis and the gravity heads in x-direction is calculated by

$$G_f = \gamma_f \Delta x\left(\frac{dx}{dz}\right),$$

V_b is the volume of a grid block and $b_f = B_f^{-1}$.

The vector equation **R** is defined as

$$\mathbf{R}(\mathbf{u},\mathbf{p};x,t) = \left\{R_o, R_w, R_g\right\}^T. \tag{2.12}$$

The vector equation **R** in (2.12) must be solved for the state variable **u** in each grid block. However, these equations are not linear. The accumulation term consists of a product of phase saturation and pressure dependent quantities as porosity and volume factors. The expression for flow terms contains saturation dependent relative permeabilities, pressure dependent PVT-terms and phase potential. The well terms are also non-linear. The only way to solve the equations is to use linear approximations. In this work, the Newton-Raphson method [Aziz and Settari, 1979] has been applied to linearize the flow equations (2.9)-(2.11). This method is shown below:

The model equation is given as

$$\mathbf{R}(\mathbf{u}^{n+1}) = \mathbf{0}. \tag{2.13}$$

This non-linear system of equations is solved by:

$$\mathbf{u}^{(k)} - \mathbf{u}^{(k-1)} = -\left[\mathbf{J}^{(k-1)}\right]^{-1}\mathbf{R}^{(k-1)} \tag{2.14}$$

where $\mathbf{J}$ is the Jacobian of the vector function $\mathbf{R}(\mathbf{u})$:

$$\mathbf{J}^{(k-1)} = \left(\frac{\partial \mathbf{R}(\mathbf{u})}{\partial \mathbf{u}}\right)^{(k-1)}. \tag{2.15}$$

This gives

$$\mathbf{J}^{(k-1)}\left(\mathbf{u}^{(k)} - \mathbf{u}^{(k-1)}\right) = -\mathbf{R}^{(k-1)} \tag{2.16}$$

for iteration index $k \geq 1$ and initial guess

$\mathbf{u}^{(0)} = \mathbf{u}^{n}$.

The above equations are solved iteratively and the iterations proceed until a convergence criterion $\left|\mathbf{u}^{(k)} - \mathbf{u}^{(k-1)}\right| \leq \varepsilon$ is reached. The forward solution is then given as

$$\mathbf{u}^{n+1} = \mathbf{u}^{(k)}, \tag{2.17}$$

and this iterative procedure continues for each time step until a stop-criterion has been reached.

2.1.4 Flow Function Representation

In this work, a methodology for determination of two- and three-phase relative permeability and two-phase capillary pressure functions will be proposed. If the properties are to be estimated accurately, it is necessary that the functional representations be capable of representing the actual (unknown) relative permeability and capillary pressure curves. Various functional representations such as Corey exponential [Corey et al., 1956] use only a few parameters when representing the flow functions. It has been shown [Kerig and Watson, 1986] that functional representations as this is not flexible enough to represent the flow functions and therefore introduce bias error. B-splines have been used to represent the relative permeability and capillary

pressure functions in several applications for multiphase flow in porous media [Kerig and Watson, 1986; Nordtvedt and Kolltveit, 1993; Mejia et al., 1995; Mejia et al., 1996]. B-splines has the quality that for a sufficient number of knots, any continuous function can be accurately represented [Schumaker, 1981].

Generally a B-splines function for two-phase flow is given as

$$g_1(S_f) = \sum_{j=1}^{n} c_j^f B_j^m(S_f, \mathbf{y}), \quad f = w, nw. \tag{2.18}$$

In the two-phase case, relative permeability and capillary pressure may be written as follows:

$$\begin{aligned} k_{rf}(S_f) &= g_1(S_f) \quad f = w, nw \\ P_c(S_w) &= g_1(S_w) \end{aligned} \tag{2.19}$$

and Figure 2.2 illustrates the two-phase oil relative permeability and corresponding B-splines basis functions. Here, $B_j^m(S_f, \mathbf{y})$ is the basis function of order $(m\text{-}1)$ that can be evaluated at any value of saturation S_f in the partition $\mathbf{y}$. c_j^f is the B-splines coefficients that are the parameters to be determined by the parameter estimation method. The two-phase parameter vector $\mathbf{p}$ consists of the B-splines coefficients c_j^f:

$$\mathbf{p} = \left\{ c_1^w, \ldots, c_{N_w}^w, c_1^{nw}, \ldots, c_{N_{nw}}^{nw}, c_1^{P_c}, \ldots, c_{N_{P_c}}^{P_c} \right\}^T.$$

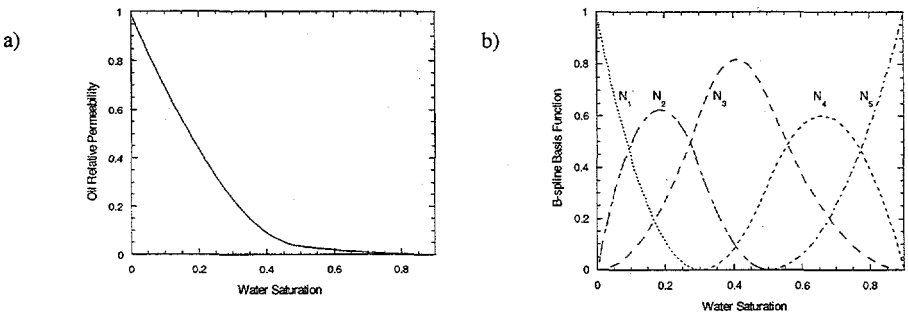

Figure 2.2 a) Two-phase oil relative permeability function, and b) corresponding B-splines basis functions.

For three-phase properties, relative permeability is represented by tensor-product B-splines [Schumaker, 1981]. A general function can be written as [from Paper II]

$$g_2(S_1,S_2)=\sum_{i=1}^{m_1+K_1}\sum_{j=1}^{m_2+K_2}c_{ij}^{f}N_{ij}^{m}(S_1,\mathbf{y}_1,S_2,\mathbf{y}_2), \tag{2.20}$$

where $\mathbf{y}_1$ and $\mathbf{y}_2$ denote the extended partition, and S_1 and S_2 the independent saturations. N_{ij}^{m} are the tensor-products B-splines basis functions.

Three-phase relative permeability may then be represented as

$$k_{rf}(S_1,S_2)=g_2(S_1,S_2)\quad\begin{cases}S_1=S_f\\ S_2=\begin{cases}S_w & if \quad f\neq w\\ S_g & if \quad f=w\end{cases}\end{cases}. \tag{2.21}$$

Figure 2.3 illustrates the three-phase oil relative permeability function with corresponding water and gas B-splines basis functions.

The two capillary pressure functions dependent on one saturation may be represented by B-splines as follows:

$$\begin{aligned}P_{c,ow}&=g_1(S_w)\\ P_{c,og}&=g_1(S_g)\end{aligned} \tag{2.22}$$

The unknown parameters in the three-phase model will be the coefficients c_{ij}^{f} in the tensor-product B-splines representation of three-phase relative permeability and capillary pressure functions. These coefficients are arranged in $\mathbf{p}$ as follows:

$$\mathbf{p}=\left\{c_{11}^{w},\ldots,c_{N_{w1}N_{w2}}^{w},c_{11}^{o},\ldots,c_{N_{o1}N_{o2}}^{o},c_{11}^{g},\ldots,c_{N_{g1}N_{g2}}^{g},c_{1}^{ow},\ldots,c_{N_{ow1}}^{ow},c_{1}^{og},\ldots,c_{N_{og1}}^{og}\right\}^{T}.$$

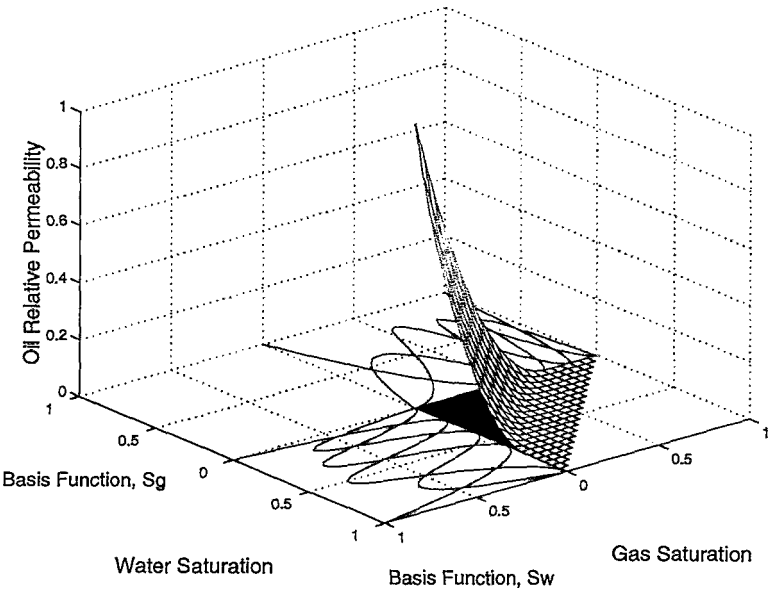

Figure 2.3 Three-phase oil relative permeability in 3D with corresponding B-splines basis functions.

2.2 Solutions of Inverse Problems

In contrast to the forward solution ($\mathbf{F(p)}+\varepsilon$ in Figure 2.4), the inverse problem seeks to find the unknown parameter $\mathbf{p}$ when continuous or discrete observations of state $\mathbf{u}$ or derived measurements $\mathbf{F(u)}$ are given ($\mathbf{R(Z)}$ in Figure 2.4). To determine flow function estimates $\hat{\mathbf{p}}$, the non-linear parameter estimation problem defined by

$$J(\hat{\mathbf{p}}) = [\mathbf{F}(\hat{\mathbf{p}}) - \mathbf{Z}]^T \mathbf{W}[\mathbf{F}(\hat{\mathbf{p}}) - \mathbf{Z}] \tag{2.23}$$

subject to the constraints

$$\mathbf{Gp} \geq \mathbf{p}^c. \tag{2.24}$$

must be solved. Figure 2.4 illustrates the relationship between measurement space and parameter space. In (2.23), $J(\hat{\mathbf{p}})$ is a performance criterion that measures the error between the model output, $\mathbf{F}(\hat{\mathbf{p}})$ and observations $\mathbf{Z}$ (of state $\mathbf{u(p)}$ or $\mathbf{F(u,p)}$) when $\mathbf{p}$ is a vector of model parameters. These observations can be measurements of the state variables $\mathbf{u} = \{S_w, S_g, P_o\}^T$ at discrete positions at various times, or at specified positions

as functions of times, or derived measurements such as pressure drop or production of one or more fluid phases.

In this work a fully implicit three-phase, one-dimensional black-oil simulator is used to calculate $\mathbf{F}(\hat{\mathbf{p}})$. $\mathbf{W}$ is selected to be the inverse of the covariance matrix of the estimate, and hence maximum-likelihood estimates result [Bard, 1974]. The parameter estimation problem is solved using a trust-region based Levenberg-Marquard algorithm [Gill et al., 1981]. Least-squares [Neuman and Yakowitz, 1979; Carrera and Neuman, 1986a; Carrera and Neuman, 1986b], least-squares with regularization [Watson, 1988; Liu, 1993; Helseth et al., 1996] or least-squares with Bayesian estimation [Gavalas et al., 1976; Shah et al., 1978; Watson et al., 1993] give different ways to compose the performance criterion, $J(\hat{\mathbf{p}})$. These criteria can include prior information (Bayesian estimation) and smoothing (regularization) to reduce the parameter space and give stable solutions of the inverse problem. This will be discussed later.

Note that with the approach used here, data from several separate two- and three-phase experiments can be utilized simultaneously. However, to attempt to solve (2.23) as a single parameter estimation problem, while including all the data from all the experiments, is not likely to be fruitful because of the large dimensionality of the parameter space. Also, it is likely that local, non-global solutions to the problem may result. For two-phase situations, this problem has been solved as a series of minimization problems with increased dimensionality or as a series of largely decoupled problems [Watson et al., 1988]. This methodology is developed for three-phase flow [Mejia et al., 1996] and further developed in this work (details in Paper II).

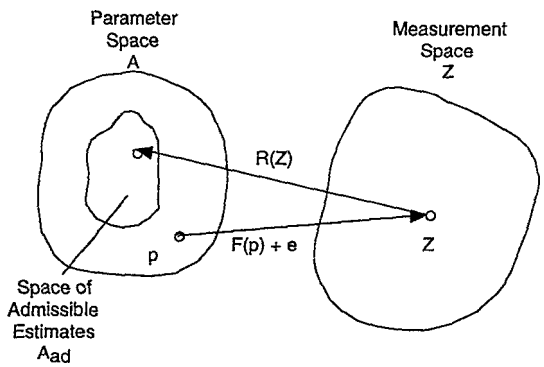

Figure 2.4 Relationship between parameter and measurement spaces for the inverse problems in porous media.

2.2.1 Nonlinear Least Squares and Maximum Likelihood Methods

Nonlinear least squares methods and related regression techniques are widely used to match experimental models to data [Bard, 1974]. Weighted least squares estimates minimize the performance criterion given as

$$J(\hat{\mathbf{p}}) = [\mathbf{F}(\hat{\mathbf{p}}) - \mathbf{Z}]^T \mathbf{W} [\mathbf{F}(\hat{\mathbf{p}}) - \mathbf{Z}]. \tag{2.25}$$

The forward equations vector (2.9)-(2.11) will generate data corresponding to the measurement vector $\mathbf{Z}$ with an additive random measurement error $\boldsymbol{\varepsilon}_z$: $\mathbf{Z} = \mathbf{F}(\mathbf{p}) + \boldsymbol{\varepsilon}_z$. The measurement error is often assumed to be Gaussian in order to facilitate statistical analysis of the results [Bard, 1974]. Numerical solutions of the nonlinear least squares problem are generally found with iterative search algorithms such as the Gauss-Newton or gradient methods (discussed in the next section).

The least squares estimator found from minimizing (2.25) is equivalent to a Gaussian maximum likelihood estimator with known statistical properties found from minimizing

$$p_{Z|p}(\mathbf{z}|\mathbf{p}) = p_v[\mathbf{Z} - \mathbf{F}(\mathbf{p})] \tag{2.26}$$

where $p_{Z|p}$ is the likelihood function (conditional density) [Neuman and Yakowitz, 1979; Carrera and Neuman, 1986a; Carrera and Neuman, 1986b]. The statistical properties such as mean and variance of maximum likelihood (and least square) estimate $\hat{\mathbf{p}}$ can be computed in a linearized covariance analysis (discussed in a later section).

Since maximum likelihood estimation, like least squares estimation, assumes that $\mathbf{p}$ is an unknown deterministic parameter, the only source of randomness in the formulation is measurement error. Therefore, in order to be useful, the concept of measurement error must be extended to include such things as scale discrepancies (e.g., differences between model discretization and well scales) and modeling errors. This generalization of the measurement error concept is particularly important in least squares and maximum likelihood methods since there is no other way to account for uncertainty [McLaughlin and Townley, 1996].

2.2.2 Solution Criteria

Solution criteria are now presented for validating estimates of relative permeability and capillary pressure functions from laboratory data. The solution of the estimation of parameters in 2.25 is compared to the statistical expectations of the least squares estimator. The sum of squared residuals is given as [Dougherty, 1990]:

$$SSR = [\mathbf{F}(\hat{\mathbf{p}}) - \mathbf{Z}]^T [\mathbf{F}(\hat{\mathbf{p}}) - \mathbf{Z}].$$

Minimization of *SSR* results in a sample regression line that best fits the observational data [Dougherty, 1990]. The sum of squared residuals (*SSR*) is satisfactory when the quantity $\sqrt{SSR/(N_m - N_p - 1)}$ gives a reasonable estimate of the standard deviation of the observation data. $SSR/(N_m - N_p - 1)$ is an unbiased estimator of σ^2 (the variance of each measurement).

Another solution criterion is the number of runs. This quantity is the number of times the residuals changes sign and is expected to be $\frac{N_M}{2}+1$. This property gives additional information to the *SSR* criterion when we want to determine if bias error is present in our estimates [Watson et al., 1990] and [Grimstad et al., 1997].

2.2.3 Regularization

Finding the minimum of the non-linear least squares problem in (2.23) is not trivial. When noisy data is used, stability in the optimization can be a problem. To stabilize the solution of the inverse problem, regularization is introduced. The regularization is based on ideas first advanced by Tikhonov [1977] in the solution of ill-posed integral equations. For some $\beta \geq 0$, a regularization term is added to the objective functional as

$$J_\beta(\mathbf{p}) = J(\mathbf{p}) + \frac{\beta}{2}\|\mathbf{p}\|_R^2. \tag{2.27}$$

Regularization has been implemented in porous media applications for estimation of porosity and permeability properties [Watson, 1980; Watson, 1988]. An important issue in regularization is to determine a suitable value of β for the given noisy data, especially where the noise level may or may not be known. A general formulation of β is not found, and the value has to be chosen for each problem according to various criterion [Liu, 1993; Helseth et al., 1996; Lee et al., 1987; Watson, 1988].

2.2.4 Bayesian Estimation

Another approach to reduce instability in the estimates is to include prior information in the objective function. Bayesian estimation methods include prior information and have been applied to parameter identification in multiphase flow [Gavalas et al., 1976].

Prior information of the system can be incorporated into the problem as a modified regularization. $\mathbf{p}_0$ contains the initial guess for $\mathbf{p}$ based on the prior information or guess about the solution from e.g. geological data. The regularized function J_β in (2.27) can be written as

$$J_\beta(\mathbf{p}) = J(\mathbf{p}) + \frac{\beta}{2}\|\mathbf{p} - \mathbf{p}_0\|_R^2. \tag{2.28}$$

This approach gives Bayesian estimates for a given distribution of the observations $\mathbf{Z}$ and parameters $\mathbf{p}$. Suppose the data $\mathbf{Z}$ are related to $\hat{\mathbf{p}}$ by

$$\mathbf{Z} = \mathbf{F}(\hat{\mathbf{p}}) + \varepsilon_Z \tag{2.29}$$

and that $\mathbf{p}_0$ satisfies

$$\hat{\mathbf{p}} = \mathbf{p}_0 + \varepsilon_p \tag{2.30}$$

for random variables ε_z and ε_p. If the underlying probability distributions on these random variables are Gaussian, then minimization of J_β as given by (2.28) has a Bayesian interpretation for suitably chosen $\|\cdot\|_z$, $\|\cdot\|_R$, and β. In particular, if ε_z and ε_p have zero mean and covariance matrices $\sigma^2\mathbf{V}$ and $\tau^2\Sigma$, respectively, and if

$$\left.\begin{aligned} \|\mathbf{z}\|_z^2 &= \mathbf{z}^T\mathbf{V}^{-1}\mathbf{z} \\ \|\mathbf{p}\|_R^2 &= \mathbf{p}^T\Sigma^{-1}\mathbf{p} \end{aligned}\right\} \Rightarrow \beta = \frac{\sigma^2}{\tau^2} \tag{2.31}$$

then minimization of J_β as given in (2.28) gives Bayesian maximum likelihood estimates [Watson et al., 1993]. This expression for β is especially enlightening: it shows that the optimal β is that which equally balances the weight given to the mean-squared error in $\mathbf{Z}$ and the mean squared error in $\mathbf{p}$.

Shah et al. [1978] showed that if reliable prior information is available, Bayesian estimation would lead to a smaller variance error of the estimated parameters.

2.2.5 Search Methods

The solution of scalar optimization problems, as the weighting method in (2.23), has been extensively discussed by many authors in the past. Numerical solutions can be classified into the following three categories: Gauss-Newton, gradient search, and direct search methods [Gill et al., 1981].

The Gauss-Newton method and related methods have been extensively used in the solution of the inverse problem [Watson et al., 1988; Sun and Yeh, 1990a; Mejia et al., 1996]. The Gauss-Newton direction, $\mathbf{d}$, is found from

$$(\mathbf{A}_k^T\mathbf{A}_k - \lambda_k\mathbf{I})\mathbf{d}_k = -\mathbf{A}_k^T\mathbf{F}_k \tag{2.32}$$

where the vector $\mathbf{d}$ is the solution of the sub-problem

$$\min_{\mathbf{d}\in\mathbf{R}^n} \tfrac{1}{2}\left\|\mathbf{A}_k\mathbf{d}+\mathbf{F}_k\right\|_2^2 \tag{2.33}$$

subject to

$\|\mathbf{d}\|_2 < \Delta$.

In order to obtain the Gauss-Newton direction it is necessary to calculate the total sensitivity matrix **A** in each iteration k of the non-linear least squares minimization where $a_{ij} = \partial F(\mathbf{u},\mathbf{p})_i / \partial \mathrm{p}_j$ is the sensitivity coefficient of the model response $F(\mathbf{u},\mathbf{p})_i$ with respect to the discretized unknown parameter p_j.

Gradient search methods [Chavent et al., 1975; Neuman et al., 1980; Carrera and Neuman, 1986b] are designed to avoid the calculation of the sensitivity matrix **A**, therefore, in principle, they require less computer time. However, more iteration may be required for convergence.

2.3 Sensitivity Analysis and Non-Linearity Measure

The sensitivity in the model equation to the parameters, or coefficients in a parameterization of the parameter functions, is essential in parameter estimation, i.e. when computing **A**. However, several aspects have to be investigated in order to find an optimal solution with high accuracy. In this section the main steps in a linearized covariance analysis are presented. In this analysis, the impact of measurement error on the estimated flow functions is computed. Finally, a short discussion on non-linearity and sensitivity is addressed.

2.3.1 Covariance Analysis

Several assumptions and sources of error accompany parameter estimation. First, we assume the mathematical model of the physical process is correct. Second, we assume that the model is linear in the parameters close to the minimum when the global minimum is found. Third is bias error, which is the result of using functional representations that are incapable of representing the true (although unknown) functional relationship. Finally, the variance error is a result of the inexact nature of measured data. The mathematical model (2.9)-(2.11) presented before is assumed to describe multiphase flow in porous media.

In this work we want to determine the two- and three-phase relative permeability and two-phase capillary pressure functions. If accurate estimates of these flow properties are to be obtained, it is necessary that the bias error and variance error is small. Choosing functional representations of the flow functions with very large numbers of parameters will reduce bias error due to increased flexibility. However, this does not ensure accurate estimates of the properties. In fact, while increasing the flexibility of the candidate functional representation decreases the bias error in the estimates, it tends to increase the variance error because of estimating more parameters on the basis of the

same amount of information [Kerig and Watson, 1986]. This trade off between the bias error and variance error must be investigated in an experimental design.

In the absence of significant bias error, the variance error of the estimates can be readily evaluated in a linearized covariance analysis.

If we assume the model function $\mathbf{F}$ is correct, we can write $\mathbf{Z} = \mathbf{F}(\mathbf{p}) + \varepsilon_Z$ for parameter vector $\mathbf{p}$ and measurement errors ε_Z. We assume that the error element $\varepsilon_{Z,i}$ has a normal distribution with zero mean and variance σ_i, i.e. $\mathbf{Z}$ is normally distributed with $\mathbf{F}(\mathbf{p})$ mean and covariance matrix Σ. We further assume the model function $\mathbf{F}(\mathbf{p})$ is linear with respect to the parameters $\mathbf{p}$ near the solution. When a set of unknown parameters $\mathbf{p}$ is to be estimated by minimization of an objective function of the form of (2.23), the accuracy of the parameter estimate may be obtained by a linearized covariance analysis.

The objective function to minimize is given as

$$J(\mathbf{p}) = [\mathbf{Z} - \mathbf{F}(\mathbf{p})]^T \mathbf{W} [\mathbf{Z} - \mathbf{F}(\mathbf{p})] = \sum_{i=1}^{m} \frac{1}{\sigma_i^2} (Z_i - F_i(\mathbf{p}))^2 . \tag{2.34}$$

The expected value of the residual vector, $\varepsilon_Z = \mathbf{Z} - \mathbf{F}(\mathbf{p})$, is given as

$$E\left[(Z_i - F_i(\mathbf{p}))^T (Z_i - F_i(\mathbf{p}))\right] = E\left[\varepsilon_Z{}^T \varepsilon_Z\right] = \begin{bmatrix} \sigma_1^2 & \cdots & 0 \\ \vdots & \ddots & \vdots \\ 0 & \cdots & \sigma_1^2 \end{bmatrix} = \Sigma . \tag{2.35}$$

A Taylor expansion about the true parameters $\mathbf{p}_0$ are given as

$$J(\mathbf{p} + \Delta\mathbf{p}) \approx J(\mathbf{p}_0) + \frac{\partial J(\mathbf{p}_0)}{\partial \mathbf{p}} (\mathbf{p} - \mathbf{p}_0) + \frac{1}{2} (\mathbf{p} - \mathbf{p}_0)^T \frac{\partial^2 J(\mathbf{p}_0)}{\partial \mathbf{p}^2} (\mathbf{p} - \mathbf{p}_0). \tag{2.36}$$

Instead of minimizing the (2.23), we minimize the expansion about the true parameters and neglect the second order terms. When the model function is linear, this expansion is exact, and the objective function is exact. To find the minimum of the objective function, we differentiate (2.36) with respect to the parameter vector $\mathbf{p}$ and set the resulting equation equal to zero.

$$\frac{\partial J(\mathbf{p})}{\partial \mathbf{p}} \approx \frac{\partial J(\mathbf{p}_0)}{\partial \mathbf{p}} + \frac{\partial^2 J(\mathbf{p}_0)}{\partial \mathbf{p}^2} (\mathbf{p} - \mathbf{p}_0) = 0 \tag{2.37}$$

Differentiating the original objective function (2.23) gives the normal equations

$$\frac{\partial J(\mathbf{p}_0)}{\partial \mathbf{p}} = -2\left[\frac{\partial \mathbf{F}(\mathbf{p}_0)}{\partial \mathbf{p}}\right]^T \mathbf{W}[\mathbf{Z}-\mathbf{F}(\mathbf{p}_0)]$$
$$\frac{\partial^2 J(\mathbf{p}_0)}{\partial \mathbf{p}^2} = -2\left[\frac{\partial^2 \mathbf{F}(\mathbf{p}_0)}{\partial \mathbf{p}^2}\right]^T \mathbf{W}[\mathbf{Z}-\mathbf{F}(\mathbf{p}_0)] + 2\left[\frac{\partial \mathbf{F}(\mathbf{p}_0)}{\partial \mathbf{p}}\right]^T \mathbf{W}\left[\frac{\partial \mathbf{F}(\mathbf{p}_0)}{\partial \mathbf{p}}\right]. \quad (2.38)$$

We assume that **F** is linear in the parameters in the minimum, i.e., the first term in (2.38) vanishes. We define the sensitivity matrix as the partial derivative of the model output with respect to the parameters in **p**

$$\mathbf{A}_{N_m \times N_p} = \left[\frac{\partial \mathbf{F}(\mathbf{p}_0)}{\partial \mathbf{p}}\right]. \quad (2.39)$$

Combining the last equations gives

$$\mathbf{A}^T \mathbf{W}[\mathbf{Z}-\mathbf{F}(\mathbf{p}_0)] = \mathbf{A}^T \mathbf{W} \mathbf{A}(\hat{\mathbf{p}}-\mathbf{p}_0). \quad (2.40)$$

Now, we introduce the covariance matrix of the parameter estimate, **P**, as

$$\mathbf{P}_{N_p \times N_p} = E\left[(\hat{\mathbf{p}}-\mathbf{p}_0)(\hat{\mathbf{p}}-\mathbf{p}_0)^T\right]. \quad (2.41)$$

After some matrix operations and introduction of the inverse of the weighting matrix **W** as the covariance matrix of the observation error Σ, we get an expression for the covariance of the parameter estimate as a function of the sensitivity matrix and the covariance matrix of measurement error, details are found in Kerig and Watson [1986] and Paper III.

$$\mathbf{P}_{N_p \times N_p} = \left(\mathbf{A}^T \Sigma^{-1} \mathbf{A}\right)^{-1}. \quad (2.42)$$

Further can the covariance of the flow functions be found using

$$\mathbf{C}_{N_q \times N_q}(S_f) = \mathbf{D}^T(S_f) \mathbf{P} \mathbf{D}(S_f), \quad (2.43)$$

where $\mathbf{D}_{N_p \times N_q} = \left[\frac{\partial \mathbf{f}(\mathbf{p})}{\partial \mathbf{p}}\right]$. N_q is the number of flow functions to be estimated and **f** is a vector of the different flow functions, i.e.

$$\mathbf{f} = \left\{k_{rw}(S_w, S_g), k_{ro}(S_w, S_g), k_{rg}(S_w, S_g), P_{c,ow}(S_o, S_w), P_{c,og}(S_w, S_g)\right\}^T.$$

Since the variance of the measurement error is unknown and we use an estimate of this variance in Σ, the t distribution (also called student's t distribution) is used when the confidence intervals are computed. The upper and lower $(1-\frac{\alpha}{2})$ level confidence intervals for each flow function f_i at a specific saturation is given as

$$\hat{f}_i \pm t_{N_m - N_p}(1-\tfrac{\alpha}{2})\sqrt{c_{ii}}. \tag{2.44}$$

2.3.2 Measure of Non-Linearity

One of the assumptions in the previous section was that the model was linear close to the parameter minimum. If this assumption fails, the confidence intervals computed from the linearized covariance analysis will be too optimistic [Bates and Watts, 1980; Liu, 1993]. Therefore, a measure of the non-linearity of the model is necessary. Expressions which indicate the adequacy of a linear approximation and its effects on inferences are called measures of non-linearity [Bates and Watts, 1980]. Bates and Watts introduced the concept of curvature as a measure of non-linearity. Leikvoll [1995] investigated error analysis methodologies for nonlinear least squares problems arising within porous media applications.

Assume that the model function $\mathbf{F}$ defines a N_p-dimensional surface S in the N_m-dimensional sample space when the parameters in $\mathbf{p}$ vary through their allowed values. The measure of non-linearity becomes the maximum curvature tangential to S (the parameter-effect curvature) and orthogonal to S (the intrinsic curvature). The curve $\eta_{\mathbf{h}}(\beta)$ on the surface S is defined by

$$\eta_{\mathbf{h}}(\beta) = \mathbf{F}(\mathbf{p}(\beta)) = \mathbf{F}(\hat{\mathbf{p}} + \beta\mathbf{h}) \tag{2.45}$$

where β is a real number and $\mathbf{h}$ an arbitrary nonzero vector in the parameter space. Assume that the mapping $\mathbf{F}(\mathbf{p})$ is smooth enough so that the curve $\eta_{\mathbf{h}}$ will have a tangent and acceleration in $\hat{\mathbf{p}}$. The tangent to $\eta_{\mathbf{h}}$ at $\beta = 0$ is the derivative of $\eta_{\mathbf{h}}$ with respect to β

$$\dot{\eta}_{\mathbf{h}} = \left.\frac{d\eta_{\mathbf{h}}(\beta)}{d\beta}\right|_{\beta=0} = \sum_i \left.\frac{\partial \mathbf{F}}{\partial p_i}\right|_{\hat{\mathbf{p}}} \left.\frac{dp_i}{d\beta}\right|_{\beta=0} = \mathbf{A}\mathbf{h}. \tag{2.46}$$

The acceleration of the curve $\eta_{\mathbf{h}}$ at $\beta = 0$ can be calculated from

$$\ddot{\eta}_{\mathbf{h}} = \left.\frac{d^2\eta_{\mathbf{h}}(\beta)}{d\beta^2}\right|_{\beta=0} = \sum_j \left.\frac{\partial \mathbf{Ah}}{\partial p_j}\right|_{\hat{\mathbf{p}}} \left.\frac{dp_j}{d\beta}\right|_{\beta=0} = \mathbf{h}^T\mathbf{H}\mathbf{h}. \tag{2.47}$$

The acceleration is then decomposed into orthogonal and parallel planes

$$\ddot{\eta}_{\mathbf{h}} = \ddot{\eta}^n_{\mathbf{h}} + \ddot{\eta}^t_{\mathbf{h}}$$

where the normal curvature in the direction of **h** is given by

$$K^n_{\mathbf{h}} = \frac{\left\|\ddot{\eta}^n_{\mathbf{h}}\right\|}{\left\|\dot{\eta}_{\mathbf{h}}\right\|^2} \tag{2.48}$$

and the tangential curvature is given by

$$K^t_{\mathbf{h}} = \frac{\left\|\ddot{\eta}^t_{\mathbf{h}}\right\|}{\left\|\dot{\eta}_{\mathbf{h}}\right\|^2}. \tag{2.49}$$

The normal curvature is a property of the surface, S, and not affected by a reparameterization of **F**. $K^n_{\mathbf{h}}$ is the intrinsic curvature. The tangential curvature $K^t_{\mathbf{h}}$ is dependent on the parameterization and is called the parameter-effects curvature. A non-linear reparameterization of the model can change the parameter-effect curvature considerably. To assess the effect of non-linearity on inference, the $K^n_{\mathbf{h}}$ and $K^t_{\mathbf{h}}$ are converted to standardized relative curvatures which are invariant under changes of scale in the response. The relative curvatures can then be used to compare not only different parameterizations for a given problem, but also different data sets for the same or different models.

The curvature measure can then be used in an experimental design to evaluate the different designs with respect to non-linearity around a global minimum. An experimental design with low degree of non-linearity is preferable during parameter estimation. When the non-linearity is low, the sensitivity of the parameters will be high [Liu, 1993], and this improves the stability in the search around the global minimum [McLaughlin et al., 1996].

3 Analytical Sensitivity Coefficients

The background chapter shows that the sensitivity coefficients play an important role in determination parameters in parameter estimation, computation of accuracy of estimated parameters in linearized covariance analysis and for determination of non-linearity of model close to global minimum. In this chapter different methods for computation of sensitivity coefficients are first reviewed. Since the direct method is favorable due to the way the model equation is solved, this method is extended from the work by Anterion [1984] and Vignes [1993] on two-phase flow to the methodology of determination of three-phase flow properties.

3.1 Perturbation Method

In the perturbation method the *j*th row of the sensitivity matrix $\mathbf{A}^T$ is approximated by [Tortorelli et al., 1994]:

$$a_{ij} = \frac{\partial F_i}{\partial \mathrm{p}_j} \approx \frac{F_i(\mathbf{p} + \Delta \mathrm{p}_j \mathbf{e}_j) - F_i(\mathbf{p})}{\Delta \mathrm{p}_j} \qquad \begin{matrix} i = 1,\ldots,N_m \\ j = 1,\ldots,N_p \end{matrix} \tag{3.1}$$

where $\Delta \mathrm{p}_j$ is the small increment of p_j and $\mathbf{e}_j$ is the *j*th unit vector. The values of $F_i(\mathbf{p} + \Delta \mathrm{p}_j \mathbf{e}_j)$ and $F_i(\mathbf{p})$ are obtained by solving the model equation (by simulation) subject to the initial and boundary conditions. This method is therefore easy to implement since the computer code for computing $F_i(\mathbf{p})$ and $F_i(\mathbf{p} + \Delta \mathrm{p}_j \mathbf{e}_j)$ already exist. However, the method requires perturbing each parameter one at a time. If there are N_p parameters to be identified, the model equation has to be solved $(N_p + 1)$ times for each iteration in the non-linear least squares minimization to numerically produce the sensitivity coefficients. The value of $\Delta \mathrm{p}_j$ is usually determined on a trial-and-error basis, and it will vary for each parameter and each case.

3.2 Adjoint Method

Jacquard and Jain [1965] first used this method (frequently called the variational method) for solving the inverse problem of parameter identification. It has later been used when solving oil and water two-phase flow problems in porous media [Seinfeld and Chen, 1978; Watson et al., 1980]. Consider the general form of the problem equations (2.9)-(2.11) and a general performance criterion

$$J(\mathbf{u}, \mathbf{p}) = \int_{t_0}^{t_f} \int_{(\Omega)} F(\mathbf{u}, \mathbf{p}; x, t) d\Omega dt \tag{3.2}$$

where $F(\mathbf{u},\mathbf{p};x,t)$ is a function specified by the user. The first-order variation of J is

$$\delta J(\mathbf{u},\mathbf{p}) = \int_{t_0}^{t_f}\int_{(\Omega)}\left(\frac{\partial F}{\partial \mathbf{u}}\delta\mathbf{u} + \frac{\partial F}{\partial \mathbf{p}}\delta\mathbf{p}\right)d\Omega dt. \tag{3.3}$$

In order to find the functional derivative of $J(\mathbf{u},\mathbf{p})$ with respect to the unknown parameter vector $\mathbf{p}$, the unknown term associated with $\delta\mathbf{u}$ in (3.3) must be eliminated. Adjoint operators are introduced together with an adjoint state variable ϕ. A set of adjoint model equations is introduced, in the same manner as the model equation in (2.9)-(2.11). The adjoint model equations are solved in the same way as the simulator equations. Sun and Yeh [1990a] have a detailed description of the method and they include an example from two-phase oil-water flow in reservoirs given by Huyakorn and Pinder [1983].

For any unknown parameter p_j, the partial functional derivative is given as

$$\frac{\partial J(\mathbf{u},\mathbf{p})}{\partial \mathrm{p}_j} = \int_{t_0}^{t_f}\int_{(\Omega)}\left[\nabla_p^{+}\mathbf{R}\phi + \frac{\partial F}{\partial \mathbf{p}}\right]_j d\Omega d. \tag{3.4}$$

By solving the model equation one time only and solving the adjoint equation for each interval in the function specified by the user, all sensitivity coefficients can be produced [Sun and Yeh, 1990a]. This method is expensive to implement compared to the perturbation method since a set of adjoint model equations must be derived and solved. However, it requires less computations and it is the most efficient method in those situations where the state sensitivities are not necessary, i.e. those situations where only the sensitivity of the performance criterion is needed (as in gradient search methods in parameter estimation). Since numerical differentiation is avoided, the method is more accurate and stable than the perturbation method.

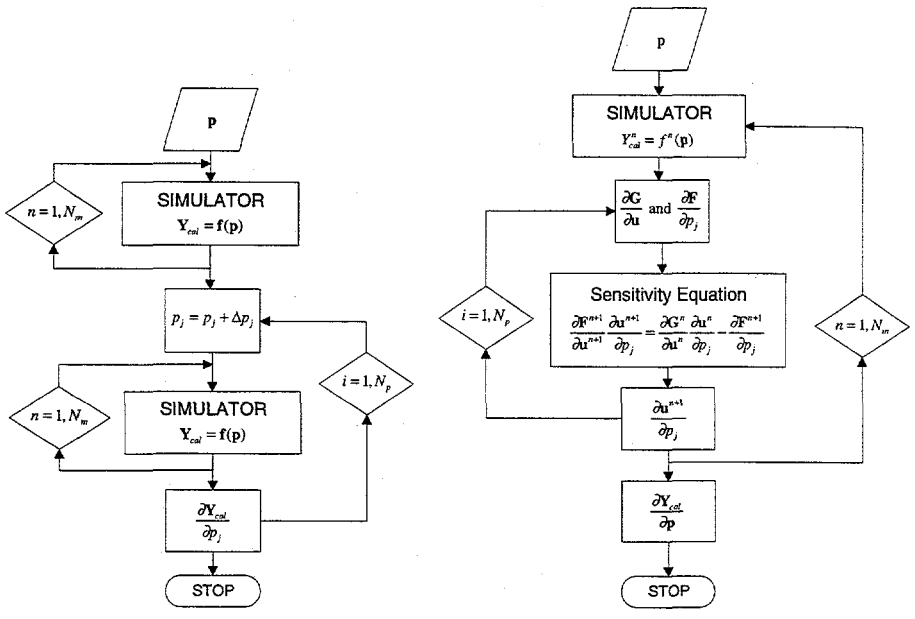

Figure 3.1 Flow chart for computation of sensitivity coefficients by a) the perturbation method and b) the direct method.

3.3 Direct Method

In the direct method the sensitivity equation is solved after the simulator equation at each time step, since data from the solution of the simulator equation are utilized in solving the sensitivity equation. The sensitivity equation is first solved for the state sensitivities, then the derived sensitivities used in estimation and experimental design are computed [Tortorelli et al., 1994].

3.3.1 State Sensitivities

The model equation has previous been given as

$$\mathbf{R}(\mathbf{u}, \mathbf{p}; x, t) = \mathbf{0}. \tag{3.5}$$

This vector function can be separated into terms at time step $n+1$ (=**F**), and at time step n (=**G**). This gives the vector equation

$$\mathbf{F}(\mathbf{u}, \mathbf{p})^{n+1} = \mathbf{G}(\mathbf{u})^n. \tag{3.6}$$

The non-linear equation (3.5) has been solved by the Newton-Raphson method, see section 2.2 which yields, as a side product, the Jacobian

$$\mathbf{J}(\mathbf{u},\mathbf{p}) = \frac{\partial \mathbf{R}(\mathbf{u},\mathbf{p})}{\partial \mathbf{u}} = \frac{\partial \mathbf{F}(\mathbf{u},\mathbf{p})}{\partial \mathbf{u}}. \tag{3.7}$$

The sensitivity in the model (3.5) with respect to the parameters is expressed in the sensitivity coefficients, defined within the *sensitivity equation* as

$$\frac{\partial \mathbf{F}^{n+1}}{\partial \mathbf{u}^{n+1}} \frac{\partial \mathbf{u}^{n+1}}{\partial \mathbf{p}} = \frac{\partial \mathbf{G}^{n}}{\partial \mathbf{u}^{n}} \frac{\partial \mathbf{u}^{n}}{\partial \mathbf{p}} - \frac{\partial \mathbf{F}^{n+1}}{\partial \mathbf{p}}. \tag{3.8}$$

The sensitivity matrix (i.e., the state sensitivity coefficients) is given by

$$\mathbf{A} = \left[A_{ij}\right] = \frac{\partial \mathbf{u}}{\partial \mathbf{p}} = \left[\frac{\partial u_i}{\partial p_j}\right]. \tag{3.9}$$

When simulating fluid flow in porous media and utilizing Newton-Raphson method, the Jacobian will be computed at each time step. Further, the sensitivity equation is linear in the sensitivity coefficients. Hence, the sensitivity equation can easily be solved if the functional representation of the flow functions is known. In this work, the functional representation of the flow properties is known (B-splines and tensor-product B-splines), and $\partial \mathbf{F}^{n+1}/\partial \mathbf{p}$ can be computed analytically. $\partial \mathbf{G}^{n}/\partial \mathbf{u}^{n}$ can easily be computed and $\partial \mathbf{u}^{n}/\partial \mathbf{p}$ is the sensitivity coefficient at the previous time step. The Jacobian is independent of the sensitivity coefficients and of the parameter vector $\mathbf{p}$, i.e., solving the sensitivity equation (3.8) requires computing N_p right hand sides and a backward substitution for each time step. Since stability of the sensitivity matrix $\mathbf{A}$ is connected to properties of the Jacobian (3.7), the sensitivity calculations inherit the stability properties of the simulator equation. After the simulator equation is discretized, here by finite difference, the computation of sensitivity coefficients are performed analytically, hence the name "analytical sensitivity coefficients".

Most of the work associated with solving the sensitivity equation (3.8) is calculation of the term $\partial \mathbf{F}^{n+1}/\partial \mathbf{p}$ for various boundary conditions. The sensitivity equation will be solved for two- and three-phase flow in section 3.6 and in Appendix A.

3.3.2 Derivable Sensitivities

From the state sensitivities $\partial \mathbf{u}^{n+1}/\partial \mathbf{p}$, derivable sensitivities can be computed, depending on the injection and production scheme.

Considering a one dimensional, two-phase oil-water case with injection of water at constant rate and production against constant well pressure. The oil production is then given as

$$V_o = \sum_{i=1}^{N_x} V_{b,i}\varphi_i b_{o,i}\left[S_{w,i} - S_{w(init),i}\right], \tag{3.10}$$

where N_x is the number of grid blocks in the x-direction. Differentiation of the oil production (3.10) with respect to a model parameter p_j is given as

$$\frac{dV_o}{d\mathrm{p}_j} = \frac{\partial V_o}{\partial \mathrm{S}_w}\frac{dS_w}{d\mathrm{p}_j} + \frac{\partial V_o}{\partial \mathrm{p}_j} = \sum_{i=1}^{N_x} V_{b,i}\varphi_i b_{o,i}\frac{dS_{w,i}}{d\mathrm{p}_j}. \tag{3.11}$$

The differential pressure is given as

$$\Delta P = p_{x=L} - p_{x=0} = P_{const} - p_{w,1} - G_w + \frac{q_w b_w}{\Sigma PI_f} = P_{const} - p_{o,1} + P_{c,ow} - G_w + \frac{q_w b_w}{\Sigma PI_f} \tag{3.12}$$

where

$$\Sigma PI_f = PI_o + PI_w = \frac{b_o k_{ro}}{\mu_o} + \frac{b_w k_{rw}}{\mu_w}. \tag{3.13}$$

q_w is the constant water injection rate, and P_{const} is the constant outlet well pressure. Differentiation of the differential pressure with respect to a model parameter p_j is given as

$$\frac{d\Delta P}{d\mathrm{p}_j} = \frac{\partial \Delta P}{\partial p_o}\frac{dp_o}{d\mathrm{p}_j} + \frac{\partial \Delta P}{\partial S_w}\frac{dS_w}{d\mathrm{p}_j} + \frac{\partial \Delta P}{\partial \mathrm{p}_j}. \tag{3.14}$$

This gives

$$\begin{aligned}\frac{d\Delta P}{d\mathrm{p}_j} = &\left\{-1 + \left[q_w\frac{\partial b_w}{\partial p_o}\Sigma PI_f - q_w b_w\frac{\partial \Sigma PI_f}{\partial p_o}\right]/\Sigma PI_f{}^2\right\}\frac{dp_o}{d\mathrm{p}_j} \\ &+\left\{\frac{\partial P_{c,ow}}{\partial S_w} + \left[-q_w b_w\frac{\partial \Sigma PI_f}{\partial S_w}\right]/\Sigma PI_f{}^2\right\}\frac{dS_w}{d\mathrm{p}_j} \\ &+\frac{\partial P_{c,ow}}{\partial \mathrm{p}_j} + \left[-q_w b_w\frac{\partial \Sigma PI_f}{\partial \mathrm{p}_j}\right]/\Sigma PI_f{}^2.\end{aligned} \tag{3.15}$$

Derived sensitivities for other boundary conditions have also been implemented:

1. Injection of oil at constant rate and production against constant well pressure.
2. Simultaneous injection of water and oil at constant rate and production against constant well pressure.

3. Injection of gas at constant rate and production against constant well pressure.
4. Simultaneous injections of water and oil and gas at constant rate and production against constant well pressure.

Details on these computations can be found in Appendix B.

3.4 Sources of Error

The different methods for sensitivity coefficient computation inherits different types of errors and these errors magnify depending on method and parameterization of sensitivity coefficient calculations. Below, truncation error, conditional error and round-off error are discussed.

3.4.1 Truncation error

When the derivative is approximated by a Taylor series, the truncation error is introduced due to neglecting higher order terms. The Taylor series up to second order is given as [Gill et al., 1981]:

$$F_i(\mathbf{p}+\Delta \mathrm{p}_j \mathbf{e}_j) = F_i(\mathbf{p}) + \Delta \mathrm{p}_j \frac{\partial F_i(\mathbf{p})}{\partial \mathbf{p}} + \frac{1}{2}\Delta \mathrm{p}_j^2 \frac{\partial^2 F_i(\mathbf{p})}{\partial \mathbf{p}^2}$$

and the sensitivity coefficients are defined in the perturbation method as

$$a_{ij}(F_i, \Delta \mathrm{p}_j) = \frac{F_i(\mathbf{p}+\Delta \mathrm{p}_j \mathbf{e}_j) - F_i(\mathbf{p})}{\Delta \mathrm{p}_j}.$$

The truncation error is given as

$$T_j(\Delta \mathrm{p}_j) = a_{ij}(F_i, \Delta \mathrm{p}_j) - \frac{\partial F_i(\mathbf{p})}{\partial \mathbf{p}} = \frac{1}{2}\Delta \mathrm{p}_j \frac{\partial^2 F_i(\mathbf{p})}{\partial \mathbf{p}^2}. \tag{3.16}$$

Hence, the truncation error is a linear function of $\Delta \mathrm{p}_j$ and will decrease when the perturbation decreases.

3.4.2 Conditional error

Condition error is introduced since function values calculated at a computer will be subject to errors due to inaccurate representation of numbers [Gill et al., 1981]. This is given as

$$\hat{F}(\mathbf{p}) = \hat{F}(\mathbf{p}) + \sigma$$
$$\hat{F}(\mathbf{p} + \Delta p_j \mathbf{e}_j) = \hat{F}(\mathbf{p} + \Delta p_j \mathbf{e}_j) + \sigma_{\Delta p_j}$$

where σ and $\sigma_{\Delta p_j}$ are the absolute error in $\mathbf{F}$ at $\mathbf{p}$ and $\mathbf{p} + \Delta p_j \mathbf{e}_j$. If the inexact function values are used for computation of sensitivity coefficients, and no other errors are made, then the computed value of a_{ij} is given by

$$a_{ij}(\hat{F}_i, \Delta p_j) = \frac{\hat{F}_i(\mathbf{p} + \Delta p_j \mathbf{e}_j) - \hat{F}_i(\mathbf{p})}{\Delta p_j}$$

and hence

$$a_{ij}(\hat{F}_i, \Delta p_j) = \frac{F_i(\mathbf{p} + \Delta p_j \mathbf{e}_j) - F_i(\mathbf{p})}{\Delta p_j} + \frac{\sigma_{\Delta p_j} - \sigma}{\Delta p_j} = a_{ij}(F_i, \Delta p_j) + C(a_{ij}, \Delta p_j). \tag{3.17}$$

The error $C(a_{ij}, \Delta p_j)$ due to inaccurate values of F is termed the conditional error (also called cancellation error). The conditional error is a linear function of $1/\Delta p_j$, hence increasing the perturbation will reduce the conditional error.

3.4.3 Rounding error

Given $\hat{F}(\mathbf{p})$ and $\hat{F}(\mathbf{p} + \Delta p_j \mathbf{e}_j)$, the calculation of the sensitivity coefficient involves rounding errors when performing subtraction and division. However, these errors are generally negligible with respect to the truncation and condition errors [Gill et al.,1981].

3.5 Comparison of Methods

The perturbation method will generally be less accurate due to truncation and conditional error. In this method the parameter increment must be chosen with care since decreasing the perturbation decreases the truncation error but increases the conditional error and vice versa. Actually, the method will require an analysis of the "best" size of the increment for each parameter. However, due to its simplicity, the method is popular. But for the cases considered in this work where the accuracy in the sensitivity coefficients is crucial, the method is not satisfactory.

For cases where only the gradient vector is required, the adjoint method is very efficient. In this work, the state sensitivities are necessary and due to the complexity of solving a new set of adjoint simulator equations, this method is not applied.

Since the simulator equations are solved using the Newton-Raphson method most of the computations in the direct method is already performed [Kabala and Milly, 1990]. Therefore, this method is chosen for sensitivity coefficient computations.

Previously, several authors [Dogru and Seinfeld, 1981; Yeh, 1986; Skaggs and Barry, 1996] have derived expressions for when the direct and adjoint methods are most efficient. These computations depend on the discretization (number of grid blocks), the number of parameters and the number of performance measures (number of times the performance criterion is computed). However, these comparisons differ depending on the algorithm applied to solve the problem for the different authors. These comparisons do not take into account the computer savings using the Newton-Raphson method when the simulator equations are solved. The analytical comparison results are therefore not discussed here. However, in Paper V, one case is presented where the perturbation and direct method are compared with respect to computer time and number of iterations before the solution is reached in parameter estimation. These results are also discussed in chapter four.

3.6 Implementation of Analytical Sensitivity Coefficients

3.6.1 Solving the Sensitivity Equation

When the simulator equation is solved for time step $n+1$, the Jacobian is computed and can be used to solve the sensitivity equation. However, two other terms must be calculated before the sensitivity equation is solved; $\partial \mathbf{G}^n / \partial \mathbf{u}^n$ and $\partial \mathbf{F}^{n+1} / \partial \mathrm{p}_j$ (from equation (3.8)).

The vector equation $\mathbf{G}^n(\mathbf{u})$ for three-phase flow is given as

$$\mathrm{G}^n_{o,i}(\mathbf{u}) = -\frac{V_b}{\Delta t}\left(\varphi b_o (1 - S_w - S_g)\right)^n \tag{3.18}$$

$$\mathrm{G}^n_{w,i}(\mathbf{u}) = -\frac{V_b}{\Delta t}\left(\varphi b_w S_w\right)^n \tag{3.19}$$

$$\mathrm{G}^n_{g,i}(\mathbf{u}) = -\frac{V_b}{\Delta t}\left(R_s \varphi b_o S_o + \varphi b_g S_g\right)^n . \tag{3.20}$$

Differentiating the vector equation $\mathbf{G}^n(\mathbf{u})$ with respect to the state variable vector $\mathbf{u}$ in each grid block gives

$$\frac{\partial \mathrm{G}_o^n}{\partial p_o} = -\frac{V_b}{\Delta t}\left[S_o(\varphi' b_o + \varphi b_o')\right]^n$$
$$\frac{\partial \mathrm{G}_o^n}{\partial S_w} = \frac{V_b}{\Delta t}\left[\varphi b_o\right]^n \tag{3.21}$$
$$\frac{\partial \mathrm{G}_o^n}{\partial S_g} = \frac{V_b}{\Delta t}\left[\varphi b_o\right]^n.$$

$$\frac{\partial \mathrm{G}_w^n}{\partial p_o} = -\frac{V_b}{\Delta t}\left[S_w(\varphi' b_w + \varphi b_w')\right]^n$$
$$\frac{\partial \mathrm{G}_w^n}{\partial S_w} = \frac{V_b}{\Delta t}\left[\varphi(S_w b_w' P_{c,ow}' - b_w)\right]^n \tag{3.22}$$
$$\frac{\partial \mathrm{G}_w^n}{\partial S_g} = 0.$$

$$\frac{\partial \mathrm{G}_g^n}{\partial p_o} = -\frac{V_b}{\Delta t}\left[\left(1-S_w-S_g\right)\left(R_s'\varphi b_o + R_s\varphi' b_o + R_s\varphi b_o'\right) + S_g(\varphi' b_g + \varphi b_g')\right]^n$$
$$\frac{\partial \mathrm{G}_g^n}{\partial S_w} = \frac{V_b}{\Delta t}\left[\varphi b_o R_s\right]^n \tag{3.23}$$
$$\frac{\partial \mathrm{G}_g^n}{\partial S_g} = -\frac{V_b}{\Delta t}\left[-R_s\varphi b_o + \varphi b_g + S_g\varphi b_g' \frac{\partial P_{c,og}}{\partial S_g}\right]^n.$$

The elements in vector equation $\mathbf{F}^{n+1}(\mathbf{u},\mathbf{p})$ are

$$\begin{aligned}\mathrm{F}_{o,i}(\mathbf{u},\mathbf{p})^{n+1} = {} & T_{o,i+\frac{1}{2}}(p_{o,i+1} - p_{o,i} - G_o)^{n+1} - T_{o,i-\frac{1}{2}}(p_{o,i} - p_{o,i-1} - G_o)^{n+1} \\ & + T_{o,i}(p_{well} - p_{o,i} - G_o)^{n+1} - \frac{V_b}{\Delta t}\left(\varphi b_o(1-S_w-S_g)\right)^{n+1}\end{aligned} \tag{3.24}$$

$$\begin{aligned}\mathrm{F}_{w,i}(\mathbf{u},\mathbf{p})^{n+1} = {} & T_{w,i+\frac{1}{2}}(p_{w,i+1} - p_{w,i} - G_w)^{n+1} - T_{w,i-\frac{1}{2}}(p_{w,i} - p_{w,i-1} - G_w)^{n+1} \\ & + T_{w,i}(p_{well} - p_{w,i} - G_w)^{n+1} - \frac{V_b}{\Delta t}\left(\varphi b_w S_w\right)^{n+1}\end{aligned} \tag{3.25}$$

$$
\begin{aligned}
\mathrm{F}_{g,i}(\mathbf{u},\mathbf{p})^{n+1} = {} & R_{s,i+\frac{1}{2}} T_{o,i+\frac{1}{2}} (p_{o,i+1} - p_{o,i} - G_o)^{n+1} - R_{s,i-\frac{1}{2}} T_{o,i-\frac{1}{2}} (p_{o,i} - p_{o,i-1} - G_o)^{n+1} \\
& + T_{g,i+\frac{1}{2}} (p_{g,i+1} - p_{g,i} - G_g)^{n+1} - T_{g,i-\frac{1}{2}} (p_{g,i} - p_{g,i-1} - G_g)^{n+1} \\
& + R_{s,i} T_{o,i} (p_{well} - p_{o,i} - G_o)^{n+1} + T_{g,i} (p_{well} - p_{g,i} - G_g)^{n+1} \\
& - \frac{V_b}{\Delta t} \left(R_s \varphi b_o S_o + \varphi b_g S_g \right)^{n+1}
\end{aligned}
\tag{3.26}
$$

Differentiating the vector equation $\mathbf{F}^{n+1}(\mathbf{u},\mathbf{p})$ with respect to the model parameters $\mathbf{p}$ gives

$$
\begin{aligned}
\frac{\partial \mathrm{F}_{o,i}(\mathbf{u},\mathbf{p})^{n+1}}{\partial \mathrm{p}_j} = {} & \frac{\partial T_{o,i+\frac{1}{2}}}{\partial \mathrm{p}_j} (p_{o,i+1} - p_{o,i} - G_o) \\
& - \frac{\partial T_{o,i-\frac{1}{2}}}{\partial \mathrm{p}_j} (p_{o,i} - p_{o,i-1} - G_o) \\
& + \frac{\partial T_{o,i}}{\partial \mathrm{p}_j} (p_{well} - p_{o,i} - G_o)
\end{aligned}
\tag{3.27}
$$

$$
\begin{aligned}
\frac{\partial \mathrm{F}_{w,i}(\mathbf{u},\mathbf{p})^{n+1}}{\partial \mathrm{p}_j} = {} & \frac{\partial T_{w,i+\frac{1}{2}}}{\partial \mathrm{p}_j} (p_{w,i+1} - p_{w,i} - G_w) + T_{w,i+\frac{1}{2}} \left(\frac{\partial P_{c,ow,i}}{\partial \mathrm{p}_j} - \frac{\partial P_{c,ow,i+1}}{\partial \mathrm{p}_j} \right) \\
& - \frac{\partial T_{w,i-\frac{1}{2}}}{\partial \mathrm{p}_j} (p_{w,i} - p_{w,i-1} - G_w) + T_{w,i-\frac{1}{2}} \left(\frac{\partial P_{c,ow,i-1}}{\partial \mathrm{p}_j} - \frac{\partial P_{c,ow,i}}{\partial \mathrm{p}_j} \right) \\
& + \frac{\partial T_{w,i}}{\partial \mathrm{p}_j} (p_{well} - p_{w,i} - G_w) + T_{w,i} \left(\frac{\partial P_{c,ow,i}}{\partial \mathrm{p}_j} \right)
\end{aligned}
\tag{3.28}
$$

$$
\begin{aligned}
\frac{\partial \mathrm{F}_{g,i}(\mathbf{u},\mathbf{p})^{n+1}}{\partial \mathrm{p}_j} &= R_{s,i+\frac{1}{2}} \frac{\partial T_{o,i+\frac{1}{2}}}{\partial \mathrm{p}_j}(p_{o,i+1} - p_{o,i} - G_o) \\
&\quad - R_{s,i-\frac{1}{2}} \frac{\partial T_{o,i-\frac{1}{2}}}{\partial \mathrm{p}_j}(p_{o,i} - p_{o,i-1} - G_o) \\
&\quad + \frac{\partial T_{g,i+\frac{1}{2}}}{\partial \mathrm{p}_j}(p_{g,i+1} - p_{g,i} - G_g) + T_{g,i+\frac{1}{2}}\left(\frac{\partial P_{c,og,i+1}}{\partial \mathrm{p}_j} - \frac{\partial P_{c,og,i}}{\partial \mathrm{p}_j}\right) \\
&\quad - \frac{\partial T_{g,i-\frac{1}{2}}}{\partial \mathrm{p}_j}(p_{g,i} - p_{g,i-1} - G_g) - T_{g,i-\frac{1}{2}}\left(\frac{\partial P_{c,og,i}}{\partial \mathrm{p}_j} - \frac{\partial P_{c,og,i-1}}{\partial \mathrm{p}_j}\right) \\
&\quad + R_{s,i} \frac{\partial T_{o,i}}{\partial \mathrm{p}_j}(p_{well} - p_{o,i} - G_o) \\
&\quad - \frac{\partial T_{g,i}}{\partial \mathrm{p}_j}(p_{well} - p_{g,i} - G_g) + T_{g,i}\left(\frac{\partial P_{c,og,i}}{\partial \mathrm{p}_j}\right)
\end{aligned}
\tag{3.29}
$$

where the transmissibility T_f is differentiated with respect to the model parameters as

$$\frac{\partial T_{f,i}}{\partial \mathrm{p}_j} = c \frac{\partial k_{rf,i}}{\partial \mathrm{p}_j}.$$

Now, all the terms but $\partial \mathbf{u}^{n+1}/\partial \mathrm{p}_j$ is known, and the sensitivity equation (3.8) is solved with respect to the state sensitivity coefficient and then the derivable sensitivities are computed.

3.6.2 Differentiation of Flow Functions with Respect to Parameters

When solving the sensitivity equation (3.8), the term $\partial \mathbf{F}^{n+1}/\partial \mathbf{p}$ can be computed analytically if the functional form of the flow functions is known. In this work, B-splines are chosen to represent the two-phase functions, and tensor-product B-splines represents the three-phase functions.

Differentiating the two-phase flow functions described in section 2.1.4 with respect to the parameters in $\mathbf{p}$ gives

$$\frac{\partial g_1(S_f)}{\partial \mathrm{p}_j} = B_j^m(S_f, \mathbf{y}), \quad f = w, nw \tag{3.30}$$

and differentiating the three-phase flow functions with respect to parameter $p_k = c_{ij}^f$ gives

$$\frac{\partial g_2(S_1, S_2)}{\partial \mathrm{p}_k} = N_{ij}^m(S_1, \mathbf{y}_1, S_2, \mathbf{y}_2). \tag{3.31}$$

The derivatives of two-phase relative permeability and capillary pressure functions are

$$\begin{aligned}\frac{\partial k_{rf}(S_f)}{\partial \mathrm{p}_j} &= \frac{\partial g_1(S_f)}{\partial \mathrm{p}_j} \quad f = w, nw \\ \frac{\partial P_c(S_w)}{\partial \mathrm{p}_j} &= \frac{\partial g_1(S_w)}{\partial \mathrm{p}_j},\end{aligned} \tag{3.32}$$

and the derivatives of three-phase relative permeability and capillary pressure functions are

$$\frac{\partial k_{rf}(S_1, S_2)}{\partial \mathrm{p}_j} = N_{ij}^m(S_1, \mathbf{y}_1, S_2, \mathbf{y}_2) \quad \begin{cases} S_1 = S_f \\ S_2 = \begin{cases} S_w & if \quad f \neq w \\ S_g & if \quad f = w \end{cases} \end{cases} \quad f = w, o, g \tag{3.33}$$

$$\begin{aligned}\frac{\partial P_{c,ow}(S_w)}{\partial \mathrm{p}_j} &= B_j^m(S_w, \mathbf{y}) \\ \frac{\partial P_{c,og}(S_g)}{\partial \mathrm{p}_j} &= B_j^m(S_g, \mathbf{y}).\end{aligned} \tag{3.34}$$

3.6.3 Parameter Estimation

The direct method to compute the sensitivity matrix is implemented in PEST [Parameter ESTimation program, developed at Texas A&M University and RF-Rogaland Research]. In this program the sensitivity coefficients have previous been computed by the perturbation method, i.e. the simulator has been called N_p times to compute **A** in the flow chart in Figure 3.2. Analytical sensitivity coefficients have been implemented for two- and three-phase flow with the boundary conditions noted in section 3.3.2. Details on the implementation can be found in Appendix B.

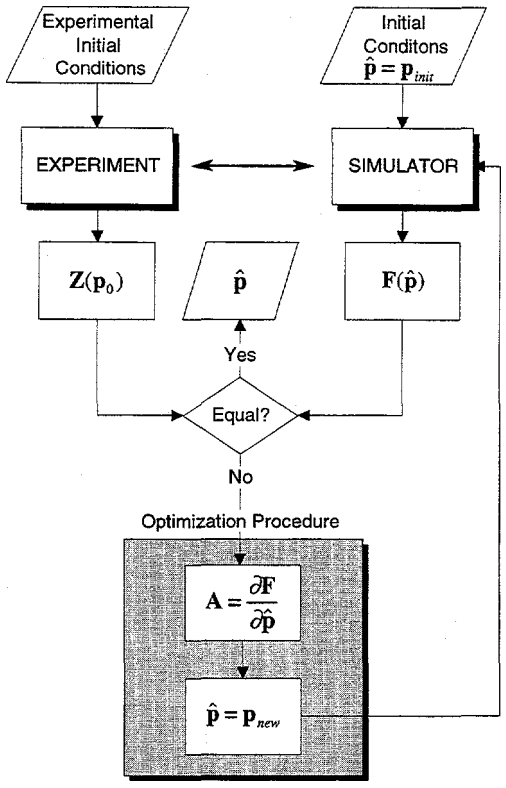

Figure 3.2 Flow chart for estimation of parameters.

3.6.4 Covariance Analysis

When the parameters in the model equation have been found in the parameter estimation procedure described above, the accuracy of these estimates can be computed in a linearized covariance analysis. These computations are dependent on the values of the sensitivity coefficients, as given by equation (2.43):

$$\mathbf{C} = \mathbf{D}^T\mathbf{P}\mathbf{D}$$

and the confidence intervals are found from the diagonal elements of **C**, see equation (2.44). Hence, the accuracy of confidence interval computations depends on the accuracy of the sensitivity matrix **A**. The accuracy and robustness together with speed of computations have motivated the implementation of analytical sensitivity coefficients when assessing the accuracy of the estimated parameters.

The direct method for computation of sensitivity coefficients has been implemented for various injection and production strategies in COVAN (COVariance ANalysis) [Urkedal, 1994]. This program is based on a linearized covariance analysis, and the perturbation method has been used to compute the sensitivity matrix.

The new algorithm for COVAN is given below:

1. Input: estimated or initial guess for the parameter vector **p**, estimate of the measurement errors, **Σ**.
2. Call the simulator:

   for $i \leftarrow 1, N_m$

   - compute the corresponding row in the sensitivity matrix, $\mathbf{A}_i$.
3. $\mathbf{P} \leftarrow (\mathbf{A}^T \mathbf{\Sigma} \mathbf{A})^{-1}$
4. for all saturations (i):
   - compute the sensitivity of the flow functions, **D**.
   - $\mathbf{C} \leftarrow \mathbf{D}^T \mathbf{P} \mathbf{D}$
   - $\left.\begin{matrix}\text{upper conf. interval} \\ \text{lower conf. interval}\end{matrix}\right\rangle \hat{f}_i \pm t_{N_m - N_p}(1-\frac{\alpha}{2})\sqrt{c_{ii}}$

Two parts in the algorithm is changed; the sensitivity matrix **A** is now computed analytically, and the sensitivity of the flow functions with respect to the parameters, **D**, is computed analytically.

3.7 Conclusions

The direct method for computation of sensitivity coefficients is extended from two-phase to three-phase flow in this work. This method is superior for computation of sensitivity coefficients when the Newton-Raphson method is used for solving the model equation. The direct method takes advantages of that the Jacobian is already computed, hence, the main computations are already performed. Further, the problems of choosing the right parameter increments in the perturbation method are avoided. The method is implemented in procedures both for parameter estimation and assessment of accuracy in two-phase and three-phase flow. The improvements of accuracy in sensitivity coefficients, stability of the parameter estimation and computer time reduction will be discussed in the next chapter where the direct method is tested for two- and three-phase cases.

4 Experimental Design

In this chapter optimal experimental design for two- and three-phase displacement experiments are derived. The optimality criterion is the covariance of the unbiased estimated parameters or the size of the confidence region around the estimated flow functions. The design problem is then to minimize the covariance of the estimated parameters, i.e., minimize the confidence intervals around the flow functions [Pukelsheim, 1993].

One problem that must be addressed first is the identifiability of the parameters. The contribution of observations, CTB, can be used to design the necessary experimental design to obtain identifiability of the parameters. The experiments must be designed so that the parameters can be identified within a certain resolution. Further they must be designed so that the accuracy is acceptable for certain saturation intervals. When an optimal design is found, this implies a high sensitivity in the data with respect to the parameters in the flow function representation. High degree of sensitivity implies a low degree of non-linearity in the parameter minimum and that the inverse problem is well-posed.

Although there is no general theory for constructing well-posed inverse problems, there are methods for dealing with ill-posedness. These methods can be the use of transient data, adding more or new kinds of measurements, and constraining the set of admissible parameter functions. It is important to note that ill-posedness does not imply that an inverse problem is meaningless. It merely indicates that the problem formulation must be modified or supplemented in some way before an acceptable solution can be obtained [McLaughlin and Townley, 1996]. The important thing is to recognize the circumstances that may or may not allow solution of the inverse problem and, if a solution is possible, to impose on it the proper limitations so as to make it mathematically well-behaved and physically meaningful [Sun and Yeh, 1990a; Sun and Yeh, 1990b]. In the experimental design discussed here the information content in the data, parameterization of the flow functions, the identifiability of the parameters and the stability and uniqueness are addressed, and an optimal combination of data sets is proposed for determination of two- and three-phase flow functions.

4.1 Background

4.1.1 Experimental Design for Interval Identifiability

In this section the necessary conditions for δ -interval identifiabilty will be discussed. The question of identifiability is equivalent to ask whether different parameter sets may lead to the same model response, if so, the parameters are unidentifiable. The uniqueness of the inverse solution may be relaxed if the identified parameters are not "too far" from the true parameters, i.e. the identified parameters are within the predefined resolution ($=\delta$ -interval) of parameters [Sun and Yeh, 1990b].

When the identifiability of the model parameters are analyzed prior to the experiment, the true parameters will be known, $\mathbf{p}_0$, together with an estimate of the covariance of the parameters, $\mathbf{C}_p$ and measurements, Σ. With an estimate of the upper bound of residuals of the least squares problem $\bar{\delta}$ and the upper limit of the experimental error $\bar{\varepsilon}$, the sufficiency of an experimental design for the δ-identifiability can be tested. This is done by solving the optimization problem:

$$\min_{\mathbf{p}\in Ad} \left\|\mathbf{F}(\mathbf{p})-\mathbf{Z}\right\|_{\mathrm{w}}^2 \tag{4.1}$$

subject to

$$\left\|\mathbf{p}-\mathbf{p}_0\right\|_{\mathbf{C}_p}^2 \geq 1$$

If the minimum of the problem is $\delta^2 \geq \left(\bar{\delta}+\bar{\varepsilon}\right)^2$, we can conclude that the experimental design is sufficient for the δ-interval identifiability when random noise ε is included in its observations [Sun and Yeh, 1990b]. An important problem that requires explanation is the determination of $\bar{\delta}$, the upper bound of residuals of the least squares problem (2.23). As a residual, $\left\|\mathbf{F}(\mathbf{p})-\mathbf{Z}\right\|_{\mathrm{w}}$ is always less than $\left\|\mathbf{F}(\mathbf{p}_0)-\mathbf{Z}\right\|_{\mathrm{w}}$ because $\mathbf{p}$ is the minimizer of the objective function $\left\|\mathbf{F}(\mathbf{p})-\mathbf{Z}\right\|_{\mathrm{w}}$ (since $\mathbf{p}_0=\mathbf{p}+\varepsilon$). Therefore a conservative estimate of $\bar{\delta}$ is $\bar{\delta}=\bar{\varepsilon}$. For the observation noise ε we only need to know the estimation of the upper bound of $\left\|\varepsilon\right\|_{\mathrm{w}}$, independent of its statistical distribution [Sun and Yeh, 1990b].

The concept of identifiability will be used later as the first step in the experimental design of two- and three-phase experiments.

4.1.2 Optimal Parameter Dimension

The identification of parameters in a distributed parameter system should, in principle, include the determination of both the parameter structure and its value. Shah et al. [1978] showed the relationship between the optimal dimension of parameterization and observations in considerable depth. The dimension of parameterization is directly related to the quantity and quality of data (observations). In practice, the number of observations is limited and observations are corrupted with noise. Without controlling parameter dimension, instability often occurs [Yakowitz and Duckstein, 1980]. If instability occurs in the inverse problem solution, parameters will become unreasonably small (sometimes negative, which is physically impossible) and/or large, if parameters are not constrained. In the constrained minimization, instability is characterized by the fact that during the solution process parameter values are bouncing back and forth between the upper and lower bounds [Liu, 1993; McLaughlin and Townley, 1996]. Reduction of parameter dimension or changing parameterization can make the inverse solution stable. When the number of parameters increase, the bias error (and modeling error) decrease while the variance error (or error in parameter uncertainty) increase. A

trade off of the two types of errors can then be made from which an optimum parameter dimension can be determined. Watson et al. [1988] used a regression based method where the number of parameters were increased and the variance error controlled.

4.1.3 Contribution of Observations

The interval identifiability allows an experimental design to guarantee the predetermined accuracy or resolution (given in $\mathbf{C}_P$) of the identified parameters. Obviously, if we limit ourselves only to the problem of parameter estimation, then we do not know how to design weighting matrix $\mathbf{C}_P$. The determination of $\mathbf{C}_P$ must depend upon other criterion, for instance, the consideration of the requirements of model applications [Sun and Yeh, 1990b].

When solving the inverse problem, the identified model parameters are generally allowed to be different from the true parameters within a certain range, provided that the required accuracy of model application is assured [Yeh and Sun, 1990]. Let η_j be the range, or resolution, of parameter p_j. The parameter is said to be interval identifiable if the identified value $\hat{\mathrm{p}}_j$ of the parameter satisfies

$$\left|\hat{\mathrm{p}}_j - \mathrm{p}_{0,j}\right| < \eta_j \tag{4.2}$$

where $\mathrm{p}_{0,j}$ is the true value of parameter p_j. The problem of whether a parameter p_j is interval identifiable for a given η_j depends upon the quantity and quality of observations.

To evaluate the data requirements of a system in connection with parameter identification, the concept of "contribution of observation F_i in the identification of parameter p_j", denoted CTB(F_i,p_j), is introduced by Yeh and Sun [1990]. The contribution of observation F_i to parameter p_j in the experimental design can be represented as

$$CTB(F_i,\mathrm{p}_j) = \frac{\eta_j}{\varepsilon_i}\left|\int_{(\Omega_j)} \frac{\partial F_i}{\partial \mathrm{p}_j} d\Omega\right| \tag{4.3}$$

where F_i is a component of model response vector $\mathbf{F}(\mathbf{p})$; p_j is a component of parameter vector $\mathbf{p}$, η_j is a given admissible error of the identified parameter p_j (or resolution), which can be seen as the element η_j of weighting matrix ($\mathbf{C}_P$); ε_i is the upper bound of observation noise associated with F_i; and $\partial F_i / \partial \mathrm{p}_j$ is the sensitivity coefficient of observation $\mathbf{F}$ with respect to parameter $\mathbf{p}$ and (Ω_j) is a region associated with parameter p_j.

Sun and Yeh [1990b] proved that a necessary condition for the interval identifiability is that there is at least one observation for each component for the unknown parameters whose contribution is larger than 1. See Sun and Yeh [1990b] for details.

4.1.4 Experimental Design Procedure

The concept of interval identifiability, contribution of observations and estimated confidence intervals give different criteria for evaluation of experimental designs. First, identifiability is addressed, then an experimental design is proposed with emphasize on three-phase flow.

To improve the identifiability of the parameters, different approaches can be investigated:

1. Increase η_j; implying a greater recognition of uncertainty in the identified parameter.
2. Decrease ε_i, implying raising the accuracy of observations.
3. Reduce the parameter dimension, i.e. reduce the flexibility of the B-splines functions.
4. Increase sensitivity coefficients, implying changing the experimental design.

However, the first three points are difficult to change since the accuracy of the observations are limited by the experimental apparatus and we do not want to compromise on the resolution of the parameters, or the flexibility of the flow functions. The fourth point indicates that changing the experimental design might give an improved identifiability.

The proposed experimental design for determination of multiphase flow functions concises of the following steps:

1. Select core and fluid properties. Select an initial relative permeability and capillary pressure function.
2. Select a way of conducting the experiments (steady state, unsteady state, centrifuge), select the type (low-rate, high-rate, multi-rate), location (in time and space), and give an estimate of the accuracy of the measured data, ε_i. Set a maximum resolution for each parameter; η_j.
3. Perform a sensitivity analysis:
    - Compute the contribution of observations (CTB).
    - Compute the confidence interval around the selected flow functions.
4. Evaluate each parameter with respect to the CTB to ensure that the parameters can be identifiable with the proposed design and that the flow functions can be estimated with acceptable accuracy (check confidence intervals in the saturation regions of interest). Otherwise, go to step 2 and reevaluate the experimental setup, data and accuracy.

This experimental design gives a *quantitative* measure of the identifiability of the different parameters and the accuracy of the estimated flow functions.

Three-phase experiments need special attention. Due to the increased complexity in three-phase flow compared to two-phase flow, the number of data sets necessary for an accurate estimation of the flow functions has increased considerably. Since the three-phase flow functions must be flexible, a considerably higher number of parameters must be determined compared to the two-phase case. The proposed three-phase experimental design comprises the following extra items:

1. Determine or limit the three-phase saturation region where the three-phase flow properties must be accurate determined.
2. Evaluate how many experiments, different data types and accuracy of the data that is necessary for identifiability of the parameters and to obtain the requested accuracy in estimated flow functions.

4.2 Design of Two-Phase Flow Experiments

In this section various experimental designs for determination of two-phase flow properties from experimental data will be proposed. The various designs are discussed with respect to the information content in the data for accurate determination of the flow functions.

4.2.1 Experimental Design

As described in an earlier section, identifiability of parameters can be investigated in various experimental designs before any experiment is conducted. In Paper III different experimental designs were discussed for the purpose of estimating oil and water relative permeability and capillary pressure functions simultaneously. Finding the "best" injection scheme in the experimental design was addressed. Three scenarios were discussed; one, two, and six steady state oil injection steps. In Paper VI we also included new data when estimating two-phase flow functions. Here the water saturation profiles using nuclear magnetic resonance imaging (MRI) were measured and the additional data included for estimation.

In Paper III the results show that the last scenario with six injection steps gives lowest confidence intervals on the estimated relative permeability and capillary pressure functions, i.e., these data contain most information on the flow functions. This observation is also supported by the results from computation of the contribution of observations ($CTB(F_i, \mathrm{p}_j)$ presented in section 4.1.3). Using interval identifiability, it can be shown that only the last scenario (with six injection steps) is capable of identifying the parameters. In this analysis an admissible error (or resolution) of 2.5% of the true value of each parameter is used (η_j), and an upper bound of observation noise of 1% of the observations is used ($\bar{\varepsilon}_i$).

Figure 4.1 shows the data discussed in design A1 and A3 in Paper III. Figures 4.2-4.4 show the contribution of pressure drop data on water and oil relative permeability and

capillary pressure parameters. Part a) in these figures shows the results on pressure drop data from experimental design A1 where only one injection step has been used. Here, all the contributions are below 1. This means that the computed observations $\mathbf{F}(\mathbf{u},\mathbf{p})$ are unable to differentiate two parameters within the given resolution η_j and accuracy $\bar{\varepsilon}_i$ on the observations. Part b) in these figures shows that the last experimental design, A3

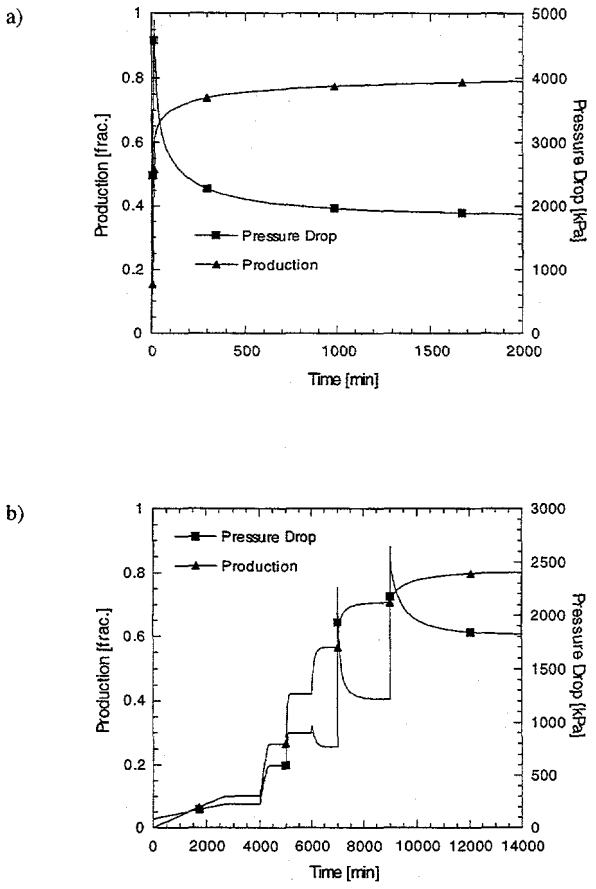

Figure 4.1 Pressure and production data for a) experimental design A1, and b) experimental design A3 (figure from Paper III).

(with six injection steps) gives data where $CTB(F_i, \mathrm{p}_j) > 1$ for most of the parameters. Hence, the parameters are identifiable with the current experimental design, resolution and measurement error. This is also the conclusion after the confidence intervals are computed. The confidence intervals in Figure 4.5 (Figure 3 from Paper III) are narrow in a large saturation range for experimental design A3.

a)

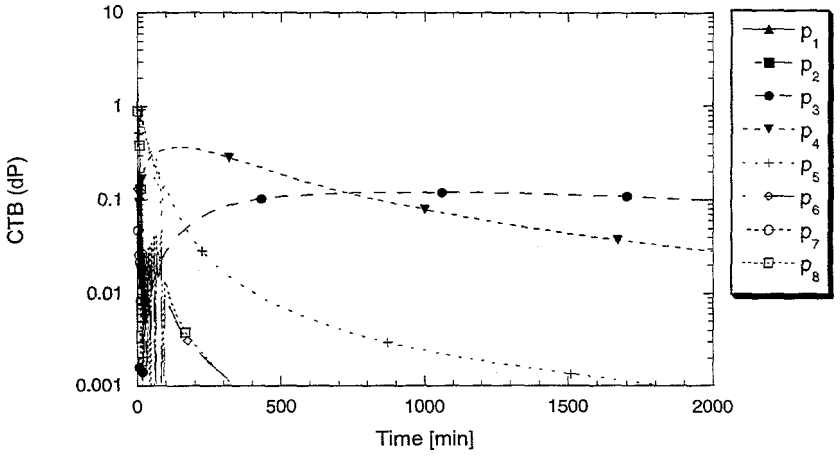

b)

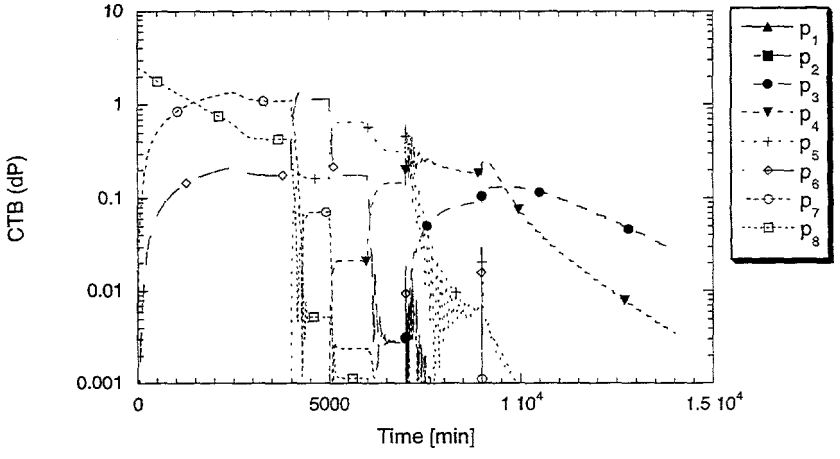

Figure 4.2 Contribution of observations (ΔP) versus time for water relative permeability parameters in a) design A1 and b) design A3 (both cases described in Paper III).

a)

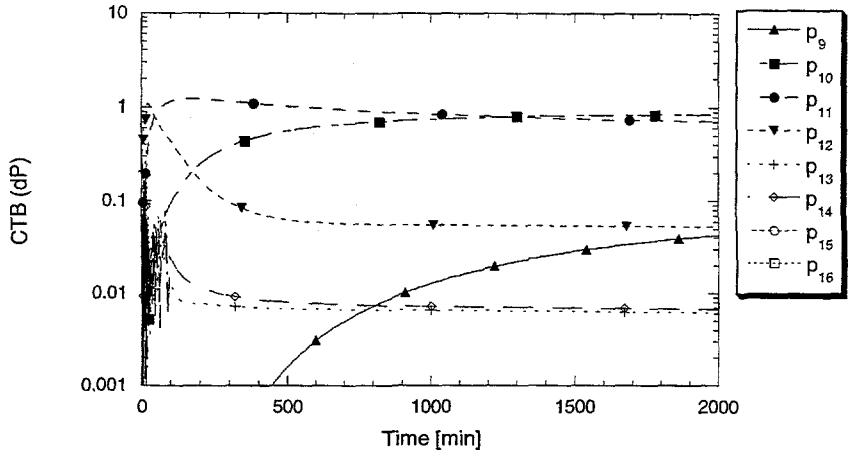

b)

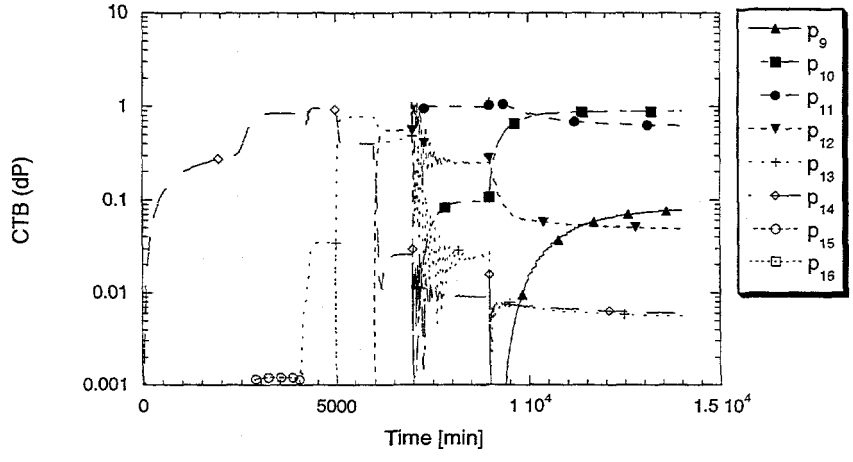

Figure 4.3 Contribution of observations (ΔP) versus time for oil relative permeability parameters in a) design A1 and b) design A3 (both cases described in Paper III).

a)

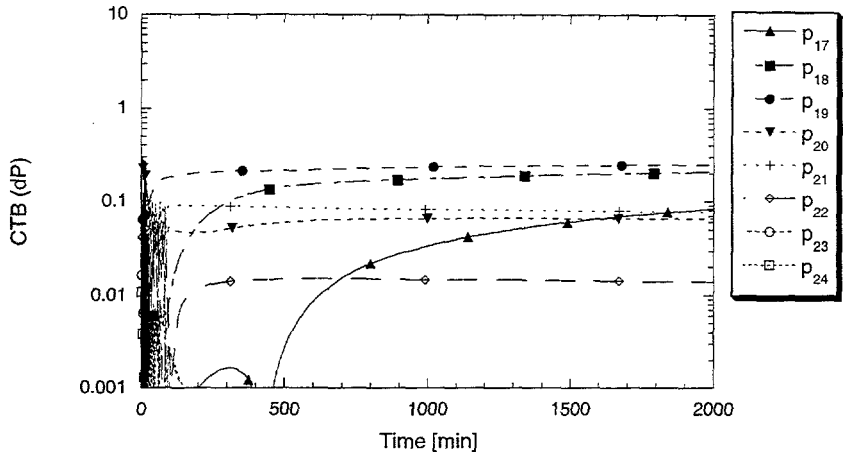

b)

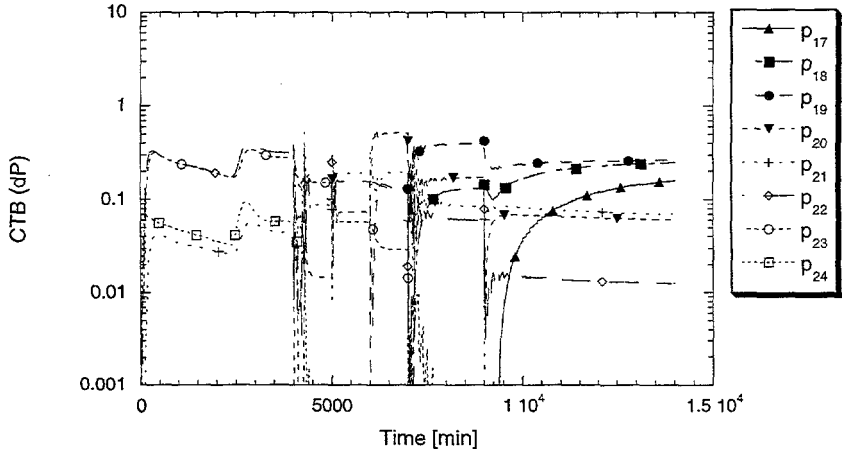

Figure 4.4 Contribution of observations (ΔP) versus time for capillary pressure parameters in a) design A1 and b) design A3 (both cases described in Paper III).

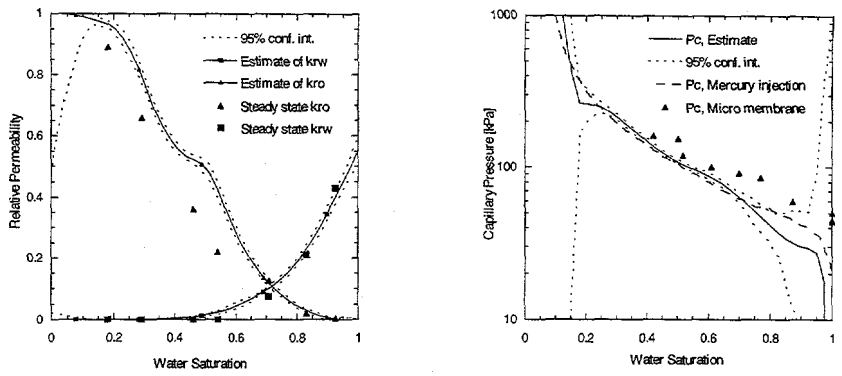

Figure 4.5 Estimated two-phase relative permeability and capillary pressure functions with 95% confidence intervals (figure from Paper III).

Now consider parameter 8 in detail. In Figure 4.2 the contribution of pressure drop data on the water relative permeability parameters is considered. In Figure 4.2b is $CTB(\Delta P, \mathrm{p}_8) > 1$ which means that this parameter can be identified with the given accuracy in data, ε_i, and with the resolution in the parameters, η_j. Here, parameter 8 (the last parameter in the representation of water relative permeability, see Table 4.1) has support for $S_w = [0.85, 1.0]$, and the contribution of observations for this parameter will of course be highest in the beginning of the experiment since this parameter has support in the saturation region that first is introduced to the oil injected. $CTB(\Delta P, \mathrm{p}_j) < 1$ for the rest of the parameters in figure 4.2a, i.e., $|\mathrm{p}_j^1 - \mathrm{p}_j^2| > \eta_j$ for the rest of the parameters, hence the experimental design is not sufficient for identifiability of the parameters. Experimental design A3 is then considered. In this design pressure drop and production data from a multi-step oil injection are analyzed. The new design gives $CTB(\Delta P, \mathbf{p}) > 1$ for several parameters, see Figure 4.2b. The situation is the same for the oil relative permeability parameters in Figure 4.3b. From the values of the CTB for water and oil relative permeability, most of these parameters were identified for a multi-step injection design.

Table 4.1 Parameters and location of knots for two-phase experimental designs (A1 and A3).

p (k_{rw})	0.0	0.1e-6	0.5e-3	0.5e-2	0.5e-1	0.15	0.35	1.0
p (k_{ro})	1.0	1.0	0.55	0.3	0.15	0.5e-1	0.1e-4	0.0
p (P_c)	5.0e+3	9.0e+2	4.5e+2	3.5e+2	3.0e+2	2.7e+2	2.5e+2	2.0e+2

a)

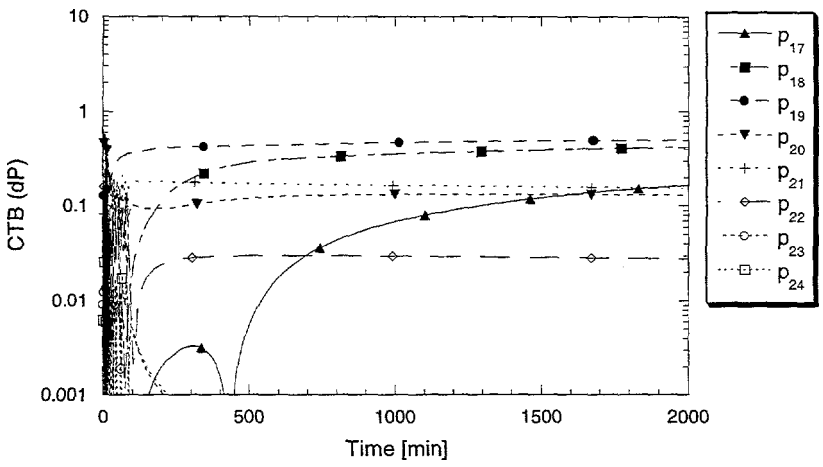

b)

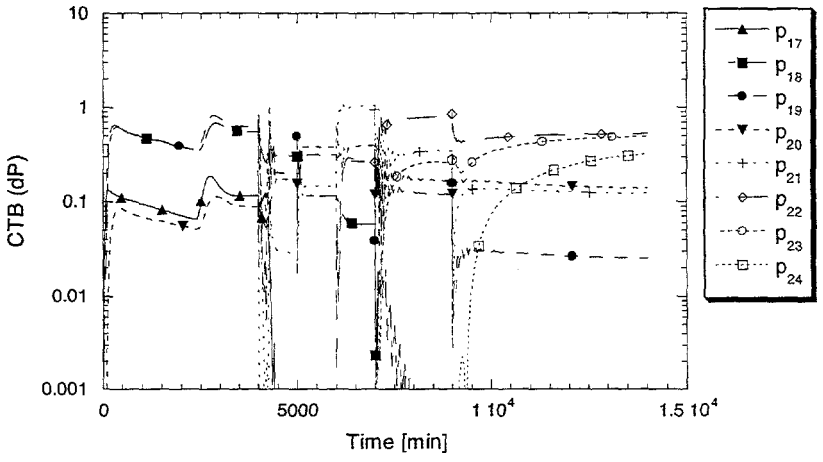

Figure 4.6 Contribution of observations (ΔP) versus time for capillary pressure parameters in a) design A1 and b) design A3 (both cases described in Paper III) with increased resolution on the parameters (η_j=5%).

Figure 4.3b) clearly illustrates that the different parameters that have support (see discussion on support of parameters in Paper II) in different saturation regions, will be identified by the data at different times. To identify parameter p_{14}, the pressure drop data in the time interval $t \in [0,6000]$ is necessary, and parameter p_{11} can be identified by pressure drop data in the time interval $t \in [7000,10000]$. Only parameter p_{10}, p_{11}, p_{12} can be identified by the pressure drop data in design A1, see Figure 4.3a), i.e., the parameters with support for $S_w = [0,0.5]$, which is the saturations at the end of the experiment (just before and after breakthrough).

The capillary pressure data in the first design is unable to identify the parameters with η_j equal to 2.5% of the true parameter values, see Figure 4.4a). The result is the same for the multi-step design, however, the CTB is higher for the last design, see Figure 4.4b). Figure 4.6 shows the CTB-results when the accepted resolution of the capillary pressure parameters are increased to 5%. Some of the parameters can then be identified in the multi-rate experiment, while the identifiability still is too low when data from the single-rate injection (A1) are used.

These results coincide with the results from Paper III. In Paper III a very good agreement between experimental and predicted pressure drop and production data is obtained. The values of the SSR for pressure drop and production data are in agreement with the estimated standard deviation for these data (here are the estimates of measurement errors based on analysis of experimental equipment) and a further reduction of the SSR will not likely be obtained. Still, the number of runs is below the expected value due to some bias error for some saturation intervals. This is the first time experimental data have been reconciled and that the SSR meets the statistical criteria. The corresponding confidence intervals are quite narrow for most of the saturation interval, see Figure 4.5. Since the sensitivity matrix is computed and used in both the computations of CTB and confidence intervals, we see the same results with respect to choice of experimental design in the confidence intervals and CTB. The parameters that were identifiable within the resolution of η_j have been found with high accuracy. The capillary pressure parameters were identified within higher resolution than the relative permeabilities, and the accuracy of the estimated capillary pressure functions is lower than for the other functions, see Figure 4.5.

Another approach to improve the accuracy of estimates is to measure data that contain additional information. In Paper VI the use of MRI for observing fluid saturation within the core sample and the use of those data in estimation of flow properties are demonstrated. An excellent match of pressure drop, production and the saturation profiles were obtained, except for low water saturations for the water saturation profiles. This may be due to the relative small number of data in this area. However, the confidence intervals are larger than desired and this suggests that the preferred experimental design may be to use a multi step injection scheme and *in situ* saturation measurements for estimation of two-phase flow properties.

4.3 Design of Three-Phase Flow Experiments

The three-phase flow properties concise of the three-phase relative permeability and capillary pressure. Here the capillary pressures for water-oil and gas-oil are treated as in two-phase flow, i.e., $P_{c,ow} = P_{c,ow}(S_w)$ and $P_{c,og} = P_{c,og}(S_g)$. In this section, the design of three-phase flow experiments is proposed, the method for estimation of the multiphase flow properties is derived and the proposed method is applied on two- and three-phase experimental data. Next, details concerning the sensitivity coefficients and their impact on "false" sensitivity, support, identifiability, pressure drop and production data and confidence intervals are discussed.

4.3.1 Design, Method and Results

There is a huge variety of ways of performing experiments leading to three-phase relative permeability estimates. For example, one may inject one, two, or three phases simultaneously into a core sample, or conduct some constant pressure drop experiments. Obviously, it is desirable to keep the number of experiments needed for three-phase relative permeability determination as low as possible, yet the accuracy with which these functions are determined as high as possible. In Paper I a systematic approach for designing the three-phase experiments leading to accurate determination of the three-phase relative permeability functions has been presented. This procedure is based on the results from the linearized covariance analysis described in section 2.3.1 and the proposed procedure in section 4.1.4. In Paper I, the accuracy with which the relative permeability functions may be determined from six different experimental designs have been investigated. The cases considered are:

- Ia and Ib: Determination of oil and water relative permeability functions using differential pressure and production data from one three-phase experiment (Ia corresponds to a steady state and Ib to an unsteady state fluid injection).
- IIa and IIb: Determination of water, oil and gas relative permeability functions using differential pressure and production data from two three-phase experiments.
- IIIa and IIIb: Determination of water, oil and gas relative permeability functions using differential pressure and production data from two three-phase experiments and one two-phase gas injection.

An overall observation is that the relative permeabilities are well determined in saturation regions corresponding to regions represented in the data even for a limited number of data. The accuracy of the estimated flow functions is highest when the steady-state type data are used in estimation, i.e. for the cases Ia, IIa and IIIa described above.

After this first analysis of a possible experimental design, the methodology was further developed in Paper II. The different parameters in the flow function representation has support for a limited saturation region, and this characteristic of the functional representation is used to design the experiments so that they produce data in saturation regions where the unknown flow function parameters have support. In this paper, a synthetic case with pressure and production data from a two-phase experiment and a

three-phase experiment was analyzed. Three-phase relative permeabilities were estimated from the synthetic data and the accuracy of these estimates was computed. The results of the estimation were investigated by examination of the final sum of squared residuals (*SSR*) and the number of runs. The results were that when a flexible functional representation of the flow functions was used, the three three-phase relative permeability functions were accurately estimated in the saturation region corresponding to the experimental data. Hence, the experimental design proposed in Paper I was confirmed to give accurate estimates of the flow functions in the region of interest. Next, the proposed experimental design and interpretation method was used on experimental data. Pressure drop and production data from one two-phase oil-water experiment and one oil-gas-water experiment were used to determine the three-phase relative permeability functions and two-phase oil-water and oil-gas capillary pressure functions. This was the first time, to the best of the authors knowledge, that three-phase flow functions have been estimated from experimental data and that two- and three-phase data have been simultaneously reconciled by simulations.

In Paper IV, the analysis of experimental data has been further developed. In this paper, the experimental apparatus constructed for two- and three-phase displacement experiments at reservoir conditions is presented. Then three-phase relative permeability functions and two-phase oil-water and oil-gas capillary pressure functions have been estimated simultaneously from pressure drop and production data from two three-phase experiments and one two-phase experiment. The predictive model by Stone has also been investigated. The three-phase relative permeabilities have been calculated with that method using the estimated two-phase relative permeabilities as input. Then the Stone three-phase relative permeabilities have been used to simulate the three-phase pressure drop and production data, and the results were compared with the experimental data. The results showed that the Stone predictive model overpredicted the oil production and the pressure drop, as described by Baker [1988].

4.3.2 Sensitivity Coefficients

In this section, the impact of the sensitivity coefficients on "false" sensitivity, support, identifiability, pressure drop and production data and confidence intervals will be discussed.

The background chapter shows that both the estimation of parameters and assessing accuracy of the estimated functions depend on the sensitivity coefficients. In Paper V, the sensitivity coefficients are computed both analytically and numerically. The impact of error in the numerical sensitivity coefficients on parameter estimation and accuracy computations will now be illustrated. The proposed three-phase experimental design from Paper I has been further developed in Paper V.

Due to the complexity in three-phase flow where the relative permeabilities are allowed to be functions of two saturations, each parameter to be estimated will have support in a limited area. The oil relative permeability function is given as

$$k_{ro}(S_w, S_g) = \sum_{i=1}^{m_w+K_w} \sum_{j=1}^{m_g+K_g} c_{ij} B_{w,i}^{m_w} B_{g,j}^{m_g}(S_w, \mathbf{y}_w, S_g, \mathbf{y}_g)$$

where e.g. coefficient c_{12} correspond to region 1 and 2 in Figure 4.7a) (from Paper V). To estimate this parameter, we need experimental data for water saturation $S_w \in [0,0.2]$ and oil saturation $S_o \in [0,0.3]$. The bold line in the two-phase region from $(S_w, S_g) = (0,0)$ to $(S_w, S_g) = (0.8,0.0)$ and into the three-phase region $(S_w, S_g) = (0.2,0.6)$ shows the saturation trajectory for the single three-phase experimental case studied in Paper V. As discussed in this paper, coefficient c_{12} can not be estimated from these data since there are almost no experimental data in this region. However, the numerical sensitivity coefficient showed some unrealistic high values due to numerical differentiation and the concept of "false" sensitivity was introduced, see Figure 4.8 (Figure 8a from Paper V). Another parameter, c_{22}, has support in a larger saturation region $S_w \times S_o = [0,0.4] \times [0,0.3]$ corresponding to area 1-4 in Figure 4.7a. This parameter can be estimated from the experimental data, i.e. from data after t=2500 min (see Figure 4.8b). Hence, the identifiability of the parameters differs depending on the way the sensitivity coefficients are computed since the identifiability is proportional to the sensitivity coefficients. The numerical sensitivity coefficients tend to overestimate the sensitivity coefficients, especially for parameters with support in regions with low sensitivity, see Figure 4.8a) and discussion in section 3.5. Numerical sensitivity coefficients become huge and indicate a sensitive region, but there are no data in this region. As a result, the contribution of observations for these parameters will be larger using numerical sensitivity coefficients than analytical sensitivity coefficients and it can look like they are identifiable with the current experimental design. This "false" sensitivity leads to a decrease in the convergency rate in the parameter estimation since the gradient step is computed from erroneous sensitivity coefficients.

The identifiability of parameters in the three-phase case is considerable more difficult than for the two-phase case. The sensitivity coefficients will generally be lower since the number of parameter increase, i.e., we will need more data. The measurement error will be the same but this requires a highly advanced three-phase apparatus, as described by Ebeltoft et al. [1998]. The resolution of the parameters is the same. Figure 4.9 shows the CTB of pressure drop and production data for parameter c_{52} using both analytical and numerical sensitivity coefficients. Parameter c_{52} has support for $S_w \times S_o = [0.4,1.0] \times [0.0,0.3]$, i.e., area 5-8 in Figure 4.7a). This parameter has support in an area that covers most of the area where we have high degree of information in the data, hence the sensitivity coefficients for this parameter will be large for all the data points. With a resolution of 5% on the parameter ($c_{52} = 0.005 \pm 0.00025$), an upper bound of 1% on the pressure drop data and 1% error in the production data (but a minimum of 0.001 PV), the contribution of observations (CTB) for pressure drop and oil production data are given in Figure 4.9.

a)

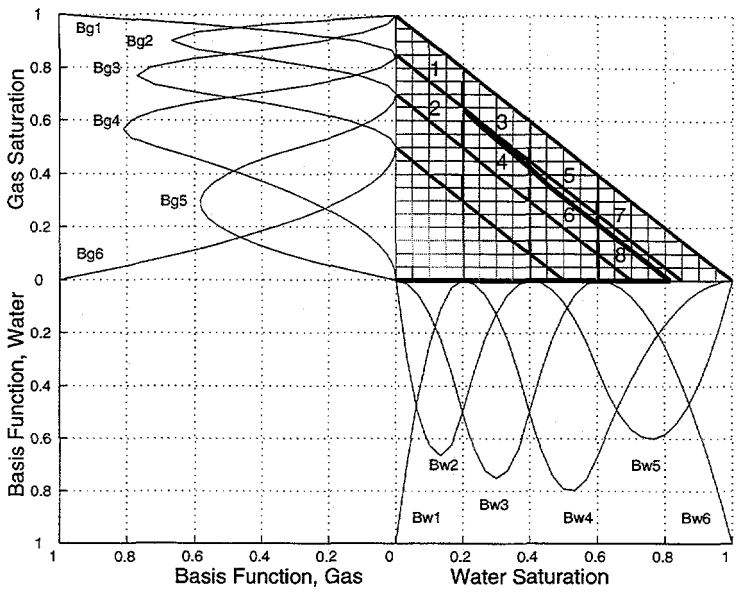

b)

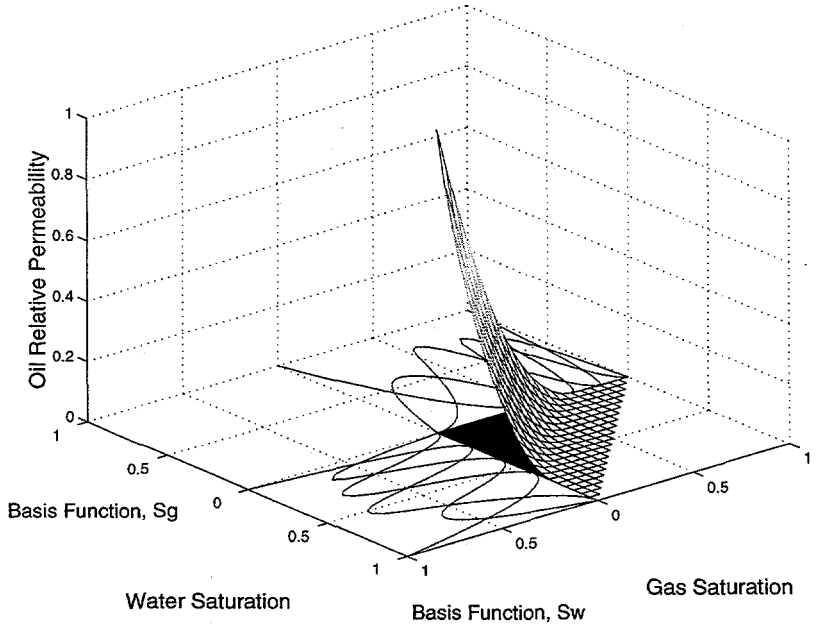

Figure 4.7 a) Three-phase oil relative permeability seen from above. The water and gas B-splines basis functions are also plotted. The saturation trajectory corresponding to a three-phase experiment is also plotted (bold line), b) Three-phase oil relative permeability in 3D.

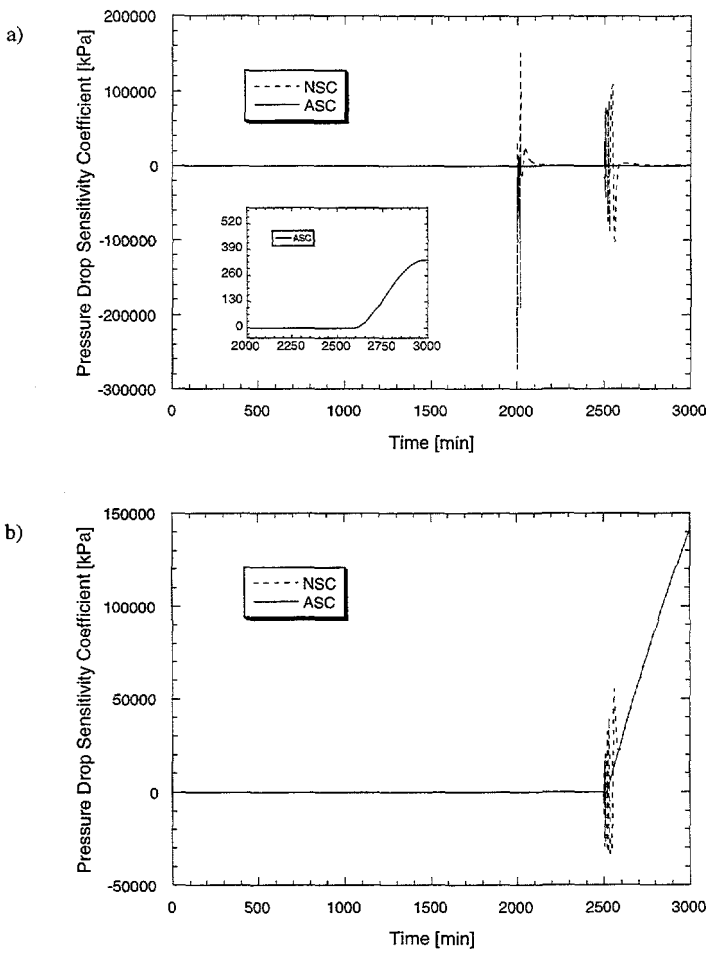

Figure 4.8 a) Sensitivity coefficient for parameter c_{12}, illustrating "false" sensitivity in low sensitivity regions, and b) Sensitivity coefficient for parameter c_{22}, illustrating oscillation in numerical sensitivity coefficients (figure from Paper V).

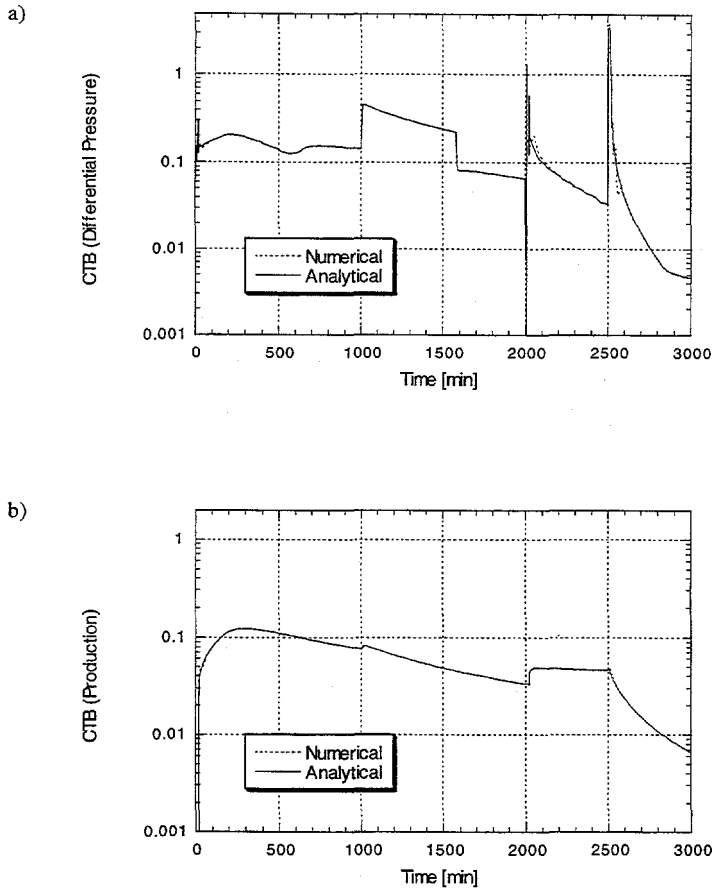

Figure 4.9 a) Contribution of pressure drop data on parameter c_{52}, and b) contribution of production data on parameter c_{52} using analytical and numerical sensitivity coefficients (figure from Paper V).

This analysis shows the importance of accurate computations of the sensitivity coefficients since these are the key element when estimating parameters and assessing accuracy of the estimates. Further, an experimental design must be conducted before the experiment to evaluate the information content in the data which is going to be used later for estimation of flow function parameters. This analysis shows that the information content in the pressure drop data is higher than the production data, see Figure 4.9. Actually, we will not be able to identify the parameter discussed (c_{52}) using production data with the given experimental design, error and resolution on the parameter as given above (CTB<1 in Figure 4.9b)). Only the pressure drop data in the last two injection steps will be necessary for identifying this parameter, Figure 4.9a).

The confidence intervals have been computed for the oil relative permeability using both numerical and analytical sensitivity coefficients and data from one three-phase

trajectory. The difference between these two surfaces is plotted in Figure 4.10. This figure shows that the confidence intervals are narrow along the saturation path corresponding to the experimental data trajectory (actually, they are both low and the difference between them is low). However, the confidence intervals computed using numerical sensitivity coefficients are smaller than the confidence interval computed using analytical sensitivity coefficients. Hence, for the low sensitivity region (outside the experimental trajectory) the difference is huge due to the "false" sensitivity in the numerical sensitivity coefficient.

This analysis of contribution of observations and the analysis of confidence intervals in Paper V show that parameters with support in those saturation regions with high quality data can be estimated with an acceptable accuracy. However, when solving the inverse problems we are dependent on accurate sensitivity coefficients and for several cases, numerically sensitivity coefficients introduce "false" sensitivity and then slow down the convergency rate in the estimation procedure. This "false" sensitivity also results in narrow confidence intervals, indicating that the information content in the data is higher than it really is.

As discussed in chapter two, the non-linearity in the model is inverse proportional with the sensitivity [Liu, 1993]. Therefore, the proposed experimental design with analytical sensitivity coefficients will give a low degree of non-linearity for several parameters characterizing the three-phase flow functions. Hence, the assumption that the model is linear close to the global minimum can actually be tested.

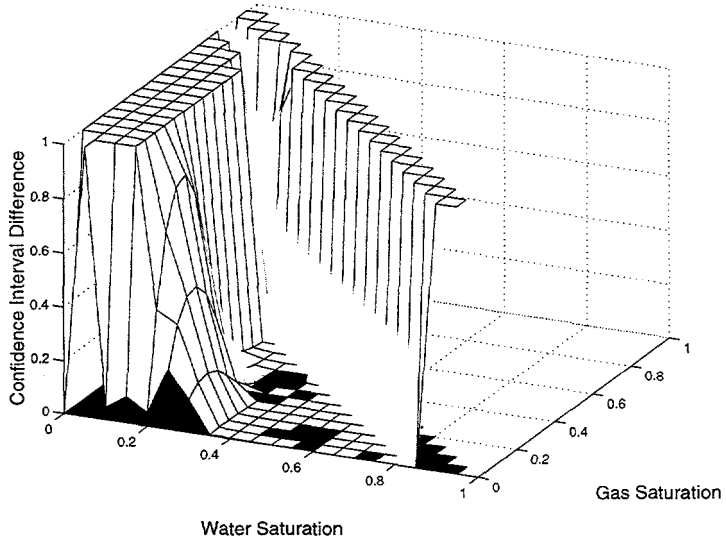

Figure 4.10 Difference between upper confidence intervals (for three-phase oil relative permeability) computed from analytical and numerical sensitivity coefficients (figure from Paper V).

As shown in chapter two, the non-linearity decreases with increasing sensitivity. McLaughlin et al. [1996] discussed the stability problems in parameter estimation around minimum with low sensitivity, generally a ill-posed problem. For the case considered here, the stability of the estimation can be illustrated by the number of iterations necessary to find the minimum. Due to the "false" sensitivity introduced by numerical sensitivity coefficients, the parameter estimation is considerably more difficult and time consuming than in the case when analytical sensitivity coefficients were applied, see Figure 4.11. In this figure the number of iterations in a parameter estimation is compared when the perturbation and direct method are used for sensitivity coefficient computations. As seen, the analytical sensitivity coefficients give a faster solution to the problem.

a)

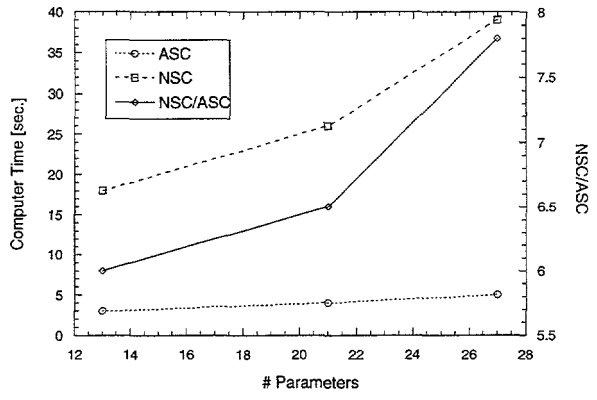

b)

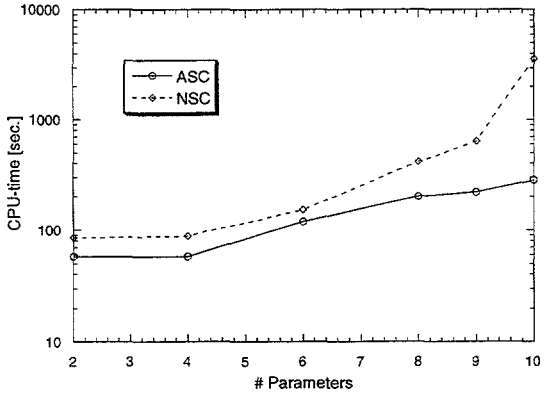

c)

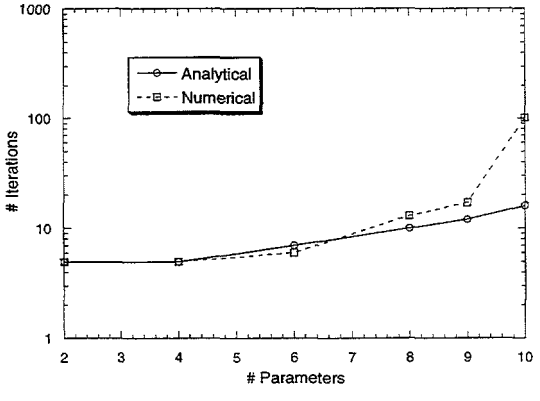

Figure 4.11 a) Number of parameters vs. CPU-time in direct computation of sensitivity matrix in Case 1, b) Number of parameters vs. CPU time, and c) Number of parameters vs. number of iterations after estimation of oil relative permeability surface in Case 2.

4.4 Conclusions

The direct method for computing sensitivity coefficients has been implemented for simulation of two- and three-phase flow (Paper V). This method is superior when the Newton-Raphson method is used for solving the simulator equation. The problem with choosing perturbations in the perturbation method is now avoided since the sensitivity coefficients are computed analytically after a discretization scheme is chosen. The direct method gives accurate sensitivity coefficients and the problem with "false" sensitivity in regions with low or no sensitivity is eliminated. The computational savings using the direct method is demonstrated and proves to be huge. The methodology for estimating three-phase flow functions has been further developed in Paper V since the concept of contribution of observations has been implemented for determination of the identifiability of the parameters.

The proposed experimental design for both two- and three-phase flow make it possible to evaluate several experiments with respect to a predefined accuracy (or resolution) on the parameters, identifiability, accuracy of estimated flow functions, different experimental scenarios, sensitivity of parameters, and non-linearity of the model. Therefore, a careful experimental design is essential for determination of the three-phase flow functions. Accurate sensitivity coefficients are essential for the experimental design procedure. Hence, the development of analytical sensitivity coefficients was necessary for the development and reliability of the experimental design procedure.

We have developed, tested and verified on synthetic data (Paper I and Paper II) that with a suitable experimental design, three-phase flow functions can be estimated simultaneously with high accuracy in saturation regions where we have high quality data.

For the first time, simultaneous reconciliation of two- and three-phase displacement experiment data has been presented (Paper IV). These multiple sets of experimental data have been interpreted for estimation of three-phase relative permeability and capillary pressure functions.

It has been shown (in Paper III), that accurate and simultaneous estimates of two-phase relative permeability and capillary pressure functions can be achieved using the inverse approach. Experimental data have been reconciled by simulations and the solution satisfies the statistical criteria, hence the solution is within the estimated standard deviation in the data. An analysis of the identifiability of the parameters in this work shows that the parameters are identifiable when a multi-rate injection scheme has been applied. In Paper VI also *in situ* saturation profiles are reconciled by simulation. However, since a one-step injection scheme has been used in the experiment, the accuracy of the estimates is not satisfactory in the entire saturation interval. Therefore, the proposed experimental design for two-phase flow experiments is to use a multi-step injection scheme. The accuracy of the estimates will be further increased if *in situ* saturation profile data are measured.

5 Future Work

5.1 Two-Phase Flow

This work shows that two-phase experimental data (pressure drop and production) have been reconciled within the statistical criteria for a solution, Paper III. In Paper VI also *in situ* saturation profiles have been reconciled. However, there are still some issues in two-phase flow that should be investigated in more detail.

First, hysteresis has not been addressed in this work. Two-phase experiments including hysteresis loops can be performed and each experiment can be interpreted go get the envelope curve and scanning curves directly. However, in the future, a model including only a few extra parameters should be developed (or existing models can be tested) and verified experimentally so that the relative permeability and capillary pressure envelope and scanning curves can be estimated simultaneously.

Second, the experimental design procedure can be extended to include experimental cost. Today, the two-phase steady-state-type experimental data are quite costly to measure. Therefore, the future experimental design research work should emphasize on reducing the cost without compromising the accuracy of the two-phase flow functions in specific saturation intervals. The experimental procedure should consider the following steps:

Decide the saturation interval where accurate relative permeability and/or capillary pressure must be achieved. For this interval:

- Consider cost and time for steady state, unsteady state and centrifuge experiments.
- Consider cost and time for pressure drop, production, *in situ* saturation and pressure data.
- Consider single rate or multi-rate injection scheme and different injection rates.

A full investigation of all possible experimental designs as presented above is a huge project, but it will provide general guidelines for how two-phase experiments can be conducted to achieve quality data for determination of the flow properties in a specific saturation interval.

5.2 Three-Phase Flow

A major problem regarding three-phase model studies is the shortness on good quality experimental data. A limited number of three-phase data sets have been published during the last 50 years. Several of the data sets are supplied with insufficient information about saturation history and rock and fluid properties and the analysis of experimental three-phase data has often been based on several simplifications such as neglecting capillary pressure, uniform saturation profiles and incompressible fluids. Therefore, high quality three-phase experiments should be performed where the flow processes are controlled. The experiments should include *in situ* saturation for verification of the three-phase model and for controlling the saturation paths in three-phase flow.

Next, hysteresis in relative permeability and capillary pressure functions has not been investigated in this work. When hysteresis is included, the relative permeabilities will also be dependent on the saturation history in the experiment. Several models for three-phase hysteresis have been proposed over the years [Land 1966; Killough, 1976; Carlson, 1981; Eikje et al., 1992; Skauge et al., 1994], but these models consider the relative permeability and capillary pressure to be dependent on only one saturation. Therefore, a proposed strategy for determination of hysteresis in three-phase flow functions is to further develop the inverse approach where the flow functions are represented as functions of two independent saturations. With a hysteresis model including the concept of envelope curves and scanning curves from the two-phase models, then relative permeability and capillary pressure in thre-phase flow will truly depend on the saturation history. However, development of such a model must be followed by analysis of three-phase experimental data to include the hysteresis effects obtained there.

The cost and complexity of three-phase experiments are considerable and the pitfalls are many. This is the reason for lacking three-phase experimental data today. Therefore, when high quality three-phase data are available, existing and new three-phase predictive models can be tested and developed. The set of three-phase experimental data interpreted in this work can be used to verify several predictive models. The Stone [1970] model was analyzed in this work, but several others discussed in Baker's [1988] work can be analyzed with respect to their ability to reconcile the three-phase experimental data. Ultimately, predictive three-phase flow models based on accurate two-phase data will be preferable due to the high cost, difficulties and time associated with three-phase flow experiments.

Nomenclature

$\mathbf{A}$	Sensitivity matrix
B/b	Volume factor
B	B-splines basis function
$\mathbf{C}$	Covariance matrix of flow functions
$\mathbf{C}_P$	Initial estimate of covariance matrix of estimated parameters
c	B-splines coefficient
$\mathbf{D}$	Sensitivity of flow functions with respect to model parameters
$\mathbf{d}$	Direction towards the minimum of problem
$\mathbf{F}$	Model response
$\mathbf{F}$	Vector function at time step $n+1$
$\mathbf{f}$	Vector of flow functions
$\mathbf{G}$	Constrain matrix
$\mathbf{G}$	Vector function at time step n
G	Gravity head
$\mathbf{g}$	Gravity acceleration vector
g	General function
$\mathbf{H}$	Hessian matrix
$\mathbf{h}$	Arbitrary nonzero vector in the parameter space
$\mathbf{J}$	Jacobian matrix
J	Performance criteria
K	Curvature
$[k]$	Permeability tensor
k_r	Relative permeability
N_{ij}	Tensor-products B-splines basis function
N_m	Number of observations
N_p	Number of parameters
N_q	Number of flow functions
N_x	Number of grid blocks in x-direction
$\mathbf{n}$	Normal vector
$\mathbf{P}$	Covariance matrix of parameter estimates
P_c	Capillary pressure
P_{well}	Well pressure
$\mathbf{p}$	Vector of parameters
$\hat{\mathbf{p}}$	Estimated parameter vector
$\mathbf{p}_0$	True parameter vector
p	Pressure
Q	Volumetric flow rate
q	Injection rate, rate term
$\mathbf{R}$	Vector function
R_s	Solution gas/oil ratio
S	Saturation
T	Transmissibility
t	Time
$\mathbf{u}$	Vector of state variables
$\boldsymbol{u}$	Fluid velocity, Darcy velocity
V	Volume of produced fluids

$\mathbf{V}$	Covariance matrix
V_b	Volume of grid block
$\mathbf{W}$	Weighted matrix of measurement error
x	X-direction
$\mathbf{y}$	B-splines partition
$\mathbf{Z}$	Observations
z	Z-direction

Greek letters

α	Level of confidence interval
β	Regularization index
Δ	Convergence criterion
δ	Accepted resolution of parameters
ε	Convergency criteria
ε_i	Upper bound of observation noise
ε_Z	Random error in observations
ε_P	Random error in parameters
ϕ	Adjoint state variable vector
Γ	Boundary
γ	Gravity term
η_h	Curve on surface S in the direction of **h**
η	Admissible error of the identified parameter vector
λ	Non-negative scalar
φ	Porosity
μ	Fluid viscosity
ρ	Density
Σ	Covariance of measurement errors
σ	Measurement error
τ	Parameter error

Subscripts

f	Phase
g	Gas
i	Block index
k	Iteration index
nw	Non-wetting phase
o	Oil
og	Oil and gas
ow	Oil and water
RC	Reservoir conditions
SC	Standard conditions
w	Water, wetting phase

Superscript

f	Phase
k	Iteration index
m	B-splines order
n	Time index, normal
t	Tangential

References

Anterion, F., Eymard, R., Karcher, B.: "Use of Parameter Gradients for Reservoir History Matching," in Proceedings of the SPE Symposium on Reservoir Simulation, Houston, TX, Feb. 6-8, 1989, pp. 339-354.

Aziz, K., Settari, A.: *Petroleum Reservoir Simulation*, Elsevier Applied Science Publishers Ltd., London, 1979.

Baker, L.E.: "Three-Phase Relative Permeability Correlations," in Proceedings of the SPE/DOE Enhanced Oil Recovery Symposium, Tulsa, Oklahoma, April 17-20, 1988, pp. 539-554.

Bard, Y.: *Nonlinear Parameter Estimation*, Academic, San Diego, Calif., 1974.

Bates, D.M., Watts, D.G.: "Relative Curvature Measures of Nonlinearity," *J. R. Statist. Soc.*, Vol. 42, No. 1, 1980, pp. 1-25.

Buckley, S.E., and Leverett, M.C.: "Mechanism of Fluid Displacement in Sands," *Trans. AIME*, 146, 1942, pp. 107.

Carlson, F.M.: "Simulation of Relative Permeability Hysteresis to the Nonwetting Phase," in Proceedings of the 56th Annual Fall Technical Conference and Exhibition of the Society of Petroleum Engineers of Aime, San Antonio, Texas, October 5-7, 1981, pp. 1-10.

Carrera, J., Neuman, S.P.: "Estimation of Aquifer Parameters Under Transient and Steady State Conditions: 1. Maximum Likelihood Method Incorporating Prior Information," *Water Resour. Res.*, Vol. 22, No. 2, 1986a, pp. 199-210.

Carrera, J., Neuman, S.P.: "Estimation of Aquifer Parameters Under Transient and Steady State Conditions: 2. Uniqueness, Stability, and Solution Algorithms," *Water Resour. Res.*, Vol. 22, No. 2, 1986b, pp. 211-227.

Chavent, G., Dupuy, M., Lemonnier, P.: "History matching by use of optimal control theory," *SPE Journal*, Feb. 1975, pp. 74-86.

Chen, S., Qin, F., Kim, K.-H., Watson, A.T.: "NMR Imaging of Flow in Porous Media," *AIChE J.*, Vol. 39, 1993, pp. 925.

Chen, S., Qin, F., Watson, A.T.: "Determination of Fluid Saturations During Multiphase Flow Experiments Using NMR Imaging Techniques," *AIChE J.*, Vol. 40, 1994, pp. 1238.

Corey, A.T., Rathjens, C.H., Henderson, J.H., Wyllie, M.R.: "Three-Phase Relative Permeability," *Petroleum Transactions Aime*, Vol. 207, 1956, pp. 349-351.

Darcy, H.: "Les fontaines publiques de la ville de Dijon," Dalmont, Paris, 1856.

Dogru, A.H., Seinfeld, J.H.: "Comparison of Sensitivity Coefficient Calculation Methods in Automatic History Matching," *SPE Journal*, 1981, pp. 551-558.

Dougherty, E.R.: *Probability and Statistics for the Engineering, Computing and Physical Science*, Prentice-Hall Inc., USA, 1990.

Dullien, F.A.L.: *Porous Media, Fluid Transport and Pore Structure*, Academic Press Inc., London, 1992.

Ebeltoft, E., Iversen, J.E., Vatne, K.O., Andersen, M.A., Nordtvedt, J.E.: "A Novel Experimental Apparatus for Determination of Three-Phase Relative Permeabilities at Reservoir Conditions," *Journal of Petroleum Science and Engineering*, Vol 19, 1998, pp. 119-132.

Eikje, E., Jakobsen, S.R., Lohne, A., Skjævland, S.M.: "Relative Permeability Hysteresis in Micellar Flooding," *Journal of Petroleum Science and Engineering*, Vol. 7, 1992, pp. 91-103.

Forbes, P.L.: "Simple and Accurate Methods for Converting Centrifuge Data into Drainage and Imbibition Capillary Pressure Curves," paper presented at the 1991 Society of Core Analysts Annual Technical Conference, San Antonio, August 20-22, 1991, 15p.

Gavalas, G.R., Shah, P.C., Seinfeld, J.H.: "Reservoir history matching by Bayesian estimation," *SPE Journal*, 16, 1976, pp. 337-350.

Gill, P.E., Murray, W., Wright, M.H.: *Practical Optimization*, Academic Press Inc., New York, 1981.

Grimstad, A.A., Kolltveit, K., Nordtvedt, J.E., Watson, A.T., Mannseth, T., Sylte, A.: "The Uniqueness and Accuracy of Porous Media Multiphase Properties Estimated from Displacement Experiments," in Proceedings of the 1997 International Symposium of the Society of Core Analysts, Calgary, Canada, September 7-10, 1997.

Hammervold, W.L.: "Capillary Pressure and Wettability Measurements by Improved Diaphragm Method," Ph.D. Dissertation, Høgskolen i Stavanger, Norway, 1994.

Hassler, G.L., Brunner, E.: "Measurement of Capillary Pressures in Small Core Samples," *Petroleum Technology*, 1945, pp. 114-123.

Helset, H.M., Nordtvedt, J.E., Skjæveland, S.M., Virnovsky, G.A.: "Three-Phase Relative Permeabilities from Displacement Experiments with Full Account for Capillary Pressure," in Proceedings of the 1996 SPE Annual Technical Conference and Exhibition, Denver, Colorado, USA, October 6-9, 1996, pp. 1-11.

Honarpour, M.M., Koederitz, L., Harvey, A.H.: *Relative Permeability of Petroleum Reservoirs*, 1994.

Huyakorn,, P.S., Pinder, G.F.: *Computational Methods in Subsurface Flow*, Academic, San Diego, Calif., 1983.

Jacquard, P., Jain, C.: "Permeability Distribution from Field Pressure Data," *SPE Journal*, Vol. 5, No. 4, 1965, pp. 281-294.

Johnson, E.F., Bossler, D.P., and Naumann, V.O.: "Calculation of Relative Permeability from Displacement Experiments," *Trans. AIME*, 216, 1959, pp. 370.

Kabala, Z.J., Milly, P.C.D.: "Sensitivity Analysis of Flow in Unsaturated Heterogeneous Porous Media: Theory, Numerical Model, and Its Verification," *Water Resour. Res.*, Vol. 26, No. 4, April 1990, pp 593-610.

Kerig, P.D., Watson, A.T.: "Relative Permeability Estimation From Displacement Experiments: An Error Analysis," *SPE Reservoir Engineering*, Vol.1, No. 2, 1986, pp. 175-182.

Killough, J.E.: "Reservoir Simulation with History-Dependent Saturation Functions," *SPE Journal*, 1976, pp. 37-48.

Land, C.S.: "Calculation of Imbibition Relative Permeability for Two- and Three-Phase Flow from Rock Properties," *SPE Journal*, 1966, pp. 149-156.

Lee, T.-Y., Seinfeld, J.H.: "Estimation of Absolute and Relative Permeabilities in Petroleum Reservoirs," *Inverse Problems*, Vol. 3, 1987, pp. 711-728.

Leikvoll, T.: "Error Analysis Methodologies for Nonlinear Least Squares Problems with Application to Flow Through Porous Media," Master Thesis, NTNU, Trondheim, Norway, 1995.

Liu, J.: "A Multiresolution Method for Distributed Parameter Estimation," *SIAM Journal on Scientific Computing*, Vol. 14, No. 2, 1993, pp. 389-405.

Manjnath, A., Honarpour, M.M.: "An Investigation of Three-Phase Relative Permeability," in Proceedings of the 1984 Rocky Mountain Regional Meeting, Casper, WY, May 21-23, 1984, pp. 205-223.

Marle, C.M.: *Multiphase Flow in Porous Media*, Editions Technip, Paris, 1981.

Mejia, G.M., Mohanty, K.K., Watson, A.T.: "Use of In Situ Saturation Data in Estimation of Two-Phase Flow Functions in Porous Media," *Journal of Petroleum Science and Engineering*, Vol. 12, 1995, pp. 233-245.

Mejia, G.M., Watson, A.T., Nordtvedt, J.E.: "Estimation of Three-Phase Flow Functions in Porous Media," *AIChE Journal*, Vol. 42, No. 7, 1996, pp. 1957-1967.

McLaghlin, D., Townley, L.R.: "A reassessment of groundwater inverse problem," *Water Resour. Res.*, Vol. 32, No. 5, May 1996, pp. 1131-1161.

Neuman, S.P., Yakowitz, S.: "A statistical approach to the inverse problem of aquifer hydrology, 1, Theory," *Water Resour. Res.*, Vol. 15, No. 4, 1979, pp. 845-860.

Neuman, S.P., Fogg, G.E., Jacobson, E.A.: "A statistical approach to the inverse problem of aquifer hydrology, 2, Case study," *Water Resour. Res.*, Vol. 16, No. 1, 1980, pp. 33-58.

Nordtvedt, J.E., Kolltveit, K.: "Capillary Pressure Curves From Centrifuge Data by Use of Spline Functions," *SPE Reservoir Engineering*, Vol. 6, No. 4, 1991, pp. 497-501.

Nordtvedt, J.E., Mejia, G., Yang, P.-H., Watson, A.T.: "Estimation of Capillary Pressure and Relative Permeability Functions from Centrifuge Experiment," *SPE Reservoir Engineering*, Vol 8, 1993, pp. 292.

Oak, M.J., Ehrlich, R.: "A New X-Ray Absorption Method for Measurement of Three-Phase Relative Permeability," *SPE Reservoir Engineering*, Vol. 3, No. 1, 1988, pp. 199-206.

Oak, M.J., Baker, L.E., Thomas, D.C.: "Three-Phase Relative Permeability of Berea Sandstones," *Journal of Petroleum Technology*, 1990, pp. 1054-1061.

Pukelsheim, F.: *Optimal Design of Experiments* J. Wiley & Sons, Inc., New York 1993.

Richmond, P.C., Watson, A.T.: "Estimation of Multiphase Flow Functions From Displacement Experiments," *SPE Reservoir Engineering*, Vol. 5, Feb. 1990, pp. 121-127.

Robinson, R.L., Slattery, J.C.: "Estimation of Three-Phase Relative Permeabilities," *Transport in Porous Media*, Vol. 16, 1994, pp. 263-287.

Schumaker, L.L.: *Spline Functions: Basic Theory*, J. Wiley & Sons Inc., New York 1981.

Seinfeld, J.H., Chen, W.H.,: "Identification of petroleum reservoir properties," Distributed Parameter System: Identification, Estimation and Control, ed. Ray, W.H. and Lainiotis, D.G., New York, Dekker, 1978, pp. 497-554.

Shah, P.C., Gavalas, G.R., Seinfeld, J.H.: "Error analysis in history matching: optimum level of parameterization," *SPE Journal*, 18, 1978, pp. 218-228.

Skaggs, T.H., Barry, D.A.: "Sensitivity methods for time-continuous, spatially discrete groundwater contaminant transport models," *Water Resour. Res.*, Vol. 32, No. 8, Aug. 1996, pp. 2409-2420.

Skauge, A., Larsen, J.A.: "Three-Phase Relative Permeabilities and Trapped Gas Measurements Related to WAG Processes," in Proceedings of the 1994 International Symposium of The Society of Core Analysts, Stavanger, Norway, September 1994.

Slobod, R.L., Chambers, A., Prehn Jr, W.L.: "Use of Centrifuge for Determining Connate Water, Residual Oil, and Capillary Pressure Curves of Small Core Samples," *Petroleum Transactions Aime*, Vol. 192, 1951, pp. 127-134.

Stone, H.L.: "Probability Model for Estimating Three-Phase Relative Permeabilities," *JPT*, 1970, pp. 214.

Sun, N.-Z., Yeh, W. W.-G.: "Coupled Inverse Problems in Groundwater Modeling 1. Sensitivity Analysis and Parameter Identification," *Water Resour. Res.*, Vol 26, No. 10, Oct. 1990a, pp. 2507-2525.

Sun, N-Z., Yeh, W.W.-G.: "Coupled Inverse Problems in Groundwater Modeling 2. Identifiability and Experimental Design," *Water Resour. Res.*, Vol 26, No. 10, Oct. 1990b, pp. 2527-2540.

Tao, T.M., Watson, A.T.: "Accuracy of JBN Estimates of Relative Permeability: Part 2 - Algortihms," *SPE Journal*, 1984, pp. 215-223.

Tikhonov, A.N., Arsenin, V.Y.: *Solution of Ill-Posed Problems*, John Wiley, New York, 1977.

Tortorelli, D.A., Michaleris, P.: "Design Sensitivity Analysis: Overview and Review," *Inverse Problems in Engineering*, Vol. 1, No. 1, 1994, pp. 71-105.

Urkedal, H.: "Sensitivity Analysis and Estimation of Relative Permeability and Capillary Pressure Functions from Transient and Equilibrium Steady State Data," Cand. Scient Thesis, Department of Physics, University of Bergen, July 1994.

Vignes, O.: "Application of optimization methods in oil recovery problems," Ph.D. Dissertation, NTNU, Trondheim, Norway, Oct. 1993.

Virnovsky, G.A.: "Determination of Relative Permeabilities in a Three-Phase Flow in a orous Medium," *Izvestiya Akademii Nauk SSSR*, No. 5, 1984, pp. 187-189.

Watson, A.T., Lane, H.S., Gatens, J.M.: "History Matching With Cumulative Production Data," *JPT*, January 1990.

Watson, A.T., Richmond, P.C., Kerig, P.D., Tao, T.M.: "A Regression-Based Method for Estimating Relative Permeabilities from Displacement Experiments," *SPE Reservoir Engineering*, Vol. 3, No. 3, 1988, pp. 953-958.

Watson, A.T., Seinfeld, J.H., Gavalas, G.R., Woo, P.T.: "History Matching in Two-Phase Petroleum Reservoirs," *SPE Journal*, Des. 1980.

Watson, A.T., Wade, J.G., Ewing, R.E.: "Parameter and System Identification for Fluid Flow in Underground Reservoirs," in Proceedings from Conference on Inverse Problems and Optimal Design in Industry, Philadelphia, Pa., July 8-10, 1993.

Welge, H.J.: "A Simplified Method for Computing Recovery by Gas or Water Drive," *Trans. AIME*, 195, 1952, pp. 91.

Yakowitz, S., Duckstein, L.: "Instability in aquifer identification: Theory and case study," *Water Resour. Res.*, Vol. 16, No. 6, 1980, pp.1045-1064.

Yeh, W.W.-G.: "Review of Parameter Identification Procedures in Groundwater Hydrology: The Inverse Problem," *Water Resour. Res.*, Vol. 22, No. 2, Feb. 1986, pp. 95-108.

Yeh, W.W.-G., Sun, N.-Z.: "Variational Sensitivity Analysis, Data Requirements, and Parameter Identification in a Leaky Aquifer System," *Water Resour. Res.*, Vol. 26, No. 9, Sept. 1990, pp. 1927-1938.

Appendix A Differentiation of Model Equations

The model equation is given in (3.6) as:

$\mathbf{F}(\mathbf{u},\mathbf{p})^{n+1} = \mathbf{G}(\mathbf{u},\mathbf{p})^{n}$.

This vector equation is solved for each grid block i at each time step n. Hence, $\mathbf{F}$ is a diagonal matrix where the size depend on how many grid blocks there are and how many state variables. There is also a $\mathbf{F}$ matrix for each phase. $\mathbf{G}$ is a vector, the size depending on the number of grid blocks. $\mathbf{p}$ is the vector of model parameters and $\mathbf{u}$ is the vector of state variables.

Oil Equation

Using the finite difference scheme with block centred grid system, the discretized form of (3.6) can be written in the following form:

$$\begin{aligned}\mathrm{F}_{o,i}(\mathbf{u},\mathbf{p})^{n+1} &= T_{o,i+\frac{1}{2}}(p_{o,i+1} - p_{o,i} - G_o)^{n+1} - T_{o,i-\frac{1}{2}}(p_{o,i} - p_{o,i-1} - G_o)^{n+1} \\ &\quad + T_{o,i}(p_{well} - p_{o,i} - G_o)^{n+1} - \frac{V_b}{\Delta t}\left(\varphi b_o(1 - S_w - S_g)\right)^{n+1} \qquad \text{(A.1)} \\ \mathrm{G}_{o,i}(\mathbf{u},\mathbf{p})^{n} &= -\frac{V_b}{\Delta t}\left(\varphi b_o(1 - S_w - S_g)\right)^{n}.\end{aligned}$$

Differentiating the right hand side, G_o, with respect to the state variables in each grid block gives

$$\begin{aligned}\frac{\partial \mathrm{G}_o^n}{\partial p_o} &= -\frac{V_b}{\Delta t} S_o(\varphi' b_o + \varphi b_o') \\ \frac{\partial \mathrm{G}_o^n}{\partial S_w} &= \frac{V_b}{\Delta t}\varphi b_o \qquad \text{(A.2)} \\ \frac{\partial \mathrm{G}_o^n}{\partial S_g} &= \frac{V_b}{\Delta t}\varphi b_o.\end{aligned}$$

Differentiating the vector equations $\mathbf{F}$ and $\mathbf{G}$ with respect to the parameters $\mathbf{p}$ gives

$$\frac{\partial \mathrm{G}_o(\mathbf{u},\mathbf{p})^n}{\partial \mathrm{p}_j} = 0 \qquad \text{(A.3)}$$

and

$$\frac{\partial \mathrm{F}_{o,i}(\mathbf{u},\mathbf{p})^{n+1}}{\partial \mathrm{p}_j} = \frac{\partial T_{o,i+\frac{1}{2}}}{\partial \mathrm{p}_j}(p_{o,i+1} - p_{o,i} - G_o) - \frac{\partial T_{o,i-\frac{1}{2}}}{\partial \mathrm{p}_j}(p_{o,i} - p_{o,i-1} - G_o) + \frac{\partial T_{o,i}}{\partial \mathrm{p}_j}(p_{well} - p_{o,i} - G_o) \tag{A.4}$$

where the transmissibility is differentiated with respect to the parameters as

$$\frac{\partial T_{o,i}}{\partial \mathrm{p}_j} = C\frac{\partial k_{ro,i}}{\partial \mathrm{p}_j}.$$

Water Equation

Using the finite difference scheme with block centred grid system, the discretized form of (3.6) can be written in the following form:

$$\mathrm{F}_{w,i}(\mathbf{u},\mathbf{p})^{n+1} = T_{w,i+\frac{1}{2}}(p_{w,i+1} - p_{w,i} - G_w)^{n+1} - T_{w,i-\frac{1}{2}}(p_{w,i} - p_{w,i-1} - G_w)^{n+1} + T_{w,i}(p_{well} - p_{w,i} - G_w)^{n+1} - \frac{V_b}{\Delta t}(\varphi b_w S_w)^{n+1} \tag{A.5}$$

$$\mathrm{G}_{w,i}(\mathbf{u},\mathbf{p})^{n} = -\frac{V_b}{\Delta t}(\varphi b_w S_w)^{n}.$$

Differentiating the right hand side, G_w, with respect to the state variables in each grid block gives

$$\frac{\partial \mathrm{G}_w^n}{\partial p_o} = -\frac{V_b}{\Delta t}S_w(\varphi' b_w + \varphi b_w')$$

$$\frac{\partial \mathrm{G}_w^n}{\partial S_w} = \frac{V_b}{\Delta t}\varphi(S_w b_w' P_{c,ow}' - b_w) \tag{A.6}$$

$$\frac{\partial \mathrm{G}_w^n}{\partial S_g} = 0.$$

Differentiating the vector equations **F** and **G** with respect to the parameters **p** gives

$$\frac{\partial \mathrm{G}_w(\mathbf{u},\mathbf{p})^n}{\partial \mathrm{p}_j} = 0 \tag{A.7}$$

and

$$\begin{aligned}\frac{\partial \mathrm{F}_{w,i}(\mathbf{u},\mathbf{p})^{n+1}}{\partial \mathrm{p}_j} = &\frac{\partial T_{w,i+\frac{1}{2}}}{\partial \mathrm{p}_j}(p_{w,i+1} - p_{w,i} - G_w) + T_{w,i+\frac{1}{2}}\left(\frac{\partial P_{c,ow,i}}{\partial \mathrm{p}_j} - \frac{\partial P_{c,ow,i+1}}{\partial \mathrm{p}_j}\right) \\ &- \frac{\partial T_{w,i-\frac{1}{2}}}{\partial \mathrm{p}_j}(p_{w,i} - p_{w,i-1} - G_w) + T_{w,i-\frac{1}{2}}\left(\frac{\partial P_{c,ow,i-1}}{\partial \mathrm{p}_j} - \frac{\partial P_{c,ow,i}}{\partial \mathrm{p}_j}\right) \\ &+ \frac{\partial T_{w,i}}{\partial \mathrm{p}_j}(p_{well} - p_{w,i} - G_w) + T_{w,i}\left(\frac{\partial P_{c,ow,i}}{\partial \mathrm{p}_j}\right)\end{aligned} \tag{A.8}$$

where the transmissibility is differentiated with respect to the parameters as

$$\frac{\partial T_{w,i}}{\partial \mathrm{p}_j} = C\frac{\partial k_{rw,i}}{\partial \mathrm{p}_j}.$$

Gas Equation

Using the finite difference scheme with block centred grid system, the discretized form of (3.6) can be written in the following form:

$$\begin{aligned}\mathrm{F}_{g,i}(\mathbf{u},\mathbf{p})^{n+1} = &R_{s,i+\frac{1}{2}}T_{o,i+\frac{1}{2}}(p_{o,i+1} - p_{o,i} - G_o)^{n+1} - R_{s,i-\frac{1}{2}}T_{o,i-\frac{1}{2}}(p_{o,i} - p_{o,i-1} - G_o)^{n+1} \\ &+ T_{g,i+\frac{1}{2}}(p_{g,i+1} - p_{g,i} - G_g)^{n+1} - T_{g,i-\frac{1}{2}}(p_{g,i} - p_{g,i-1} - G_g)^{n+1} \\ &+ R_{s,i}T_{o,i}(p_{well} - p_{o,i} - G_o)^{n+1} + T_{g,i}(p_{well} - p_{g,i} - G_g)^{n+1} \\ &- \frac{V_b}{\Delta t}\left(R_s\varphi b_o S_o + \varphi b_g S_g\right)^{n+1} \\ \mathrm{G}_{g,i}(\mathbf{u},\mathbf{p})^n = &-\frac{V_b}{\Delta t}\left(R_s\varphi b_o S_o + \varphi b_g S_g\right)^n.\end{aligned} \tag{A.9}$$

Differentiating the right hand side, G_o, with respect to the state variables in each grid block gives

$$\frac{\partial G_g^n}{\partial p_o} = -\frac{V_b}{\Delta t}\left[\left(1-S_w-S_g\right)\left(R_s^{'}\varphi b_o + R_s\varphi^{'} b_o + R_s\varphi b_o^{'}\right) + S_g(\varphi^{'} b_g + \varphi b_g^{'})\right]$$

$$\frac{\partial G_g^n}{\partial S_w} = \frac{V_b}{\Delta t}\varphi b_o R_s \tag{A.10}$$

$$\frac{\partial G_g^n}{\partial S_g} = -\frac{V_b}{\Delta t}\left[-R_s\varphi b_o + \varphi b_g + S_g\varphi b_g^{'}\frac{\partial P_{c,og}}{\partial S_g}\right].$$

Differentiating the vector equations **F** and **G** with respect to the parameters **p** gives

$$\frac{\partial \mathrm{G}_g(\mathbf{u},\mathbf{p})^n}{\partial \mathrm{p}_j} = 0 \tag{A.11}$$

and

$$\begin{aligned}
\frac{\partial \mathrm{F}_{g,i}(\mathbf{u},\mathbf{p})^{n+1}}{\partial \mathrm{p}_j} = {} & R_{s,i+\frac{1}{2}}\frac{\partial T_{o,i+\frac{1}{2}}}{\partial \mathrm{p}_j}(p_{o,i+1}-p_{o,i}-G_o) \\
& -R_{s,i-\frac{1}{2}}\frac{\partial T_{o,i-\frac{1}{2}}}{\partial \mathrm{p}_j}(p_{o,i}-p_{o,i-1}-G_o) \\
& +\frac{\partial T_{g,i+\frac{1}{2}}}{\partial \mathrm{p}_j}(p_{g,i+1}-p_{g,i}-G_g)+T_{g,i+\frac{1}{2}}\left(\frac{\partial P_{c,og,i+1}}{\partial \mathrm{p}_j}-\frac{\partial P_{c,og,i}}{\partial \mathrm{p}_j}\right) \\
& -\frac{\partial T_{g,i-\frac{1}{2}}}{\partial \mathrm{p}_j}(p_{g,i}-p_{g,i-1}-G_g)-T_{g,i-\frac{1}{2}}\left(\frac{\partial P_{c,og,i}}{\partial \mathrm{p}_j}-\frac{\partial P_{c,og,i-1}}{\partial \mathrm{p}_j}\right) \\
& +R_{s,i}\frac{\partial T_{o,i}}{\partial \mathrm{p}_j}(p_{well}-p_{o,i}-G_o) \\
& -\frac{\partial T_{g,i}}{\partial \mathrm{p}_j}(p_{well}-p_{g,i}-G_g)+T_{g,i}\left(\frac{\partial P_{c,og,i}}{\partial \mathrm{p}_j}\right)
\end{aligned} \tag{A.12}$$

where the transmissibility is differentiated with respect to the parameters as

$$\frac{\partial T_{g,i}}{\partial \mathrm{p}_j} = C\frac{\partial k_{rg,i}}{\partial \mathrm{p}_j}.$$

Derivative of Production Terms

The production terms are a part of the left hand side, and the terms will form the diagonal of the Jacobi matrix since all terms are computed at grid block *i*. They are given as

$$q_o = -PI_o\left(p_{well} - p_o - G_o\right)$$

$$q_w = -PI_w\left(p_{well} - p_w - G_w\right) = -PI_w\left(p_{well} + P_{c,ow} - p_o - G_w\right)$$

$$q_g = -PI_g\left(p_{well} - p_g - G_g\right) = -PI_g\left(p_{well} - P_{c,og} + p_o - G_g\right)$$

$$R_s q_o = -R_s PI_o\left(p_{well} - p_o - G_o\right)$$

Differentiating the production terms with respect to the model parameters gives

$$\frac{\partial q_o}{\partial \mathrm{p}_j} = -\frac{\partial PI_o}{\partial \mathrm{p}_j}\left(p_{well} - p_o - G_o\right)$$

$$\frac{\partial PI_o}{\partial \mathrm{p}_j} = c\frac{b_o}{\mu_o}\frac{\partial k_{ro}}{\partial \mathrm{p}_j}$$

$$\frac{\partial q_w}{\partial \mathrm{p}_j} = -\frac{\partial PI_w}{\partial \mathrm{p}_j}\left(p_{well} + P_{c,ow} - p_o - G_w\right) - PI_w\frac{\partial P_{c,ow}}{\partial \mathrm{p}_j}$$

$$\frac{\partial PI_w}{\partial \mathrm{p}_j} = c\frac{b_w}{\mu_w}\frac{\partial k_{rw}}{\partial \mathrm{p}_j}$$

$$\frac{\partial q_g}{\partial \mathrm{p}_j} = -\frac{\partial PI_g}{\partial \mathrm{p}_j}\left(p_{well} - P_{c,og} + p_o - G_g\right) + PI_g\frac{\partial P_{c,og}}{\partial \mathrm{p}_j}$$

$$\frac{\partial PI_g}{\partial \mathrm{p}_j} = c\frac{b_g}{\mu_g}\frac{\partial k_{rg}}{\partial \mathrm{p}_j}$$

$$\frac{\partial R_s q_o}{\partial \mathrm{p}_j} = -R_s\frac{\partial PI_o}{\partial \mathrm{p}_j}\left(p_{well} - p_o - G_o\right).$$

Appendix B Differentiation of Boundary Conditions

Several boundary conditions are implemented in the model: injection of water or oil or gas at constant rate or injection of all phases simultaneously at constant total rate and production against constant well pressure or at constant rate. For these boundary conditions are the derivative of production and pressure drop with respect to the model parameters computed.

Injection of oil at constant reservoir rate

Considering a one dimensional, two-phase oil-water case with injection of oil at constant rate and production of water against constant well pressure. The water production is then

$$V_w = \sum_{i=1}^{N_x} V_{b,i}\varphi_i b_{w,i}\left[S_{o,i} - S_{o(init),i}\right] = \sum_{i=1}^{N_x} V_{b,i}\varphi_i b_{w,i}\left[1 - S_{w,i} - S_{o(init),i}\right],$$

where N_x is the number of grid blocks in the x-direction. Differentiation of the water production with respect to a model parameter p_j is given as

$$\frac{\partial V_w}{\partial p_j} = -\sum_{i=1}^{N_x} V_{b,i}\varphi_i b_{w,i}\frac{\partial S_{w,i}}{\partial p_j}.$$

The differential pressure is given as

$$\Delta P = p_{x=L} - p_{x=0} = P_{const} - \left[p_{o,1} + G_o - \frac{q_o b_o}{\Sigma PI_f}\right]$$

where

$$\Sigma PI_f = PI_w + PI_o = \frac{b_o k_{ro}}{\mu_o} + \frac{b_w k_{rw}}{\mu_w},$$

q_o is the constant oil injection rate, and P_{const} is the outlet well pressure. Differentiation of the differential pressure with respect to a model parameter p_j is given as

$$\frac{d\Delta P}{dp_j} = \frac{\partial \Delta P}{\partial p_o}\frac{\partial p_o}{\partial p_j} + \frac{\partial \Delta P}{\partial S_w}\frac{\partial S_w}{\partial p_j} + \frac{\partial \Delta P}{\partial p_j}.$$

This gives

$$\frac{d\Delta P}{dp_j} = \left\{-1 + \left[q_o \frac{\partial b_o}{\partial p_o}\Sigma PI_f - q_o b_o \frac{\partial \Sigma PI_f}{\partial p_o}\right] / \Sigma PI_f^{\,2}\right\}\frac{\partial p_o}{\partial p_j}$$
$$+\left\{\left[-q_o b_o \frac{\partial \Sigma PI_f}{\partial S_w}\right] / \Sigma PI_f^{\,2}\right\}\frac{\partial S_w}{\partial p_j}$$
$$+\left[-q_o b_o \frac{\partial \Sigma PI_f}{\partial p_j}\right] / \Sigma PI_f^{\,2}.$$

Simultaneous injection of water and oil at constant reservoir rate

Considering a one dimensional, two-phase oil-water case with injection of oil at constant rate and production of water against constant well pressure. The water production is then

$$V_o = \sum_{i=1}^{N_x} V_{b,i}\varphi_i b_{o,i}\left[S_{w,i} - S_{w(init),i}\right],$$

where N_x is the number of grid blocks in the x-direction. Differentiation of the oil production with respect to a model parameter p_j is given as

$$\frac{\partial V_o}{\partial p_j} = \sum_{i=1}^{N_x} V_{b,i}\varphi_i b_{o,i}\frac{\partial S_{w,i}}{\partial p_j}.$$

The differential pressure is given as

$$\Delta P = p_{x=L} - p_{x=0} = P_{const} - \left[p_{o,1} + \frac{-(q_w + q_o) + PI_o G_o + PI_w(G_w - P_{c,ow})}{\Sigma PI_f}\right]$$

where

$$\Sigma PI_f = PI_w + PI_o = \frac{b_o k_{ro}}{\mu_o} + \frac{b_w k_{rw}}{\mu_w}$$

q_o and q_w is the constant oil and water injection rate, and P_{const} is the outlet well pressure. Differentiation of the differential pressure with respect to a model parameter p_j is given as

$$\frac{d\Delta P}{dp_j} = \frac{\partial \Delta P}{\partial p_o}\frac{\partial p_o}{\partial p_j} + \frac{\partial \Delta P}{\partial S_w}\frac{\partial S_w}{\partial p_j} + \frac{\partial \Delta P}{\partial p_j}.$$

This gives

$$\frac{d\Delta P}{dp_j} = \left\{-1 - \left[\begin{array}{l}\left(G_o\frac{\partial PI_o}{\partial p_o} + \frac{\partial PI_w}{\partial p_o}(G_w - P_{c,ow})\right)\Sigma PI_f \\ -\left(-(q_w + q_o) + PI_o G_o + PI_w(G_w - P_{c,ow})\right)\frac{\partial \Sigma PI_f}{\partial p_o}\end{array}\right] / \Sigma PI_f^{\,2}\right\}\frac{\partial P_o}{\partial p_j}$$

$$+\left\{-\left[\begin{array}{l}\left(G_o\frac{\partial PI_o}{\partial S_w} + \frac{\partial PI_w}{\partial S_w}(G_w - P_{c,ow}) - PI_w\frac{\partial P_{c,ow}}{\partial S_w}\right)\Sigma PI_f \\ -\left(-(q_w + q_o) + PI_o G_o + PI_w(G_w - P_{c,ow})\right)\frac{\partial \Sigma PI_f}{\partial S_w}\end{array}\right] / \Sigma PI_f^{\,2}\right\}\frac{\partial S_w}{\partial p_j}$$

$$+\left\{-\left[\begin{array}{l}\left(G_o\frac{\partial PI_o}{\partial p_j} + \frac{\partial PI_w}{\partial p_j}(G_w - P_{c,ow}) - PI_w\frac{\partial P_{c,ow}}{\partial p_j}\right)\Sigma PI_f \\ -\left(-(q_w + q_o) + PI_o G_o + PI_w(G_w - P_{c,ow})\right)\frac{\partial \Sigma PI_f}{\partial p_j}\end{array}\right] / \Sigma PI_f^{\,2}\right\}$$

Injection of gas at constant reservoir rate

Considering a one dimensional, two-phase oil-gas case with injection of gas at constant rate and production against constant well pressure. The oil production is then

$$V_o = \sum_{i=1}^{N_x} V_{b,i}\varphi_i b_{o,i}\left[S_{g,i} - S_{g(init),i}\right],$$

where N_x is the number of grid blocks in the x-direction. Differentiation of the oil production with respect to a model parameter p_j is given as

$$\frac{\partial V_o}{\partial p_j} = \sum_{i=1}^{N_x} V_{b,i}\varphi_i b_{o,i}\frac{\partial S_{g,i}}{\partial p_j}.$$

The differential pressure is given as

$$\Delta P = p_{x=L} - p_{x=0} = P_{const} - \left[p_{o,1} + G_w + P_{c,og} - \frac{q_g b_g}{\Sigma PI_f}\right]$$

where

$$\Sigma PI_f = PI_o + PI_g = \frac{b_o k_{ro}}{\mu_o} + \frac{b_g k_{rg}}{\mu_g},$$

q_g the constant gas injection rate and P_{const} is the outlet well pressure. Differentiation of the differential pressure with respect to a model parameter p_j is given as

$$\frac{d\Delta P}{dp_j} = \frac{\partial \Delta P}{\partial p_o}\frac{\partial p_o}{\partial p_j} + \frac{\partial \Delta P}{\partial S_g}\frac{\partial S_g}{\partial p_j} + \frac{\partial \Delta P}{\partial p_j}.$$

This gives

$$\begin{aligned}\frac{d\Delta P}{dp_j} = &\left\{-1 + \left[q_g \frac{\partial b_g}{\partial p_o}\Sigma PI_f - q_g b_g \frac{\partial \Sigma PI_f}{\partial p_o}\right] / \Sigma PI_f{}^2\right\}\frac{\partial p_o}{\partial p_j} \\ &+ \left\{-\frac{\partial P_{c,og}}{\partial S_g} + \left[-q_g b_g \frac{\partial \Sigma PI_f}{\partial S_g}\right] / \Sigma PI_f{}^2\right\}\frac{\partial S_g}{\partial p_j} \\ &- \frac{\partial P_{c,og}}{\partial p_j} + \left[-q_g b_g \frac{\partial \Sigma PI_f}{\partial p_j}\right] / \Sigma PI_f{}^2.\end{aligned}$$

Simultaneous injection of water, oil, and gas at constant reservoir rate

Considering a one dimensional, three-phase oil-water-gas case with injection of oil, water and gas at constant rate and production of oil against constant well pressure. The oil production is then

$$V_o = \sum_{i=1}^{N_x} V_{b,i}\varphi_i b_{o,i}\left[S_{w,i} + S_{g,i} - S_{w(init),i} - S_{g(init),i}\right],$$

where N_x is the number of grid blocks in the x-direction. Differentiation of the oil production with respect to a model parameter p_j is given as

$$\frac{\partial V_o}{\partial p_j} = \sum_{i=1}^{N_x} V_{b,i} \varphi_i b_{o,i} \left[\frac{\partial S_{w,i}}{\partial p_j} + \frac{\partial S_{g,i}}{\partial p_j} \right].$$

The differential pressure is given as

$$\begin{aligned} \Delta P &= p_{x=L} - p_{x=0} \\ &= P_{const} - \left[p_{o,1} + \frac{-(q_w + q_o + q_g) + PI_o G_o (1 + R_s) + PI_w (G_w - P_{c,ow}) + PI_g (G_g + P_{c,og})}{\Sigma PI_f + PI_o R_s} \right] \end{aligned}$$

where

$$\Sigma PI_f = PI_w + PI_o = \frac{b_o k_{ro}}{\mu_o} + \frac{b_w k_{rw}}{\mu_w} + \frac{b_g k_{rg}}{\mu_g}$$

q_o, q_w and q_g is the constant oil, water and gas injection rate, and P_{const} is the outlet well pressure. Differentiation of the differential pressure with respect to a model parameter p_j is given as

$$\frac{d\Delta P}{dp_j} = \frac{\partial \Delta P}{\partial p_o} \frac{\partial p_o}{\partial p_j} + \frac{\partial \Delta P}{\partial S_w} \frac{\partial S_w}{\partial p_j} + \frac{\partial \Delta P}{\partial S_g} \frac{\partial S_g}{\partial p_j} + \frac{\partial \Delta P}{\partial p_j}.$$

This gives:

$$\frac{\partial \Delta P}{\partial p_o}\frac{\partial p_o}{\partial \mathrm{p}_j}=\left\{-1-\left[\begin{array}{l}\left(\dfrac{\partial PI_o}{\partial p_o}G_o(1+R_s)+PI_oG_o\dfrac{\partial R_s}{\partial p_o}\right.\\ \left.+\dfrac{\partial PI_w}{\partial p_o}(G_w-P_{c,ow})+\dfrac{\partial PI_g}{\partial p_o}(G_g+P_{c,og})\right)\\ \left(\Sigma PI_f+PI_oR_s\right)\\ -\left(\begin{array}{l}-(q_w+q_o+q_g)+PI_oG_o(1+R_s)\\ +PI_w(G_w-P_{c,ow})+PI_g(G_g+P_{c,og})\end{array}\right)\\ \left(\dfrac{\partial \Sigma PI_f}{\partial p_o}+\dfrac{\partial PI_o}{\partial p_o}R_s+PI_o\dfrac{\partial R_s}{\partial p_o}\right)\end{array}\right]/\left(\Sigma PI_f+PI_oR_s\right)^2\right\}\frac{\partial P_o}{\partial \mathrm{p}_j}$$

$$\frac{\partial \Delta P}{\partial S_w}\frac{\partial S_w}{\partial \mathrm{p}_j}=\left\{-\left[\begin{array}{l}\left(\dfrac{\partial PI_o}{\partial S_w}G_o(1+R_s)+\dfrac{\partial PI_w}{\partial S_w}(G_w-P_{c,ow})\right.\\ \left.-PI_w\dfrac{\partial P_{c,ow}}{\partial S_w}+\dfrac{\partial PI_g}{\partial S_w}(G_g+P_{c,og})\right)\\ \left(\Sigma PI_f+PI_oR_s\right)\\ -\left(\begin{array}{l}-(q_w+q_o+q_g)+PI_oG_o(1+R_s)\\ +PI_w(G_w-P_{c,ow})+PI_g(G_g+P_{c,og})\end{array}\right)\\ \left(\dfrac{\partial \Sigma PI_f}{\partial S_w}+\dfrac{\partial PI_o}{\partial S_w}R_s\right)\end{array}\right]/\left(\Sigma PI_f+PI_oR_s\right)^2\right\}\frac{\partial S_w}{\partial \mathrm{p}_j}$$

$$\frac{\partial \Delta P}{\partial S_g}\frac{\partial S_g}{\partial \mathrm{p}_j}=+\left\{-\left[\begin{array}{l}\left(\dfrac{\partial PI_o}{\partial S_g}G_o(1+R_s)+\dfrac{\partial PI_w}{\partial S_g}(G_w-P_{c,ow})\right.\\ \left.+\dfrac{\partial PI_g}{\partial S_g}(G_g+P_{c,og})+PI_g\dfrac{\partial P_{c,og}}{\partial S_g}\right)\\ \left(\Sigma PI_f+PI_oR_s\right)\\ -\left(\begin{array}{l}-(q_w+q_o+q_g)+PI_oG_o(1+R_s)\\ +PI_w(G_w-P_{c,ow})+PI_g(G_g+P_{c,og})\end{array}\right)\\ \left(\dfrac{\partial \Sigma PI_f}{\partial S_w}+\dfrac{\partial PI_o}{\partial S_w}R_s\right)\end{array}\right]/\left(\Sigma PI_f+PI_oR_s\right)^2\right\}\frac{\partial S_g}{\partial \mathrm{p}_j}$$

$$\frac{\partial \Delta P}{\partial p_j} = -\left[\begin{array}{l} \left(\begin{array}{l} \dfrac{\partial PI_o}{\partial p_j} G_o(1+R_s) + \dfrac{\partial PI_w}{\partial p_j}(G_w - P_{c,ow}) \\ -PI_w \dfrac{\partial P_{c,ow}}{\partial p_j} + \dfrac{\partial PI_g}{\partial p_j}(G_g + P_{c,og}) + PI_g \dfrac{\partial P_{c,og}}{\partial p_j} \end{array}\right) \\ \left(\Sigma PI_f + PI_o R_s\right) \\ -\left(\begin{array}{l} -(q_w + q_o + q_g) + PI_o G_o(1+R_s) \\ +PI_w(G_w - P_{c,ow}) + PI_g(G_g + P_{c,og}) \end{array}\right) \\ \left(\dfrac{\partial \Sigma PI_f}{\partial p_j} + \dfrac{\partial PI_o}{\partial p_j} R_s\right) \end{array}\right] / \left(\Sigma PI_f + PI_o R_s\right)^2$$

Paper I

Design of Three-Phase Relative Permeability Experiments

H. Urkedal,[1] K. Langaas,[1] J.E. Nordtvedt,[1] and A.T. Watson[2]

[1] RF – Rogaland Research, P.O. Box 2503 Ullandhaug, N-4004 Stavanger, Norway
[2] Texas A&M University, Dept. of Chem. Eng., College Station, TX 77843-3122, USA

Abstract

This paper presents, for the first time, a systematic approach to the selection of experimental designs leading to accurate determination of the three-phase relative permeability functions. The approach is based on a linearized covariance analysis which is utilized to determine the confidence intervals on estimated relative permeabilities. These confidence intervals define the accuracy with which the relative permeabilities can be determined for the given data, their acccuracy, and the chosen flooding scenario. In this paper, the confidence intervals are utilized to quantitatively assess the utility of different designs towards accurate three-phase relative permeability determination. For the cases considered here, we demonstrate that accurate estimates may be obtained in the parts of the saturation region which are reflected in the experimental data.

Introduction

Two- and three-phase relative permeabilities are important properties of porous media. In order to perform reservoir forcasting in a multi-phase situation, these functions will have to be specified at all locations within the considered porous structure. Since one usually does not have sufficient field data available for analyses leading to relative permeability estimates, the properties are most commonly inferred through analyses of data acquired during some process imposed on a sample extracted from the reservoir. These data will typically be from some type of displacement experiment, in which one or several fluids are injected into a saturated core. The data (called flooding data hereafter) may comprise fluid production and pressure drop as a function of time, and, possibly, *in situ* saturation and/or phase pressures as functions of time and position.

For two-phase situations, a sound approach has been developed for determining the relative permeabilities[15]. In this approach, the relative permeability functions are determined through a solution of a series of linear inequality constrained least-squares problems (a regression-based approach), the idea being that the properties are chosen such that the measured flooding data "match" the ones calculated using a numerical simulator. In each step in the regression-based approach, the functions are represented by a set of parameters. For a number of two-phase experimental scenarios, it has been demonstrated that relative permeability and capillary pressure functions may be accurately determined utilizing this approach, e.g., dynamic displacement experiments[12, 6], centrifuge experiments[7], and modified steady-state experiments[8]. This methodology has proven to be quite superior to the more frequently used JBN method[3] (see analysis in [11]), and has the advantage of being able to determine both capillary pressure and relative permeability functions simultaneously from a given set of data. One particularly important characteristic of the regression-based

approach is that it allows for the determination of *functions*, rather than sets of discrete points, the latter being the output of the JBN-type interpretation of displacement data.

In the three-phase case, however, the estimation of functions, as opposed to sets of discrete points, has just recently been addressed[5]. Most of the effort up to now has been concentrated on extending the JBN-method to three-phase situations (see, e.g.,[13]), and utilization of the steady-state technique (see, e.g.,[9, 10]). Both these methods provides relative permeability values (i.e., *points*) along one or several trajectories in the three-phase diagram. However, the entire relative permeability functions need to be determined if the estimates should be of any utility in reservoir simulation or forecasting. Furthermore, as the capillary pressure is neglected in both these approaches, the relative permeability points determined from these analyses will suffer from this modeling error[4]. Although the regression-based approach circumvents previous problems, the experiments need to be carried out in such a manner that sufficient information is extracted for accurate estimation of the three-phase relative permeability functions over a relatively large saturation region.

This paper addresses the design of three-phase experiments leading to accurate determination of relative permeability functions. We will investigate different types of data and different flooding scenarios and their impact on the accuracy of the estimated relative permebility functions.

Design of Experiments

There is a huge variety of ways of performing experiments leading to three-phase relative permeability estimates. For example, one may inject one, two, or three phases simultaneously into a core sample, or conduct some constant pressure drop experiments. Obviously, it is desirable to keep the number of experiments needed for three-phase relative permeability determination as low as possible, yet the accuracy with which these functions are determined as high as possible. This section presents a systematic approach for designing the three-phase experiments leading to accurate determination of the three-phase relative permeability functions. By *design* of three-phase experiments, we mean the manner in which the experiments are conducted (e.g., a series of injections of gas into a sample initially saturated with oil and water) *and* the experimental flooding data measured (both type of data and location of each datapoint (in time and/or space), as well as the accuracy with which the data are measured).

The evaluation of the designs will be based upon measures of the accuracy with which the relative permeabilities may be determined from a given set of data. In the two-phase situation, accuracy measures have been obtained through a linearized covariance analysis[4]. In the covariance analysis, it is assumed that a mathematical model capable of describing the physics of the considered process exists. It is further assumed that we can adequately represent the relative permeability functions by a set of parameters, that the mathematical model is linear in these parameters near the solution, and, finally, that the errors in the measurements are additive with zero mean and a given standard deviation; see Kerig and Watson[4] for details. The parameters are taken to be estimated through solution of the constrained least-squares problem defined by:

$$min\ J(\vec{\beta}) = [\vec{Y}_m - \vec{Y}_s(\vec{\beta})]^T \mathbf{W} [\vec{Y}_m - \vec{Y}_s(\vec{\beta})] \quad (1)$$

$$subject\ to\ \mathbf{G}\vec{\beta} \geq \vec{b}. \quad (2)$$

Here, $\vec{Y}_m$ is the vector of measured data, and $\vec{Y}_s(\vec{\beta})$ is the corresponding vector of simulated quantities. W is the weighting matrix, and $\vec{\beta}$ contains the parameters in the functional representation of the relative permeability and/or capillary pressure functions. By choosing W to be the inverse of the covariance matrix of the measurements ($W = C^{-1}$), the solution of Eqs. 1- 2 becomes the maximum-likelihood estimates of the parameters, $\vec{\beta}$[1]. It can then be shown that the covariance matrix of the parameter estimates is given by[4]

$$P = (A^T C^{-1} A)^{-1}, \tag{3}$$

where A is the sensitivity matrix (with elements $a_{ij} = \partial Y_{s,i}/\partial \beta_j$), and C is the covariance matrix of the measurements. Linearizing the relative permeability functions around the true parameter values, a (pointwise) relative permeability confidence interval can be calculated for any saturation value.

This analysis has been used for determining confidence intervals for the estimates of the relative permeability functions for a number of two-phase situations, see[6, 7, 8, 11]. Also, three-phase situations have recently been considered[5]. In this work, we have extended the analysis to three-phase situations in which data from several three-phase experiments can be considered simultaneously.

Note that these accuracy measures are obtained from knowledge of the simulated experimental data ($\vec{Y}_s(\vec{\beta})$), the parameters in the functional representation of the relative permeabilities ($\vec{\beta}$), and the covariance matrix of the measurements (C). Thus, to determine the accuracy with which the relative permeabilities may be determined from a particular experimental design, the core sample and fluid properties will first have to be selected, along with injection strategies, types of data and time, position, and accuracies with which these measurements are going to be acquired, and finally, the parameters in the functional representation of the relative permeabilities. Then, using this selected experimental design, $\vec{Y}_s(\vec{\beta})$ can be calculated using a numerical simulator; in this work, $\vec{Y}_s(\vec{\beta})$ is calculated using the fully implicit, black-oil, coreflood simulator CENDRA[2]. The sensitivity materix, **A**, is determined by perturbing (in turn) each element in $\vec{\beta}$, and calculating each a_{ij} by a first order finite difference approximation. Finally, P is calculated through Eq. 3 and thus the relative permeability confidence intervals may be found. Note that no actual experimental data are needed in this analysis.

Our evaluation of the experimental designs comprises the following steps:

1. Select core and fluid properties, and select a set of relative permeability and capillary pressure functions;

2. Select an experimental design (i.e., select a way of conducting the experiments and the types of data and location for those data (in time and space));

3. Perform the covariance analysis, i.e., calculate the confidence intervals around the selected relative permeability functions; and

4. Analyze the confidence intervals with respect to desired accuracy in the estimated functions;

In this manner, quantitative measures of the potential performance of different chosen designs of the experiment can be obtained. We will next discuss items 1 and 2 in the above evaluation procedure.

The adequacy of this approach depends on the suitability of the representation for the relative permeability functions. In two-phase situations, univariate B-splines[14] adequately represent the relative permeability functions[4]. In this work, we have used a bivariate extension of this B-spline representation. The relative permeability surfaces are given by

$$k_{rl}(S_1, S_2) = \sum_{i_1=1}^{m_1+K_1} \sum_{i_2=1}^{m_2+K_2} c_{i_1,i_2} N_{i_1}^{m_1}(S_1, \vec{y}^{\,i_1}) N_{i_2}^{m_2}(S_2, \vec{y}^{\,i_2}), \tag{4}$$

where $l = w, o, g$, as we will consider water, oil, and gas cases. For convenience we will define $S_1 = 1 - S_l$, and $S_2 = S_w$ if $l \neq w$ and $S_2 = S_g$ otherwise. This representation is a tensor-product expansion of the univariate B-spline in the directions along S_1 and S_2. m_i is the order of the spline along direction i, and K_i is the corresponding number of knots. One can increase the flexibility of the surface by increasing the number of knots (in one or both directions) and/or by increasing the corresponding spline order. The spline coefficients c_{i_1,i_2} will constitute the parameter vector $\vec{\beta}$.

Table 1: Core properties.

Porosity [$frac.$]	0.35
Permeability [mD]	2.0
Core length [cm]	30
Core area [cm^2]	11.22
Oil formation volume factor	1.635
Water formation volume factor	1.0
Water viscosity [cP]	0.34
Oil viscosity [cP]	0.3625
Gas viscosity [cP]	0.0515
Initial Water Saturation [$frac.$]	1.0

The properties of the fluid and core sample considered in this study are given in Table 1. The capillary pressure functions used are shown in Figure 1. In our analysis, we will investigate the determination of the relative permeability functions, assuming that the core and fluid properties as well as capillary pressure functions are known. The analysis works equally well for estimating the accuracy with which other properties may be determined (e.g., the capillary pressure functions); however, such considerations are outside the scope of the present paper. The relative permeability functions used in this study are shown in Figure 2. These functions are tensor-product B-splines of order 3 with 2 knots in each direction, i.e., they are represented by 20 parameters each, giving a total of 60 parameters. Some of the corresponding B-splines do not have support within the saturation area of interest (as $S_w + S_o + S_g = 1$, e.g., $S_w = S_o = 1$ is not a possible saturation combination), which decreases the number of effective parameters to 51. The functions are selected by utilizing three-phase relative permeability points acquired by Oak[9]. The representation in Eq. 4 is fitted to the data through solution of the linear least-squares problem defined by $min\|\vec{k}_{rl}^{m} - \vec{k}_{rl}^{s}(\vec{\beta}, S_1, S_2)\|_2^2$, where $\vec{k}_{rl}^{m}$ is the vector of measured relative permeability values, and $\vec{k}_{rl}^{s}(\vec{\beta}, S_1, S_2)$ is the corresponding vector of calculated quantities (calculated through Eq. 4). The solution is obtained subject to some constraints, see Eq. 2; we have in this work imposed monotonicity constraints on these relative permeability surfaces.

Table 2: Overview of the experiments considered (W: Water; O: Oil; G: Gas.) All steady-state experiments stops at 80000 *min*, while the unsteady-state experiments stops at 40000 *min*.

	q_w[cc/min]	q_o[cc/min]	q_g[cc/min]	**Start time** [min]
Experiment 1SS				
WO injection	0.020	0.030	0.000	0.0
WOG injection	0.002	0.010	0.040	10000.0
WOG injection	0.001	0.005	0.150	20000.0
OG injection	0.000	0.002	0.500	30000.0
G injection	0.000	0.000	1.000	50000.0
Experiment 2SS				
WO injection	0.014	0.014	0.000	0.0
WOG injection	0.014	0.014	0.016	10000.0
WOG injection	0.002	0.002	0.040	20000.0
WOG injection	0.001	0.001	0.160	30000.0
G injection	0.000	0.000	0.500	40000.0
G injection	0.000	0.000	1.000	60000.0
Experiment 3SS				
WG injection	0.095	0.000	0.005	0.0
WG injection	0.090	0.000	0.010	10000.0
WG injection	0.050	0.000	0.050	20000.0
WG injection	0.001	0.000	0.099	30000.0
G injection	0.000	0.000	1.000	40000.0
G injection	0.000	0.000	5.000	60000.0
Experiment 1USS				
WO injection	0.020	0.030	0.000	0.0
G injection	0.000	0.000	1.000	10000.0
Experiment 2USS				
WO injection	0.014	0.014	0.000	0.0
G injection	0.000	0.000	1.000	10000.0
Experiment 3USS				
G injection	0.000	0.000	5.000	0.0

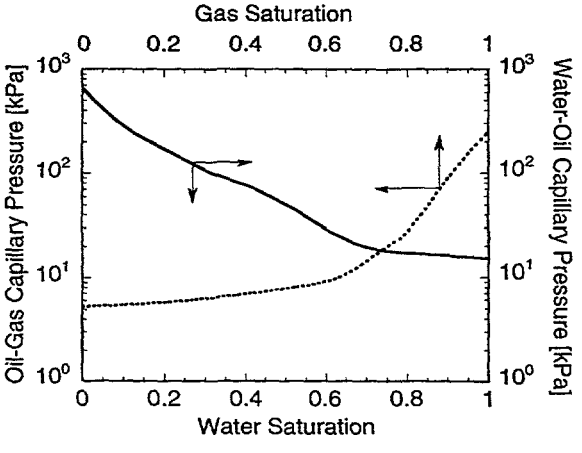

Figure 1: Water-oil and oil-gas capillary pressure functions.

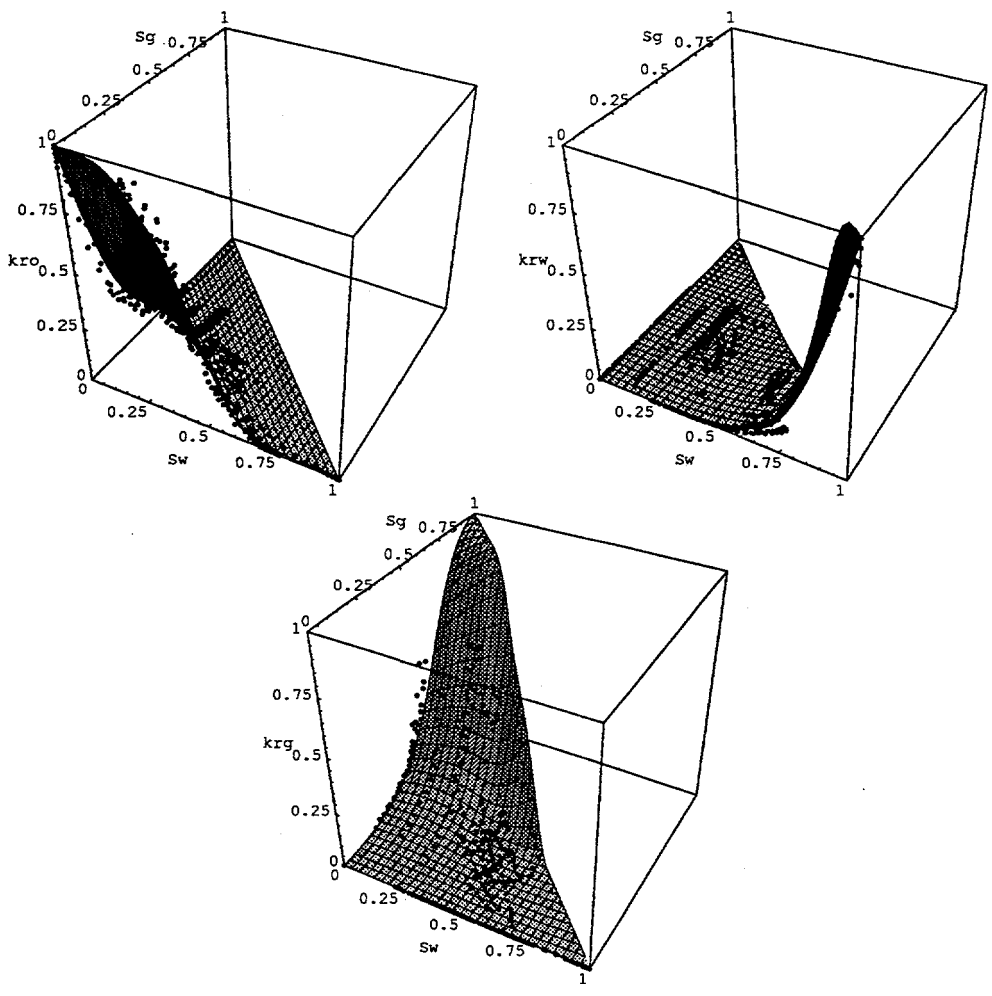

Figure 2: Relative permeabilitity functions used in analysis. Upper left: k_{ro}; upper right: k_{rw}; and lower: k_{rg}

In this work, we have investigated the accuracy with which the relative permeability functions may be determined from 6 different experimental designs, all of which can be considered as modified DDI (decreasing water saturation, decreasing oil saturation, and increasing gas saturation) reservoir condition cases, see Figure 3a). The cases are performed to study how the relative permeabilities in three-phase apparatuses similar to that at RF – Rogaland Research can be determined. In this set-up, three phases can be injected simultaneously at

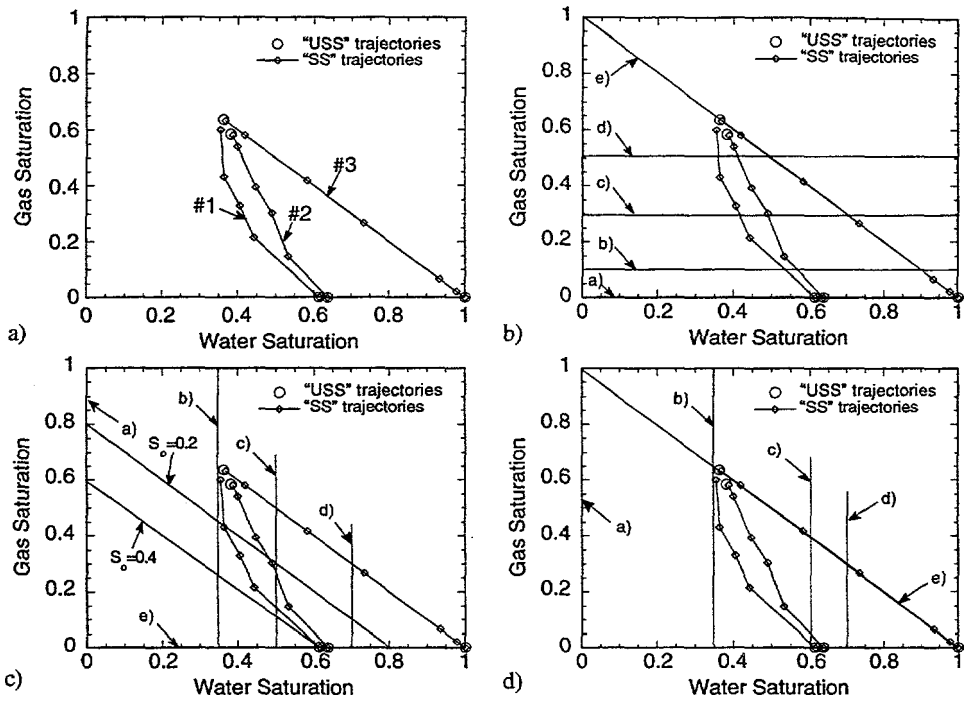

Figure 3: a) Trajectories for all the experiments; b) Sections for study of water relative permeability; c) Sections for study of oil relative permeability; d) Sections for study of gas relative permeability.

reservoir pressure and temperature, and the production of each of the phases and the pressure drop across the core can be measured as a function of time, and the three-phase saturation profiles can be measured at any steady-state situation. Each of the experimental designs is comprised of one to three experiments. Table 2 shows an overview of the injection strategies in all the experiments. The details of these experiments will be discussed next.

In steady-state experiment 1 (1SS; see Table 2 for details on the injection strategy for this experiment), oil and water are first injected into a fully water saturated core sample, and data are "collected" until a near equilibrium situation is reached in both production and pressure drop accross the core (i.e., a close to steady-state situation is attained). Then gas is introduced into the core sample. This is done through a series of steady-state steps. From one steady-state to the next, we decrease the flow rate of liquids (water and oil) and increase the gas rate. In the two last steps, we first maintain the gas flow rate, but let the liquid flow rate go to zero, and then, finally, increase the gas flow rate. The latter is done to establish a high final gas saturation. This procedure follows Oak[9] with only minor modifications. A total of 5 steps are utilized for experiment 1SS. In Figure 3a) the average saturation at the near steady-state condition (i.e, prior to each of the rate changes) is shown as "trajectory" #1. (Note that all of the trajectories starts at unity water saturation.) A similar procedure

is utilized for experiment 2SS (trajectory #2 in Figure 3a)). Experiment 3SS (trajectory #3 in Figure 3a)) is a gas-water injection in a fully water saturated sample. Here, the rate fraction of gas is increased while the water rate is decreased in 6 steps.

Table 3: Overview of the cases considered.

Case	Experiment used	Surfaces considered	# parameters	# datpoints
Case Ia	1SS	k_{rw}, k_{ro}	34	1800
Case Ib	1USS	k_{rw}, k_{ro}	34	1800
Case IIa	1SS, 2SS	k_{rw}, k_{ro}, k_{rg}	51	3600
Case IIb	1USS, 2USS	k_{rw}, k_{ro}, k_{rg}	51	3600
Case IIIa	1SS, 2SS, 3SS	k_{rw}, k_{ro}, k_{rg}	51	5400
Case IIIb	1USS, 2USS, 3USS	k_{rw}, k_{ro}, k_{rg}	51	5400

For the first unsteady-state experiment (1USS), oil and water are first injected into a fully water saturated core sample to establish a two phase oil-water situation in the sample. When a near equilibrium state is obtained, only gas is injected at the same rate fraction as the last gas rate in the corresponding steady-state experiment (i.e., experiment 1SS). A similar procedure is utilized for experiment 2USS. For experiment 3USS gas is injected into a fully water saturated core sample in only 1 step. The end points for gas injections as well as oil-water equilibrium average saturations are shown in Figure 3a) for the three unsteady-state type experiments.

From the 6 experiments we form 6 different experimental designs (referred to as cases) for consideration, see details in Table 3. In the analysis of each of the cases, we assume that we measure production of two phases (water and oil), and the pressure drop across the core as a function of time. The measurement errors are taken to be $\sigma_V = 0.005\ PV$ and $\sigma_{\Delta P} = 20\ kPa$ for the produced phase volumes and the pressure drop, respectively. In Case Ia we investigate determination of the water and oil relative permeability surfaces with data from experiment 1SS. I.e., we assume that the gas relative permeability function is known *a priori*, and investigate only the determination of the water and oil relative permeabilities. The dimension of $\vec{\beta}$ is 34. Case Ib is the corresponding unsteady-state case (i.e., using data from experiment 1USS). For Case Ia and Ib we have chosen 1200 production data and 600 pressure data. In Case IIa, we study the determination of all relative permeability surfaces using data from experiments 1SS and 2SS; Case IIb is the corresponding unsteady-state case. Finally, in Case IIIa, we investigate the determination of all of the surfaces from experiments 1SS, 2SS, and 3SS. Again, Case IIIb is the corresponding unsteady-state case; see Table 3 for details.

Results and Discussion

The results from each of these cases are shown in Figure 4 to 6. The figures are constructed to compare the performance of steady-state and unsteady-state type experiments. For each surface the results are shown as cross sections, e.g., the water relative permeability surface with confidence intervals are shown for constant values of the gas saturations in Figures 4a) to 4e). Each of the selected sections are plotted in Figure 3b) together with all the trajectories

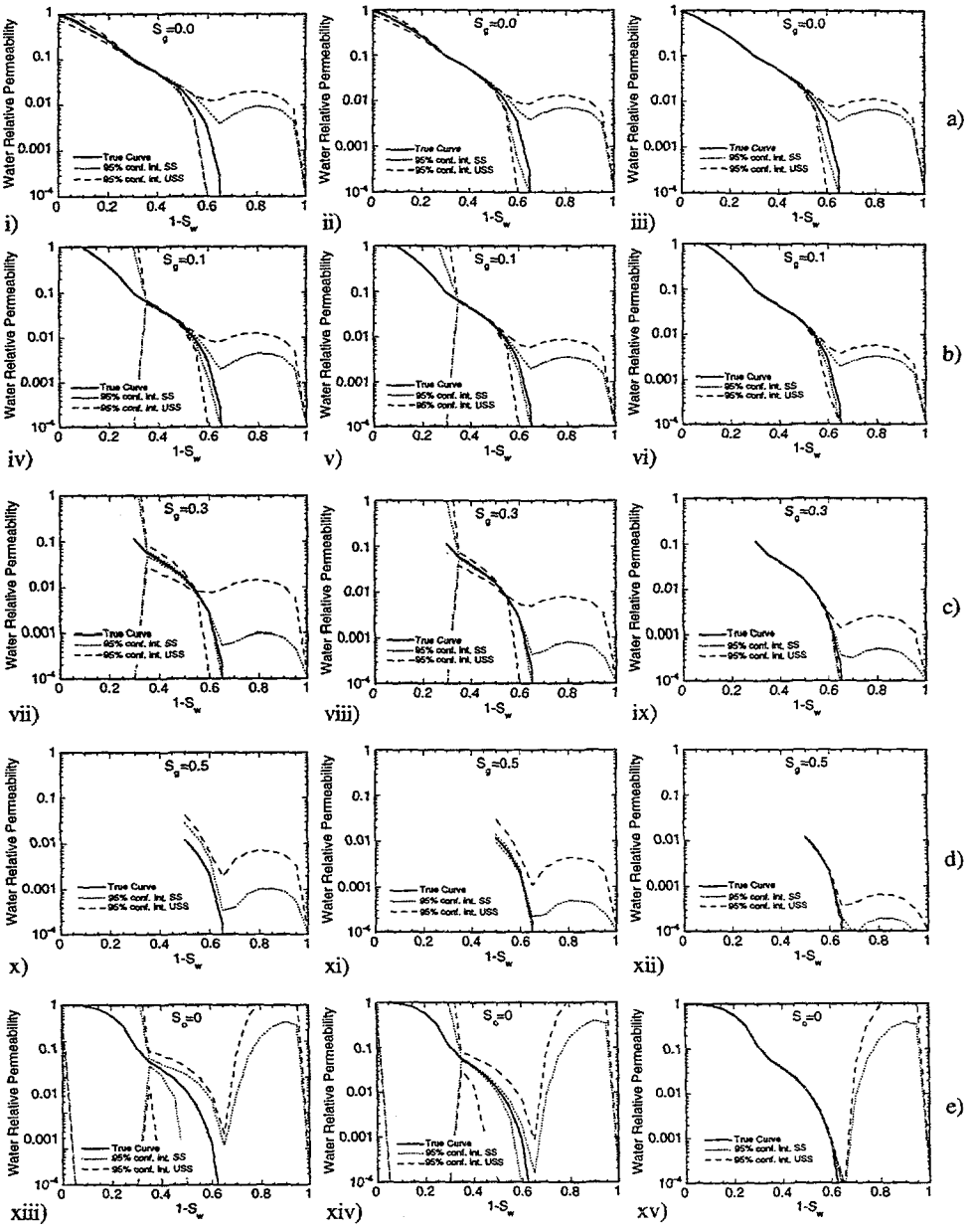

Figure 4: Water relative permeability sections for all the cases. Plots in left column shows results for Case Ia and Ib, in the middle column for Case IIa and IIb, and in the right column for Case IIIa and IIIb. See Figure 3b) for details on the sections.

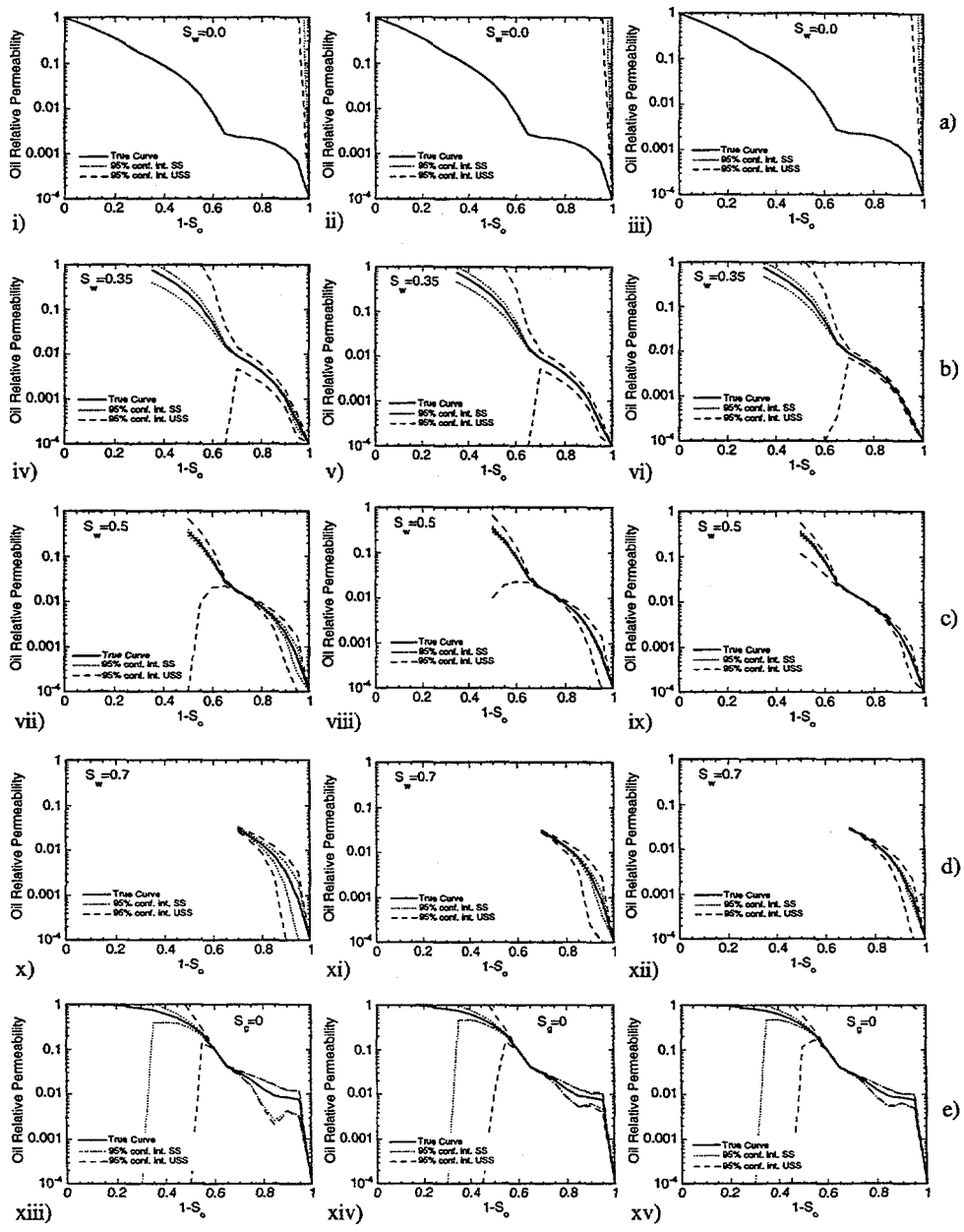

Figure 5: Oil relative permeability sections for all the cases. Plots in left column shows results for Case Ia and Ib, in the middle column for Case IIa and IIb, and in the right column for Case IIIa and IIIb. See Figure 3c) for details on the sections.

(both from steady-state as well as unsteady-state type experiments). The corresponding results for determination of the oil relative permeability are plotted in Figure 5a) to 5e), with cross sections in Figure 3c), and, finally, the results for the gas relative permeability are shown in Figure 6a) to 6e), with cross sections in Figure 3d).

Note that each relative permeability surface appears to be well determined whenever its "own" phase saturation is zero. In our analyses we have utilized the *a priori* information that $k_{ri}(S_i = 0) = 0$. Consequently, the corresponding parameters are eliminated from the covariance analysis, leading to zero confidence intervals whenever $S_i = 0$.

An overall observation is that the relative permeabilities are well determined in saturation regions corresponding to regions represented in the data. For the cases considered here, this region is approximately given by the triangle defined by the intervals $S_w \in [0.3, 1]$ and $S_g \in [0, 0.6]$, and the line $S_o = 0$; see trajectories in Figure 3a) and Figures 4-6.

For $S_g = 0$, the confidence intervals of the water relative permeability are narrow (i.e., k_{rw} is expected to be well determined from the data) for all the cases in a saturation region from unity down to about $S_w = 0.3$. This is the saturation region which is represented in the data from experiments 1SS, 2SS, 1USS, and 2USS; see Figures 4a). For Case Ia, Ib, IIa, and IIb, the water relative permeability will only be well determined in a relatively small S_w-interval whenever $S_g > 0$; see Figure 4b)-d). The reason for this is that the data from the experiments along trajectories #1 and #2 will only reveal relative permeability information in a saturation region close to the trajectories. This means that we should not expect to be able to determine the water relative permeability with any high degree of accuracy for water saturations outside the interval $S_w \in [0.3, 0.6]$, whenever $S_g > 0$. For example, for Case Ia, the confidence interval is relatively large for S_w values higher than 0.6 for $S_g = 0.3$; see Figure 4vii). However, as data along trajectory #3 is added in Case IIIa and IIIb, the water relative permeability surface becomes well determined for S_w values higher than 0.4 for any fixed value of the gas saturation, see Figures 4iii), 4vi), 4ix), and 4xii). Note that while k_{rw} was very poorly determined along the gas-water axis from data from Case Ia, Ib, IIa, and IIb, data from Case IIIa and IIIb determine the relative permeability well along this axis for gas saturation higher than 0.6; compare Figure 4xiii) and 4xiv) with 4xv). Also, note that steady-state type data better determine the water relative permeability surfaces for all the cases and for all the selected sections (frequently by an order of magnitude).

For all the cases, the oil relative permeability is well determined along parts the oil-water axis ($S_g = 0$), see Figures 5e). Generally, k_{ro} is well determined in saturation areas close to the trajectories for the particular case. For example, for $S_w = 0.5$ (see Figures 5c)), the k_{ro} is relatively poorly determined for $S_o \in [0, 0.3]$, as this saturation interval is not represented in the data. For S_o approximately between 0.3 and 0.4, k_{ro} is well determined. This area corresponds to the trajectories #1 (and #2), see Figure 3c) for details on oil saturation vs. trajectory saturations. Again, steady-state type data determine the surface better than unsteady-state data.

For Case IIa and IIb, the gas relative permeability is quite well determined for saturation values corresponding to the trajectories #1 and #2, see Figures 6i), 6iii), 6v), 6vii), and 6ix). However, for high water saturation values, as well as along the water-gas axis, k_{rg} is poorly determined, see Figures 6v) and 6vii). This is because this saturation region is not represented in the data used in Case IIa and IIb. When the gas injection is added (Case IIIa and IIIb), these regions becomes well determined (see Figures 6viii) and 6x)); in fact, the gas relative permeability is quite well determined for approximately $S_w \geq 0.35$ and $S_g < 0.6$.

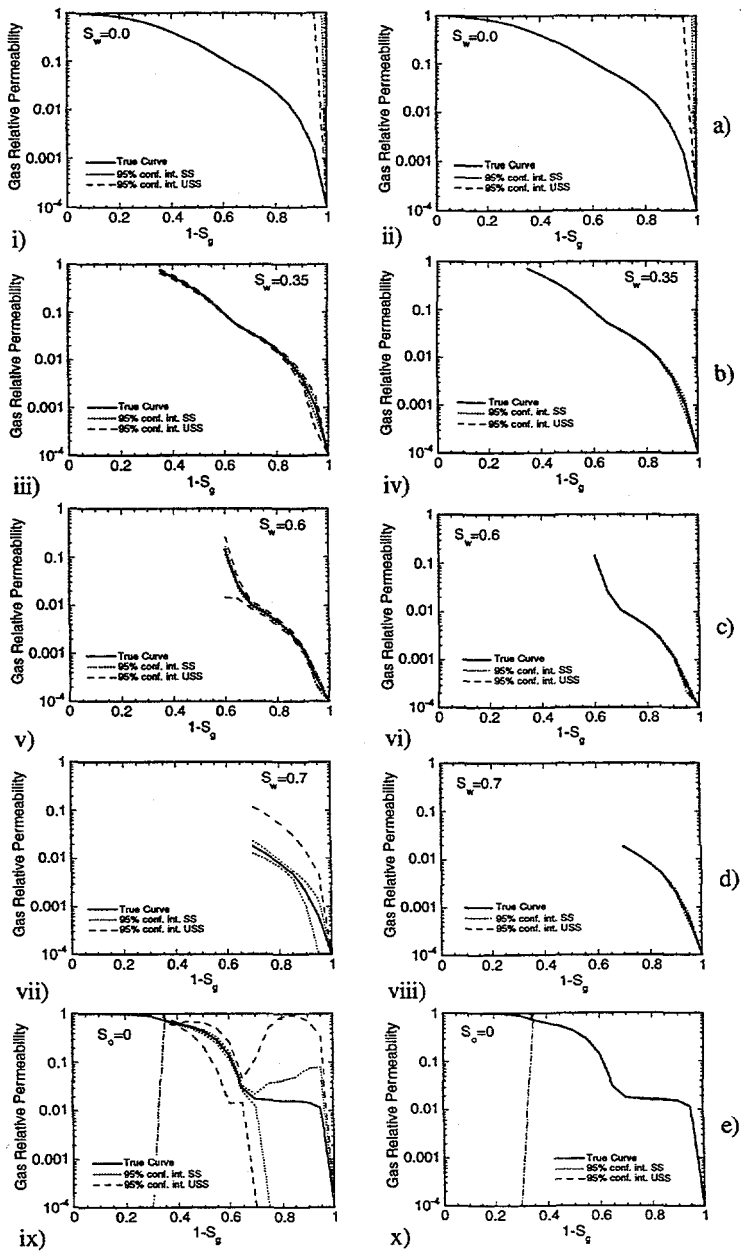

Figure 6: Gas relative permeability sections for all the cases. Plots in left column shows results for Case Ia and Ib, in the middle column for Case IIa and IIb, and in the right column for Case IIIa and IIIb. See Figure 3d) for details on the sections.

Although most pronounced for Case IIa and IIb, the steady-state type data are superior to the unsteady-state type.

Although we limit here the discussion to 6 DDI experimental designs, this approach can be utlized to design experiments of any kind, and the estimation of capillary pressure may also be considered. The outlined method is particularly fruitful for the design of three-phase relative permeability experiments for field applications. In a reservoir engineering context, one may know reasonably well the saturation region that is expected to occur in the reservoir. While it can be quite acceptable to have poorly determined three-phase relative permeabilitites outside this "window," it is imperative to accurately determine the functions within. Our methodology provides a quantitative means for designing experiments leading to accurate relative permeability determination in saturation regions of interest.

Conclusions

1. A systematic method for quantitative evaluation of designs of three-phase relative permeability experiments leading to accurate determination of the relative permeability surfaces has been presented. The evaluation procedure is based on a linearized covariance analysis, and can consider data from several three-phase experiments simultaneously.

2. Six different DDI experimental designs have been analyzed. The analysis show that from the DDI designs considered here, we are able to determine the relative permeability surfaces accurately in a relatively large saturation region, even for a limited number of experiments. Also, the inclusion of water-gas data seems to potentially give significant improvements in analyses leading to relative permeability estimates.

Nomenclature

a_{ij}	Element in sensitivity matrix
$\mathbf{A}$	Sensitivity matrix
$\vec{b}$	Constraint vector
$\vec{\beta}$	Vector of parameters in representation of relative permeabilities
c	Spline coefficients
$\mathbf{C}$	Covariance matrix
$\mathbf{G}$	Constraint matrix
J	Objective function
k	Permeability
K	Number of knots
m	Spline order
N	Normalized B-spline basis function
S	Saturation
$\sigma_{\Delta P}$	Measurement error in the pressure drop data
σ_V	Measurement error in the production data
$\mathbf{P}$	Covariance matrix of parameters
$\vec{y}$	Spline partition

$\vec{Y}$	Vector of measured or simulated data
$\mathbf{W}$	Weighting matrix

Subscripts / Superscripts

c	Capillary
g	Gas
m	Measured
o	Oil
r	Relative
s	Simulated
w	Water

Acknowledgements

This work is a part of an RF – Rogaland Research project within three-phase relative permeability estimation. The project is financed by Amoco Norway Oil Company, whose support we gratefully acknowledge.

References

[1] Bard, Y.: *Nonlinear Parameter Estimation*, Academic Press, Inc., Washington, DC (1974).

[2] Guo, Y., Nordtvedt, J.E., Olsen, H.: "Development and Improvement of CENDRA+," Report RF-183/93, Confidential.

[3] Johnson, E.F., Bossler, D.P., Naumann, V.O.: "Calculation of Relative Permeability from Displacement Experiments" *Trans.*, AIME, 1958, 370.

[4] Kerig, P.D., Watson, A.T.: "Relative Permeability Estimation From Displacement Experiments: An Error Analysis," *SPE Reservoir Engineering*, Jan. 1986, 175.

[5] Mejia-Velazquez, G.M.: "A Method for Estimating Three-Phase Flow Functions," *PhD Dissertation*, Texas A&M University, College Station, TX, Aug. 1992.

[6] Mejia, G.M., Mohanty, K.K., Watson, A.T.: "Use of *In Situ* Saturation Data in Estimation of Two-Phase Flow Functions in Porous Media," *Journal of Petroleum Science and Engineering*, **12**, 1995, 233.

[7] Nordtvedt, J.E., Mejia, G., Yang, P.-H., Watson, A.T.: "Estimation of Capillary Pressure and Relative Permeability Functions From Centrifuge Experiments," *SPE Reservoir Engineering*, Nov. 1993, 292.

[8] Nordtvedt, J.E., Urkedal, H., Watson, A.T., Ebeltoft, E., Kolltveit, K., Langaas, K., Øxnevad, I.E.I.: "Estimation of Relative Permability and Capillary Pressure Functions

Using Transient and Equilibrium Data From Steady-State Experiments," *Reviewed Proceedings of the 1994 International Symposium of the Society of Core Analysts*, Stavanger, Norway, September 12-14, 1994 197.

[9] Oak, M. J.: "Three-Phase Relative Permeability of Water-Wet Berea," *paper SPE 20183 presented at the SPE/DOE Seventh Symposium on Enhanced Oil Recovery*, Tulsa, OK, April 22-25, 1990.

[10] Oak, M. J., Baker, L. E., Thomas, D. C.: "Three-Phase Relative Permeability of Berea Sandstone," *J. Pet. Tech.*, 1990, 1054.

[11] Richmond, P.C., Watson, A.T.: "Comparison of Implicit and Explicit Methods for Interpreting Displacement Data," *SPE Reservoir Engineering*, Aug. 1990, 389.

[12] Richmond, P.C., Watson, A.T.: "Estimating Multiphase Flow Functions From Displacement Experiments," *SPE Reservoir Engineering*, May 1990, 121.

[13] Sarem, A. M.: "Three-Phase Relative Permeability Measurements by Unsteady-State Method," *Soc. Pet. Eng. J.*, 1966, 199.

[14] Schumaker, L. L.: *Spline Functions: Basic Theory*, John Wiley & Sons, New York (1981).

[15] Watson, A.T., Richmond, P.C., Kerig, P.D., Tao, T.M.: "A Regression-Based Method for Estimating Relative Permeabilities From Displacement Experiments," *SPE Reservoir Engineering*, Aug. 1988, 953.

Paper II

Estimation of Three-Phase Relative Permeability and Capillary Pressure Functions

NORDTVEDT, Jan-Erik, RF-Rogaland Research, NORWAY
LANGAAS, Kaare, RF-Rogaland Research, NORWAY
SYLTE, André, RF-Rogaland Research, NORWAY
URKEDAL, Hege, RF-Rogaland Research, NORWAY
WATSON, A. Ted, Texas A&M University, USA

Paper presented at the 5th European Conference on the Mathematics of Oil Recovery, Leoben, Austria, 3-6 Sept. 1996

ABSTRACT

In this paper, three-phase relative permeability and capillary pressure functions are estimated simultaneously from laboratory experiments. The three-phase flow functions are represented by tensor-product B-splines, and the coefficients in the expansions are determined through solution of a series of linearly constrained nonlinear parameter estimation problems. We demonstrate that data from both two- and three-phase experiments can be reconciled simultaneously by simulations. Measures of the accuracy of the estimates are provided, showing that the flow functions can be accurately determined.

INTRODUCTION

Simulation of fluid flow in porous media is a key exercise for sound reservoir management. The properties of the porous medium must be specified in order to simulate reservoir behavior. For multiphase situations, relative permeability and capillary pressure functions (i.e., the flow functions) are to be specified at all locations throughout the reservoir model. Consequently, accurate determination of multiphase flow functions is an issue of great concern to the oil industry. As there is typically insufficient information to determine reliable estimates of these functions from data gathered from field tests or production history, they are generally determined through analyses of data gathered from laboratory experiments on small porous medium samples. For two-phase situations, accurate determination of the relative permeability and capillary pressure functions is possible from such experiments through solution of the inverse problem associated with the mathematical model of the displacement process and the measured data[7,10,11,16,22]. In this methodology, the flow functions are parameterized, and the parameters that minimize the sum of squared differences between the experimental data and corresponding values calculated through the simulation of the experimental process are determined.

To reveal information about three-phase flow functions, two approaches have traditionally been utilized: one based on prediction of three-phase relative permeability values from two-phase data, and one based on interpretation of three-phase experiments. The first approach (see, e.g., Stone[18]) is very tractable if reliable, as it would make time consuming three-phase experimentation unnecessary. However, even though a number of such models have been proposed (see Baker[1] for an overview), they remain virtually untested since there are insufficient published three-phase relative permeability data available for testing purposes. In the second approach, three-phase relative permeability values have been determined either through steady-state[7,9,14] or unsteady-state experiments[5,21]. In both these types of experiments, the capillary pressure effects have been ignored. Also, the unsteady-state method generally suffers from allowing the relative permeabilities to be functions of one saturation only. Although this may be overcome[21], the problem of error magnification by differentiation of functions defined by noisy experimental data remains. For both types of experiments, only discrete values of relative permeabilities and corresponding saturations have been determined, i.e., the relative permeability *functions* were not estimated.

Recently, Mejia[8] et al. published a method for simultaneous determination of three-phase flow functions. In this work, we further develop that methodology. First, we develop constraints on the three-phase flow functions, and secondly, we address the issue of selecting a flexible functional representation allowing for accurate representation of the true (although unknown) flow functions with a limited number of parameters. Note that in this

approach, each flow function may depend on two saturations, and hence can be represented as a surface when plotted against the saturations. We use tensor product B-splines to represent the surfaces[17]. The parameters in these functions are determined through a series of linearly constrained nonlinear least-squares parameter estimation problems. We demonstrate the methodology using both synthetic as well as experimental three-phase data. To the best of our knowledge, this is the first time that three-phase flow functions have been estimated from experimental data.

METHODOLOGY

The basic methodology we use for estimating the multiphase flow functions is an implicit approach first reported by Mejia[8] et al. The selected experimental design is simulated with a suitable mathematical model of the experiment, and estimates of the multiphase flow functions are obtained so that predictions of the measured data match those obtained during the experiment. Two key components of this process - the selection of functional representations for the unknown properties, and the determination of coefficients within these representations, are discussed below in two subsections.

There is a large variety of experimental designs that can be used for estimating three-phase flow functions. Basically, one can start experiments at saturations for which one, two, or three fluid phases are mobile, and inject, at any fraction, one, two, or three fluid phases. We have directed our work to the use of injection schemes giving average saturation paths similar to those expected for the reservoir flow processes. We have previously investigated different three-phase experimental designs and evaluated the accuracy with which the flow function may be determined through analyses of the corresponding data[20]. In that study, a linearized covariance analysis was utilized. Mejia[8] et al. estimated all flow functions using synthetic data from a single three-phase experiment. Conclusions from these studies are that simultaneous and accurate estimates of the flow functions corresponding to saturation regions spanned by the experiment can be obtained. Here we further these studies by developing constraints on the properties and select parameters within the functional representations that need to be estimated. Also, we develop and test a procedure for estimating those parameters.

We investigate estimation of flow functions from both two-phase as well as three-phase displacement experiments, and utilize pressure drop and production (of two phases) data. We are using data from experiments in which several fluid phases are injected simultaneously into a core sample. In these experiments, we select the rate fractions so that we gradually (in time) access a larger and larger range of saturations (see Nordtvedt[11] et al. and Urkedal[20]et al. for a discussion of this type of experimental design for two-phase and three-phase experiments, respectively). The advantage with this design is that a limited saturation range is accessed for each rate fraction, and hence a time interval will correspond to a certain (and limited) range of saturation. This feature is utilized in our estimation procedure.

Flow Function Representation

A key aspect in estimating multiphase flow functions from measured data is the representation of the unknown functions. It is essential that the functions have sufficient degrees of freedom to represent the true (although unknown) properties; yet, it is desirable that the degrees of freedom be limited whenever there is insufficient information content in the experimental data. B-spline functions have been successfully used for representation of the univariate flow functions when estimating relative permeability and capillary pressure functions from two-phase experiments[7,9,10,11,22]. A key advantage of these functions is the degree of control one can exert through selection of the partition. While any smooth function can be represented arbitrarily accurately with sufficient numbers of knots[17], the representation is also very efficient since relatively few knots, and hence degrees of freedom, can provide for many different function shapes. Through selection of the partition, one can effectively maximize the information content in the experimental data by providing sufficient degrees of freedom in regions where the information content is high, while reducing the degrees of freedom where the experimental data provide relatively little information about the properties.

For situations with three flowing fluid phases, the flow functions are bivariate since the properties may depend upon two saturation values (the third saturation value is not independent). Thus, the relative permeability and capillary pressure functions represent surfaces when plotted as a function of two saturations. We represent each of these properties using two sets of univariate B-splines $\{N_{i_1}(S_1,\bar{y}_1)\}_{i_1=1}^{m_1+K_1}$ and $\{N_{i_2}(S_2,\bar{y}_2)\}_{i_2=1}^{m_2+K_2}$ defined along coordinates S_1 and S_2. S_1 and S_2 may be taken to be any two fluid saturations, or any two linear combination of the saturations. Our selection will be discussed later in this section. $\bar{y}_1$ and $\bar{y}_2$ denote the respective extended partitions ($\bar{y}_i = [y_{i1},\ldots,y_{i,m_i+K_i}]^T$). We define

$$N_{i_1 i_2}(S_1,S_2) = N_{i_1}^{m_1}(S_1) N_{i_2}^{m_2}(S_2) \qquad (1)$$

as the tensor-product B-splines. The space spanned by these $(m_1+K_1)(m_2+K_2)$ bases is a linear space of bivariate polynomial splines of dimension $(m_1+K_1)(m_2+K_2)$ (simple knots are used here). Each function f in this space can be written as a linear combination of the tensor-product B-splines;

$$f(S_1,S_2)=\sum_{i_1=1}^{m_1+K_1}\sum_{i_2=1}^{m_2+K_2}c_{i_1i_2}N_{i_1i_2}(S_1,S_2) \tag{2}$$

The tensor-product B-splines have rectangular support. Using, e.g., quadratic splines ($m_1=m_2=3$) with one interior knot in each coordinate ($K_1=K_2=1$), there will be a total of 16 basis functions and coefficients (i.e., degrees of freedom). Figure 1 illustrates the tensor product basis function generated by the first and the fourth basis functions in coordinate S_1 and S_2, respectively.

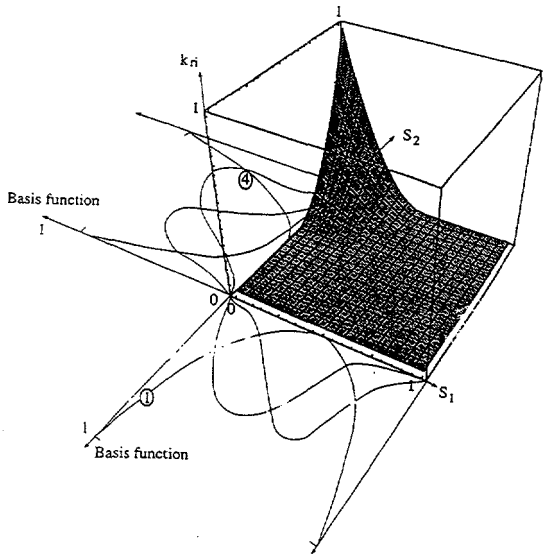

Figure 1: Basis function in the case of quadratic spline functions with one knot in each direction. Basis function N_{14} is shown.

The coordinates S_1 and S_2 are selected for convenience in establishing correct values for the flow functions corresponding to certain lines in the saturation plane. For example, for $k_{ro}(S_w,S_g)$, we know that $k_{ro}=0$ along the line $S_w+S_g=1$. Similar expressions will be valid for each of the two other relative permeabilities as well as the capillary pressures. Thus, to have a simple and uniform manner for constraining the flow functions to zero at specific lines in the plane, we represent the three relative permeabilities through the following tensor-product B-spline expansion:

$$k_{rl}=f(S_1,S_2)\quad \begin{matrix} S_1=S_l \\ S_2=\begin{cases} S_w & if \quad l\neq w \\ S_g & if \quad l=w \end{cases}\end{matrix} \tag{3}$$

The capillary pressures are represented by:

$$\begin{matrix} P_{cow}=f(S_1,S_2) & S_1=S_w \\ P_{cog}=f(S_1,S_2) & S_2=S_g \end{matrix} \tag{4}$$

f is given by Eq. 2.

The tensor-product expansions of the flow functions will contain relatively large numbers of spline coefficients to be estimated. On the other hand, not all saturation values may be encountered in the experiments, so there may be certain regions of the functions which can not be determined from the experimental data (see Urkedal[20] et al. for a discussion). We will reduce the number of parameters to be estimated by including appropriate constraints that represent our knowledge about the functions, and by not attempting to estimate coefficients corresponding to basis function with support in saturation regions which are not represented in the experiment.

The coefficients corresponding to basis functions which have no support inside the accessible saturation region given by $S_1+S_2\le 1$ need not be estimated. The indices (i,j) for these basis functions are implicitly given by:

$$y_{2j}\ge -y_{1i}\quad \begin{matrix} m_1+1\le i\le m_1+K_1 \\ m_2+1\le j\le m_2+K_2 \end{matrix} \tag{5}$$

So, the coefficients c_{ij} for integer values (i,j) satisfying Eq.5 will not be estimated.

Our expectations on admissible values and shapes of the flow functions can be used to reduce the parameter space that needs to be considered. The relative permeability to phase l will be zero whenever $S_l=0$ (similarly for the capillary pressure functions). This condition can be maintained by setting $c_{ij}=0$ for $i=1$ and $j=1,\ldots,m_2+K_2$, for all three phases (see Eq.2). We also expect the flow functions to have the following properties:

$$k_{rl}\le 1 \qquad for \quad S_l=1. \tag{6a}$$

$$\frac{\partial k_{rl}}{\partial S_l}\ge 0 \qquad for \quad 0\le S_l\le 1. \tag{6b}$$

$$\frac{\partial P_{com}}{\partial S_i}\le 0 \quad for \quad i=1,2,\ m=w,g \tag{6c}$$

We have shown that these inequality constraints are linear in the parameters when implemented for any specific saturation value. In principle, monotonicity can be guaranteed by imposing constraints at a finite number of saturation values. In the univariate case, this can be conveniently handled for linear and quadratic splines by use of constraints at the knots[19]. There does not appear to be such a convenient implementation for the bivariate case. However, we have found that when using a limited number of basis functions, implementation of linear constraints at a few hundred saturation values will suffice. All constraints specified by Eq.6 can be implemented as:

$$G\vec{\beta} \le \vec{\beta}^{con} \tag{7}$$

where $\vec{\beta}$ is the collection of all spline coefficients.

These functional representations are quite flexible, and should provide for accurate approximations of the flow functions. The use of these functions for representing relative permeabilities can be illustrated by fitting a tensor-product B-spline surface to a large number of experimental steady-state oil relative permeability points acquired by Oak[13]. To do so, we determine the coefficients that solve the linear least square problem defined by

$$\min \left\| k_{ro}^{cal}(\vec{\beta}) - k_{ro}^{meas} \right\|_2^2 \tag{8}$$

subjected to the constraints given by Eq. 7. In this case, we impose monotonicity constraints at 231 points, giving a total number of 463 constraint equations. The result of the estimation is shown in Figure 2. As can be seen, the tensor-product spline representation provides for a smooth surface that fairly precisely represents the relative permeability values.

Estimation Procedure

To determine flow function estimates, we solve the nonlinear parameter estimation problem defined by

$$J(\vec{\beta}) = \left[\vec{Y}^{cal}(\vec{\beta}) - \vec{Y}^{meas} \right]^T W \left[\vec{Y}^{cal}(\vec{\beta}) - \vec{Y}^{meas} \right] \tag{9}$$

subject to the linear inequality constraints given by Eq.7. Here, $\vec{Y}^{meas}$ and $\vec{Y}^{cal}(\vec{\beta})$ are the measured and predicted data, respectively, and W is the weighting matrix. In this work, we use a fully implicit three-phase, one dimensional black-oil simulator to calculate $\vec{Y}^{cal}(\vec{\beta})$[4]. W is selected to be the inverse of the covariance matrix of the estimate, and hence maximum-likelihood estimates result. The parameter estimation problem is solved using a trust-region based Levenberg-Marquardt algorithm.

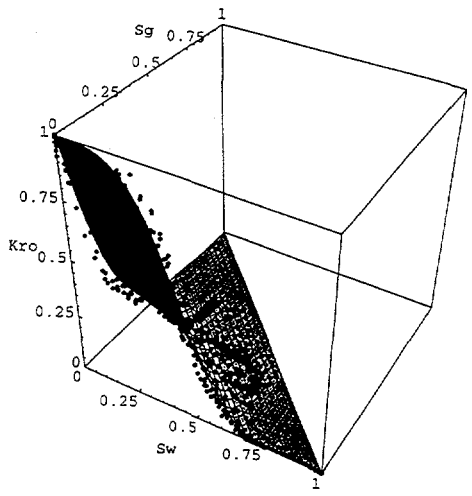

Figure 2: k_{ro} as a function of water and gas saturations estimated from Oak's data[13].

Note that with the approach used here, we can utilize simultaneously data from several separate two- and three-phase experiments. To the best of our knowledge, this is the first time this has been implemented and demonstrated. However, to attempt to solve Eq.9 as a single parameter estimation problem, while including all the data from all the experiments, is not likely to be fruitful because of the large dimensionality of the parameter space. Also, it is likely that local, nonglobal solutions to the problem may result. For two-phase situations, this problem has been solved as a series of minimization problems with increased dimensionalities or as a series of largely decoupled problems. For three-phase problems, we propose the following procedure.

First, we analyze all the available data from the two-phase experiments. Instead of simply estimating the univariate functions, as might typically be done, we use the three-phase representations and estimate only those coefficients corresponding to basis functions that have support in saturation regions accessed by the particular two-phase experiments. The regression-based approach[22] is utilized for selection of the partitions. Analyzing the three-phase data, we start using the partitions and coefficients that will reconcile the two-phase data; hence the flow functions are kept equal to the two-phase estimates in the two-phase regions. Consequently, relatively flexible representations for each of the flow functions are used in the initial phase in the analysis of the three-phase data. We then analyze only parts of the three-phase data, and estimate the parameters corresponding to basis functions with support in the saturation region corresponding to the

data used. With fixed partitions, we gradually increase the amount of three-phase data utilized. Finally, if necessary, we will increase the flexibility of the representations. A knot will be added in a saturation region corresponding to data which are not well matched, and to the function expected to have the highest sensitivity in that saturation region.

For the cases considered here, we have available two-phase oil/water and oil/gas data. From the two-phase estimation, nonzero coefficients corresponding to the basis functions along the two independent directions will result. For the water and gas relative permeability, the only nonzero coefficients will be those corresponding to basis functions along the water and gas saturation axis, respectively. Therefore, we initially keep the oil relative permeability function fixed at the estimate from the two-phase data, and obtain an initial estimate for the water and gas relative permeabilites utilizing all three-phase data. In this estimation, the two capillary pressure functions are also kept at the two-phase estimates. Next, we estimate all flow functions utilizing only data from the first, say, two rate fractions. We estimate the coefficients corresponding to the saturation range spanned by these data. We then increase the amount of data used in the estimation (by including data corresponding to an increased number of rate fractions), and repeat the above described step. Now, coefficients estimated in the previous step can be kept constant, if the added data represent a saturation region not accessed by the corresponding basis functions. We repeat this procedure until no more data is available. This estimation procedure can be used with any combination of two- and three-phase data.

RESULTS AND DISCUSSION

Two test cases are reported to demonstrate the method; one synthetic and one experimental case. In the synthetic case, we generate experimental data using the simulator; the true flow functions are then known. Such cases are very useful for testing purposes, as the error in the estimation can be found directly by comparing the estimated and true functions. The experimental case was designed to determine water, oil and gas relative permeability functions simultaneously with the capillary pressure functions when water is injected into an oil and gas filled zone in the field. Table 1 gives the core and fluid properties for the two cases.

Table 1: Core and fluid properties for the two cases.

	Synthetic Case	Experimental Case
Porosity [frac.]	0.4	0.398
Permeability [mD]	2.0	2.27
Core length [cm]	10.0	12.27
Core area [cm^2]	10.0	11.34
Water viscosity [cP]	1.0	1.280
Oil viscosity [cP]	1.19	1.238
Gas viscosity [cP]	0.02	0.0187
Initial oil saturation [frac.]	1.0	1.0

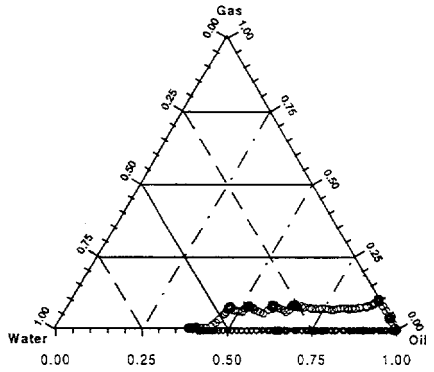

Figure 3: Trajectories for the synthetic case.

Analysis of Synthetic Data

In the synthetic case, two "experiments" were conducted using the simulator. We have chosen to investigate experimental scenarios close to those possible for our experimental apparatus, in order to investigate to what extent and with what accuracy we can expect to determine the flow functions. We select water, oil, and gas to be the three phases, and investigate two different experimental scenarios; one IDC[1] (a two-phase oil/water experiment denoted E1) and one CDI (a two-phase oil/gas experiment) followed by an IDD (E2). Both experiments were started at 100% oil saturation. During the IDD experiment, oil and gas rates were kept constant while the water rate was increased in steps. Figure 3 shows the ternary diagram of the trajectory (i.e., the average saturation of the three phases at different times during the experiments).

In this synthetic case, the true relative permeability functions are represented with tensor-product B-splines

1 The notation IDC refers to increasing water saturation, decreasing oil saturation, and constant gas saturation, and follows Oak[13]. The three letters indicate the direction saturation changes of each fluid phase within the core sample.

of order 3 with two interior knots in each direction (located at 0.3 and 0.6; see Figure 4a) for the true oil relative permeability functions. The capillary pressure functions are kept constant in this analysis, and are represented by univariate B-splines; here we only investigate the estimation of the relative permeability functions. From the simulation of the experiments using the stated relative permeability surfaces, and fluid and core properties as given in Table 1, we select 2320 data points (pressure drops and production of two phases) to be used in the analysis. We add a random error to these "true" data points to simulate the measurement process. This error has zero mean and a given standard deviation; we assumed the standard deviation in the oil production, gas production and the pressure drop to be 0.1 cc, 0.15 cc and 5.0 kPa, respectively. These values are based on an analysis of our experimental equipment[3].

We perform three different estimations in the synthetic case, using different numbers of knots for the relative permeability surfaces:

1. Zero knots in each direction (i.e., a total of 27 parameters);
2. One knot (at 0.45) in each direction (i.e., a total of 48 parameters);
3. Two knots (at 0.25 and 0.55) in each direction (i.e., a total of 75 parameters):

These estimations are performed to illustrate the utility of our estimation procedure and the importance of having a functional representation capable of representing the true (although unknown) properties. The lack of such a representation will result in estimates which depart from the true solution, and the predicted and measured data will not match. This effect has been investigated extensively for two-phase cases (see Kerig and Watson[7]), in which exponential type relative permeability correlations are shown to be inadequate for accurate estimates of the two-phase functions (and for data reconciliation). Here, we show corresponding results for the three-phase case. Note that we have not utilized exponential type relative permeability correlations in this study (as, e.g., suggested by Parmeswar et al.[15]). The lack of success of these models in the two-phase case suggest that they will not be useful for the three-phase case.

The results of the estimation are investigated by examining the final sum of squared residuals (*SSR*) and the number of runs, *R* (i.e., the number of times the time series of the residuals crosses the zero line). By using the inverse of the covariance of the measurements as the weighting matrix, the *SSR* should approach the number of datapoints, *M*. At the same time, *R* should approach $(M + 1) / 2$.

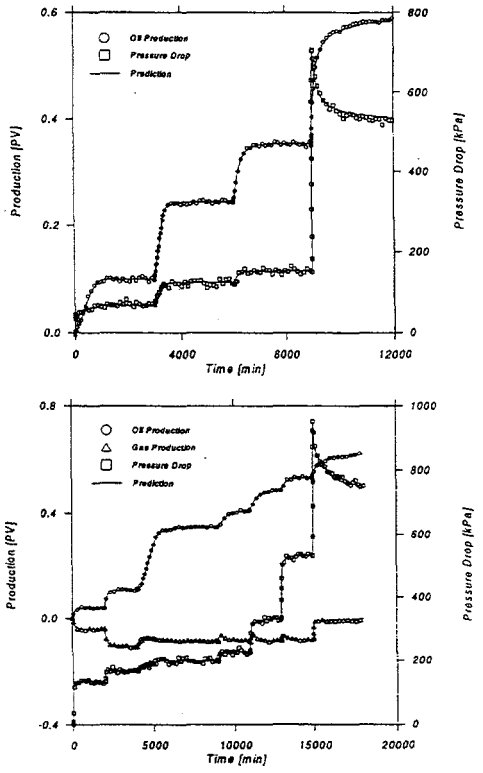

Figure 4: Predicted and measured data for estimated functions with two knots in each direction; Upper figure: Two-phase trajectory results; Lower figure: Three-phase trajectory results.

The *SSR* and *R* values for all these estimations are shown in Table 2. In Figure 4 we show the simulated and experimental data for the case with two knots. The estimated oil relative permeability surfaces are shown in Figure 5. We see that a low estimation error is obtained using two knots for the oil relative permeability. As shown in Table 2, the number of runs and the *SSR* also approach the expected values for the two-knot case. In Figure 6 we show the estimation error (difference between estimated and true relative permeability values) for all the three surfaces. As can be seen, all three functions are accurately estimated in the saturation region for which we have data in the experiments (along the trajectories indicated with a thick line on the plots). Figure 7 shows the error in the estimation of oil relative permeability for the cases with zero, one, and two knots; the estimation error is reduced as the number of knots is increased. Figure 8 shows the confidence intervals at two constant water saturations for the oil relative permeability surface. The confidence intervals calculated using a linearized covariance analysis[20] is consistent with the absolute errors shown in Figure 5c).

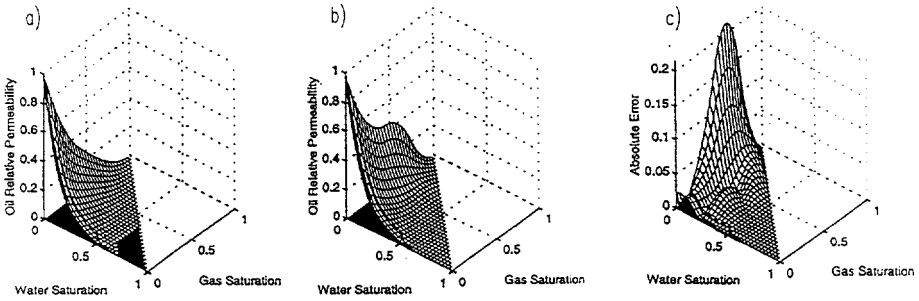

Figure 5: Estimation of k_{ro} with two knots in each direction. a) True k_{ro}.; b) Estimated k_{ro}; c) Absolute error.

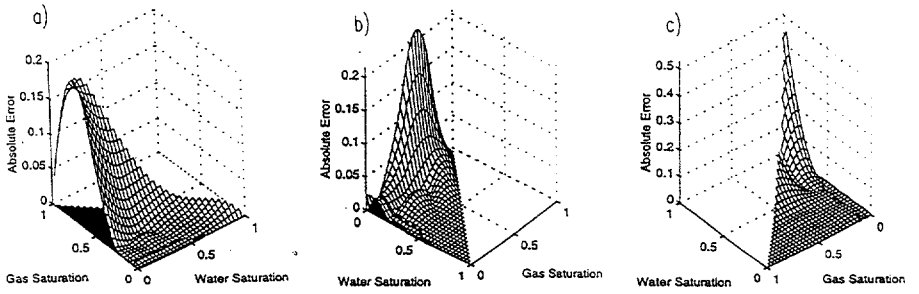

Figure 6: Absolute error for all three relative permeability functions; a) Gas; b) Oil; c) Water.

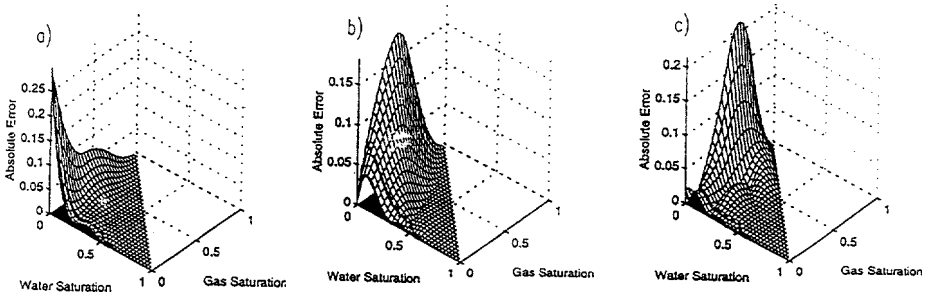

Figure 7: Absolute error for estimated oil relative permeability functions; a) Zero knots; b) One knot; c) Two knots.

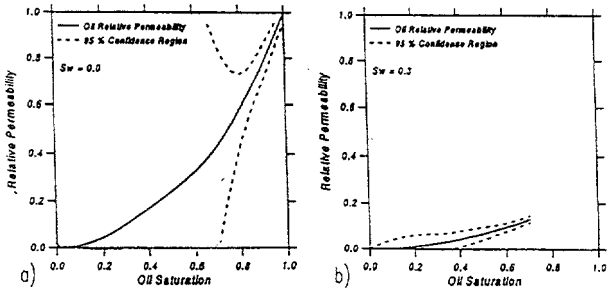

Figure 8: Confidence intervals around true k_{ro} for constant water saturation; a) $S_w = 0$; b) $S_w = 0.3$.

Analysis of Experimental Data

Two experiments were conducted in our three-phase flooding apparatus[3]. Both these experiments were initiated at 100% oil saturation. First, a two phase water-oil flow experiment was conducted (IDC); E1. Upon completion, the core was again brought to 100% oil saturation. Then, a two phase oil-gas flood was conducted to an intermediate gas saturation (a CDI to approximately 40% gas saturation), before water was injected (in a series of steady-state steps) simultaneously with oil and gas (IDD); E2. During the IDD experiment, oil and gas rates were kept constant while the water rate was increased in steps. Figure 9 show the ternary diagram of the trajectory. Production of all phases were measured together with the differential pressure across the sample as a function of time. For details of the experimental apparatus and detailed analyses of results, see Ebeltoft[3] et al. and Nordtvedt[12] et al., respectively.

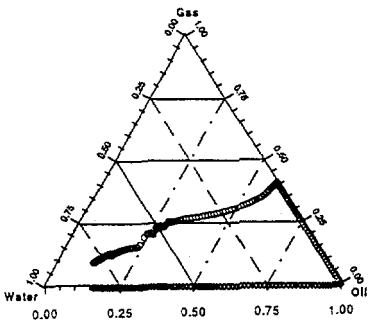

Figure 9: Trajectories for the experimental case.

Table 2: Estimation results for Synthetic Case

	P	*SSR*	*R*
S1: (850 data points)			
Zero knots	8	4161	146
One knot	15	1537	293
Two knots	18	854	396
True partition	18	814	412
S1+S2 (2320 data poinst)			
Zero knots	18	15400	424
One knot	25	7585	617
Two knots	39	2760	1042
True partition	39	2164	1108

In the experimental case, we first estimate the relative permeability to oil and water as well as the oil-water capillary pressure functions from the two-phase oil/water data (Experiment E1; trajectory along the axis with zero gas saturation in Figure 9). An estimate with a quadratic tensor-product B-spline representation for the oil and water relative permeabilities with 4 knots in each direction results. For the oil-water capillary pressure function, we use univariate quadratic B-splines with 6 knots.

We then utilize the two-phase gas-oil data to determine the oil and gas relative permeabilities for zero water saturation (two-phase part of Experiment E2; trajectory along the axis with zero water saturation in Figure 9). The same partition as above was utilized for the oil relative permeability; for gas a quadratic expansion with 4 knots along the water axis and 2 knots along the gas axis was used. The oil-gas capillary pressure was represented by univariate quadratic B-splines with 4 knots.

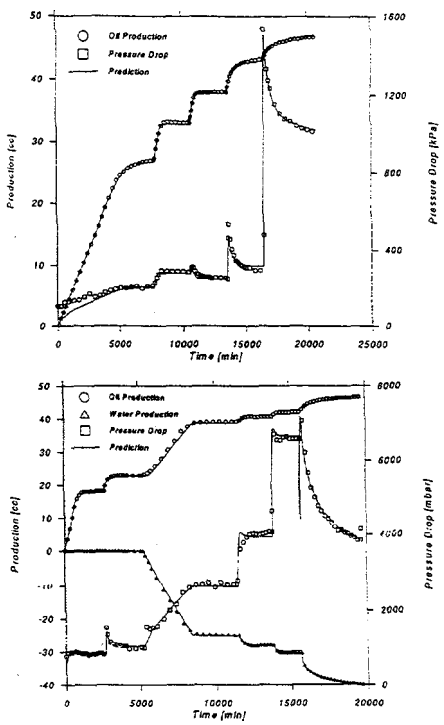

Figure 10: Predicted and measured data for experimental case; Upper figure: Two-phase trajectory results; Lower figure: Three-phase trajectory results.

Finally, we started analyzing the three-phase data (three-phase part of Experiment E2; trajectory into the three-phase region in Figure 9). In this work, we fix the capillary pressure functions at the estimate resulting from the two-phase data (i.e., our estimate of the three-phase capillary pressure is univariate). We follow the estimation procedure outlined above. The estimates of the relative permeability and capillary pressure functions are shown in Figure 11. Figure 10 shows simulated and experimental data. As can be seen, a close match is obtained. To the best of the authors'

knowledge, this is the first time that three-phase flow functions have been estimated from experimental data and that two- and three-phase data have been simultaneously reconciled by simulations.

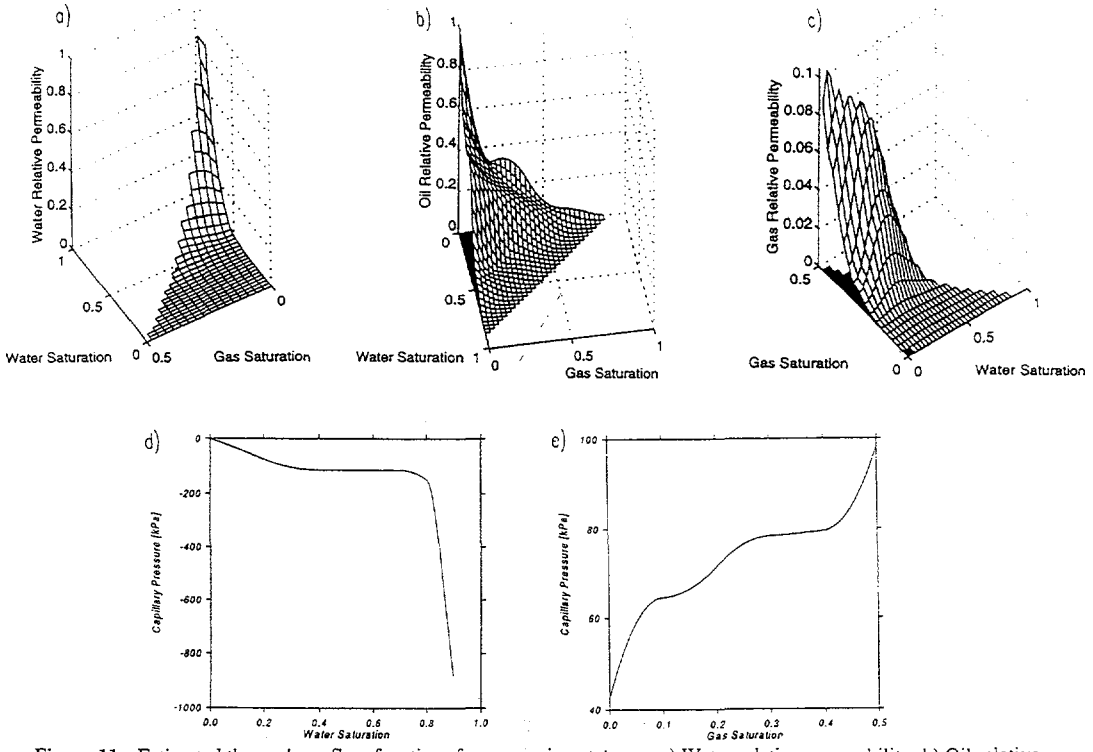

Figure 11: Estimated three-phase flow functions from experimental case; a) Water relative permeability; b) Oil relative permeability; c) Gas relative permeability; d) Oil-water capillary pressure; e) Oil-gas capillary pressure.

CONCLUSIONS

1. We have developed and tested a method for estimating three-phase flow functions using data from several two- and three-phase flooding experiments simultaneously in the analysis. Realistic constraints are imposed on the flow functions, and a regression-based approach is utilized for estimating the functions.
2. For the first time, simultaneous reconciliation of two- and three-phase flooding experiments by simulation has been presented.
3. Our analysis of the synthetic case shows that accurate estimates of the flow functions can be obtained in saturation regions for which we have data.

NOMENCLATURE

$\tilde{\beta}$	Parameters
c	Spline coefficients
f	Function defined by Eq. 2
G	Constraint matrix
K_i	Number of knots in direction i
M	Number of data points
m_i	Spline order in direction i
N	Spline basis function
P	Number of parameters
R	Number of runs
SSR	Sum of Squared Residuals
S	Saturation
$\tilde{Y}$	Vector of data
$\tilde{Y}$	Weighting matrix

Subscript/Superscript

c	Capillary
cal	Calculated
con	Constraint
g	Gas
$meas$	Measured
r	Relative
o	Oil
w	Water

ACKNOWLEDGEMENTS

This work is a part of an RF - Rogaland Research project within three-phase relative permeability estimation. The project is financed by Amoco Norway Oil Company, whose support we gratefully acknowledge. One of the authors (H. Urkedal) is sponsored through our Strategic Institute Program within Advancing System and Parameter Identification. This program is financed by the Norwegian Research Council, whose support we gratefully acknowledge.

REFERENCES

[1] Baker, L.: "Three-Phase Relative Permeability Correlations", *SPE/DOE Symposium on Enhanced Oil Recovery*, Tulsa, USA, 1988.

[2] Corey, A.T., Rathjens, R.J., Henderson, J.H., Wyllie, M.J.: "Three-Phase Relative Permeability", *Trans. AIME*, Vol. 207, 1956, 349.

[3] Ebeltoft, E., Iversen, J.E., Vatne, K.O., Andersen, M.A., Nordtvedt, J.E.: "A Novel Experimental Apparatus for Determination of Three-Phase Relative Permeabilities at Reservoir Conditions", *reviewed proceedings of the 1996 SCA International Symposium*, Montpellier, France, September 8-10, 1996.

[4] Guo, Y.: "Simulation of Three-Phase Core Flood Experiments with CENDRA", RF - Rogaland Research Report *RF-140/93*, Confidential, 1993.

[5] Grader, A.S., O'Meara, D.J.: "Dynamic Displacement Measurements of Three-Phase Relative Permeabilities Using Three Immiscible Liquids", *proceedings of the SPE Technical Conference and Exhibition*, Houston, USA, 1988, 325.

[6] Johnson, E.F., Bossler, D.P., Naumann, V.O.: "Calculation of Relative Permeability from Displacement Experiments", *Trans.; AIME*, 1958, 370.

[7] Kerig, D.P., Watson, A.T.: "A New Algorithm for Estimating Relative Permeabilities From Displacement Experiments", *SPE Reservoir Engineering*, Vol. 2, 1987, 103.

[8] Mejia, G.M., Watson, A.T., Nordtvedt, J.E.: "Estimation of Three-Phase Functions in Porous Media", *AIChE Journal*, Vol. 42, No. 7, 1996.

[9] Nordtedt, J.E., Kolltveit, K.: "Capillary Pressure Curves From Centrifuge Data by Use of Spline Functions", *SPE Reservoir Engineering*, Vol. 6, No. 4, Nov. 1991, 501.

[10] Nordtvedt, J.E., Mejia, G., Yang, P., Watson, A.T.: "Estimation of Capillary Pressure and Relative Permeability Functions From Centrifuge Experiments", *SPE Reservoir Engineering*, Vol. 8, No. 4, Nov. 1993, pp. 292-298.

[11] Nordtvedt, J.E., Urkedal, H., Watson, A.T., Ebeltoft, E., Kolltveit, K., Langaas, K., Øxnevad, I.E.I.: "Estimation of Relative Permeability and Capillary Pressure Functions Using Transient Data from Steady-State Experiments", *reviewed proceedings of the 1994 SCA International Symposium*, Stavanger, Norway, September 12-14, 1994, 197.

[12] Nordtvedt, J.E., Ebeltoft, E., Iversen, J.E., Sylte, A., Urkedal, H., Vatne, K.O., Watson, A.T.: "Determination of Three-Phase Relative Permeabilities From Flooding Experiments", *paper SPE 36683, proceedings of the 71th ATCE 96*, Denver, USA, October 6-9, 1996, to appear.

[13] Oak, M.J.: "Three-Phase Relative Permeabilities of Water-Wet Berea", *SPE/DOE Symposium on Enhanced Oil Recovery*, Tulsa, USA, 1990.

[14] Oak, M.J., Baker, L.E., Thomas, D.C.: "Three-Phase Relative Permeability of Berea Sandstone", *J. Pet. Tech.*, 1990, 1054.

[15] Parmeswar, R., Marefat, N.L.: "A Comparison of Methods for the Representation of Three-Phase Relative Permeability Data", *Proc. California Regional Meeting of SPE*, Oakland, USA, 1986, 151.

[16] Richmond, P.C., Watson, A.T.: "Estimation of Multiphase Flow Functions From Displacement Experiments," *SPE Reservoir Engineering*, Vol. 5, No.1., 1990, 121.

[17] Schumaker, L.L.: *Spline Functions: Basic Theory*, Wiley, New York, 1981.

[18] Stone, H.L.: "Probability Model for Estimating Three-Phase Relative Permeabilities", *J. Petr. Tech.*, 1970, 214.

[19] Tao, T.M., Watson, A.T.: "A Data-Fitting Algorithm With Shape Preserving Features," *AIChE Journal*, Vol. 33, No. 9, 1987, 1567.

[20] Urkedal, H., Langaas, K., Nordtvedt, J.E., Watson, A.T.: "Design of Three-Phase Relative Permeability Experiments", *reviewed proceedings of the 1995 SCA International Symposium*, San Francisco, USA, September 12-14, 1995, 1.

[21] Virnovsky, G.A.: "Determination of Relative Permeabilities in a Three-Phase Flow in Porous Media", *Izv. Akad. Nauk. SSSR. Mekh. Zhidk. Gaza*, No. 5, 1984 (in Russian), *Fluid. Dyn.*, English trans., 1985.

[22] Watson, A.T., Richmond, P.C., Kerig, P.D., Tao, T.M., "A Regression-Based Method for Estimating Relative Permeabilities From Displacement Experiments", *SPE Reservoir Engineering*, Vol. 3, 1988, 953.

Paper III

A New Design of Steady-State Type Experiments for Simultaneous Estimation of Two-Phase Flow Functions

H. Urkedal, E. Ebeltoft, J.E. Nordtvedt; RF-Rogaland Research,
A.T. Watson; Texas A&M University

Summary

We have developed a new design of steady-state type experiments so that relative permeability and capillary pressure functions (collectively called multiphase flow functions) can be estimated simultaneously from all measured pressure drop and production data. The multiphase flow functions are represented by B-splines to ensure a flexible representation, and the coefficients in the representation are determined using a regression-based approach. Through this method of determining relative permeability and capillary pressure functions, we were able to reconcile all pressure drop and production data from the steady-state type experiment conducted. An analysis of the accuracy of the estimated functions showed that they were accurately determined over a large saturation interval.

Introduction

Relative permeability and capillary pressure functions are important properties of porous media and essential for understanding multiphase flow behavior. Accurate estimates of these properties are important input for reservoir production forecasting. Since the reservoir itself is inaccessible for determination of relative permeability and capillary pressure functions, these properties are commonly determined through laboratory experiments on small core samples. Relative permeability and capillary pressure functions are inferred from analysis of various experimental data.

The multiphase flow functions are defined through the system of equations that describes the flow in porous media[11]. The relative permeabilities enter into Darcy's law (or the flow equations) which relates the superficial velocities of each individual phase to the corresponding pressure gradient and viscosity ($u_i = -(kk_{ri}/\mu_i)(\partial P_i/\partial x)$), i.e., the relative permeabilities are empirical properties defined by these equations. Darcy's law is generally assumed to be adequate for describing capillary dominated flow through porous media, i.e., flow for which the capillary number (ratio of viscous-to-capillary forces) is relatively low[3]. As the reservoir flow generally will be capillary dominated (with the possible exception of the near-well flow), the relative permeabilities should be determined in the corresponding capillary number region.

Conventional methods are generally incapable of determining relative permeabilities under such conditions. In the most commonly used method for analyzing unsteady-state data, the Johnson, Bossler, and Neuman[8] method, capillary pressure is neglected altogether. This has computational advantages, as the system of equations describing flow through porous media then can be solved analytically, and relative permeability values are calculated explicitly. Experimentally, elimination of capillary effects would require high injection rates with correspondingly large capillary numbers, possibly

outside the range of interest. The relative permeabilities are computed as points after breakthrough, i.e., on a very limited saturation interval. High flow rates are also required in steady-state experiments[3,5] to overcome capillary effects and get uniform saturation profiles, unless the sample is placed between porous discs (semi permeable membranes). The relative permeability points are computed directly from Darcy's law when the average saturation and the pressure drop across the core are measured. This method gives relative permeability points distributed over the entire saturation interval. In both these methods, the capillary pressure must be found by independent experiments[6,7,15]. This requires multiple experiments on the same core sample, including reestablishing the same initial states and wetting conditions. This procedure is both difficult and time consuming. Therefore, neighboring core samples are often used to determine the flow functions. However, this may lead to errors of unknown magnitude since the properties of core samples may differ even on small scales. It is much more desirable to determine the relative permeability and capillary pressure functions simultaneously and from a single experiment.

By designing experiments so the measured data contain information of both relative permeability and capillary pressure effects, simultaneous estimates of these functions can be found through the solution of the appropriate inverse problem. In such an approach, we estimate porous media properties so that the solution of the mathematical model for the process "matches" the measured data. This methodology has been demonstrated by analyzing both unsteady-state (pressure drop and production data) as well as centrifuge displacement (production data) experiments [16,18]. Although the relative permeability and capillary pressure curves can, in principle, be identified in those conventional experiments[16,18], the accuracy may not be adequate due to insufficient "information content" of the measured data. This situation can be improved by measuring additional data, such as *in situ* saturation or pressure[1,12,13]. However, this approach requires substantial investments in equipment and training, and has not yet been sufficiently demonstrated with actual data.

In this work, we present a method which provides accurate estimates of relative permeability and capillary pressure functions using steady-state equipment and pressure drop and production measurements. We first design a low-rate steady-state type experiment, for which the measured data contain information about relative permeability and capillary pressure effects. During the experiment, we need not wait until a steady-state saturation distribution has been obtained since we utilize all the measured data when estimating the relative permeability and capillary pressure functions. Hence, both time and cost of the experiment is reduced compared to the conventional steady-state experiment. The proposed method reconciles the experimental data and we show it is superior compared to the steady-state method.

New Experimental Design

This section presents a systematic approach for designing experiments leading to simultaneous and accurate estimates of relative permeability and capillary pressure functions, and analyses of the new design. By *design of experiments*, we mean the manner in which the experiments are conducted (e.g., injection /production strategy) and an evaluation of which experimental flooding data should be measured (both type of data and location of each datum as well as the accuracy with which the data will be measured). The experimental design comprises the following steps:

1. Measure core and fluid properties, and give reasonable estimates for the relative permeability and capillary pressure functions.

2. Select a way of conducting the experiment(s). The types of data and location of the data (in time and space) that will be measured in the experiment(s) are predicted from the data given in step 1 using a numerical simulator.

3. Perform a covariance analysis[9] and calculate the confidence intervals around the initial relative permeability and capillary pressure functions based on estimates of the measurement error in the simulated experimental data.

4. Analyze the confidence intervals with respect to desired accuracy in the estimated functions. If the confidence intervals are large, continue from step 2 and select another way to conduct the experiment or include other sets of data.

A variety of different types of data, gathered at different costs may be measured in displacement experiments (see **Fig. 1**). Using different proposed experimental designs, we can compare the relative accuracies of the estimated functions to the different costs of performing the various experiments.

We have considered the design of a drainage experiment, and investigated three different injection schemes, referred to as Case A-1, Case A-2, and Case A-3 in **Table 1**. The core and fluid properties in these simulated drainage experiments are those referred to as Case A in **Table 2.** In this design phase, we want to investigate whether there is an injection scheme for the steady-state type experiment that will provide pressure drop and production data with sufficient information content so that both relative permeability and capillary pressure functions can be accurately estimated. That is, we want to find a way of conducting the experiment so that the flow functions can be estimated with acceptable accuracy without including *in situ* data.

Simulated data for Case A-1 (one injection step) and Case A-2 (two injection steps) are plotted in **Fig. 2a**, while **Fig. 2b** shows the data for Case A-3 (six injection steps). The impact of measurement error on estimated flow functions is computed using a linearized covariance analysis; see **Appendix A** for details on this analysis. The 95% confidence intervals are computed and plotted around the relative permeability and capillary pressure functions for each case, see **Fig. 3**. For Case A-1, the generally wide confidence intervals show that the data contain little information about the relative permeability and capillary pressure functions for water saturation from 1.0 down to 0.5. In Case A-2 the confidence intervals are generally more narrow. This is due to the two-step injection scheme where data are measured during two breakthrough sequences, and consequently the information content in these data is higher. For every case, the confidence intervals become very large when the water saturation is less than 0.2, as saturation does not take on values in that range during the experiments (0.2 is approximately the lowest water saturation in all three cases after the oil injection, see saturation profiles for Case A in **Fig. 4**, solid line). By injecting oil in two steps as in Case A-2, we decrease the confidence intervals in **Fig. 3**, but they are still not satisfactory. A further reduction in the confidence intervals can be achieved by including other sets of data[13] (i.e., saturation profiles or *in situ* pressure and saturation data). However, the narrow confidence intervals in **Fig. 3** for Case A-3 show that an injection strategy with six rate fractions with production and pressure drop data

measurements will provide accurate estimates of the relative permeability and capillary pressure functions in saturation regions corresponding to those where experimental data are represented, i.e., from water saturation equal to 1.0 and down to approximately 0.2.

We have also used the experimental design to evaluate how estimates will depend upon the degree of capillary effects. We compare two cases; Case A (low absolute permeability) and Case B (high absolute permeability). The relative permeability functions are set equal for these two cases, but the capillary pressure is reduced for Case B with a factor of 10. The calculated steady-state equilibrium relative permeability points are plotted in **Fig. 3a,b**, and the saturation profiles in **Fig. 4**. These points are not accurate estimates of the relative permeability. The reason for the errors is that the saturation distributions are not uniform, as is assumed in the steady-state analysis. **Fig. 4** shows that the degree of capillary effects is most pronounced for the high permeability case, i.e., the saturation profiles are non-uniform throughout the entire core sample. In the low absolute permeability case the saturation profile is uniform except at the end of the core due to the capillary end effects. So, even though the two cases reach almost the same average saturation, the shape of the saturation profiles in Case B show that the capillary forces dominate the flow in the entire core, while fore Case A the capillary forces only cause a small end effect. This indicates that data from a high permeable medium might contains more information about the capillary pressure, and consequently, the capillary pressure function can be estimated more accurately than for a low permeable medium.

We have plotted the pressure drop and production data for Case A and Case B in **Fig. 5a,b**. Here we compare the data computed using the steady-state relative permeability equilibrium points, as plotted in **Fig. 3a,b**, with the true data. A B-spline[19] function is fitted to these points and then used to simulate pressure drop and production data. These figures show that the equilibrium relative permeabilities do not reconcile the true data, and this will be more pronounced for high absolute permeability cases, i.e., for cases with higher degree of capillary effects.

These results show that the conventional way of conducting steady-state experiment do not provides for accurate determinations of relative permeabilities. Now, we want to demonstrate the new methodology when relative permeabilities and capillary pressure functions are simultaneously estimated from conventional data measured during steady-state type experiments.

Estimation of Flow Functions

The relative permeability and capillary pressure functions are represented by B-splines[19] and given as

$$k_{ri}(S_w) = \sum_{j=1}^{N_i} C_j^i B_j^m(S_w, \vec{y}^i), \quad i = w, nw \tag{1}$$

$$P_c(S_w) = \sum_{j=1}^{N_c} C_j^c B_j^m(S_w, \vec{y}^c). \tag{2}$$

The functions are defined on $0 \le S_w \le 1$ and are specified by the order m, the spline coefficients C and the extended partition $\vec{y}$. The vector of unknown parameters becomes

$$\vec{\beta} = \left[C_1^{nw}, \ldots, C_{N_{nw}}^{nw}, C_1^{w}, \ldots, C_{N_w}^{w}, C_1^{c}, \ldots, C_{N_c}^{c} \right]. \tag{3}$$

The parameter vector $\vec{\beta}$ is estimated in a regression-based approach[22]. We seek a solution to the non-linear least squares problem defined by

$$J(\vec{\beta}) = \left[\vec{Y}_m - \vec{Y}_s(\vec{\beta}) \right]^T \mathbf{W} \left[\vec{Y}_m - \vec{Y}_s(\vec{\beta}) \right], \tag{4}$$

subject to the constraints $\mathbf{G}\vec{\beta} \ge \vec{b}$. Here $\vec{Y}_m$ is a vector containing the measured data while $\vec{Y}_s(\vec{\beta})$ contains the corresponding values calculated using a mathematical model for the process (in this work, the fully implicit core flood simulator CENDRA[4] has been utilized), and $\boldsymbol{G}$ and $\vec{b}$ are a constraint matrix and vector, respectively. $\mathbf{W}$ is the weighting matrix. By choosing $\mathbf{W}$ to be the inverse of the covariance matrix of the measurements ($\mathbf{W}=\Sigma^{-1}$), the solution of Eq. 4 becomes the maximum-likelihood estimates of the parameters, $\vec{\beta}$. Details on the estimation algorithm can be found in Richmond[17].

In the cases investigated here, particular characteristics of the steady-state process are used to help select the extended partition. Consider, for simplicity, a primary drainage process (similar arguments are valid for secondary drainage as well as an imbibition process). After injection at the initial rate fraction has begun, the wetting phase saturation will decrease, eventually approaching equilibrium. The data collected during that period reflect the relative permeability and capillary pressure curves for a range of saturations from unity down to the minimum wetting saturation in the sample, say $S_{w,1}$ (see the plot of saturation profiles in **Fig. 4**). As the rate fraction of the non-wetting phase is increased, the measured data will reflect a larger range of saturations. Data corresponding to the *n*th rate fraction will reflect the relative permeability and capillary pressure curves corresponding to a range of saturations from unity down to $S_{w,n}$, where $S_{w,n}$ represents the lowest saturation value experienced in the *n*th rate fraction. All the $S_{w,i}$ values will form a descending sequence. This feature can be utilized beneficially in selecting the extended partition.

In this work, we investigate the residuals (i.e., $\vec{Y}_m - \vec{Y}_s(\vec{\beta})$), corresponding to the sequence of rate fractions, in order to locate the first rate fraction for which the data are not well predicted (i.e., has large residuals). By inspecting the saturation profiles corresponding to that rate fraction, the saturation region for which the properties are not well determined will be obtained. Flexibility is then added by inserting a spline knot in the saturation region that is least well determined and to the function which we consider to have the largest impact in that region.

An initial estimate of the relative permeability functions may be obtained by fitting a spline function to the relative permeability points obtained from Darcy's law using the equilibrium (or near equilibrium) data.

Results and Discussion

Demonstration of Methodology. To demonstrate how experiments are designed and flow functions estimated from the measured data, a simulated case is first considered. Relative permeability and capillary pressure functions are plotted in **Fig. 6c,d**. Cubic splines were used to represent the functions, including 4, 4, and 5 interior knots for the water and oil relative permeability and capillary pressure functions, respectively. Core and fluid properties (see Case A in **Table 2**) were selected. Based on the previous discussion on different experimental designs, the new design of steady-state type experiments with a six step injection scheme has been used (see Case A in **Table 3**). The simulator CENDRA was then used to compute pressure drop and production data. Random errors, with zero mean and a given standard deviation, were drawn from a normal distribution and added to the simulated data, giving us a set of synthetic data.

We estimated the relative permeability and capillary pressure functions using the procedure described in the previous section. We started with an initial guess of the relative permeability and capillary pressure functions where the partition (the way the spline knots were distributed) was different from the true one for each function. For the relative permeability functions, we used the steady-state relative permeability points as an initial estimate. By systematically adding knots (and thereby flexibility) to the flow functions, an improved match between the synthetic and estimated data was obtained. **Fig. 6a** shows the results from the estimation and **Fig. 6b** the residuals ($\vec{Y}_m - \vec{Y}_s(\vec{b})$). The match was very good as seen from the residual plot. The residuals of the production oscillate around zero with a mean residual of approximately 0.005, which is the value of standard deviation of the noise we added to the data. The noise we added to the pressure drop data increased after 7000 minutes (due to increasing pressure drop) and this is seen as an increase in residuals from 5 to 14 kPa. **Table 4** lists some statistical results for this case. The sum of squared residuals is satisfactory since the quantity $\sqrt{\frac{SSR}{M-N-1}}$ gives a reasonable estimate of the standard deviation in the data (which is known when we are working with synthetic data). $\frac{SSR}{M-N-1}$ is an unbiased estimator of σ^2 (the variance of each measurement)[2]. The number of runs are approximately the same as the expected value, which is $\frac{M}{2}+1$. The number of runs tells how often the residual is crossing the zero line. This property gives additional information to the SSR when we want to determine if bias error is present in our estimates (for further details on errors in measurements, see Watson *et al.*[21]). Since the SSR and the number of runs are close to the expected values for these quantities, the estimated functions must be close to the true functions.

The estimated and true flow functions with 95% confidence intervals are plotted in **Fig. 6c,d**. Here, the 95% confidence intervals are computed around the estimated functions, and the true functions are within these intervals. The plots in **Fig. 6a,b** show that we can reconcile the measured pressure drop and production data, and that we can estimate the "true" relative permeability and capillary pressure functions simultaneously. This design of experiments for estimating flow functions has also been used for estimating three-phase relative permeability functions (see Urkedal *et al.*[20] and Nordtvedt *et al.*[14]).

Experimental results. The proposed method to determine relative permeability and capillary pressure functions has been used with experimental data. A reservoir condition steady-state flow apparatus was utilized[5] for acquiring experimental data. The apparatus consists of three major parts: a pumping system, a core holder, a high resolution

differential pressure transmitter, and an acoustic separator. These parts are assembled in order to recycle two phases simultaneously through a core sample with accurate and virtually pulse free flow rates. Production from the core sample and differential pressure across the sample are continuously monitored as a function of time. Both data acquisition and monitoring of the apparatus are automated, and performed by a personal computer; see **Appendix B** and **Fig. 9** for details.

The core used was an outcrop chalk sample from the Turonian Seaton Chalk Formation ("Beer Stone") in Devon, Southern England[23]. It was selected on the basis of having relatively homogenous CT-scan images. The core was cleaned with solvents and dried before testing, and it was water-wet. Mineral oil (Exxon Isopar H) was used as the oil phase and a simulated North-Sea chalk formation water as the water phase. Calcium is added to the formation water to ensure chemical stability of the chalk matrix. Basic core data and fluid properties are listed in **Table 2**. The new experimental design was used; details on the rate fractions are listed in **Table 3**.

The relative permeability and capillary pressure functions were estimated using the same procedure as with the synthetic data set, demonstrated in the previous section. The match between experimental and estimated data is plotted in **Fig. 7a**, and **Fig. 7b** shows the residuals. A very good agreement between the experimental and predicted pressure drop and production data is obtained. **Table 4** lists the statistical data for the experimental case. The values of the SSR for pressure drop and production data are in agreement with the estimated standard deviation for these data (estimates of measurement errors are based on analysis of experimental equipment) and a further reduction will not likely be obtained. Still, we see that the number of runs are below the expected value. This is the result of some bias error in our estimates which is seen in the residual plot when the residuals are not oscillating around zero.

The estimated functions (see **Fig. 7c,d**) were quite flexible by the end of the estimation, with seven interior knots each in the spline partition. The 95% confidence intervals computed and plotted around the estimated functions are quite narrow, which means that the information content of the data is relatively large. The steady-state equilibrium relative permeability points have been computed and plotted together with the estimated functions. These points are only equal to points on the estimated functions for water saturation higher than 0.8. This deviation shows that effects of capillary pressure are significant. This is consistent with the relatively narrow confidence intervals around the estimated capillary pressure functions (see **Fig. 7d**). For water saturations below 0.2, the confidence intervals are large since saturation does not take on values in that range during the experiment. Nevertheless, estimates of the functions are obtained. This has been done to avoid making *a priori* assumptions with respect to irreducible water saturation in the analyses (i.e., the irreducible water saturation has been kept equal to zero throughout the analyses). This is desirable as there is generally no *a priori* information available about the irreducible water saturation.

The capillary pressure estimate has been compared to two other experimental techniques; both the micro-membrane[7] as well as the mercury injection techniques have been utilized to obtain independent estimates (see **Fig. 7d**). In both these cases, the capillary pressure curves are obtained on a neighboring sample. This sample had a somewhat different permeability and porosity from the one used in the steady-state type experiment. The mercury injection and micro membrane curves in **Fig. 7d** are therefore

scaled so that the capillary pressure curves should be comparable to the capillary pressure function for the test sample considered here. This scaling is done using the so called Leverett J-function[10]. As can be seen from **Fig. 7d**, the three techniques provide very similar results except for high saturation values.

Finally, we compared the pressure drop and production data predicted from the steady-state relative permeability points with the results obtained from estimation of the flow functions. We fitted a smooth monotonic B-spline function through the equilibrium points in **Fig. 7c**, but kept the water relative permeability non-zero until zero water saturation to avoid the water-cut we otherwise would experience. Then the numerical simulator CENDRA was used to predict the pressure drop and production data. These data are plotted together with the estimated and experimental data in **Fig. 8**. These figures show that it is impossible to reconcile the experimental pressure drop and production data using the conventional equilibrium steady-state relative permeability points.

Conclusions

1. A method for simultaneous determination of relative permeability and capillary pressure functions from pressure drop and production data measured during steady-state type experiments has been developed and tested.

2. All experimental data are reconciled by simulation.

3. The accuracy of the estimates has been calculated using a linearized covariance analysis. The analysis shows that the relative permeability and capillary pressure functions can be determined accurately over a large saturation range.

4. The feasibility of the method has been demonstrated by analyzing simulated and actual experimental data. For the experimental case, the estimated capillary pressure is consistent with independent estimates using the micro membrane and mercury injection techniques.

Nomenclature

$\vec{a}$	Sensitivity coefficient
A	Sensitivity of simulated data to parameters
$\vec{b}$	Constrained vector
$\vec{b}$	Estimate of $\vec{\beta}$
B	Spline basis function
$\vec{\beta}$	Vector of unknown parameters
C	Spline coefficients
C	Covariance of estimated flow functions
D	Sensitivity of flow functions to parameters
G	Constraint matrix
J	Objective function
k	Permeability
M	Number of measured data
m	Spline order
μ	Viscosity

N Dimension of spline
N_c Capillary number
N_P Number of points in flow function table
P Pressure
P Covariance of estimated flow function parameters
S Saturation
σ Interfacial tension
u Darcy velocity
W Weighting matrix
x Length coordinate
$\bar{y}$ Spline partition
$\bar{Y}$ Vector of measured or simulated data
Σ Covariance of measurements

Subscripts

c Capillary
m Measured
nw Nonwetting phase
r Relative
s Simulated
w Wetting phase

Superscripts

c Capillary
nw Nonwetting phase
w Wetting phase

Acknowledgments

This work is a part of an RF - Rogaland Research multidisciplinary Strategic Technology Program for improved chalk characterization. The program is financed by the Norwegian Research Council, whose support we gratefully acknowledge.

References

1. Chardaire-Rivere, C., Forbes, P., Zhang, J.F., Chavent, G., Lenormand, R.: "Improving the Centrifuge Technique by Measuring Local Saturations," proceedings of the 67th Annual Technical Conference and Exhibition of the Society of Petroleum Engineers, Washington, DC, 1992, 193.

2. Dougherty, E.R.: *Probability and Statistics for the Engineering, Computing and Physical Science*, Prentice-Hall Inc., USA, 1990.

3. Dullien, F.A.L.: *Porous Media: Fluid Transport and Pore Structure*, Academic Press, Inc., 2nd ed., 1992.

4. Guo, Y., Nordtvedt, J.E., Olsen, H.: "Development and Improvement of CENDRA+," report RF-183/93, Confidential.

5. Guo, Y., Vatne, K.O.: "Use of a New Generation Recirculation System for Steady-State Relative Permeability Measurement," proceedings of the 7th European IOR Symposium, Vol. 1, Moscow, Russia, 1993, 161.

6. Hassler, G.L., Brunner, E.: "Measurement of Capillary Pressure in Small Core Samples," Trans., AIME, 1945, 114.

7. Hammervold, W.L., Skjæveland, S.M.: "Improvement of Diaphragm Method for Capillary Pressure Measurements with Micro Pore Membrane," Advances in Core Evaluation III, Gordon and Breach Sci. Publ., 1992, 91.

8. Johnson, E.F., Bossler, D.P., Naumann, V.O.: "Calculation of Relative Permeability from Displacement Experiments," Trans., AIME, 1958, 370.

9. Kerig, P.D., Watson, A.T.: "Relative Permeability Estimation From Displacement Experiments: An Error Analysis," SPE Reservoir Engineering, Jan. 1986, 175.

10.Leverett, M.C.: "Capillary Behavior in Porous Solids," Trans., AIME, 1941, 152.

11.Marle, C.M.: *Multiphase Flow Functions in Porous Media*, Editions Technip, Paris, 1981.

12.Mejia-Velazquez, G.M.: "A Method for Estimating Three-Phase Flow Functions," PhD Dissertation, Texas A&M University, College Station, TX, Aug. 1992.

13.Mejia-Velazquez, G.M., Mohanty, K.K., Watson, A.T.: "Use of *In Situ* Data in Estimation of Two-Phase Flow Functions in Porous Media," International Journal of Petroleum Science and Engineering, 1996.

14.Nordtvedt, J.E., Ebeltoft, E., Iversen, J.E., Sylte, A., Urkedal, H., Vatne, K.O., Watson, A.T.: "Determination of Three-Phase Relative Permeabilities From Displacement Experiments," proceedings of the SPE Annual Technical Conference and Exhibition, Dallas, Colorado, USA, Oct. 6-9, 1996.

15.Nordtvedt, J.E., Kolltveit, K.: "Capillary Pressure Curves From Centrifuge Data by Use of Spline Functions", SPE Reservoir Engineering, Nov. 1991, 497.

16.Nordvedt, J.E., Mejia, G., Yang, P.-H., Watson, A.T.: "Estimation of Capillary Pressure and Relative Permeability Functions From Centrifuge Experiments," SPE Reservoir Engineering, Nov. 1993, 292.

17.Richmond, P.C.: "Estimating Multiphase Flow Functions in Porous Media From Dynamic Displacement Experiments," PhD Dissertation, Texas A/M University, College Station, TX, Dec. 1988.

18.Richmond, P.C., Watson, A.T.: "Estimating Multiphase Flow Functions From Displacement Experiments," SPE Reservoir Engineering, May 1990, 121.

19.Schumaker, L.L.: *Spline Functions: Basic Theory*, J. Wiley & Sons Inc., New York City (1981).

20.Urkedal, H., Langaas, K., Nordtvedt, J.E., Watson, A.T.: "Design of Three-Phase Relative Permeability Experiments," Reviewed proceedings of the 1995 International Symposium of the Society of Core Analysts, San Francisco, California, Sept. 12-14, 1995.

21. Watson A.T., Lane H.S., Gatens J.M.: "History Matching With Cumulative Production Data", JPT, January 1990.

22.Watson, A.T., Richmond, P.C., Kerig, P.D., Tao, T.M.: "A Regression-Based Method for Estimating Relative Permeabilities From Displacement Experiments," SPE Reservoir Engineering, August 1988, 953.

23.Øxnevad, I.E.I., Bonnell, L., Nordtvedt, J.E.: "Improved Reservoir Characterization," proceedings of the EAPG/AAPG Special Conference on Chalk, Copenhagen, Denmark, Sept. 7-9, 1994.

Appendix A - Linearized Covariance Analysis

A linearized covariance analysis is utilized to obtain an estimate of the accuracy of the estimated functions[9]. In this analysis it is assumed that the selected functional representation, B-splines[19], adequately represent the true (although unknown) functions. It is further assumed that the simulator adequately represents the physics of flow through porous media and that the measurement errors are additive. The analysis is based upon the assumption that the objective function, **Eq. 4**, may adequately be approximated in a sufficiently large parameter region near the true parameter values, $\vec{\beta}$, by a function that is linear in the parameters. By Taylor expansion of $J(\vec{b})$ where $\vec{b}$ is the estimate of $\vec{\beta}$

$$J(\vec{b}) \approx J(\vec{\beta}) + \frac{\partial J(\vec{\beta})}{\partial \vec{\beta}}(\vec{b}-\vec{\beta}) + (\vec{b}-\vec{\beta})^T \frac{\partial^2 J(\vec{\beta})}{\partial \vec{\beta}^2}(\vec{b}-\vec{\beta}), \tag{A.1}$$

it can be shown[9] that a linear relationship exists between the parameter errors and the errors in the measurements:

$$\mathbf{P}_{N\times N} = (\mathbf{A}^T \boldsymbol{\Sigma}^{-1} \mathbf{A})^{-1}, \tag{A.2}$$

where the sensitivity matrix for the simulated data with respect to the parameters is defined as

$$\mathbf{A}_{M\times N} = \left[\frac{\partial \vec{Y}_S(\vec{\beta})}{\partial \vec{\beta}} \right]. \tag{A.3}$$

By assuming a normal distribution for the measurement errors, pointwise confidence intervals for the relative permeability and capillary pressure functions may be calculated from the covariance matrix of the estimated functions

$$\mathbf{C}_{N_p\times N_p} = \mathbf{D}^T (\mathbf{A}^T \boldsymbol{\Sigma}^{-1} \mathbf{A})^{-1} \mathbf{D} = \mathbf{D}^T \mathbf{P} \mathbf{D}, \tag{A.4}$$

where the sensitivity in the flow functions with respect to the parameters in the representation of the functions is given as

$$\mathbf{D}_{N_p\times N} = \left[\frac{\partial f(\vec{\beta})}{\partial \vec{\beta}} \right], \tag{A.4}$$

where $f(\vec{\beta})$ represent the flow functions dependent on the parameter vector $\vec{\beta}$.

Appendix B - Steady-State Experiment

A schematic of the two-phase flow apparatus is shown in **Fig. 6**. The main parts of the apparatus are a pumping system, a two-phase separator, and a core holder.

The pumping system consists of five computer controlled cylinders that have the capability of recycling two phases simultaneously through a core sample. The cylinders

are paired, and two cylinder pairs act as pumps for recycling water and oil (or a gaseous phase), respectively. Each phase is pumped into the core sample with accurate and virtually pulse free flow rates. For each of the cylinder pairs, one cylinder delivers fluid into the sample, while the other receives fluid through the return line from the separator. The receiving cylinder runs at a slightly higher rate than the delivering cylinder, which implies that the receiving cylinder is ready to deliver fluid into the sample before the delivering cylinder is empty. By continuously adjusting the rates and the pressures, the take-over between the cylinders in one pump can occur smoothly. The fifth cylinder is working in a constant pressure mode, and acts as a back pressure regulator within 7 kPa accuracy. This cylinder is connected to the water return line, but is in contact with both phases indirectly through the separator. It provides for an excellent back pressure control, and tracks any leakage that might occur throughout the experimentation. The flow rates are adjustable from 0.5 µl/min to 10 ml/min.

A two-phase separator is used for volume detection. It is an acoustic separator used for separation of produced fluids, and for continuously monitoring the production from the outlet face of the core sample. In the separator, two bores are connected to each other, and fluid from the core sample enters in one of the bores at the bottom of the separator, where they are separated. The other bore is the measuring bore, and is connected to the separation bore by two channels, one at the top of the separator and one at the bottom. An acoustic transducer is located in the bottom of the measurement bore. Through measurements of the time for an acoustic wave (generated by the transducer) to echo off the interface between the water and oil phase and a calibration stub, the distance from the transducer to the interface can be determined. From this measurement, the water volume in the separator may be calculated. The static accuracy of the volume determination is ± 0.01 ml, while the dynamic accuracy is empirically determined to be ± 0.07 ml. The accuracy is poorer when the phases are recycled due to the different rates of the delivering and receiving cylinders in one pump. This involves that cylinder five is compensating for a pressure loss caused by the higher rate of the receiving cylinder. As a consequence, the meniscus in the separator will continuously be moving up and down. The shape of the meniscus will change with the direction of movement, and hence a hysteresis effect in the volume measurements will occur. However, we have minimized this effect by covering the bores with a layer of Teflon, and thus rendered the wettability of the bore surfaces close to a neutral state.

A hydrostatic core holder is used in the apparatus. The inlet distribution plug has two separate spiral grooves for water and oil, ensuring distribution of both phases across the entire core inlet face, and a pressure port in the centre. The outlet distribution plug is of conventional type with three concentric rings and cross-hatch every 45 degrees. A wire screen is placed on the outlet distribution plug to minimize particle washout and to ensure uniform fluid flow across the outlet end face. A non-flexible stainless steel support screen with no vertical flow possibilities is placed toward each core face to prevent the relatively soft chalk sample being forced into the grooves forming the distribution plugs. Several rubber washers are placed behind each distribution plug to transmit an axial stress proportional to the confinement pressure. The core sample is completely covered with Teflon tape and a hydrogenated nitrile sleeve.

The pressure drop across the core sample is measured by a high resolution differential pressure transmitter with adjustable range. The range is zero to 3 MPa, and the accuracy during re-circulation is within 1% of the measured value.

The pumps, the separator and the core holder are all placed in a heating cabinet, and provide a closed loop and recycling of both phases up to reservoir conditions. The apparatus is capable of running either steady-state type experiments or unsteady-state type experiments, i.e. either one or two phases can be simultaneously injected into the core sample. The monitoring of the apparatus and data acquisition (pressures, volumes, temperature etc.) are automated and performed by a personal computer.

TABLE 1 - INJECTION RATES, q_o/q_w [cc/min]	
Case A-1	1.0/0.0
Case A-2	0.06/0.04, 1.0/0.0
Case A-3	0.001/0.099, 0.016/0.084, 0.060/0.040, 0.094/0.006, 0.040/0.001, 1.0/0.0

TABLE 2 - CORE AND FLUID PROPERTIES			
	Case A	Case B	Exp.
Oil viscosity [cP]	1.2	1.2	1.19
Water viscosity [cP]	0.9	0.9	1.097
Core length [cm]	6.0	6.0	6.81
Core area [cm^2]	11.1	11.1	10.927
Porosity [%]	40.0	40.0	28.4
Abs. permeability [md]	**1.0**	**100.0**	4.17
S_w, initial [frac.]	1.0	1.0	1.0

TABLE 3 - INJECTION RATES [cc/min]			
	Case A	Case B	Experiment
1) q_w/q_o	0.099/0.001	0.098/0.002	0.099/0.001
2) q_w/q_o	0.084/0.016	0.084/0.016	0.088/0.012
3) q_w/q_o	0.040/0.060	0.040/0.060	0.040/0.060
4) q_w/q_o	0.006/0.094	0.001/0.099	0.0/0.10
5) q_w/q_o	0.001/0.400	0.001/0.500	0.0/0.25
6) q_w/q_o	0.0/1.0	0.0/4.0	0.0/1.0
7) q_w/q_o			0.0/3.0

TABLE 4 - STATISTICAL DATA							
	#Points (M)	#Param. (N)	SSR	$\sqrt{\frac{SSR}{M-N-1}}$	$\hat{\sigma}$	RUNS obs.	RUNS expected
Case A, ΔP (kPa)	433	26	54564.0	11.2	5.0	225	218
Case A, V_{prod} (frac.)	417	26	0.00464	0.0033	0.005	204	210
Exp., ΔP (kPa)	366	21	20672.4	7.5	2.0	41	184
Exp., V_{prod} (frac.)	337	21	0.00518	0.0039	0.005	76	170

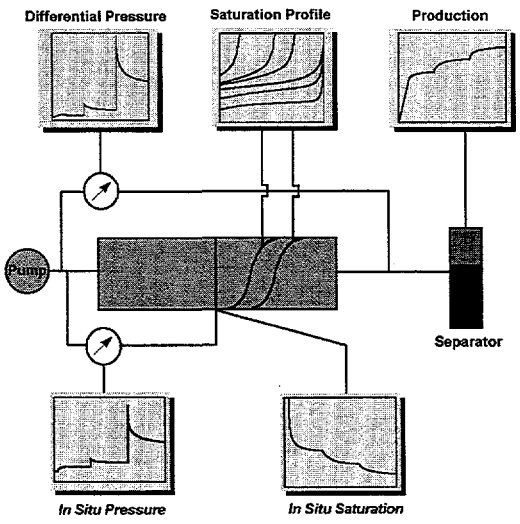

Fig. 1 - Different types of data gathered from displacement experiments.

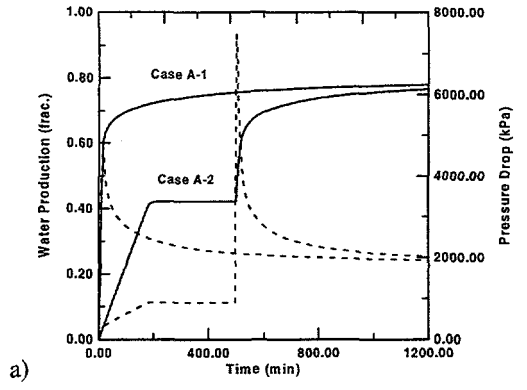

a)

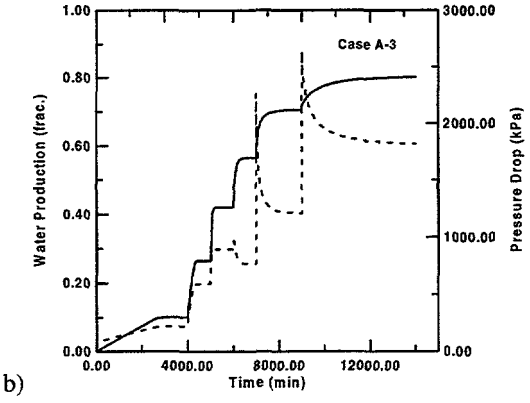

b)

Fig. 2 - Production (solid line) and pressure drop (dotted line) data for; a) Case A-1 (one injection step) and Case A-2 (two injection steps), and b) Case A-3 (six injection steps).

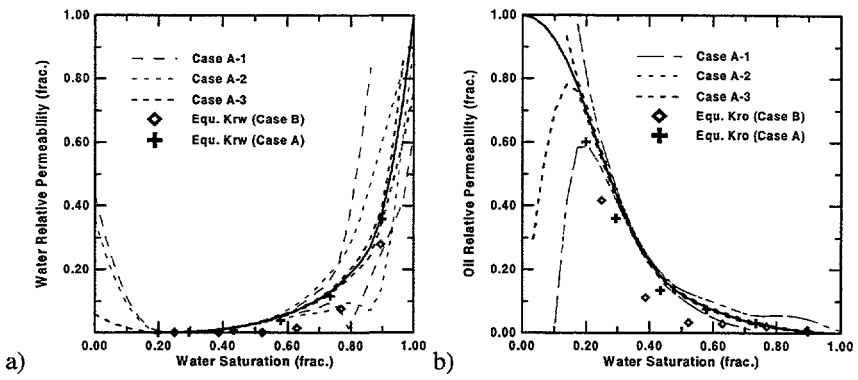

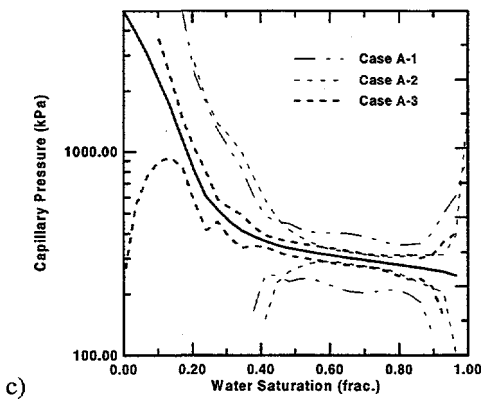

Fig. 3 - Experimental design with 95% confidence intervals for the three injection strategies; a) Water relative permeability; b) Oil relative permeability; and c) Capillary pressure.

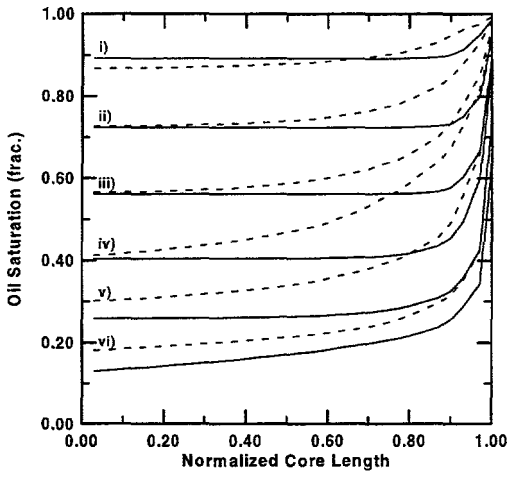

Fig. 4 - Saturation profiles for Case A (low absolute permeability), solid line and Case B (high absolute permeability), dotted line.

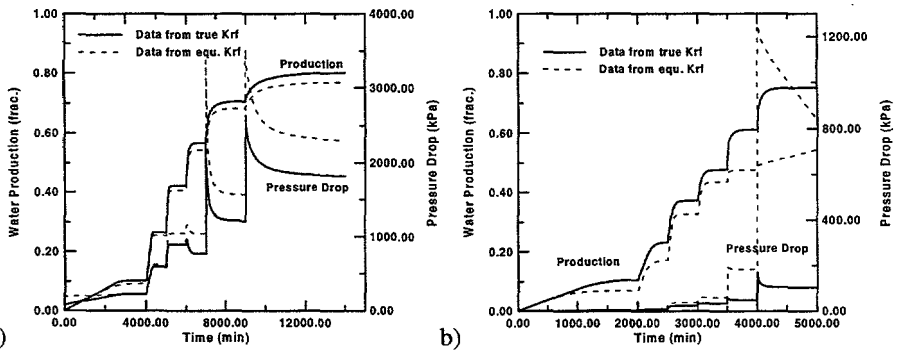

Fig. 5 - Experimental design - true pressure drop and production data, and the same data computed using equilibrium relative permeabilities; a) Case A; and b) Case B.

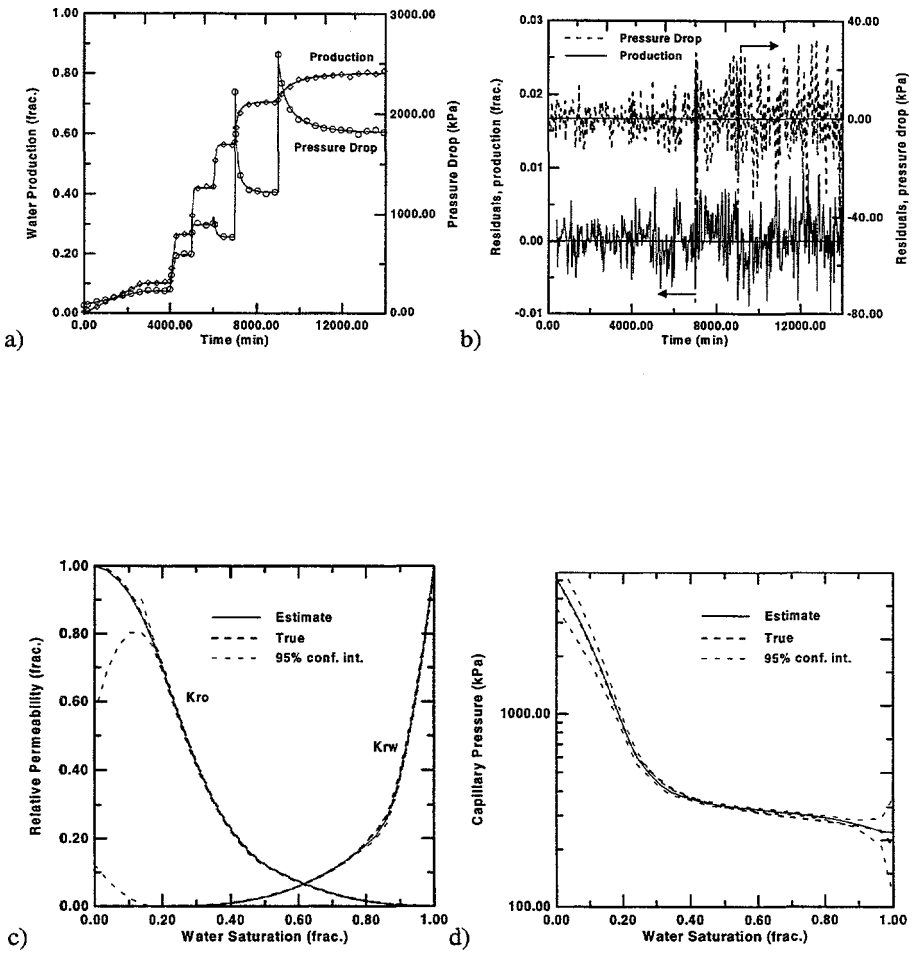

Fig. 6 - Simulated case; a) Match between synthetic and estimated data; b) Residual plot; c) Estimated and true relative permeability functions with 95% confidence intervals; and d) Estimated and true capillary pressure functions with 95% confidence intervals.

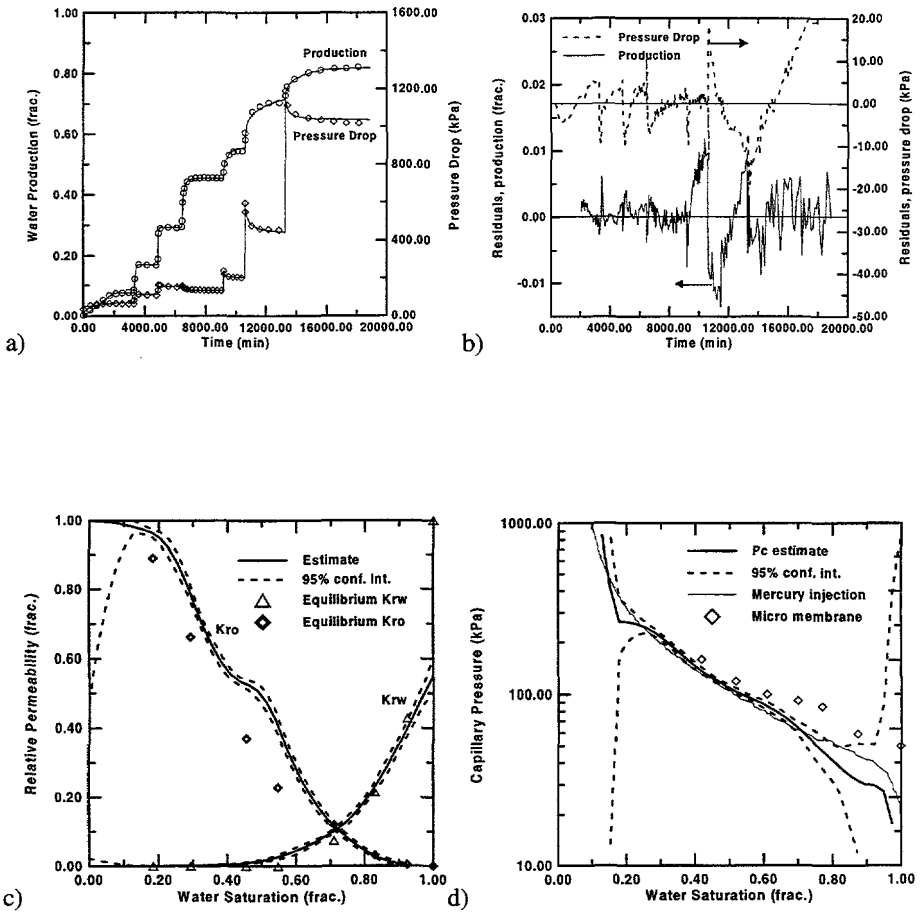

Fig. 7 - Experimental data; a) Match between experimental and estimated data; b) Residual plot; c) Estimated relative permeability functions with 95% confidence intervals; and d) Estimated capillary pressure function with 95% confidence intervals.

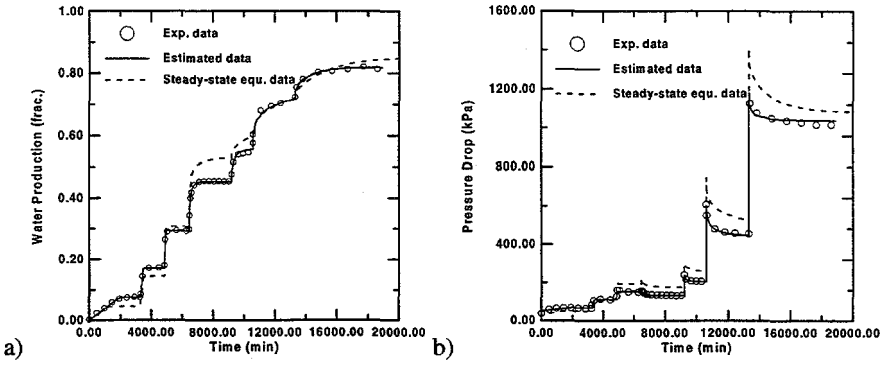

Fig. 8 - Experimental data predicted using estimated relative permeability functions and data predicted using equilibrium relative permeability points; a) Production data; and b) Pressure drop data.

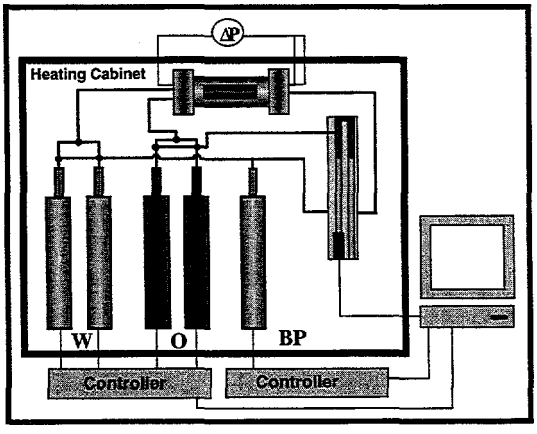

Fig. 9 - Two-phase flow apparatus.

Paper IV

Determination of Three-Phase Relative Permeabilities From Displacement Experiments

J.E. Nordtvedt, Einar Ebeltoft, J.E. Iversen, André Sylte, Hege Urkedal, and **K.O. Vatne,** RF - Rogaland Research, and **A.T. Watson,** Texas A&M U.

Summary

We describe and demonstrate a method for the determination of three-phase relative permeability functions at reservoir conditions. Two- and three-phase displacement experiments are conducted on a low-permeability chalk sample, and estimates of the three-phase relative permeability and capillary pressure functions are obtained. We also calculate three-phase relative permeabilities with the Stone predictive model, and we evaluate them by simulating the experimental data.

Introduction

Determination of relative permeability and capillary pressure properties (multiphase-flow functions) from experimental data has received a great deal of attention in the past half decade. Substantial improvements in the estimation of two-phase relative permeabilities have been made with the development of a generalized procedure for estimating multiphase-flow functions from experimental data.[1–4] The extension of this method to the determination of three-phase functions also can provide for substantial advances in that area.[5,6]

The understanding and description of three fluid phases in porous media have been hindered severely by the lack of adequate methods for determining multiphase-flow functions from experimental data. Consequently, the primary method for generating three-phase relative permeabilities has been through the use of various predictive methods that generally have never been evaluated with actual experimental data. These methods are based on simplified models whereby two-phase relative-permeability data represented with univariate saturation are extrapolated onto bivariate saturation representations.

Analysis of three-phase experimental data has been based on several generally unsupported simplifications (e.g., the neglect of capillary pressure, incompressible fluids, uniform saturation profiles, and each relative permeability being a function of its own saturation only). In an effort to meet such simplifications, experiments frequently have been conducted under flowing conditions that are unrepresentative of those encountered within reservoirs. Consequently, the estimated three-phase properties may not be suitable for describing reservoir flow.

We report the application of a method to overcome these problems. We have constructed an experimental apparatus whereby two- and three-phase displacement experiments may be performed at reservoir conditions.[7] The experimental process is modeled by a general-purpose three-phase simulator that includes the pertinent physical effects. We then choose the appropriate relative permeability and capillary pressure functions through solution of a series of optimization problems, so that the quantities calculated with the simulator are consistent with the measured values. A low-permeability chalk sample demonstrates this method.

The data measured during three-phase experiments can be used to evaluate predictive methods when the necessary two-phase relative permeabilities have been determined. We demonstrate this by use of the three-phase relative permeabilities calculated with Stone's method[8] to simulate the pressure drop and production using the conditions of the experiments and comparing the simulations to the actual measured data.

Original SPE manuscript received for review 25 October 1996. Revised manuscript received 2 September 1997. Paper peer approved 5 September 1997. Paper (SPE 36683) first presented at the 1996 SPE Annual Technical Conference and Exhibition held in Denver, Colorado, 6–9 October.

Three-Phase Flow Apparatus

Fig. 1 shows a schematic of the flow apparatus. It consists of a pumping system, a three-phase separator, a core holder, and an X-ray scanner system for in-situ saturation measurements. Here, we review the main features of the apparatus; further details on the equipment and testing may be found in Ebeltoft *et al.*[7]

The pumping system consists of eight computer-controlled cylinders that pump reservoir fluids into the core sample at reservoir conditions. Cylinders are paired to act as a pump. Three cylinder pairs are used for recycling water, oil, and gas with accurate and virtually pulse-free flow rates. For each of the cylinder pairs, one cylinder delivers fluid into the sample, while the other receives fluid through the return line from the separator. The receiving cylinder runs at a slightly higher rate than the delivering cylinder. The receiving cylinder is then ready to deliver fluid into the sample before the delivering cylinder is empty. All rates and pressures are continuously adjusted, and the switch between the cylinders occurs smoothly. The seventh cylinder acts as a back-pressure regulator and works in a constant pressure mode. This cylinder is plumbed to the oil return line, but is in connection with all three phases through the separator. It will respond to any volume and pressure changes in the system. These seven cylinders are placed in a heating cabinet, and provide a closed loop with recycling of all three phases at reservoir conditions. The eighth cylinder is placed outside the heating cabinet and is used to maintain constant overburden pressure to the core sample and for various preparation work. A personal computer monitors the apparatus and automates and performs collection of data.

Fig. 2 shows a schematic of the separator that is used to monitor the production of each fluid phase. Three bores are connected to each other, and fluids from the core sample enter into the top of the middle bore, where they are separated. Two measuring bores are connected to the separator bore by a set of channels. The volumes of the phases in the separator are inferred by means of acoustic transducers determining the distance from the transducer to the interfaces formed in the measurement bores. Using these measurements, the water and gas volume can be determined. The oil volume is determined by subtracting the water and gas volume from the total separator volume.

A carbon fiber hydrostatic core holder is used. The core holder contains an internal heating system that makes it feasible to keep the core holder outside the heating cabinet during experimentation. This may be necessary in cases when, for example, an X-ray system is used to monitor saturation changes.[7] The core sample is covered by aluminum and placed within a rubber sleeve. This arrangement is then mounted into the core holder. Distilled water is used as the fluid surrounding the core sample in the holder. The pressure in the surrounding fluid is controlled by the eighth cylinder in the pumping system. Specially designed plugs are used at the inlet to distribute the fluids over the face of the core and at the outlet to avoid hold-up of the produced fluids. Several rubber washers behind these plugs transmit an axial stress proportional to the pressure in the surrounding fluid.

The differential pressure across the core sample is measured with a high-resolution transmitter with an adjustable range. Three high-pressure titanium cells located inside the heating cabinet are used as reservoirs for the fluids (i.e., the formation water, oil, and gas). They

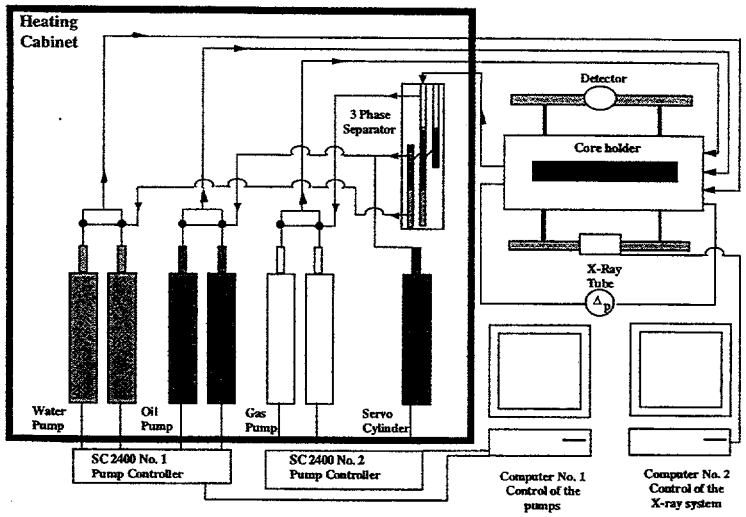

Fig. 1—Three-phase flow apparatus.

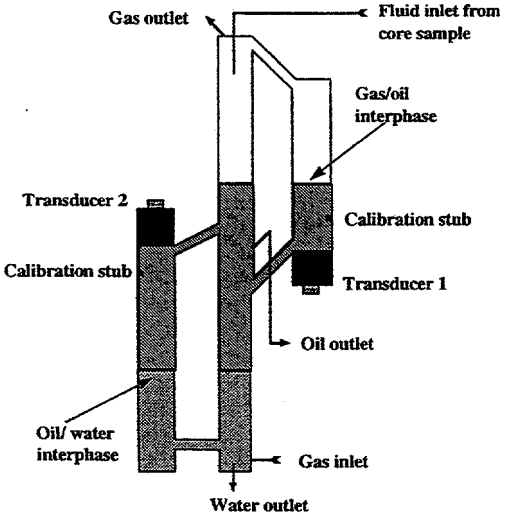

Fig. 2—Three-phase acoustic separator.

load the apparatus with live fluids at reservoir conditions. A membrane-type back-pressure regulator is used to decrease the pressure from the operating condition to atmospheric in a controlled manner when loading the system with live reservoir fluids. Both the titanium cells and the back-pressure regulator are closed off during experimentation. Everything, except the X-ray scanner and the core holder, is placed in an electrically heated cabinet.

Method

The basic method we use for estimating the multiphase flow functions is an implicit approach first reported by Mejia *et al.*[5] and further developed by Nordtvedt *et al.*[6] In this approach, the experimental physical process is represented with a suitable mathematical model, and estimates of the multiphase flow functions are obtained so that predictions of the measured data match those obtained during the experiment. The model is based on a continuum representation,[9] using equations for conservation of mass, the Darcy equations, the capillary pressure equations, and appropriate boundary and initial conditions. Important effects in this model include compressibility of fluid phases, capillary pressure, gravity, and heterogeneity. While the first two effects are taken into account explicitly, we assume gravity to be negligible, and that the core sample is homogeneous. The neglect of gravity effects for these experiments has been verified through X-ray saturation monitoring (see Ebeltoft[7] for a discussion), while a CT scanner has been used to select a homogeneous sample.

A key aspect in estimating multiphase flow functions from measured data is the representation of the unknown functions. It is essential that the functions have sufficient degrees of freedom to represent the true (although unknown) properties, yet it is desirable that the degrees of freedom be limited whenever there is insufficient information content in the experimental data. B-spline functions have been used successfully for representation of the univariate flow functions when estimating relative permeability and capillary pressure functions from two-phase experiments.[1–4]

For situations with three flowing fluid phases, the flow functions are bivariate because the properties may depend on two saturation values (the third saturation value is not independent). Thus, the relative permeability and capillary pressure functions must be represented by surfaces when plotted as a function of two saturations. This can be achieved by using tensor-product B-splines. The relative permeability surfaces are given by:

$$k_{ri}(S_1, S_2) = \sum_{i=1}^{m_1+K_1} \sum_{j=1}^{m_2+K_2} c_{ij} N_{ij}(S_1, \vec{y}_1, S_2, \vec{y}_2) \, , \ldots\ldots\ldots\ldots (1)$$

where $i = o,w,g,m_i$ is the order of the spline in direction i, K_i is the corresponding number of knots, and $\vec{y}_1$ and $\vec{y}_2$ are the extended partitions $\left[\vec{y}_i = (y_{i1}, \ldots, y_i, 2m_i + K_i)^T\right]$. One can increase the flexibility of the surface by increasing the number of knots (in one or both directions) and/or by increasing the corresponding spline order. Similar bivariate expressions can represent the capillary pressure functions. The tensor product B-spline expansion in Eq. 1 can be found from two univariate B-splines expansions in any two saturation directions.[10] For details on the functional representation, see Nordtvedt *et al.*[6]

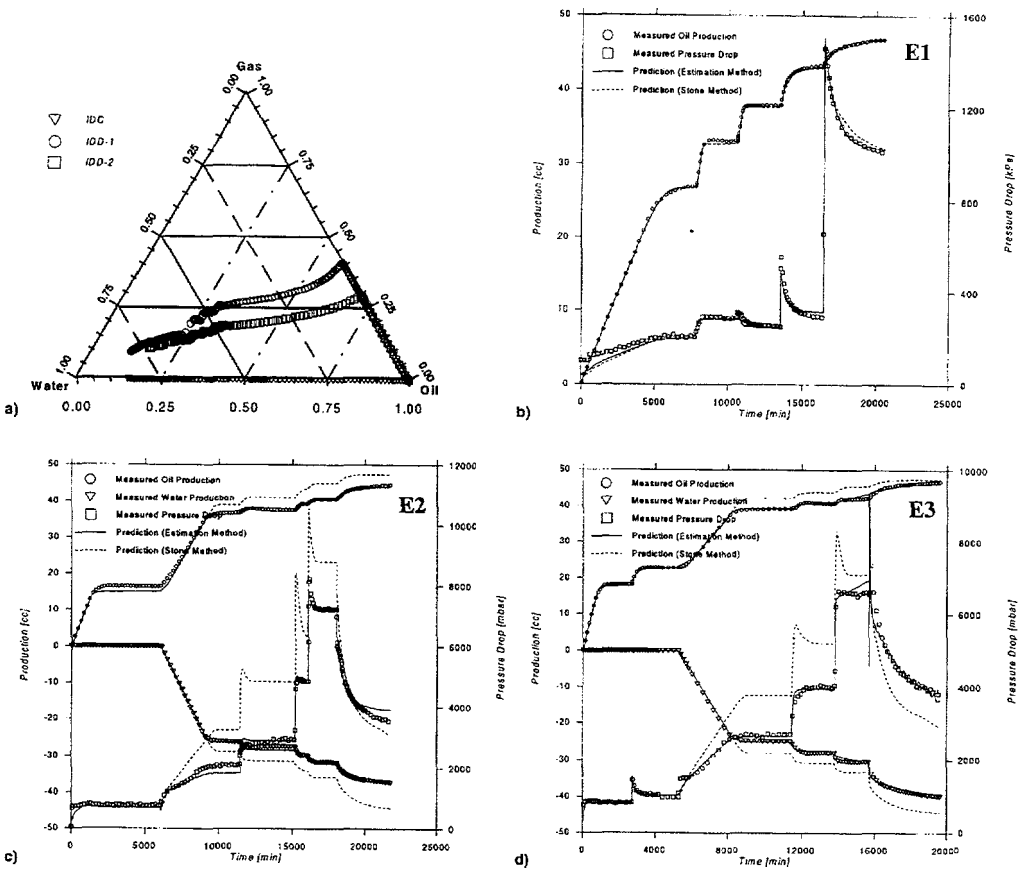

Fig. 3—Saturation trajectories and predicted and estimated data; a) saturation trajectories; b) two-phase experiment (E1); c) three-phase experiment (E2); d) three-phase experiment (E3).

To determine estimates of the flow functions, we solve the nonlinear parameter estimation problem defined by minimization of the following objective function:

$$J(\vec{\beta}) = \left[\vec{Y}^{cal}(\vec{\beta}) - \vec{Y}^{meas}\right]^T W \left[\vec{Y}^{cal}(\vec{\beta}) - \vec{Y}^{meas}\right]. \quad \ldots\ldots\ldots (2)$$

Here, $\vec{Y}^{meas}$ and $\vec{Y}^{cal}(\vec{\beta})$ are the measured and simulated data, respectively, W is the weighting matrix, and $\vec{\beta}$ is the collection of all spline coefficients. In this work, we use a fully implicit three-phase, one-dimensional black-oil simulator to calculate $\vec{Y}^{cal}(\vec{\beta})$. W is selected to be the inverse of the covariance matrix of the estimate, and hence maximum-likelihood estimates result. The parameter estimation problem is solved with a trust-region-based Levenberg-Marquardt algorithm.

In the parameter estimation procedure, it may be convenient that the estimates of the flow functions exhibit some particular shape characteristics. For example, it is desirable that the flow functions be monotonic with increasing saturation. This results in a set of linear inequality constraints on the parameters,

$$G\vec{\beta} \le \vec{\beta}^{con}, \quad \ldots\ldots\ldots\ldots\ldots\ldots\ldots\ldots\ldots\ldots\ldots\ldots (3)$$

where G is the constraint matrix.[3,6]

Note that with the approach used here, we can use data simultaneously from several separate two- and three-phase experiments. However, to attempt to solve Eq. 2 as a single-parameter estimation problem while including all the data from all the experiments is not likely to be fruitful because local, nonglobal solutions to the problem may result. For two-phase situations, this problem has been solved as a series of minimization problems with increasing dimensions of the parameter space [1,3,4] or as a series of largely decoupled problems.[1] For three-phase problems, we use the following procedure.

First, we analyze all the available data from the two-phase experiments. Instead of simply estimating the univariate functions, as might be done typically, we use the three-phase representations and estimate only those coefficients corresponding to basis functions that have support in saturation regions accessed by the particular two-phase experiments. The regression-based approach is used for selection of the partitions. Analyzing the three-phase data, we start using the partitions and coefficients that will reconcile the two-phase data; hence the flow functions are kept equal to the two-phase estimates in the two-phase regions. Consequently, relatively flexible representations for each of the flow function are used in the initial phase in the analysis of the three-phase data. We then analyze only parts of the three-phase data and estimate the parameters corre-

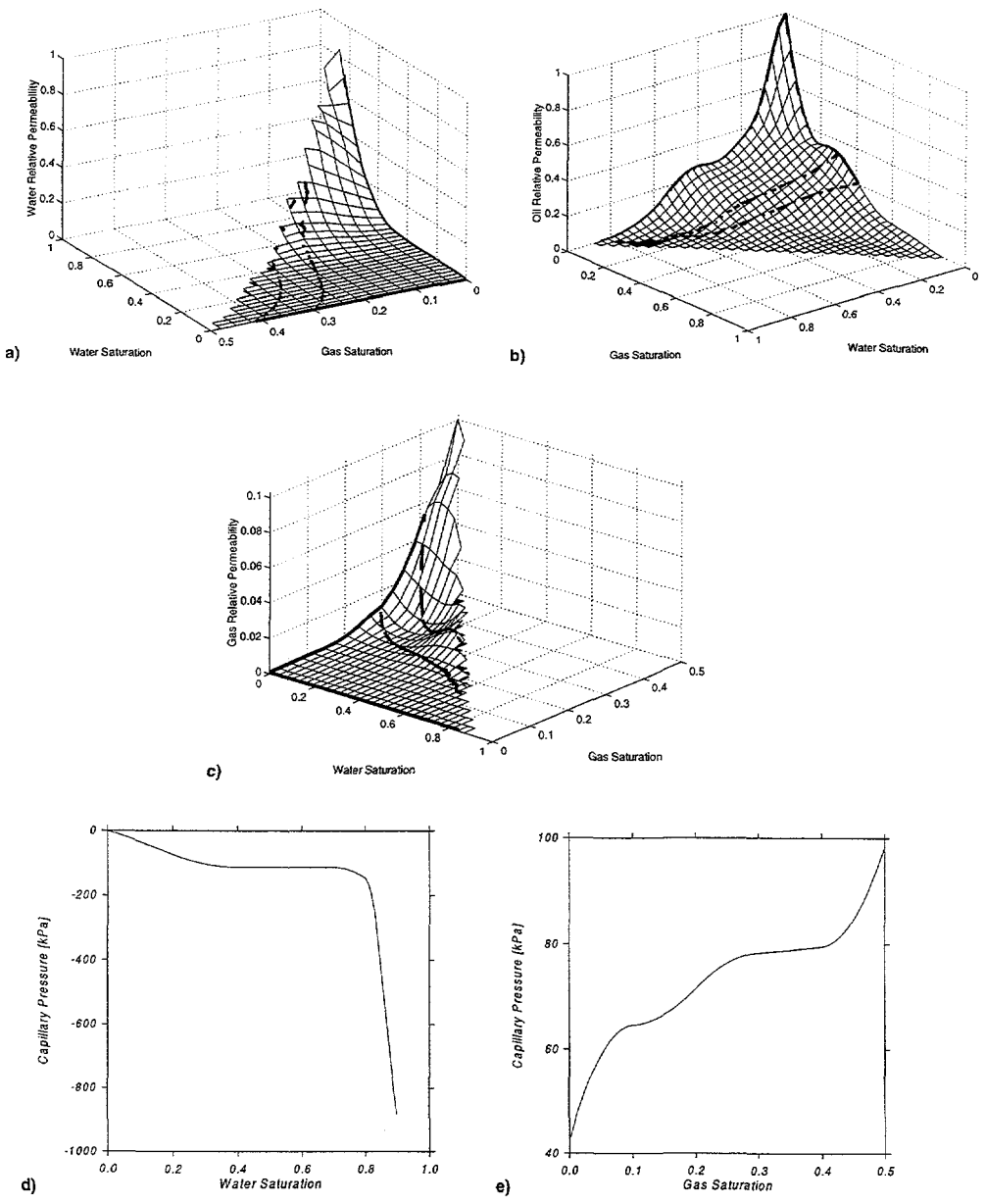

Fig. 4—Estimated three-phase flow functions; a) water relative permeability; b) oil relative permeability; c) gas relative permeability; d) oil-water capillary pressure; e) oil gas capillary pressure.

sponding to basis functions with support in the saturation region corresponding to the data used. With fixed partitions, we gradually increase the amount of three-phase data used. Finally, if necessary, we will increase the flexibility of the representations. A knot will be added in a saturation region corresponding to data that are not well matched and to the function expected to have the highest sensitivity in that saturation region. For further details on the method, see Nordtvedt *et al.*[6]

Results and Discussion

We analyzed three-phase flow in a chalk sample with the previously described apparatus and estimation method. One two-phase and two three-phase experiments were designed to determine water, oil, and gas relative-permeability functions to represent simultaneously with the capillary pressure functions for a situation in which water is injected into an oil- and gas-filled zone in the field. This means that the water should be injected into the core sample at initial low-

water saturation. Because it can be very difficult to replicate the very low initial saturations that are expected within the field in the laboratory, the core sample was saturated fully with oil. Then, we performed the two- and three-phase experiments. We conducted all experiments at 20,700 kPa and 30°C, with a net overburden pressure of 7,000 kPa. **Fig. 3a** shows, in a ternary diagram, the average saturation of the three phases as a function of time for the three experiments. For all the experiments, the production of water and oil was measured as a function of time along with the pressure drop. **Figs. 3b through d** show the measured pressure and production data.

First, we conducted a two-phase water-displacing-oil experiment (IDC). The notations IDC, CDI, and DDI describe the saturation history. The three capital letters indicate directional saturation changes of each fluid phase within the core sample, in order of water, oil and gas, to be decreasing, increasing, or remaining constant. The IDC experiment consists of a series of steady-state steps. Initially, a low-water/oil rate fraction is used, and the production of water and the pressure drop across the core sample is measured as a function of time until a near steady-state situation is attained. Then, the rate fraction of water is increased, keeping the total rate constant. Again, production and pressure are measured as functions of time. Two more steps using increasing values of the water-rate fraction (the last one corresponding to water injection only) are made. Then, the total rate is increased. This experiment is denoted E1. Fig. 3b shows the experimental data.

Upon completion of experiment E1, we cleaned the core and saturated it with oil. Then, a two-phase oil-gas flood was conducted to an intermediate gas saturation using a constant-rate fraction of gas and oil (a CDI to approximately 30% gas saturation).

In Fig. 3c, the data through the first 6,000 minutes represents the two-phase production and pressure drop. An increase in the oil production as a function of time is observed, while the pressure drop rapidly reaches a plateau value. The measured water production is zero because this is a two-phase water-gas case. Subsequently, and without halting the flow, water was injected simultaneously with oil and gas (an IDD process). During the IDD process, a series of steady-state steps was conducted in which the oil and gas rates were kept constant while the water rate was increased in steps. Fig. 3c shows the experimental data. Note that the water production is negative. This reflects the change of fluid saturation in the core sample. The experiment was initiated with a high oil and gas saturation and zero water saturation in the core. As we start injecting water, the water saturation will increase, and gas and oil will be displaced. This means that water will accumulate within the core, giving a negative production. The amount of injected fluid can be determined with the separator.[7] The CDI and IDD experiments are denoted E2. Upon completion, the core sample was again cleaned and saturated with oil. We conducted a new CDI (in two steps) followed by an IDD experiment (E3), and this time we introduced the water at a gas saturation of about 40%. Fig. 3d shows the data for experiment E3.

To determine the three-phase flow functions, we first estimate the two-phase relative permeability functions as well as the two-phase capillary pressure functions corresponding to the two-phase oil-water data (E1) and the two-phase oil-gas data (two-phase part of experiment E3). Then, we analyze the three-phase data (three-phase part of experiment E3). In this work, the capillary pressure functions resulting from estimation from the two-phase data are kept fixed (i.e., our estimate of the three-phase capillary pressure functions are univariate). Finally, we analyze the three-phase data resulting from experiment E2. Note that the two-phase data from experiment E2 (IDC) are not included in the analysis. The total number of data in the analysis was 2,443, and final value of the objective function was 17000. At the final step, the total number of parameters was 50. **Fig. 4** shows the estimates of the relative permeability and capillary pressure functions, and Fig. 3 shows the comparison between estimated and measured data. As can be seen, a close match between experimental and simulated values is obtained.

As discussed in the introduction, it is desirable to evaluate the efficacy of methods for calculating three-phase relative permeabilities from two-phase relative permeabilities. Here, we investigate the predictive model developed by Stone[8] by calculating the three-phase relative permeabilities with that method and using those properties to simulate the measured experimental data. If the calculated three-phase relative permeabilities are accurate, the simulated values should be consistent with the measured data.

In the Stone[8] predictive model, it is assumed that water and gas are spatially separated, and hence are univariate functions, while the oil relative permeability depends on two saturations. This dependency can be found from the oil/water and oil/gas two-phase relative permeabilities. To get smooth functions for the purposes of simulation, we fit a tensor-product B-spline surface to the three-phase data points obtained from the Stone predictive model. The production and pressure drop are simulated under the conditions of the experiment. Fig. 3 shows experimental data together with simulated data by use of relative permeabilities determined with the Stone predictive model. These values also can be compared with those simulated with the relative permeabilities we derived from the experiment. The figure shows clearly that relative permeabilities generated using the Stone predictive model overpredicts the oil production in E2 and overpredicts the amount of water injected in both E2 and E3. In both E2 and E3, the pressure drop is overpredicted for all rate fractions except the last one. A measure of the degree of inconsistency between the measured and simulated data is provided by the objective function. The value calculated using the Stone relative permeabilities exceeds the value obtained using our estimates by more than a factor of 20.

Conclusions

1. Three-phase relative permeability and capillary pressure functions on a low-permeable chalk sample were determined from data measured in serial two- and three-phase experiments.
2. The relative permeabilities generated using the Stone predictive model do not simulate the experiments accurately.

Acknowledgments

This work is a part of an RF-Rogaland Research project within three-phase relative permeability estimation. The project is financed by Amoco Norway Oil Co., whose support we gratefully acknowledge. One of the authors (H. Urkedal) is sponsored through our Strategic Inst. Program within Advancing System and Parameter Identification. This program is financed by the Norwegian Research Council. Their support is gratefully acknowledged.

Nomenclature

$\vec{\beta}$ = parameters
c = spline coefficients
G = constraint matrix
J = objective function (defined in Eq. 2)
K_i = number of knots in direction i
m_i = spline order in direction i
N = spline basis function
S = saturation
$\vec{y}$ = partition vector
$\vec{Y}$ = vector of data
W = weighting matrix

Subscript/Superscript

c = capillary
cal = calculated
con = constraint
g = gas
$meas$ = measured
r = relative
o = oil
w = water

References

1. Nordtvedt, J.E. *et al.*: "Estimation of Capillary Pressure and Relative Permeability Functions From Centrifuge Experiments," *SPERE* (November 1993) 292.
2. Nordtvedt, J.E. et al.: "Estimation of Relative Permeability and Capillary Pressure From Transient and Equilibrium Steady-State Data," *Proc.*, 1994 International Symposium of the Society of Core Analysis (Stavanger) 197.
3. Watson, A.T. *et al.*: "A Regression-Based Method for Estimating Relative Permeabilities From Displacement Experiments," *SPERE* (August 1988) 953.
4. Richmond, P.C. and Watson, A.I.: "Estimation of Multiphase Flow Functions From Displacement Experiments," *SPERE* (February 1990) 121.
5. Mejia, G.M., Watson, A.T., and Nordtvedt, J.E.: "Estimation of Three-Phase Functions in Porous Media," *AIChE Journal* (1996) **42**, No. 7.
6. Nordtvedt, J.E. *et al.*: "Estimation of Three-Phase Relative Permeability and Capillary Pressure Functions," *Proc.*, 1996 European Conference on the Mathematics of Oil Recovery (Leoben, Austria) 113.
7. Ebeltoft, E. *et al.*: "A Novel Experimental Apparatus for Determination of Three-Phase Relative Permeabilities at Reservoir Conditions," *Journal of Petroleum Science and Engineering*.
8. Stone, H.L.: "Probability Model for Estimating Three-Phase Relative Permeabilities," *JPT* (1970) 214.
9. Slattery, J.: "Momentum, Energy, and Mass Transfer in Continua," Krieger, New York, 1981.
10. Schumaker, L.L.: *Spline Functions: Basic Theory*, Wiley, New York, 1981.

SI Metric Conversion Factors

bar	× 1.0*	E+05 = Pa
°F	(°F–32)/1.8	= °C

*Conversion factor is exact.

SPEFE

Jan-Erik Nordtvedt is research manager for reservoir technology and IOR at RF-Rogaland Research in Bergen, Norway. His research interests include two- and three-phase flow through porous media, parameter estimation, and inverse problems. He holds MS and PhD degrees in physics from the U. of Bergen. Nordtvedt is a Technical Editor for *SPEFE*. **Einar Eboltoft** is research scientist in the Reservoir Technology Group at Rogaland Research in Bergen. His research interests are experimental techniques and interpretation of multiphase flow properties in porous media. He holds an MS degree in physics from the U. of Bergen. **Jan Erik Iversen** is a research scientist at the Reservoir/IOR group of RF-Rogaland Research. Iversen holds an MS degree in physics from the Norwegian Inst. of Technology, Trondheim. **André Sylte** is a research scientist at the Reservoir Technology Group at RF-Rogaland Research. His experience includes multiphase flow in porous media, estimation of properties, and design of experiments. He holds an MS degree in physics from the U. of Bergen. **Hege Urkedal** is a research scientist at the Reservoir Technology/Inverse Problem group at Rogaland Research. Her research interests are two- and three-phase flow in porous media, parameter estimation, and sensitivity analysis. **Kaare Olav Vatne** is a research engineer at the Reservoir/IOR group of RF-Rogaland Research. Vatne holds an MS degree in petroleum technology from Rogaland Regional College in Stavanger. **Ted Watson** is professor of chemical engineering at Texas A&M U. and senior scientific advisor at Rogaland Research. His research interests include parameter estimation and imaging methods. He holds a BS degree from the U. of Texas and a PhD degree from the California Inst. of Technology, both in chemical engineering. Watson is a member of the Editorial Review Committee.

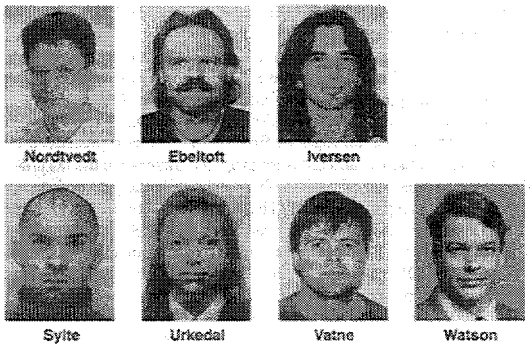

Nordtvedt Eboltoft Iversen

Sylte Urkedal Vatne Watson

Paper V

Development of Analytical Sensitivity Coefficients for Determination of Porous Media Properties

H. Urkedal, J.E. Nordtvedt; RF - Rogaland Research,
A.T. Watson; Texas A&M University

Abstract

Accurate information of the properties describing fluid flow in porous medium is important for simulation of reservoir forecasting and exploration. In estimation of these properties from laboratory data, the properties are selected so that simulated data match the observed data. The most frequent used estimation methods involve computation of the sensitivity of the model response with respect to the model parameters. These derivatives are referred to as sensitivity coefficients.

The sensitivity coefficients are traditionally calculated numerically by finite differences. This method introduces truncation and condition errors and is also computationally expensive as it requires N_p+1 base runs of the simulator (N_p is the number of parameters characterizing the properties we want to determine). In this work we establish a methodology for determination of analytical sensitivity coefficients using the direct method. Since the simultor equation is solved using the Newton-Raphson method, we can use the properties of this solution to solve the sensitivity equation and get the sensitivity coefficients in the direct method. Hence, the number of computations is reduced. The finite difference derivative computations are avoided, and we improve the accuracy of both estimation of porous media properties and the accuracy assessment.

The direct method for computation of analytical sensitivity coefficients is developed and implemented for two- and three-phase flow in porous media. Examples from parameter estimation and computation of accuracy of estimates are presented. The difference between numerical and analytical sensitivity coefficients, the impact of sensitivity coefficients on "false" sensitivity, support of parameters, identifiability of parameters and size of confidence intervals will also be discussed.

1 Introduction

To simulate a practical problem as in history matching or prediction of reservoir performance, the porous media properties which appears in terms of coefficients (and/or initial and boundary conditions) in the model equations must be specified. Typically, these quantities can not be measured directly, but must be inferred through measurement of other quantities and utilizing some inverse approach [21]. The inverse approach provides a manner in which measurements of state variables or other data sets are used to determine the unknown coefficients by matching the model response to the measurements [14]. Optimization procedures which minimize an objective function, typically the sum of squared differences between the model response and measurements are used. These optimization procedures require the partial derivative of the model equation with respect to the parameters. These derivatives are called the *sensitivity coefficients*. The sensitivity coefficients provide a quantitative measure of the change of direction and magnitude of a model response with the properties. They also contain the necessary information for calculation of accuracy of the estimates. This accuracy can be computed using a linearized covariance analysis [7,11], and utilized in designing experiments [18].

The sensitivity coefficients play an important role when estimating the properties and determining the accuracy of the estimates. Consequently, it is essential to compute accurate and robust sensitivity coefficients in an efficient manner.

There are several methods for computing sensitivity coefficients [13]. They are grouped into three methods: perturbation, direct and adjoint method. The perturbation method (also called divided difference or influence coefficient) is the simplest of the sensitivity methods and is widely used [13]. The model is first run with an estimate of the coefficients. The coefficients are then perturbed one by one followed by a simulator model run. This gives numerical sensitivity coefficients (NSC) approximate by

$$a_{ij} \approx \frac{Y_{s,i}(\theta_1,\ldots,\theta_j+\Delta\theta_j,\theta_{j+1},\ldots,\theta_{N_p}) - Y_{s,i}(\theta_1,\ldots,\theta_j,\theta_{j+1},\ldots,\theta_{N_p})}{\Delta\theta_j}. \quad (1)$$

This is divided differences or finite difference approximation of the derivatives. The sensitivity matrix A contain the $N_D \times N_P$ elements a_{ij}, where N_D is the number of data points and N_P the number of parameters. This method requires N_p+1 simulation runs. The advantage of the perturbation method is that an existing computer code can be used with only minimal additional programming. The disadvantages are that it requires repeated solutions of the simulator equation. Second, it introduces truncation error since second order and higher terms are neglected when computing the derivative. Condition error is introduced since the computed function values $Y_s(\theta)$ of $Y_s^{exact}(\theta)$ will be subject to errors as $Y_s(\theta) = Y_s^{exact}(\theta) + \sigma$. Rounding errors in performing subtraction and division are generally negligible with respect to the truncation and condition errors. Third, choosing the right perturbation is difficult. When approximating the sensitivity matrix **A** by the perturbation method in Eq. 1, the error in the computed approximation can be viewed as the sum of truncation error and condition error. The truncation error is a linear function of $\Delta\theta_j$ and the condition error is a linear function of $1/\Delta\theta_j$, and changes in $\Delta\theta_j$ will tend to have opposite effects on these errors [3]. Hence, the errors introduced in the method will give accuracy and robustness problems when the sensitivity coefficients are used in later computations.

Instead of a numerical approximation, the direct and adjoint methods (semi-analytical methods) compute the sensitivity coefficients analytically by solving the coefficients' sensitivity equations directly. The sensitivity equations are obtained by differentiating the model equations together with the associated boundary and initial conditions with respect to model parameters.

In the adjoint method (also called variational method), the adjoint simulator equations are differentiated with respect to the model parameters. This involve solving the adjoint simulator equation and integrate in space and time [4, 13]. The adjoint method also makes use of sensitivity equations, but rather than solve them directly, the sensitivities are obtained by solving the adjoint problem. Although the adjoint method can be used to compute state sensitivities [4], it is primarily used to compute the sensitivity of functionals.

The direct method (or sensitivity equation method) requires significantly less storage in comparison to the adjoint method. In addition, when the Newton-Raphson's algorithm

is used to solve the model equation, a large part of the computations can be spared in the sensitivity part, and the resulting system of sensitivity equation can be readily solved by performing just matrix back substitutions, rendering thus the direct approach computational efficient [6].

Hence, the direct and adjoint methods are much more efficient than the perturbation method since less computations are performed, and the accuracy and robustness are higher since the perturbation of the parameters and differences between very equal numbers is avoided [4, 13, 14, 20]. On the other hand, implementation of the methods requires more effort in terms of computer code development. The adjoint method will be more efficient than the direct method if the number of parameters is much larger than the number of grid blocks, due to integration in space in the adjoint method. The adjoint method also requires that a code similar to that of the original simulator be written for the adjoint variable. In this work we use relative many parameters to represent the unknown properties. However, the number of grid blocks will be in approximately the same range or larger than the number of parameters, and the direct method will therefore be the most efficient of the two semi-analytical methods. The direct method is implemented for reservoir history matching [1], and for two-phase flow in porous media [19]. It has also been showed that the method generally can be used in many applications [17].

In this paper, we will develop the direct method to compute analytical sensitivity coefficients (ASC) for two- and three-phase flow in porous media. The impact of different perturbations on truncation and conditional error and on numerical sensitivity coefficients (NSC) computed by the perturbation method will be discussed. The impact of errenous sensitivity coefficients on contribution of observations and identifiability of parameters will also be discussed. We will also present results on estimation of three-phase relative permeability and assessment of accuracy of these estimates when the direct and perturbation method have been applied to compute model sensitivity. Comparison of the two methods with respect to accuracy and CPU-time requirements will also be presented.

2 Theory

In this section, we first briefly sketch the experimental data used for determination of relative permeabilities. Then, we review the estimation and accuracy assessment methodologies, the functional representation of relative permeability and capillary pressure functions, the identifiability of parameters and the mathematical model for three-phase flow in porous media. Finally, the analytical sensitivity coefficients by the direct method developed for three-phase flow is presented.

2.1 Experimental Data

The main problem associated with determination of two- and three-phase relative permeabilities, is that the relative permeabilities are properties of the porous medium defined through the system of equations for flow through porous medium. Consequently, the relative permeabilities are not directly measurable, but have to be inferred from measurements of other quantities. The subsequent section will deal with the estimation methodologies. Here, we review the data used in such determinations.

Typically, the relative permeabilities are determined from some displacement experiment, in which one or several fluid phases are injected into a core sample at some initial saturation of the same or other fluid phases. Frequently, a constant injection rate is utilized, and the pressure drop across the core sample and the fluid production are measured as a function of time. One example of typical data from such experiments is shown in Figure 1. Other measurables are individual phase saturations as a function of time at a given location, or as a function of location for a given time (saturation profiles). Such saturation information can be acquired using e.g. NMR experiments [8]. Also, individual phase pressures can be utilized in a similar manner.

These types of data might be utilized for determination of two-phase as well as three-phase relative permeabilities. In the three-phase cases, production and pressure drop as well as *in situ* saturation of two phases need to be considered. Similarly, two individual phase pressures might be made available. Figure 2 summarize types of data from displacement experiments.

In this paper, we will focus on utilization of production and pressure drop data, see [5] for a discussion on equipment and procedures. Note that all of the data can be utilized in all the procedures discussed in this paper, and the direct method has been implemented correspondingly.

2.2 Estimation of Reservoir Properties

The estimation methodologies for two- and three-phase relative permeabilities have been developed through a series of articles, see [7, 9, 10, 11, 21]. Basically, estimates are obtained solving a series of linearly constrained nonlinear parameter estimation problems. Each of these parameter estimation problems are defined by

$$\text{minimize} \quad \mathrm{J}(\theta) = f(\theta)^T \Sigma^{-1} f(\theta) \tag{2}$$

subject to the constraints

$$\mathrm{G}\theta \geq g. \tag{3}$$

Here is $f(\theta) = Y_o - Y_s(\theta)$, where Y_o is the vector of observed data, i.e. pressure drop, production, *in situ* saturation or pressure or saturation profiles, and $Y_s(\theta)$ is the vector of the corresponding simulated data. $f(\theta)$ is the residual vector to be minimized in this problem. Σ^{-1} is the estimated variance of the observations. Hence, we find maximum-likelihood estimates. A trust region based, Levenberg-Marquardt algorithm is applied to solve the nonlinear least squares problem in Eq. 2 and 3, as described in [21]. The Levenberg-Marquardt search direction is defined in Gill [3] as the solution of the equation

$$\left[A_k{}^T A_k + \lambda_k \mathrm{I}\right] p_k = -A_k{}^T f_k. \tag{4}$$

Here, k is the iteration, λ_k is a non-negative scalar, f_k is the residual vector, and A_k is a $N_D \times N_P$ matrix of sensitivity coefficients defined as $A_{i,j} = \partial Y_{s,i}(\theta)/\partial\theta_j$. p_k is the solution of Eq. 4 and the new parameters are computed as $\theta_{new} = \theta_{old} + p_k$. The search direction and the new parameters are functions of the sensitivity coefficients through Eq. 4. Hence, the accuracy of the estimated parameters, θ_{new}, depends on an accurate computation of the sensitivity coefficients before Eq. 4 is solved. For large problems where many parameter are estimated, the method computational expense depends on the expense to compute **A**. The efficiency (cost of computing **A** and number of iterations before convergence) and robustness of the optimization will also depend on the accuracy and robustness of the computations of **A**.

2.3 Functional Representation of Reservoir Properties

Flexible representation of the relative permeabilities is a key element for successful determination of the relative permeabilities, see [7]. However, the degree of freedom must be limited whenever there is insufficient information content in the experimental data. B-spline functions have been successfully used for representing the univariate flow functions, and tensor-product B-spline functions for representing three-phase relative permeability functions [10, 9, 18]. A general function can be written as [12]

$$f(S_1, S_2) = \sum_{i=1}^{m_1+K_1} \sum_{j=1}^{m_2+K_2} c_{ij} N_{ij}^m(S_1, \vec{y}_1, S_2, \vec{y}_2), \tag{5}$$

where $\vec{y}_1$ and $\vec{y}_2$ denote the extended partition, and S_1 and S_2 the independent saturations. N_{ij}^m are the tensor-product B-splines.

Three-phase relative permeability can be represented as

$$k_{rf} = f(S_1, S_2) \quad \begin{cases} S_1 = S_f \\ S_2 = \begin{cases} S_w & if \quad f \neq w \\ S_g & if \quad f = w \end{cases} \end{cases},$$

and the capillary pressures are represented by

$$P_{c,ow} = f(S_1, S_2) \quad S_1 = S_w$$
$$P_{c,og} = f(S_1, S_2) \quad S_2 = S_g$$

The unknown parameters in the three-phase model will be the coefficients c_{ij} in the tensor-product B-splines (Eq. 5). These coefficients are arranged in the vector θ as follows

$$\theta = \left[c_{11}^w, \ldots, c_{N_{w1}N_{w2}}^w, c_{11}^o, \ldots, c_{N_{o1}N_{o2}}^o, c_{11}^g, \ldots, c_{N_{g1}N_{g2}}^g, c_1^{ow}, \ldots, c_{N_{ow1}}^{ow}, c_1^{og}, \ldots, c_1^{og}, \ldots, c_{N_{og1}}^{og}\right].$$

An example of a two-phase oil relative permeability function is plotted in Figure 3a. This function is a sum of each of the five basis functions plotted in Figure 3b multiplied by the elements in the vector $\theta = \{1.0, 0.5, 0.05, 0.00002, 0.0\}$. The basis function N_2

has support in the saturation region S_2=[0.0, 0.5]. During estimation of the parameter which is multiplied by this basis function, the experimental data must contain oil relative permeability information in this saturation region. The differential pressure sensitivity coefficient for this second oil relative permeability parameter is plotted in Figure 4.

In the three-phase case, oil relative permeability generally depends on two saturations. The surface is represented by the sum of tensor-product B-spline functions multiplied by a parameter vector. The basis functions B_{W1} to B_{W6} and B_{G1} to B_{G6} in Figure 5a are multiplied with a vector containing 36 parameters and give the oil relative permeability surface in Figure 5b. A parameter with support in e.g. region 1-2 in Figure 5a is denoted c_{21} and correspond to the basis functions B_{W2} and B_{G1}. This parameter has support in the saturation region corresponding to $S_w \times S_o = [0.0,0.5] \times [0.0,0.3]$. Hence, to estimated the parameter c_{21}, data containing three-phase oil relative permeability information in the corresponding saturation region are necessary.

2.4 Accuracy of Estimates

After the minimization problem in Eq. 2 and 3 is solved, the accuracy of the estimates can be computed using a linearized covariance analysis [7, 11]. The covariance of the parameter estimate is given as

$$P = (A^T \Sigma^{-1} A)^{-1}. \tag{6}$$

The accuracy or covariance of the estimated relative permeability and capillary pressure functions are computed by

$$C = D^T P D \tag{7}$$

where D is found from differentiating relative permeability and capillary pressure with respect to coefficients in their functional representation, i.e. for water relative permeability this is $D_{ij} = \partial k_{rw,i} / \partial \theta_j$, where i is the index for saturation and j the parameter index. From the diagonal elements in C, the confidence intervals can be computed for the estimated functions.

Again, the accuracy of these computations is highly connected to the accuracy of the elements in A. If the sensitivities are large, i.e. we predict the sensitivity in the data with respect to the parameters to be large, the confidence intervals will be small. In the accuracy computations, the CPU-time will be linearly dependent of the number of parameters.

The linearized covariance analysis is also used in experimental design to analyze the sensitivity in the model to parameters in different parameterizations of the properties, different injection strategies, and with different sets of data [18].

2.5 Contribution of Observations

When solving the inverse problem, the identified model parameters are generally allowed to be different from the true parameters within a certain range, provided that the required accuracy of model application is assured [22]. Let η_j be the range, or resolution, of parameter θ_j. The parameter is said to be interval identifiable if the identified value $\hat{\theta}_j$ of the parameter satisfies

$$\left|\hat{\theta}_j - \theta_{0,j}\right| < \eta_j \tag{8}$$

where $\theta_{0,j}$ is the true value of parameter θ_j. The problem of whether a parameter θ_j is interval identifiable for a given η_j depends upon the quantity and quality of observations.

To evaluate the data requirements of a system in connection with parameter identification, the concept of "contribution of observation F_i in the identification of parameter θ_j", denoted CTB(F_i,θ_j), is introduced by [22]. The contribution of observation F_i to parameter θ_j in the experimental design can be represented as

$$CTB(F_i,\theta_j) = \frac{\eta_j}{\varepsilon_i}\left|\int_{(\Omega_j)} \frac{\partial F_i}{\partial \theta_j} d\Omega\right| \tag{9}$$

where F_i is a component of model response vector $\mathbf{F}(\theta)$; θ_j is a component of parameter vector θ, η_j is a given admissible error of the identified parameter θ_j (or resolution), which can be seen as the element η_j of parameter weighting matrix ($\mathbf{C}_\theta$); ε_i is the upper bound of observation noise associated with F_i; and $\partial F_i / \partial \theta_j$ is the sensitivity coefficient of observation $\mathbf{F}$ with respect to parameter θ and (Ω_j) is a region associated with parameter θ_j.

Sun and Yeh [15] proved that a necessary condition for the interval identifiability is that there is at least one observation for each component for the unknown parameters whose contribution is larger than 1.

2.6 Three-Phase Flow Model

We consider three-phase flow in a homogenous porous, one dimensional medium. The model for three-phase flow is described by Darcy's law which relates the flow rate and pressure gradient for each phase. Together with the conservation law, we get a coupled partial differential equation which is discretized in space and time and solved for the

state variables, P_o, S_w, and S_g, in each grid block at each time step, see [2, 16]. The extended version of Darcy's law for multiphase flow is given as

$$u_f = -\frac{kk_{rf}}{\mu_f B_f}(\nabla P_f - \rho_f g \nabla z), \quad f = w, o, g, \tag{10}$$

where u_f is the filtration velocity and ∇P_f is the fluid pressure gradient. k_{rf}, μ_f, B_f, and ρ_f are the relative permeability, viscosity, formation volume factor, and density of phase f, respectively. k is the absolute permeability and g the gravitational constant. ∇z is the gradient in the z-direction. Mass conservation gives

$$-\nabla \cdot u_f + Q_f = \varphi \frac{\partial}{\partial t}\left(\frac{S_f}{B_f}\right), \quad f = w, o, g, \tag{11}$$

where Q_f is the source/sinc term of phase f. φ is the porosity and S_f is the saturation of phase f. The relations on saturation and capillary pressure are given as

$$S_w + S_o + S_g = 1$$

$$P_{c,ow}(S_w, S_g) = P_o - P_w .$$

$$P_{c,og}(S_w, S_g) = P_g - P_o$$

The initial conditions are chosen according to the reservoir conditions studied in each case. Various boundary conditions can be applied, depending on the process studied, e.g. simultaneous injection of several fluids at constant total rate and production against constant pressure.

Darcy's law and mass conservation together with the relations and initial and boundary conditions (depending on the type of injection and production) give the simulator equations to be solved

$$\nabla \cdot \left\{T_o(\nabla P_o + \gamma_o \nabla z)\right\} = V_b \frac{\partial}{\partial t}(\varphi b_o S_o) + Q_o$$

$$\nabla \cdot \left\{T_w(\nabla P_w + \gamma_w \nabla z)\right\} = V_b \frac{\partial}{\partial t}(\varphi b_w S_w) + Q_w \tag{12}$$

$$\nabla \cdot \left\{R_s T_o(\nabla P_o + \gamma_o \nabla z) + T_g(\nabla P_g + \gamma_g \nabla z)\right\} = V_b \frac{\partial}{\partial t}\left[\varphi(R_s b_s S_o) + \varphi b_g S_g\right] + R_s Q_o + Q_g$$

with volume factors, gravity term and transmissibility given as:

$$b_f = \frac{1}{B_f}$$

$$\gamma_f = \rho_f g$$

$$T_f = \frac{k k_{rf}}{\mu_f B_f}, \quad f = w, o, g.$$

Here, porosity and absolute permeability, $\varphi = \varphi(x)$ and $k = k(x)$, are porous media properties. Relative permeability is generally dependent on two saturations in three-phase flow, $k_{rf} = k_{rf}(S_1, S_2)$. V_b represents the pore volume of a grid block. R_s is the solution gas-oil ratio describing the mass transfer between oil and gas phases.

The discrete form of Eq. 10 can be written as

$$\Delta T_o(\Delta\Phi_o) + q_o = \frac{V_b}{\Delta t}\Delta_t(\varphi b_o S_o)$$

$$\Delta T_w(\Delta\Phi_w) + q_w = \frac{V_b}{\Delta t}\Delta_t(\varphi b_w S_w) \tag{13}$$

$$\Delta R_s T_o(\Delta\Phi_o) + \Delta T_g(\Delta\Phi_g) + R_s q_o + q_g = \frac{V_b}{\Delta t}\Delta_t(\varphi R_s b_o S_o + \varphi b_g S_g)$$

with

$$\Delta\Phi_f = P_{f,i+1} - P_{f,i} - G_f, \qquad f = w, o, g.$$

When discretization scheme is chosen (upstream weighting), the oil equation becomes

$$T^{n+1}_{o,i+\frac{1}{2}}\Delta\Phi^{n+1}_{o,i+\frac{1}{2}} - T^{n+1}_{o,i-\frac{1}{2}}\Delta\Phi^{n+1}_{o,i-\frac{1}{2}} + q^{n+1}_{o,i} = \frac{V_b}{\Delta t}\left\{(\varphi b_o S_o)^{n+1} - (\varphi b_o S_o)^n\right\}; \tag{14}$$

the equations for water and gas will follow the same principles.

The discrete equations for water, oil (Eq. 12) and gas can be written in matrix notation as

$$\mathrm{F}(u^{n+1}, \theta)\, u^{n+1} = \mathrm{G}(u^n, \theta) u^n, \tag{15}$$

where F is the vector of non-linear difference equations for each grid block and one vector for each phase, θ is the vector of parameters, and u is the vector of unknown state variables at each grid block. This leads to a non-linear equation where Eq. 12 is approximated with Taylor's series expansion about an assumed solution, written as

$$\frac{\partial \mathrm{F}(u^{(k-1)},\theta)}{\partial u^{(k-1)}}\left[u^{(k)}-u^{(k-1)}\right]=\mathrm{G}(u^{n},\theta)u^{n}-\mathrm{F}(u^{(k-1)},\theta),\qquad \left[u^{(k)}-u^{(k-1)}\right]=\begin{bmatrix}P_o^{(k)}-P_o^{(k-1)}\\ S_w^{(k)}-S_w^{(k-1)}\\ S_g^{(k)}-S_g^{(k-1)}\end{bmatrix},\quad(16)$$

where k is the iteration level and $\left[u^{(k)}-u^{(k-1)}\right]$ is the change in the unknowns between two iterations. The Jacobi matrix $\partial \mathrm{F}(u^{(k-1)},\theta)/\partial u^{(k-1)}$ is tridiagonal, so that each iteration in Eq. 14 is a linear system and solved by Gauss elimination. The exit criterion is obtained when the maximum change in the unknowns is less than the preset tolerance $\left\|u^{(k)}-u^{(k-1)}\right\|_{\infty}\le\varepsilon$. The state variables will then be updated according to $u^{n+1}=u^{k}$.

2.7 Analytical Sensitivity Coefficients by the Direct Method

In the direct method, the sensitivity coefficients are found by differentiating the model equation, Eq. 13 with respect to the model parameters.

Differentiation of the model at grid block *i* gives

$$\frac{\partial \mathrm{F}_{f,i}^{n+1}}{\partial u_i^{n+1}}\frac{\partial u_i^{n+1}}{\partial \theta_j}=\frac{\partial \mathrm{G}_{f,i}^{n}}{\partial u_i^{n}}\frac{\partial u_i^{n}}{\partial \theta_j}+\frac{\partial \mathrm{G}_{f,i}^{n}}{\partial \theta_j}-\frac{\partial \mathrm{F}_{f,i}^{n+1}}{\partial \theta_j}\qquad f=w,o,g.\qquad(17)$$

The sensitivity equation, Eq. 15, can be solved for the sensitivity coefficients $\mathrm{Y}_{i,j}^{n+1}=\partial u_i^{n+1}/\partial\theta_j$ at each time step *n+1*. In Eq. 15 we know the Jacobi matrix $\partial F_{f,i}^{n+1}/\partial u_j^{n+1}$ at iteration *(k-1)* from Eq. 9, but we can assume this is a good approximation to *n+1* since the solution of the model do not change much from iteration *k-1* to *k*. On the left hand side of Eq. 15, we must compute $\partial \mathrm{G}_{f,i}^{n}/\partial u_i^{n}$, $\partial \mathrm{G}_{f,i}^{n}/\partial\theta_j$, and $\partial \mathrm{F}_{f,i}^{n+1}/\partial\theta_j$. This is relatively straight forward, see Appendix A for details. Since the relative permeability and capillary pressure functions are known, $\partial \mathrm{G}_{f,i}^{n}/\partial\theta_j$ and $\partial \mathrm{F}_{f,i}^{n+1}/\partial\theta_j$ can be computed analytically. We then have an equation which is linearly independent in the sensitivity coefficient, and can be solved by algebraic operations. When the sensitivity coefficients, $\mathrm{Y}_{j}^{n+1}=\partial u^{n+1}/\partial\theta_j$, at each grid block are computed, the boundary conditions are differentiated with respect to the coefficients, and $\partial\Delta P/\partial\theta_j$ and $\partial V_o/\partial\theta_j$ are computed at each time step, see Appendix B. The sensitivity coefficients and the sensitivity in ΔP and V_o with respect to the model parameters are then used in parameter estimation and computation of accuracy, whenever the sensitivity in the models response to the coefficients is necessary.

3 Results and Discussion

The direct method to compute analytical sensitivity coefficients has been implemented for estimation of two- and three-phase relative permeability and capillary pressure, and for accuracy computation of these estimates.

3.1 Outline of Cases

Case 1 is a two-phase unsteady state oil injection example. This case illustrates the problem of choosing the right perturbation in the perturbation method, and its influence on accuracy of estimated parameters. Then, CPU-time spent on computing the sensitivity coefficients for an increasing number of parameters using the perturbation method are measured and compared with sensitivity coefficients computed by the direct method. The details on core and fluid properties used in this synthetic test are found in Table 1 and 2.

Sensitivity coefficients computed by the direct and perturbation method are compared for differential pressure data in the three-phase case (Case 2). Here, we focus on comparison of sensitivity in data with respect to parameters with support in high and low sensitive regions. The identifiability of the parameters is also investigated. CPU-time requirements for estimation of three-phase relative permeability functions when the two methods are applied are also measured. Details on fluid and core properties and injection strategies for this case can be found in Table 1-3.

3.2 Selection of Perturbation Parameter

The difficulties of choosing the right perturbations to compute accurate sensitivity coefficients as well as the computational effort have motivated the implementation of the direct method. Figure 4 shows the pressure drop sensitivity coefficient with respect to one parameter in the oil relative permeability representation (the parameter corresponding to basis function N_2 in Figure 3b). The sensitivity coefficients have been computed by the two methods, and for the perturbation method (numerical sensitivity coefficients, NSC) for several perturbations ($\Delta\theta$=1.0e-3, $\Delta\theta$=1.0e-5, $\Delta\theta$=1.0e-6, $\Delta\theta$=1.0e-11). The pressure drop and production data for this case is plotted in Figure 1. This figure shows that the water breakthrough is at approximately t=25 min. Figure 4 shows the tendency of numerical sensitivity coefficients to oscillate in the transient period until breakthrough at t=25 min. Figure 4a shows that the highest perturbation (1.0d-3) gives huge oscillations before breakthrough. Decreasing the perturbations decreases the oscillations around breakthrough, i.e., the truncation error decrease. But the perturbation that gave low oscillations before breakthrough, also gives oscillations after, see Figure 4b. This is a result of increasing condition error. This shows that simply choosing a low perturbation value will not be sufficient, this only minimize the truncation error. In fact, this error trade-off between truncation error and condition error imply that, in order for the perturbation method to be successful, an analysis of each individual parameter is required.

The accuracy of the estimated functions can be computed and plotted as confidence intervals. These intervals has been computed in a linearized covariance analysis [7, 11]. In this analysis the confidence intervals are linear dependent on the sensitivity

coefficients (as shown in the theory section). Figure 6 shows the oil relative permeability function with 95% confidence intervals. These intervals are computed using different perturbations in the perturbation method and they are compared with the confidence intervals calculated from analytical sensitivity coefficients. The direct method gives the largest intervals which means that the sensitivity coefficients were less than the sensitivity coefficients computed using the perturbation method. The trend is that for decreasing perturbations, the confidence intervals computed based on numerical sensitivity coefficients becomes larger and closer to the confidence intervals computed based on analytical sensitivity coefficients. The truncation error has introduced a "false sensitivity" in the numerical sensitivity coefficients. This "false sensitivity" decrease as the perturbations decrease. However, for low perturbations ($\Delta\theta$=1.0d-11), the condition error is large since the error in numerical computations is large and this introduces "false sensitivity", and consequently, the confidence intervals tend to be very narrow. This case illustrates that using the perturbation method without a careful analysis of the perturbations will result in too narrow confidence intervals and lead to underestimation of the errors in the estimated functions.

3.3 Basis Function Support and Impact on Sensitivity Coefficients and Confidence Intervals

Figure 7 shows a comparison of sensitivity coefficients computed by the direct and perturbation method for the three-phase case. The derivative of the state variables (P_o, S_w, and S_g) with respect to the parameters is first computed (as shown in the theory section). Then the pressure drop and oil production are differentiated with respect to these parameters using the state sensitivity coefficients, details on this can be found in Appendix B. The sensitivity of the differential pressure and production data with respect to one oil relative permeability parameter is plotted in Figure 7 as a function of time. The parameter correspond to the basis functions $B_{w5}B_{w3}$ which have support in the saturation region $S_w \times S_o = [0.4,1.0] \times [0.0,0.5]$ in Figure 5a. Figure 7 shows that the two methods give comparable results for this parameter. It can be noted, however, that in the transient period after the gas injection at t=2000 min and the rate increase at t=2500 min, the perturbation method will give some oscillations, as discussed in the previous section. These oscillations occur with rapid changes in the derivative, and they are a result of the truncation and condition error introduced by the numerical method used to compute sensitivity coefficients.

Next, identifiability of the parameters is investigated. The identifiability of parameters in the three-phase case is considerable more difficult than for the two-phase case. The sensitivity coefficients will generally be lower since the number of parameter increase, i.e., we will need more data. The measurement error will be the same but this requires a highly advanced three-phase apparatus, as described by [5]. The resolution of the parameters is the same. Figure 8 shows the CTB of pressure drop and production data for parameter c_{52} using both analytical and numerical sensitivity coefficients. Parameter c_{52} has support for $S_w \times S_o = [0.4,1.0] \times [0.0,0.3]$, i.e., area 5-8 in Figure 5a. This parameter has support in an area that covers most of the area where we have high degree of information in the data, hence the sensitivity coefficients for this parameter will be large for all the data points. With a resolution of 5% on the parameter ($c_{52} = 0.005 \pm 0.00025$), an upper bound of 1% on the pressure drop data and 1% error

in the production data (but a minimum of 0.001 PV), the contribution of observations (CTB) for pressure drop data and oil production are given in Figure 8. This analysis shows the importance of accurate computations of the sensitivity coefficients since these are the key element when estimating parameters and assessing accuracy of the estimates. This analysis also shows that the information content in the pressure drop data is higher than the production data. Actually, we will not be able to identify the parameter discussed (c_{52}) using production data with the given experimental design, error and resolution on the parameter as given above. The pressure drop data in the last two injection steps will be necessary for identifying this parameter.

Then sensitivity in pressure drop data with respect to two oil relative permeability parameters with support in two different saturation regions has been investigated. The first parameter (c_{12}) correspond to the basis function $B_{W1}B_{G2}$ in Figure 5a and has support in region 1 and 2 marked in the same figure, the other oil relative permeability parameter (c_{22}) corresponds to the basis function $B_{W2}B_{G2}$ with support in region 1-4. Figure 9a shows the sensitivity coefficient for c_{12} computed by both the direct and perturbation method. In this case the perturbation method gives sensitivity coefficients with high sensitivities in the transient period after the gas injection and gas rate step up at t=2000 min and t=2500min, while the direct method gives no sensitivities for these data except for data at the end of the experiment. The numerical sensitivity coefficients contain huge "false" sensitivity due to the condition error since there are no data in the saturation region 1 and 2. However, a low value of the sensitivity coefficient should be expected since the data trajectory stops at the border of the region and these data will be influenced by the relative permeability in the nearby region. This small sensitivity is computed by the analytical method, see zoomed part of Figure 9a. The sensitivity in pressure drop data with respect to c_{22} (the parameter with support in area 1-4) is plotted in Figure 9b. For this case, the two methods have computed the same sensitivity coefficient. However, the perturbation method has problems in the transient period after the second gas injection and produce huge oscillating sensitivities.

Based on sensitivity coefficients computed from the two methods, the confidence interval for the oil relative permeability is computed. The difference between the upper confidence surface computed by the two methods is plotted in Figure 10. This figure shows that analytical sensitivity coefficients gives larger confidence intervals than numerical sensitivity coefficients in regions with low sensitivity, i.e. for parameters with support in regions with no data, or data with little information on oil relative permeability. Since the confidence intervals computed from numerical sensitivity coefficients show that there are sensitivity in data in low sensitive regions, the method will produce erroneous sensitivity coefficients. However, the difference in sensitivity coefficients computed by the two methods is very low for parameters with support in regions with data containing relative permeability information. In Figure 5a, this region is marked 5-8 and corresponds to the region in Figure 10 with very low confidence intervals; $S_w \times S_o = [0.4,1.0] \times [0.0,0.3]$, i.e. around the saturation trajectory marked with bold.

3.4 Estimation and CPU-Time Requirements

The direct method for computation of sensitivity coefficients is implemented both for parameter estimation and computation of accuracy. As shown in section 3.3, the

parameters can be estimated accurately from analytical sensitivity coefficients, if the parameters have support in a sensitive region.

Figure 11 shows the results after estimating three-phase oil relative permeability parameters using the two methods for sensitivity calculations (we are here estimating 10 parameters in the three-phase oil relative permeability function, the rest of the parameters characterizing the surface is equal to the true parameters, and they are not part of the estimation). The true differential pressure and production data and the data based on the initial guess of oil relative permeability parameters are plotted together with data computed from estimated parameters. Both the direct and perturbation method have been used to compute the sensitivity coefficients used in the optimization to estimate the oil relative permeability function. Here, both the analytical and numerical method provides a good match with the true data. Since the estimated parameters have support in sensitive regions, and hence, both analytical and numerical methods for sensitivity computations can be used. However, the number of iterations to reach the solution differ for the two methods, see Table 4. In the perturbation method the number of iterations increases more rapidly than for the direct method. Due to the "false" sensitivity introduced in the perturbation method, the accuracy of each step in the search for the true parameters is reduced. The "false" sensitivity reduces the accuracy of the sensitivity coefficients and the robustness of the parameter estimation method, and consequently, slows down the convergence rate.

Finally, the CPU-time requirements for the two methods have been investigated. In Figure 12a the CPU-time vs. number of parameters when computing the sensitivity coefficients is plotted for Case 1. The computational expense in the perturbation method is clearly illustrated compared to the direct method, and Table 5 gives the results from comparison of the two methods. The direct method is approximately 8 times faster than the perturbation method when computing the sensitivity matrix **A**.

In Figure 12b the CPU-time vs. number of parameters when estimating parameters is plotted for Case 2. When the number of parameters increase, the advantage of the direct method is obvious, both due to reduction in computer time and due to reduced number of iterations, as plotted in Figure 12c. The number of iterations increase due to the "false" sensitivity introduced by the truncation and condition error.

This analysis has showed that choosing the perturbations, as well as accuracy and computational effort might be a significant problem when the perturbation method is used to compute the sensitivities. The direct method, however, has proved to be more efficient, accurate and robust for sensitivity calculations used in parameter estimation and accuracy computations in three-phase flow.

4 Conclusions

1. The direct method for computing sensitivity coefficients has been implemented to compute sensitivity coefficients for two- and three-phase flow in porous media.
2. The problem with choosing perturbations in the perturbation method is avoided since the sensitivity coefficients are computed analytically after a discretization scheme is chosen.
3. The direct method gives accurate sensitivity coefficients and the problem with "false sensitivity" in regions with low or no sensitivity is eliminated.
4. Contribution of observations can be used to check the identifiability of the parameters and the information contents in various data sets.
5. The computational savings using the direct method to compute sensitivity coefficients are huge.

Acknowledgment

This work is a part of a RF - Rogaland Research project within three-phase relative permeability estimation. The project is sponsored by the Norwegian Research Council whose support we gratefully acknowledge.

References

[1] F. Anterion, R. Eymard, B. Karcher, Use of Parameter Gradients for Reservoir History Matching, in Proceedings of the SPE Symposium on Reservoir Simulation, Houston, TX, Feb. 6-8, 1989, pp. 339-354.

[2] K. Aziz, A. Settari, *Petroleum Reservoir Simulation*, Elsevier Applied Science Publishers Ltd., London, 1979.

[3] P.E. Gill, W. Murray, M.H. Wright, *Practical Optimization*, Academic Press Inc., New York, 1981.

[4] A.H. Dogru, J.H. Seinfeld, Comparison of Sensitivity Coefficient Calculation Methods in Automatic History Matching, Society of Petroleum Engineering Journal, 1981, pp. 551-558.

[5] E. Ebeltoft, J.E. Iversen, K.O. Vatne, M.A. Andersen, J.E. Nordtvedt, A Novel Experimental Apparatus for Determining of Three-Phase Relative Permeabilities at Reservoir Conditions, Journal of Petroleum Science and Engineering, in press, 1998.

[6] Z.J. Kabala, P.C.D. Milly, Sensitivity Analysis of Flow in Unsaturated Heterogeneous Porous Media: Theory, Numerical Model, and Its Verification, Water Resour. Res., Vol. 26, No. 4, pp 593-610, April 1990.

[7] P.D. Kerig, A.T. Watson, Relative Permeability Estimation From Displacement Experiments: An Error Analysis, SPE Reservoir Engineering, Vol.1, No. 2, 1986, 175-182.

[8] G.M. Mejia, K.K Mohanty, A.T. Watson, Use of In Situ Saturation Data in Estimation of Two-Phase Flow Functions in Porous Media, Journal of Petroleum Science and Engineering, Vol. 12, 1995, pp. 233-245.

[9] J.E. Nordtvedt, E. Ebeltoft, J.E. Iversen, A. Sylte, H. Urkedal, K.O. Vatne, A.T. Watson, Determinations of Three-Phase Relative Permeabilities from Displacement Experiments, in: Proc. of the 1996 SPE Annual Technical Conference and Exhibition, Denver, Colorado, USA, October 6-9, 1996, pp. 1-13.

[10] J.E. Nordtvedt, K. Langaas, A. Sylte, H. Urkedal, A.T. Watson, Estimation of Three-Phase Relative Permeability and Capillary Pressure Functions, in Proceedings of the 5th European Conference on Mathematics of Oil Recovery, Leoben, Austria, Sept. 3-6, 1996, pp. 1-10

[11] J.E. Nordtvedt, H. Urkedal, A.T. Watson, E. Ebeltoft, K. Kolltveit, K. Langaas, I.E.I. Øxnevad, Estimation of Relative Permeability and Capillary Pressure Functions Using Transient and Equilibrium Data from Steady-State Experiments, in Proceedings of the 1994 International Symposium of the Society of Core Analysts, Stavanger, Norway, Sept., 1994, pp. 197-206.

[12] L.L Schumaker, *Spline Functions: Basic Theory*, J. Wiley & Sons Inc., New York 1981.

[13] T.H. Skaggs, D.A. Barry, Sensitivity methods for time-continuous, spatially discrete groundwater contaminant transport models, Water Resour. Res., Vol. 32, No. 8, pp. 2409-2420, Aug. 1996.

[14] N.-Z. Sun, W. W.-G. Yeh, Coupled Inverse Problems in Groundwater Modeling 1. Sensitivity Analysis and Parameter Identification, Water Resour. Res., Vol 26, No. 10, pp. 2507-2525, Oct. 1990.

[15] N.-Z. Sun, W. W.-G. Yeh, Coupled Inverse Problems in Groundwater Modeling 2. Identifiability and Experimental Design, Water Resour. Res., Vol 26, No. 10, pp. 2527-2540, Oct. 1990.

[16] G.W. Thomas, *Principles of Hydrocarbon Reservoir Simulation*, IHRDC, Publishers, Boston, 1982.

[17] D.A. Tortorelli, P. Michaleris, Design Sensitivity Analysis: Overview and Review, Inverse Problems in Engineering, Vol. 1, No. 1, pp. 71-105, 1994.

[18] H. Urkedal, K. Langaas, J.E. Nordtvedt, A.T. Watson, Design of Three-Phase Relative Permeability Experiments, in Proceedings of the 1995 International Symposium of the Society of Core Analysts, San Francisco, California, Sept. 12-14, 1995, pp. 1-15.

[19] O. Vignes, Application of optimization methods in oil recovery problems, Ph.D. dissertation, NTNU, Trondheim, Norway, Oct. 1993.

[20] A.T. Watson, Sensitivity Analysis of Two-Phase Reservoir History Matching, SPE Reservoir Engineering, Vol. 4, No. 3, 1989, pp. 319-324.

[21] A.T. Watson, P.C. Richmond, P.D. Kerig, T.M. Tao, A Regression-Based Method for Estimating Relative Permeabilities from Displacement Experiments, SPE Reservoir Engineering, Vol. 3, No. 3, 1988, pp. 953-958.

[22] W.W.-G. Yeh, N.-Z. Sun, Variational Sensitivity Analysis, Data Requirements, and Parameter Identification in a Leaky Aquifer System, Water Resour. Res., Vol 26, No. 9, pp. 1927-1938, Sept. 1990.

Appendix A Differentiation of Model Equations

The model equation is given as

$$F(u^{n+1},\theta)=G(u^n,\theta).$$

This equation is solved for each grid block i at each time step n. Hence, **F** is a diagonal matrix where the size depend on how many grid blocks there are in the problem and how many state variables. There is also a **F** matrix for each phase. **G** is a vector, the size depending on the number of grid blocks. θ is the vector of model parameters and **u** is the vector of state variables.

Oil Equation

Generally, the oil equation is given as

$$F_o^{n+1}(u^{n+1},\theta)=T_o^+(\Delta\Phi_o^+)^k-T_o^-(\Delta\Phi_o^-)^k-\frac{V_b}{\Delta t}\left(\varphi S_o b_o\right)^k-q_o^k$$

$$G_o^n(u^n,\theta)=-\frac{V_b}{\Delta t}\left(\varphi b_o(1-S_w-S_g)\right)^n.$$

The derivatives of the right hand side, G, with respect to the state variables in each grid block are

$$\frac{\partial G_o^n}{\partial P_o}=-\frac{V_b}{\Delta t}S_o(\varphi' b_o+\varphi b_o')$$

$$\frac{\partial G_o^n}{\partial S_w}=\frac{V_b}{\Delta t}\varphi b_o$$

$$\frac{\partial G_o^n}{\partial S_g}=\frac{V_b}{\Delta t}\varphi b_o.$$

For each grid block, the left hand side becomes

$$F_{o,i}^{n+1}=\frac{A}{\Delta x}\frac{k_{ro,i+\frac{1}{2}}}{\mu_o b_o}\left(P_{o,i+1}-P_{o,i}-G_{o,i+\frac{1}{2}}\right)-\frac{A}{\Delta x}\frac{k_{ro,i-\frac{1}{2}}}{\mu_o b_o}\left(P_{o,i}-P_{o,i-1}-G_{o,i-\frac{1}{2}}\right)$$
$$-\frac{V_b}{\Delta t}S_o b_o\varphi+c\frac{AK}{\Delta x}\frac{k_{ro,i}}{\mu_o b_o}\left(P_{well}-P_{o,i}-G_{o,i}\right).$$

Differentiating the model equation with respect to the coefficients gives

$$\frac{\partial F_{o,i}^{n+1}}{\partial\theta_j}=\frac{A}{\Delta x}\frac{1}{\mu_o b_o}\left(P_{o,i+1}-P_{o,i}-G_{o,i+\frac{1}{2}}\right)\frac{\partial k_{ro,i+\frac{1}{2}}}{\partial\theta_j}$$
$$-\frac{A}{\Delta x}\frac{1}{\mu_o b_o}\left(P_{o,i}-P_{o,i-1}-G_{o,i-\frac{1}{2}}\right)\frac{\partial k_{ro,i-\frac{1}{2}}}{\partial\theta_j}$$
$$-c\frac{AK}{\Delta x}\frac{1}{\mu_o b_o}\left(P_{well}-P_{o,i}-G_{o,i}\right)\frac{\partial k_{ro,i}}{\partial\theta_j}.$$

$$\frac{\partial G_o^n}{\partial \theta_j} = 0.$$

Corresponding calculations are performed for water and gas.

Derivative of Production Terms

The production terms are a part of the left hand side, and the terms will form the diagonal of the Jacobi matrix since all terms are computed at grid block *i*. They are given as

$$q_o = -PI_o\left(P_{well} - P_o - G_o\right)$$

$$q_w = -PI_w\left(P_{well} - P_w - G_w\right) = -PI_w\left(P_{well} + P_{c,ow} - P_o - G_w\right)$$

$$q_g = -PI_g\left(P_{well} - P_g - G_g\right) = -PI_g\left(P_{well} - P_{c,og} + P_o - G_g\right)$$

$$R_s q_o = -R_s PI_o\left(P_{well} - P_o - G_o\right).$$

Differentiating the production terms with respect to the model parameters gives

$$\frac{\partial q_o}{\partial \theta_j} = -\frac{\partial PI_o}{\partial \theta_j}\left(P_{well} - P_o - G_o\right)$$

$$\frac{\partial PI_o}{\partial \theta_j} = c\frac{b_o}{\mu_o}\frac{\partial k_{ro}}{\partial \theta_j}$$

$$\frac{\partial q_w}{\partial \theta_j} = -\frac{\partial PI_w}{\partial \theta_j}\left(P_{well} + P_{c,ow} - P_o - G_w\right) - PI_w\frac{\partial P_{c,ow}}{\partial \theta_j}$$

$$\frac{\partial PI_w}{\partial \theta_j} = c\frac{b_w}{\mu_w}\frac{\partial k_{rw}}{\partial \theta_j}$$

$$\frac{\partial q_g}{\partial \theta_j} = -\frac{\partial PI_g}{\partial \theta_j}\left(P_{well} - P_{c,og} + P_o - G_g\right) + PI_g\frac{\partial P_{c,og}}{\partial \theta_j}$$

$$\frac{\partial PI_g}{\partial \theta_j} = c\frac{b_g}{\mu_g}\frac{\partial k_{rg}}{\partial \theta_j}$$

$$\frac{\partial R_s q_o}{\partial \theta_j} = -R_s\frac{\partial PI_o}{\partial \theta_j}\left(P_{well} - P_o - G_o\right).$$

Appendix B Differentiation of Boundary Conditions with Respect to Model Parameters

Several boundary conditions are implemented in the model. Injection of water or oil or gas at constant rate or injection of all phases simultaneously at constant total rate. Production against constant well pressure or production at constant rate. As an example, injection of water at constant reservoir rate and production against constant well pressure is considered here. For these boundary conditions are the derivative of oil production and pressure drop with respect to the model parameters computed.

Oil Production

For injection of water, the production is given as

$$V_o = \sum_{i=1}^{N_x} V_{b,i}\varphi_i b_{o,i}\left[S_{w,i} + S_{g,i}\right],$$

where N_x is the number of grid blocks in the x-direction. Differentiation of the oil production with respect to a model parameter θ_j is given as

$$\frac{\partial V_o}{\partial \theta_j} = \sum_{i=1}^{N_x} V_{b,i}\varphi_i b_{o,i}\left[\frac{\partial S_{w,i}}{\partial \theta_j} + \frac{\partial S_{g,i}}{\partial \theta_j}\right].$$

Pressure Drop

For injection of water at constant reservoir rate and production against constant pressure, the differential pressure is given as

$$\Delta P = P_{well} - P_{o,in} = -\frac{q_w}{\Sigma PI_f} + P_{c,ow}$$

where

$$q_w = -PI_w(P_{well} - P_w - G_w)$$
$$\Sigma PI_f = PI_w + PI_o$$

The derivative of differential pressure with respect to the model parameters is then

$$\frac{d\Delta P}{d\theta_j} = \frac{d}{d\theta_j}(P_{well} - P_{o,in})$$

where

$$\frac{d\Delta P}{d\theta_j} = \frac{\partial \Delta P}{\partial P_o}\frac{\partial P_o}{\partial \theta_j} + \frac{\partial \Delta P}{\partial S_w}\frac{\partial S_w}{\partial \theta_j} + \frac{\partial \Delta P}{\partial \theta_j}.$$

This gives

$$\frac{\partial \Delta P}{\partial \theta_j} = \left\{ -\left[\frac{\partial q_w}{\partial P_o} \Sigma PI_f + q_w \frac{\partial \Sigma PI_f}{\partial P_o} \right] / \Sigma PI_f{}^2 \right\} \frac{\partial P_o}{\partial \theta_j}$$

$$+ \left\{ -\left[\frac{\partial q_w}{\partial S_w} \Sigma PI_f + q_w \frac{\partial \Sigma PI_f}{\partial S_w} \right] / \Sigma PI_f{}^2 + \frac{\partial P_{c,ow}}{\partial S_w} \right\} \frac{\partial S_w}{\partial \theta_j}$$

$$- \left[\frac{\partial q_w}{\partial \theta_j} \Sigma PI_f + q_w \frac{\partial \Sigma PI_f}{\partial \theta_j} \right] / \Sigma PI_f{}^2 + \frac{\partial P_{c,ow}}{\partial \theta_j}.$$

Tables

Table 1: Core and fluid properties, and initial state for Case 1 and Case 2.

		Case 1	Case 2
φ	Porosity [frac.]	0.3	0.3
k	Absolute permeability [mD]	500.0	10.0
L	Core length [cm]	25.0	7.0
	Grid blocks in x-direction	50x0.5	20x0.35
A	Core area [cm^2]	10.0	10.0
B_w	Water formation volume factor	1.0	1.0
B_o	Oil formation volume factor	1.0	1.0
B_g	Gas formation volume factor		1.0
μ_w	Water viscosity [cP]	0.3	0.3
μ_o	Oil viscosity [cP]	0.4	0.4
μ_g	Gas viscosity [cP]		0.02
ρ_w	Water density [kg/m^3]	980.0	1000.0
ρ_o	Oil density [kg/m^3]	915.0	900.0
ρ_g	Gas density [kg/m^3]		100.0
S_{wi}	Initial water saturation [frac.]	0.0	1.0

Table 2: Statistical data for Case 1 and Case 2.

	Case 1	Case 2
Standard deviation, ΔP data [kPa]	0.20	5.00
Number of data points, ΔP	229	195
Standard deviation, V_o data [frac.]	0.01	0.01
Number of data points, V_o	229	195

Table 3: Injection strategy for Case 2.

	TIME (min)	Q_w (cc/min)	Q_g (cc/min)	Process	Measured data
1	0.0	0.70	0.00	W1	ΔP, Vo
2	1000.0	2.00	0.00	W2	ΔP, Vo
3	2000.0	0.00	0.50	G3	ΔP, Vo
4	2500.0	0.00	40.00	G4	ΔP, Vo

Table 4: Comparison of efficiency using analytical or numerical sensitivity coefficients in parameter estimation in Case 2.

	ASC				**NSC**			
# Param.	# It.	SSR	CPU time (sec)	# Call of simulator	# It.	SSR	CPU time (sec)	# Call of simulator
2	5	407.28	58	7	5	407.28	85	30
4	5	405.93	58	7	5	405.93	88	31
6	7	405.26	119	24	6	405.20	151	50
8	10	404.66	210	41	13	404.59	414	132
9	12	403.09	219	43	17	402.41	628	206
10	16	402.02	281	51	101	433.62	10 461	1143

Table 5: Number of parameters vs. CPU time when computing sensitivity matrix for Case 1 using direct method and perturbation method.

# Parameters	CPU time, ASC	CPU time, NSC	NSC/ASC
13	4	18	6
21	5	26	6.5
27	6	39	7.8

Figures

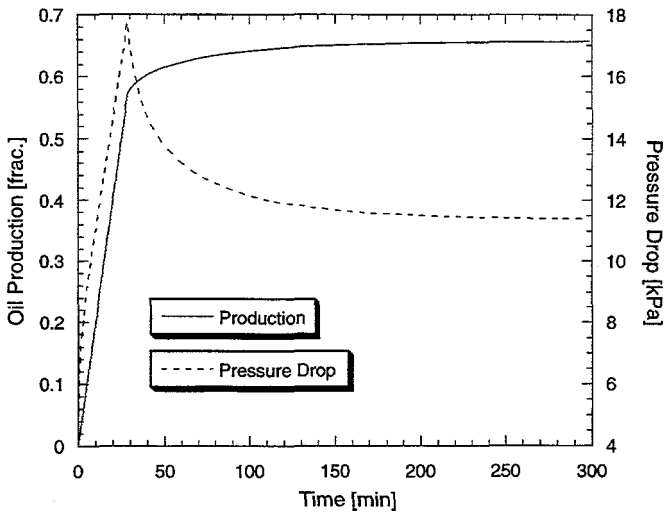

Figure 1 Pressure drop and production data for Case 1 (two-phase).

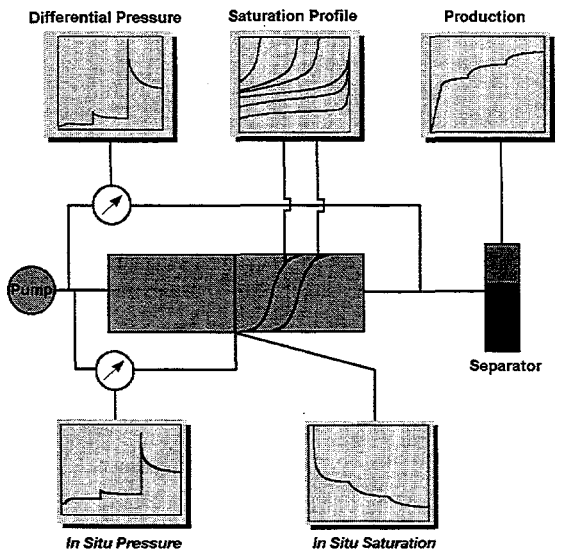

Figure 2 Different types of data gathered from displacement experiments.

a)

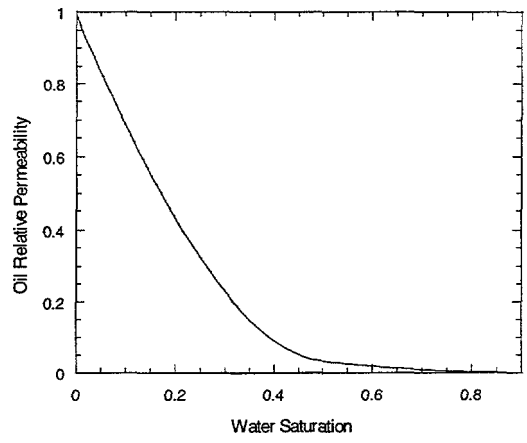

b)

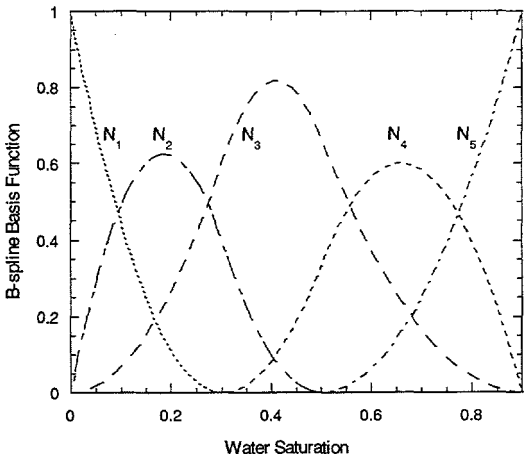

Figure 3 a) Two-phase oil relative permeability function, and b) corresponding B-splines basis functions. The derivative of oil relative permeability with respect to parameter $\theta_2=c_2$ is B-splines basis function N_2.

a)

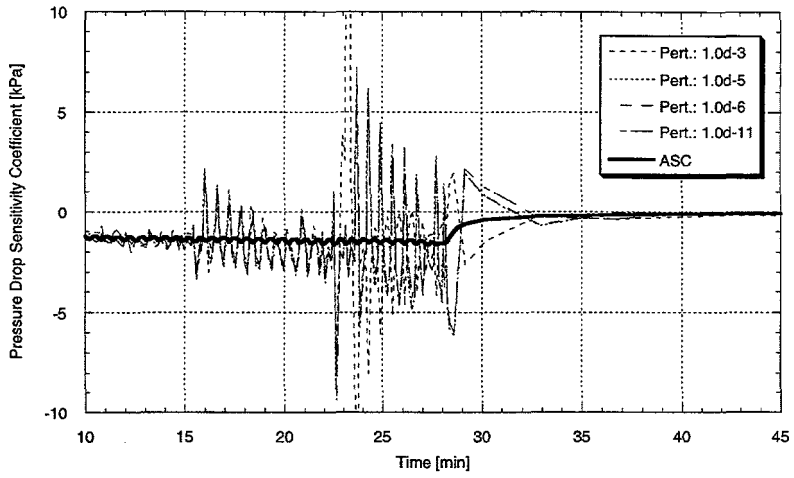

b)

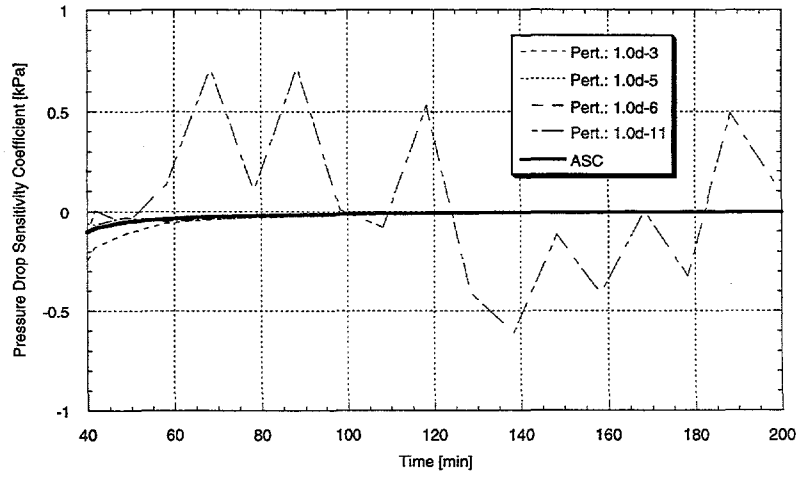

Figure 4 Analytical pressure drop sensitivity coefficient in Case 1 compared with different choices of perturbations in the numerical method.

a)

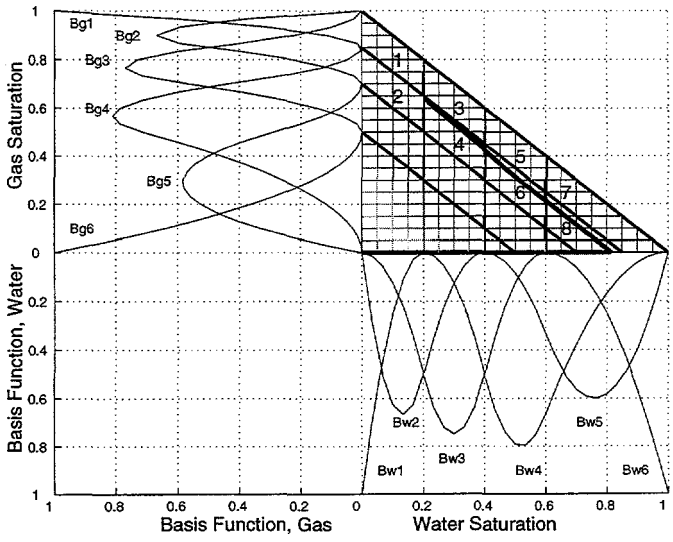

b)

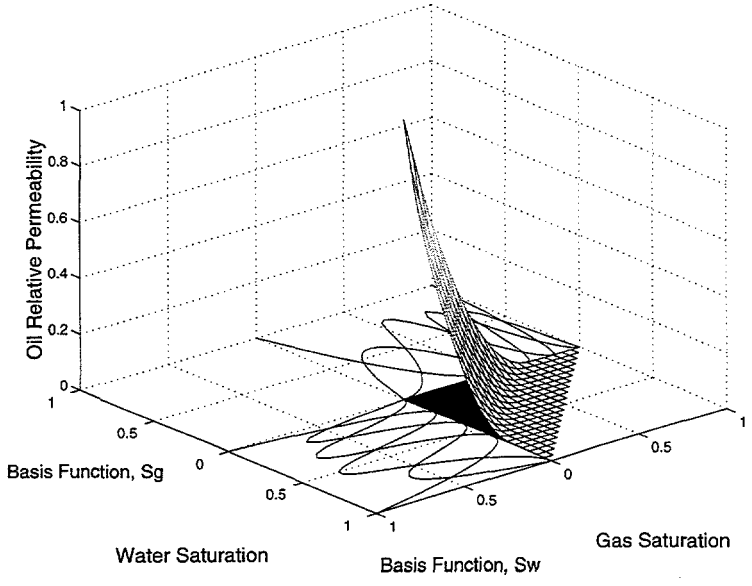

Figure 5 a) Three-phase oil relative permeability seen from above. The water and gas B-splines basis functions are also plotted. The saturation trajectory corresponding to a three-phase experiment is also plotted (bold line), b) Three-phase oil relative permeability in 3D.

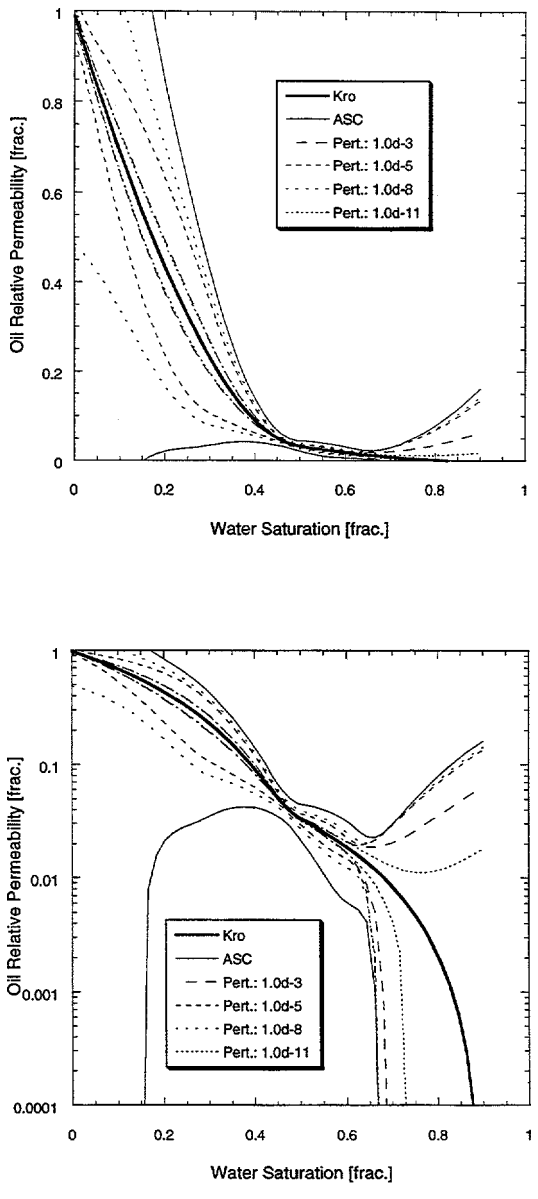

Figure 6 Oil relative permeability function for Case 1 with 95% confidence intervals in normal and log-scale. The confidence intervals are computed using the analytical method and the numerical method with different choices of perturbations.

a)

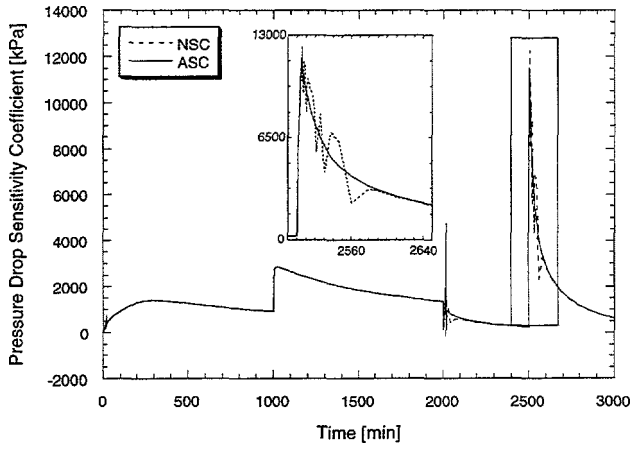

b)

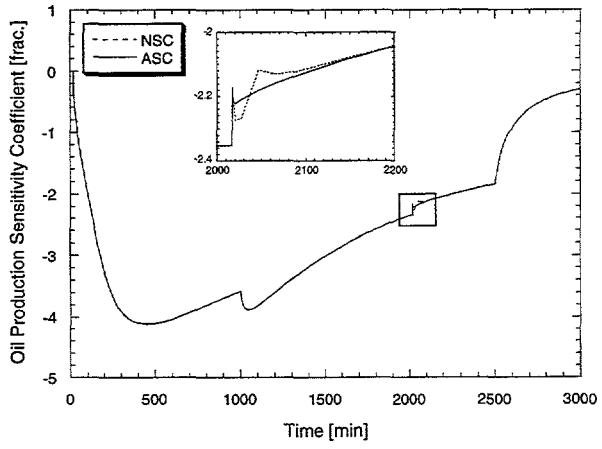

Figure 7 Numerical and analytical sensitivity coefficient in Case 2 (three-phase) for parameter c_{53}. a) pressure drop data, and b) production data.

a)

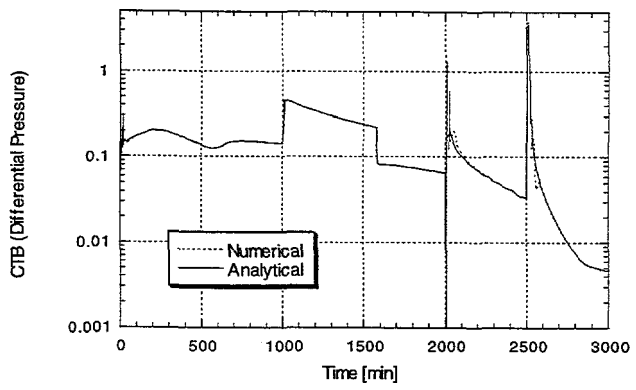

b)

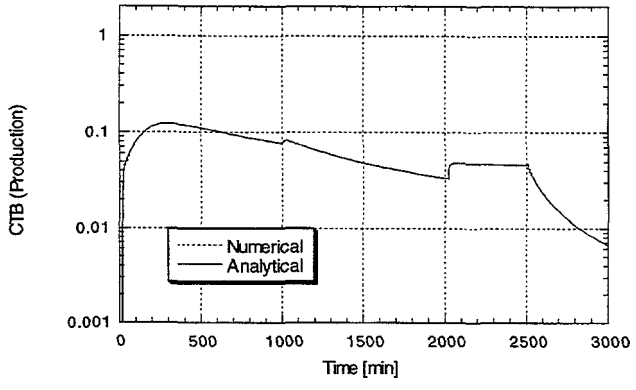

Figure 8 a) Contribution of pressure drop data on parameter c_{s2}, and b) contribution of production data on parameter c_{s2} using analytical and numerical sensitivity coefficients.

a)

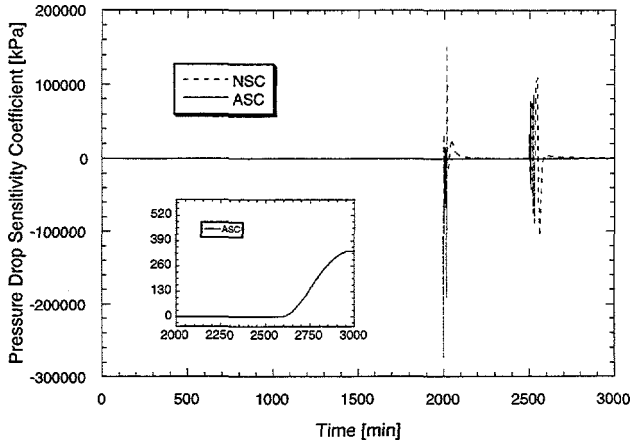

b)

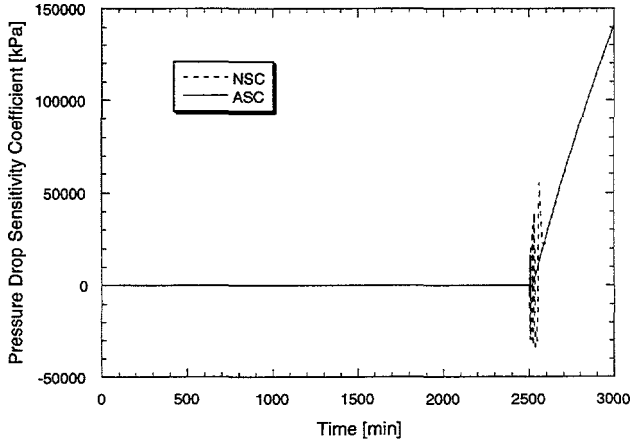

Figure 9 Analytical and numerical sensitivity coefficients for Case 2. a) Sensitivity coefficient for parameter with support in low-sensitive region, c_{12} (region 1 and 2), and b) Sensitivity coefficient for parameter with support in a sensitive region c_{22} (region 1-4).

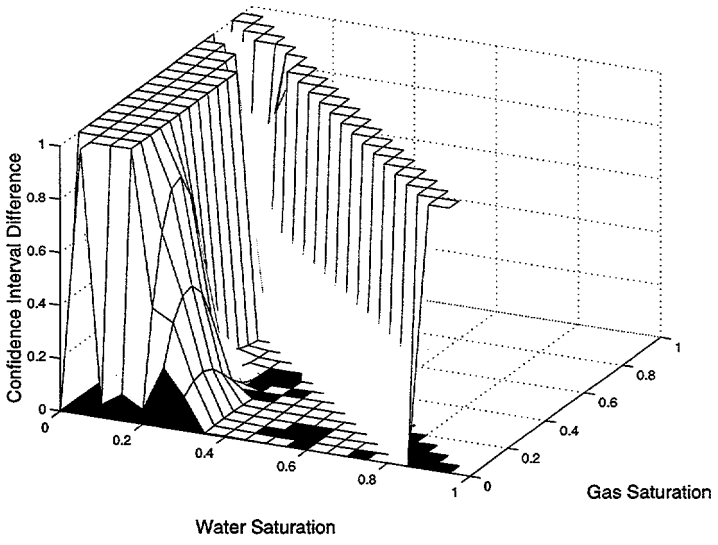

Figure 10 Difference between upper confidence intervals (for three-phase oil relative permeability) computed from analytical and numerical sensitivity coefficients.

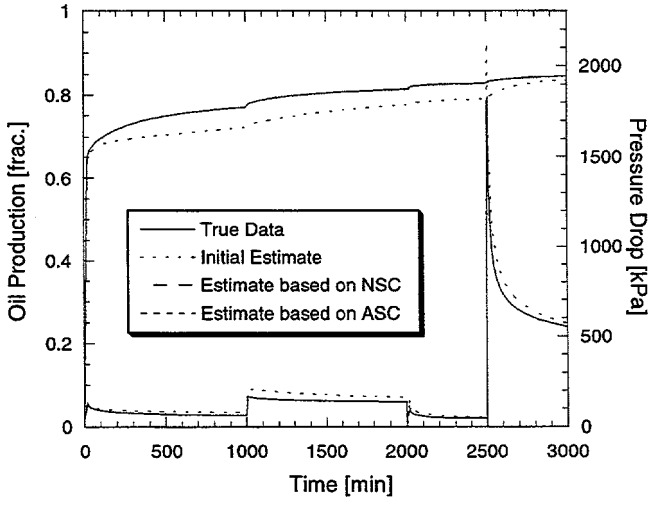

Figure 11 Differential pressure data and oil production data after parameter estimation using analytical and numerical implementation of sensitivity coefficients in Case 2.

a)

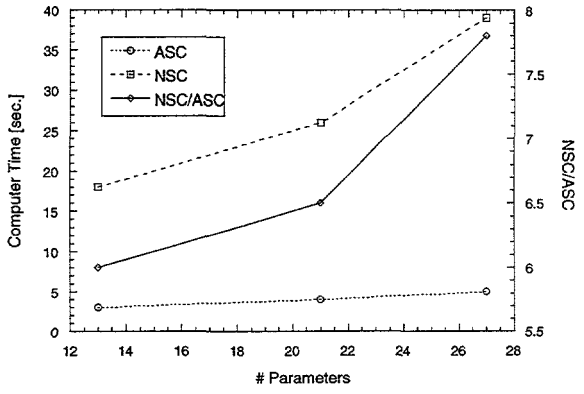

b)

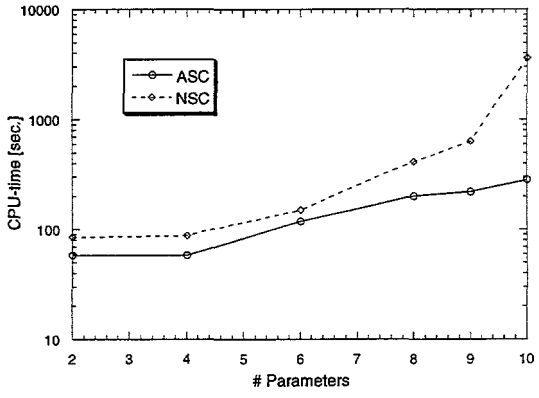

c)

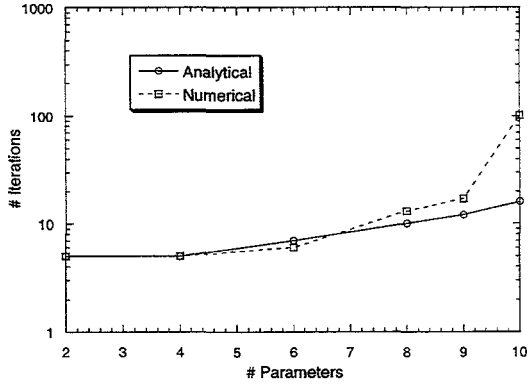

Figure 12 a) Number of parameters vs. CPU-time in direct computation of sensitivity matrix in Case 1, b) Number of parameters vs. CPU time, and c) Number of parameters vs. number of iterations after estimation of oil relative permeability surface in Case 2.

Paper VI

Estimation of Porous Media Flow Functions

A. Ted Watson,[†1] Raghavendra Kulkarni,[†] Jan-Erik Nordtvedt,[‡] Andre Sylte,[‡] Hege Urkedal[‡]

[†]Department of Chemical Engineering,
Texas A&M University, College Station, TX 77843-3122

[‡]RF-Rogaland Research, Thormøhlengt. 55, N-5008 Bergen, Norway

Abstract

Properties important for describing the flow of multiple fluid phases through porous media are represented as functions of state variables (fluid saturations). A generalized procedure is presented to obtain the most accurate estimates of the multiphase flow functions from the available experimental data. The procedure is demonstrated for several different experimental designs, including a novel experiment in which fluid saturations are measured using nuclear magnetic resonance imaging. A method to evaluate the accuracy of the estimates is presented, and its use for assessing experimental design is demonstrated.

Introduction

Accurate description of multiphase flow through porous media is important in designing and controlling a number of processes of technological significance, among those the production of fluids from underground reservoirs and remediation of underground water resources. Multiphase flow through porous media is typically modeled by continuum representations whereby the state variables are rendered continuous in space and time based on local volume averaging (Slattery, 1981; Bear, 1972). Several properties have to be specified in such models. They include fluid properties such as viscosity and density and rock properties such as porosity and absolute permeability. In situations where there are multiple fluid phases, relative permeability and capillary pressure functions are to be specified. We will refer to these collectively as multiphase flow functions.

The flow functions are effective properties defined within the mathematical model, so they must be determined through solution of some inverse problem. This is done by using observations of state variables measured during displacement experiments to infer the flow functions through the mathematical model of the experiment. This is particularly challenging since the flow functions are functions of state variables (saturations), and the models for the displacement processes are coupled partial differential equations.

Typically, a relative permeability function for each fluid phase and a capillary pressure function for each pair of fluid phases are to be estimated. Hence, for two-phase flow, three flow functions are to be estimated while for three-phase flow, five flow functions are to be estimated. Traditionally, simplified methods have been used to estimate these flow functions. Capillary pressure has been estimated independently (see e.g., Nordtvedt and Kolltveit, 1991). Methods to estimate relative permeabilities have been based upon attempts to eliminate capillary pressure effects in the experiments so that point values of the relative permeabilities can be explicitly

[1]Corresponding author

calculated (Leverett, 1940; Johnson et al., 1959) using analytical solutions of the model equations available for those simplified conditions. These methods suffer from simplifications used in trying to avoid the capillary pressure effects (Urkedal et al., 1997; Richmond and Watson, 1990) and also from the fact that the determination of a few discrete relative permeability values does not adequately reconcile the continuous relative permeability functions (Richmond and Watson, 1990). It is desirable that relative permeabilities and capillary pressure be simultaneously estimated from the same experiment.

A unified methodology can be used to estimate the multiphase flow functions simultaneously from a variety of experimental scenarios (Watson et al., 1988). The method is directed to obtaining the most accurate estimates of the unknown functions from the available data, and is not limited by the form of the mathematical model, the experimental design (which includes the manner in which the experiment is conducted, the types of data measured and the accuracy with which the data are measured), or the specification of which unknown functions are to be estimated. In this technique, the data analysis problem is formulated as an inverse problem. A mathematical model is specified which describes the fluid flow experiment and includes the properties to be estimated. Then, the flow functions are adjusted with a statistical methodology until the numerical solution of the mathematical model for the process matches the experimental data.

A key element of the technique is the suitable representation of the flow functions. Ultimately a finite number of parameters are to be estimated from the finite number of measured data. Using a suitable functional representation, the estimation of flow functions reduces to a series of parameter estimation problems. A regression-based methodology can be used to select the appropriate representations (Watson et al., 1988).

In this paper we present the unified methodology in the context of estimating two-phase flow functions. We also present a methodology to assess the accuracy of estimates which can be obtained from a given experimental design. We demonstrate the estimation method with two different experimental scenarios. In the first, the relative permeability and capillary pressure functions are estimated from a constant rate dynamic displacement experiment which incorporates novel measurements of fluid saturation distributions using magnetic resonance imaging (MRI). In the second, the flow functions are estimated from a multirate dynamic displacement experiment utilizing only effluent data. In addition, we show how the measures of accuracy of the estimates can be used to assess the experimental design.

Estimation Methodology

A particular feature of the estimation of multiphase flow functions is that these properties are functions of state variables, fluid saturations. There are several key elements to the estimation. A mathematical model is selected to represent the experiment. The model should be sufficiently complete so that all important physical effects within the experiment are represented by the model. Candidate functional representations are chosen for the multiphase flow functions to be estimated. Then, the coefficients within the functional representations are calculated as those that minimize a suitable objective functions. Each of these elements is discussed in more detail in this section.

Mathematical Model

Multiphase immiscible flow through porous media is modeled by an extension of Darcy's law for single phase flow through porous media. The state variables (saturation and pressure) are

volume averaged quantities (Slattery, 1981), and are represented as continuous functions of time as well as space. The following equations are obtained by combining the Darcy equation with continuity equation for each fluid phase (Aziz and Settari, 1979),

$$\frac{\partial}{\partial t}(\phi\rho_{nw}S_{nw}) = \nabla.\left(\frac{Kk_{nw}\rho_{nw}}{\mu_{nw}}(\nabla P_{nw} + g\nabla z)\right) \quad (1)$$

$$\frac{\partial}{\partial t}(\phi\rho_{w}S_{w}) = \nabla.\left(\frac{Kk_{w}\rho_{w}}{\mu_{w}}(\nabla P_{w} + g\nabla z)\right) \quad (2)$$

where subscripts nw and w refer to the non-wetting and wetting phases, respectively. In addition, the state variables, fluid phase saturations and pressures, are related as follows:

$$P_{nw} - P_w = P_c \quad (3)$$

$$S_{nw} + S_w = 1. \quad (4)$$

Boundary and initial conditions for the pressures and saturations are chosen according to the particular experimental design being used.

The densities and viscosities are fluid properties which can be measured independently. The porosity ϕ and permeability K are effective properties corresponding to local volume averages (Slattery, 1981). These can be determined in experiments involving a single saturating fluid phase. The relative permeabilities, k_w, k_{nw}, and capillary pressure, P_c, are effective properties which are functions of the fluid saturation. The determination of these multiphase flow functions is the objective here.

Functional Representation

The relative permeability and capillary pressure are known to be functions of fluid saturation, and are believed to be smooth and monotonic. In particular, the relative permeability of each phase in nonnegative and increases with the saturation of that phase. However, the exact functional form is unknown and should be inferred from the experimental data.

We use B-splines to represent the flow functions. B-splines are preferred because they can represent any smooth function arbitrarily accurately (Schumaker, 1981). At the same time they have many convenient computational features. The property representations are given by:

$$k_{ri}(S_w) = \sum_{j=1}^{N_i} C_j^i B_j^m(S_w, \vec{y}^i), \qquad i = w, nw \quad (5)$$

$$P_c(S_w) = \sum_{j=1}^{N_c} C_j^c B_j^m(S_w, \vec{y}^c). \quad (6)$$

The B-spline functions are specified by the order m and the extended partition $\vec{y}$. Once these are specified, the properties are estimated by determining the following parameter vector through a parameter estimation problem:

$$\vec{\beta} = [C_1^w, \ldots, C_{N_w}^w, C_1^{nw}, \ldots, C_{N_{nw}}^{nw}, C_1^c, \ldots, C_{N_c}^c]. \quad (7)$$

The parameter estimation problem is described in the next subsection.

Selection of a suitable spline partition is important for accurate estimation of flow functions. The goal is to eliminate significant basis errors, while limiting unnecessary variance errors (Watson et al, 1988; Kerig and Watson, 1986). This is accomplished by successively increasing

the number of knots (and hence the number of unknown parameters, and correspondingly the candidate solution space for the unknown functions) until suitable predictions of the measured quantities are obtained. A convenient way to assess this is to identify the point at which significant reductions in the performance index cannot be obtained with modest increases in the number of parameters. The knots are added to those regions of the properties that appear to be responsible for the greatest discrepancies between the measured and predicted data (Grimstad et al., 1997).

Parameter Estimation

For a given B-spline representation (i.e. order m and extended partition $\vec{y}$), the parameters are given by solution of the parameter estimation problem represented by:

$$\text{minimize} \qquad J(\vec{\beta}) = [\vec{Y}_m - \vec{Y}_s(\vec{\beta})]^T \mathbf{W} [\vec{Y}_m - \vec{Y}_s(\vec{\beta})] \tag{8}$$

subject to the constraints

$$\mathbf{G}\vec{\beta} \geq \vec{g}_0. \tag{9}$$

$\vec{Y}_m$ is the vector containing measured data. In the regression-based method, a variety of data can be used, including pressure drop, production, and saturations measured within the sample. $\vec{Y}_s(\vec{\beta})$ is the vector containing corresponding values calculated by numerical simulation of the displacement process through the mathematical model represented by Eqs. 1–4. $\mathbf{G}$ is the matrix specifying the linear inequality constraints on the parameters. For example, each of the functions is monotonic with saturation and the relative permeabilities are nonnegative. Such constraints can be conveniently expressed as linear inequality constraints on the unknown coefficients in the B-spline representation (Watson et al., 1988). $\mathbf{W}$ is the weighting matrix. If we assume that the measurement errors associated with the data can be represented by a normal distribution with zero mean and covariance matrix $\mathbf{\Sigma}$, maximum likelihood estimates of the parameters are obtained when the weighting matrix $\mathbf{W}$ is taken as a scalar multiple of $\mathbf{\Sigma}^{-1}$ (Watson et al., 1990). Generally, it can be taken to be a diagonal matrix with entries equal to the inverse of the estimated variances of the data measurement errors. A trust-region based, linear inequality constrained, Levenberg-Marquardt algorithm (Richmond, 1988) has been used to solve the nonlinear least squares problem represented by Eqs. 8 and 9.

Design of Experiments

The multiphase flow properties are determined by setting up a flowing experiment, whereby the state variables, or functions of the state variables, corresponding to Eqs. 1–4 can be measured. Then, estimates are obtained as discussed in the previous section, using the mathematical model represented by Eqs. 1–4 with the associated boundary and initial conditions corresponding to the particular flowing experiment. The conventional experiment is a displacement experiment, in which a single fluid phase is injected at a constant flow rate into a sample which is initially saturated with the other fluid (perhaps containing an irreducible saturation of the injected fluid phase). The pressure drop across the sample, and the production of the displaced fluid phase, are measured. The pressure drop represents the difference between state variables corresponding to spatial locations at either end of the sample. The production is a function of state variables: material balances on the fluids provide relations between integrals of saturations distributions across the sample and the production.

An important question is whether such data have sufficient information content to estimate all the unknown functions accurately. This can be evaluated using a linearized covariance analysis. In the covariance analysis, it is assumed that the mathematical model is capable of describing the physical process, that the B-spline representation can adequately represent the flow functions (no bias error), and that the model function $\vec{Y}_s(\vec{\beta})$ is linear with respect to the parameters $\vec{\beta}$ near the solution. Finally, it is assumed the measurement errors are additive (i.e., $\vec{Y}_m(\vec{\beta}) = \vec{Y}_s + \vec{\epsilon}$) for some parameter vector $\vec{\beta}$ and error vector $\vec{\epsilon}$. Suppose the error vector $\vec{\epsilon}$ has a normal distribution with zero mean and covariance matrix $\mathbf{\Sigma}$. Then, if we use the inverse of the covariance matrix $\mathbf{\Sigma}$ as the weighing matrix in equation (8), we find that the covariance matrix of the estimated parameters is given by (Kerig et al., 1986):

$$\mathbf{P} = (\mathbf{A}^T \mathbf{\Sigma}^{-1} \mathbf{A})^{-1} \tag{10}$$

where $\mathbf{A}$ is given by the sensitivity of the simulated data to the parameters. Note that since the vector of data values $\vec{Y}_m$ does not appear in this expression, no experimental data are required to compute $\mathbf{P}$. Thus, a statistical analysis of the estimation problem for a specific experimental design can be performed before actually conducting any experiments (Nordtvedt et al., 1992).

Of greater interest than the covariance matrix $\mathbf{P}$ for the parameters, is the covariance of the flow functions themselves at specific saturation values. The covariance of the flow functions, $\mathbf{C}$, can be written as(Kerig et al., 1986):

$$\mathbf{C} = \mathbf{D}^T(S_w)\mathbf{P}\mathbf{D}(S_w) \tag{11}$$

where the matrix $\mathbf{D}$ is the sensitivity of the flow functions with respect to the parameters at a specified saturation value. Using the diagonal of $\mathbf{C}$, a point-wise confidence interval can be constructed for the flow functions

$$\vec{r}^* = \vec{r} \pm q\sqrt{c_{ii}} \tag{12}$$

where $\vec{r} = [k_{rw}, k_{ro}, P_c]$ and q is the appropriate quantile for the given confidence level and distribution.

If the properties are not estimated sufficiently accurately, one should investigate alternative experimental designs. Possibilities of improving the accuracy of the estimates include measuring the data more accurately (if possible), measuring more data, and conducting the experiment differently. The accuracy of the estimates corresponding to each experimental design can be assessed, and trade-offs of the accuracy with such concerns as costs and experimental convenience can be evaluated.

Results and Discussion

We consider here the estimation of two-phase relative permeability and capillary pressure functions from laboratory displacement experiments. The basic experiment is as follows. A cylindrical sample of the porous medium, nominally an inch in diameter and three inches in length, is sealed along the periphery. The sample is saturated with one or two fluids at a known saturation. Then, one, or two, fluids are injected into one end of the sample, and production takes place at the other end. The pressure drop and production are measured, and in one experiment, the actual saturation distributions within the sample are observed. Several properties within the mathematical model can be determined independently, namely the fluid properties and those properties used to describe the flow of a single fluid phase. In one example, the porosity distribution is measured using a novel MRI experiment. Otherwise, the average porosity and

Table 1: Core and fluid properties for experimental design cases

Water viscosity (cP)	1.11
Oil viscosity (cP)	1.121
Core length (cm)	5.0
Core diameter (cm)	3.74
Porosity (%)	25.00
Absolute Permeability(mD)	100.0
Initial Water Saturation	1.0
Injection single-rate (cc/min.)	1.0
Injection multirate (cc/min.)	0.1/1.0/5.0

permeability of the samples are determined, and those properties taken to be uniform in the mathematical model. The mathematical model is solved using a fully implicit finite difference technique (Guo et al., 1993; Aziz and Settari, 1979).

We first report an investigation of experimental design that demonstrates the accuracy of estimates can be improved by simply using multiple injection rates with conventional experiments. We then demonstrate the use of novel measurements of saturation distributions for estimating the properties. Finally, we demonstrate an experimental design in which two fluid phases are injected simultaneously.

Example of Experimental Design

Traditionally, displacement experiments have been conducted using a constant flow rate, apparently because the original methods used to compute relative permeabilities were based on that assumption. However, exciting the system through manipulations in the flow rate can provide for greater accuracy of estimates of the properties. This is demonstrated by comparing the accuracy of estimates obtained using two different scenarios for conducting two-phase displacement experiments.

In both cases, oil is injected into a core sample completely saturated with water (this represents a primary drainage experiment). The measured data are taken to be the production of water from the core sample and the pressure drop across the sample. The accuracy with which the flow functions can be estimated are determined for a case in which a single, uniform injection rate is used, and a case in which multiple injection rates are used. Details of the core sample, fluid properties and injection strategy chosen are tabulated in Table 1. The irreducible water saturation is taken to be 0.2.

The estimates of the relative permeabilities and capillary pressure curves, with the associated confidence intervals, are shown in Figure 1. The left-right pairs represent the same information, but with different scales for the ordinates. (Note that since each relative permeability increases with its own saturation, the water relative permeability corresponds to the curve which has positive derivatives.) It is evident that the multirate scenario is superior to the single-rate scenario for accuracy of estimates of the flow functions. Large improvements in the accuracy of estimates of all the properties are apparent in the lower range of water saturation. This is largely the result of the greater range of saturations accessed in the multirate scenario through the use of the greater flow rate. More accurate estimates of the capillary pressure are obtained throughout

the saturation range, with the larger improvements occuring at either end of the saturation range. While there are some improvements in the accuracy of estimate of the oil relative permeability corresponding to larger values of water saturation, the accuracy of estimation of the water relative permeability remains poor. Evidently, the production and associated pressure drops in the early part of the displacement experiment (during which time the water saturations are relatively large) are largely controlled by capillary pressure effects, and to a lesser extent oil relative permeability effects, but are relatively insensitive to water relative permeability effects.

Observing Fluid Saturation Distributions

The previous example shows that the accuracy of estimates of multiphase flow functions is limited when a single injection rate is used. Multiple injection rates provide one way to enhance the accuracy of the estimates. Another approach to improve the accuracy of estimates is to measure additional data. In particular, nuclear magnetic resonance imaging (MRI) can provide a novel means for determining the fluids states within the core sample (Chen et al 1993; Chen et al 1994). Here we demonstrate the use of MRI for observing fluid saturations within the sample, and the use of those data in estimating the multiphase flow functions. Note that the measurements of the saturation distributions represent distributed observations of the system, while the previous measurements used, the production and pressure drop, represent only integral observations of fluid states.

A two-phase dynamic displacement experiment was conducted using a Texas Cream limestone sample. Oil was injected at a constant flow rate into the core sample which was completely saturated with the aqueous phase. The pressure drop and oil saturation profiles were measured until no further changes in the saturation distributions were observed. Hexadecane was used as the oleic phase and deuterium oxide was used as the aqueous phase. Oil saturation was measured using NMR imaging (Chen et al., 1994, Kulkarni et al., 1997). Water production was estimated by integration of oil saturation profiles with material balances about the initial state. Further details of the core sample, fluid and the displacement process are tabulated in Table 2.

The pressure drop, saturation profiles, and water production data were used in the regression-based approach to estimate the relative permeability and capillary pressure functions. Starting with just single knot B-spline representations for each flow function, successive parameter estimation problems were solved with increasing numbers of knots. It was found that the performance index, calculated using Eq. 8 for a B-spline representation with 7 interior knots each in the relative permeability representation and 6 interior knots in the capillary pressure representation, did not significantly decrease when additional knots were added. This representation was chosen for the final estimate. A total of 27 parameters were estimated in the final step of the regression-based approach.

The values of pressure drop, saturation distributions, and water production calculated using the estimated flow functions are shown together with the measured data in Figures 2–4. An excellent match between the data groups are seen, except for low water saturation for the water saturation profiles. This may be due to the relatively small number of data in this area. The estimated flow functions together with confidence intervals are shown in Figures 5 and 6. The measurement of the fluid saturations within the sample provide an important validation of the property estimates. Although these additional measurements do improve the accuracy as compared to just using conventional meaurements, the confidence intervals are still larger than one might desire. A preferred experimental design would be to use multirate injection experiments in addition to measurements of saturation distributions, although it is not clear that water relative permeabilities corresponding to the larger values of water saturation would

Table 2: Core and fluid properties for the single rate primary drainage experiment

Water viscosity (cP)	1.26
Oil viscosity (cP)	3.34
Core length (cm)	4.9
Core diameter (cm)	2.5
Porosity (%)	26.6
Absolute Permeability(mD)	10.2
Initial Water Saturation	1.0
Oil Injection Rate (cc/min):	0.05

be accurately from such displacement experiments.

Simultaneous Fluid Injection

While measurements of fluid distributions are desirable, equipment investments are significant, and the conduct of the experiment under reservoir conditions of temperature and pressure presents further difficulties. Yet another experimental scenario is investigated here. The experiment is carried out by injecting *both* fluid phases, as done in conventional steady state experiments (Urkedal et al., 1997). Unlike those conventional experiments, the dynamic responses are measured and used in estimating the properties.

An outcrop sample from the Turonian Seaton chalk formation ("Bear Stone") in Devon, Southern England was used. Oil and water were injected simultaneously into the core sample with the water/oil fraction decreasing in three steps. Then oil was injected at four increasing flow rates. Throughout the experiment, both transient and steady-state water production and pressure drop data were measured. Mineral oil (Exxon Isopar H) was used as the oleic phase and a simulated North-Sea chalk formation water as the aqueous phase. Calcium was added to the formation water to ensure chemical stability of the chalk matrix. Further details of the core sample, fluid and the displacement process are tabulated in Table 3.

The relative permeability and capillary pressure functions were estimated using the same procedure as the single rate primary drainage experiments. A total of 28 parameters were estimated in the final step of the regression-based methodology. The measured and simulated pressure drop and water production data are shown in Figure 7. A good agreement between the simulated and measured data are seen for both the water production and the pressure drop data. The estimated flow functions together with confidence intervals are plotted in Figures 8 and 9. Narrow intervals appear indicating that the experimental design used in this experiment is very suitable for accurate flow function estimates.

The capillary pressure estimate is compared to independent estimates obtained using two different experimental techniques: micro-membrane (Hammervold and Skjæveland,1992), and mercury injection (Wardlaw and Taylor, 1976). In both these cases, the capillary pressure curve has been obtained on a companion core sample, and thus, the properties may be expected to differ somewhat. As seen from Figure 9, the three techniques provide very similar results except for high saturation values.

Table 3: Core and fluid properties for the multirate experiment

Water viscosity (cP)	1.10
Oil viscosity (cP)	1.19
Core length (cm)	6.81
Core diameter (cm)	3.06
Porosity (%)	28.40
Absolute Permeability(mD)	4.17
Initial Water Saturation	1.0
Injection rates water / oil (cc/min):	0.099 / 0.001
	0.088 / 0.012
	0.04 / 0.06
	0.0 / 0.1
	0.0 / 0.25
	0.0 / 1.0
	0.0 / 3.0

Conclusions

A unified methodology was presented for determining properties used to describe the flow of multiple fluid phases in porous media. The method is not limited by the form of the mathematical model or the experimental design.

The accuracy of estimation of the properties was evaluated by a linearized covariance analysis and used to investigate the experimental design. Experiments and analyses demonstrated advantages of altering fluid injection strategies. A novel method for measuring distributions of the fluid states within the sample using MRI and incorporating those measurements into the estimation of the properties was presented.

Nomenclature

Roman

$\mathbf{A}$	Sensitivity matrix
B	B-spline basis functions
C	B-spline coefficients
c_{ii}	Diagonal elements of $\mathbf{C}$
$\mathbf{C}$	Covariance matrix of flow functions
$\mathbf{D}$	Sensitivity matrix of flow functions
$\mathbf{G}$	Constraint matrix
$\vec{g}_0$	Constraint vector
g	Gravitational constant
J	Objective function
K	Absolute permeability
k	Relative permeability
N	Number of parameters

$\mathbf{P}$	Covariance matrix of parameters
P	Pressure
q	Quantile for confidence level
S	Saturation
$\mathbf{W}$	Weigthing matrix
$\vec{Y}$	Vector of simulated or measured data
$\vec{y}$	B-spline partition vector

Greek

$\vec{\beta}$	Parameter vector
μ	Viscosity
ϕ	Porosity
ρ	Density
$\mathbf{\Sigma}$	Covariance matrix of measurement errors

Subscript / Superscript

c	Capillary
m	Measured
nw	Non-wetting
s	Simulated
T	Transposed
w	Wetting

References

Aziz, K., Settari, A., *Petroleum Reservoir Simulation.* Applied Science Publishers, London (1979).

Bear, J., *Dynamics of Fluids in Porous Media.* Dover Publications, Inc., New York (1979).

Chen, S., Qin, F., Kim, K.-H., Watson, A.T., "NMR Imaging of Flow in Porous Media," *AIChE J.*, Vol. 39, 925 (1993).

Chen, S., Qin, F., Watson, A.T., "Determination of Fluid Saturations During Multiphase Flow Experiments Using NMR Imaging Techniques," *AIChE J.*, Vol. 40, 1238 (1994).

Grimstad, A.A., Kolltveit, K., Nordtvedt, J.E., Watson, A.T., Mannseth, T., Sylte, A.: "The Uniqueness and Accuracy of Porous Media Multiphase Properties Estimated From Displacement Experiments, *Proceedings of the 1997 International Symposium of the Society of Core Analysts*, Calgary, Canada, September 7-10, 1997.

Guo, Y., Nordtvedt, J.E., Olsen, H., "Development and Improvement of CENDRA+," Confidential Report RF-183/93, RF - Rogaland Research, Stavanger, Norway (1993).

Hammervold, W.L., Skjæveland, S.M., "Improvement of Diaphragm Method for Capillary Pressure Measurements with Micro-Membranes," *Advances in Core Evaluation III*, Gordon and Breach Sci. Publ., 91 (1992).

Johnson, E.F., Bossler, D.P, Naumann, V.O., "Calculation of Relative Permeability From Displacement Experiments," *Trans. AIME*, Vol. 216 (1959).

Kerig, P.D., Watson, A.T., "Relative Permeability Estimation From Displacement Experiments: An Error Analysis," *SPE Reservoir Engineering*, Vol. 1, 175 (1986).

Kulkarni, R., Watson, A.T., "Robust Technique for Quantification of NMR Imaging Data," *AIChE J.*, Vol. 43, 2137 (1997).

Leverett, M.C., "Flow of Oil-Water Mixtures Through Unconsolidated Sands, *Trans. AIME*, Vol. 142 (1940).

Nordtvedt, J.E., Kolltveit, K., "Capillary Pressure Functions From Centrifuge Data Using Spline Functions," *SPE Reservoir Engineering*, Vol. 6, 497 (1991).

Nordtvedt, J.E., Aga, M., Kolltveit, K.: "Calculating the Relative Permeability and the Capillary Pressure Functions from In Situ and Effluent Measurements: An Error Analysis, *in Proceedings of the 3rd European Conference on the Mathematics of Oil Recovery*, 79 (1992).

Richmond, P.C., *Estimating Multiphase Flow Functions From Displacement Experiments.* PhD Dissertation, Texas A&M University (1988)

Richmond, P.C., Watson, A.T., "Comparison of Implicit and Explicit Methods fro Interpreting Displacement Data," *SPE Reservoir Engineering*, Vol. 5, 389 (1990).

Schumaker, L.L., *Spline Function: Basic Theory.* John Wiley & Sons, New York (1981).

Slattery, J., *Momentum, Energy and Mass Transfer in Continua.* Krieger, New York (1981).

Urekdal, H., Ebeltoft, E., Nordtvedt, J.E., Watson, A.T., "A New Design of Steady-State Type Experiments for Simultaneous Estimation of Two-Phase Flow Function," *Submitted for publication* (1997).

Wardlaw, N.C., Taylor, R.P, "Mercury Capillary Pressure Curves and the Interpretation of Pore Structure and Capillary Behavior in Reservoir Rocks, *Bulletin of Canadian Petroleum Geology*, Vol. 24, 225 (1976).

Watson, A.T., Lane, H.S., Gates III, J.M., "History Matching With Cumulative Production Data," *J. Pet. Technol.*, Vol. 42, 96 (1990).

Watson, A.T., Richmond, P.C., Kerig, P.D., Tao, T.M., "A Regression-Based Method fro Estimating Relative Permeabilities From Displacement Experiments," *SPE Reservoir Engineering*, Vol. 3, 953 (1988).

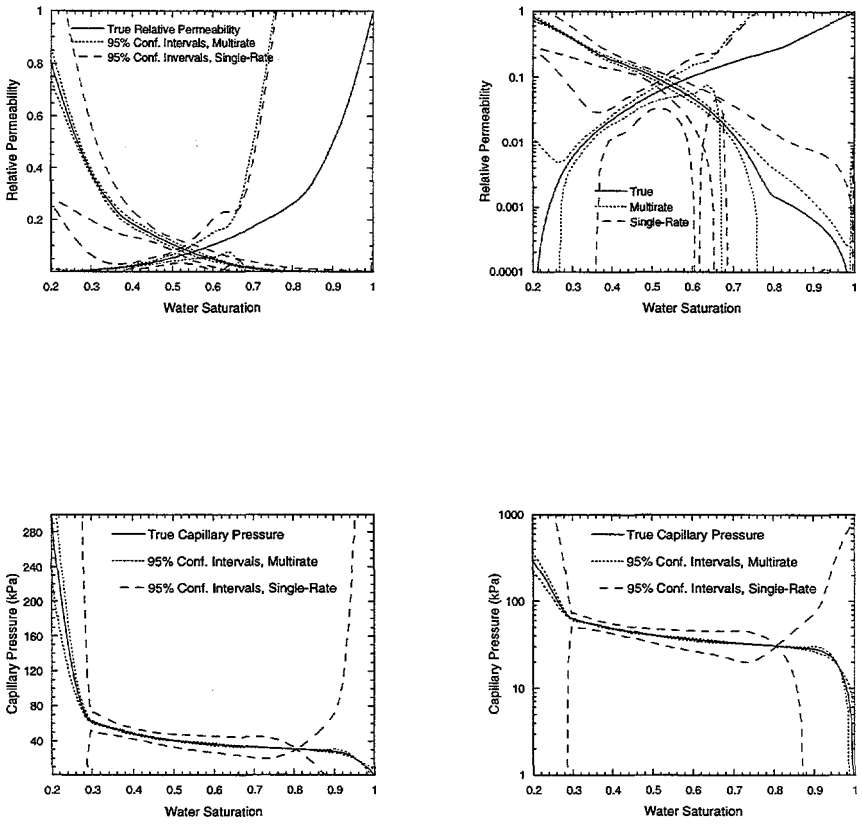

Figure 1: Results from the experimental design study. Upper row: Relative permeabilities and 95% confidence intervals. Lower row: Capillary pressure and 95% confidence intervals.

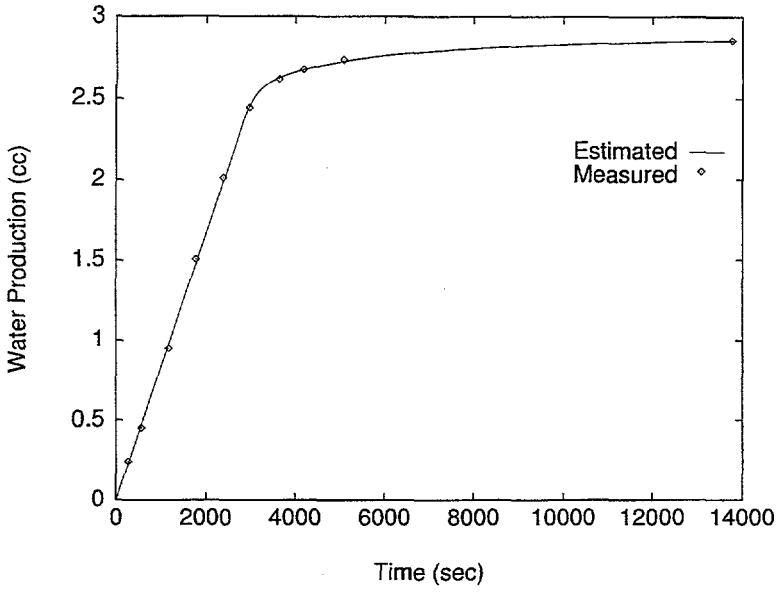

Figure 2: Estimated and measured water production data in single-rate primary drainage experiment.

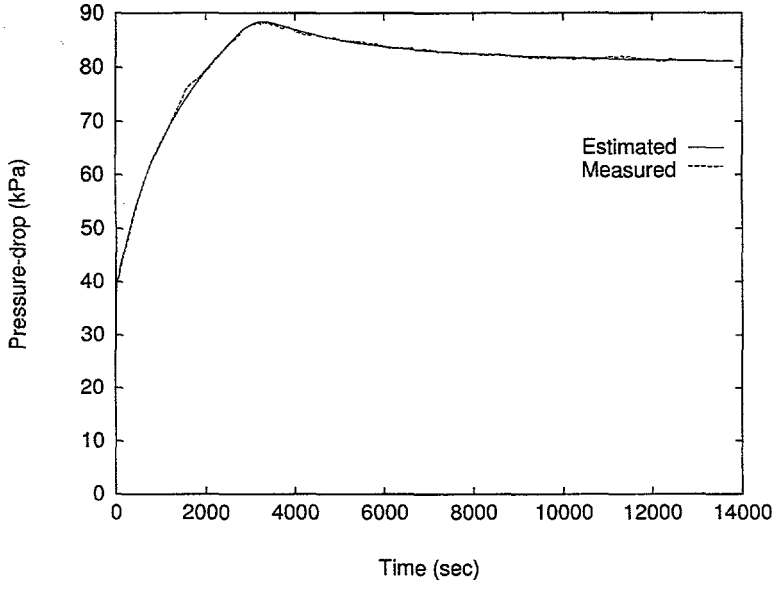

Figure 3: Estimated and measured pressure drop data in single-rate primary drainage experiment.

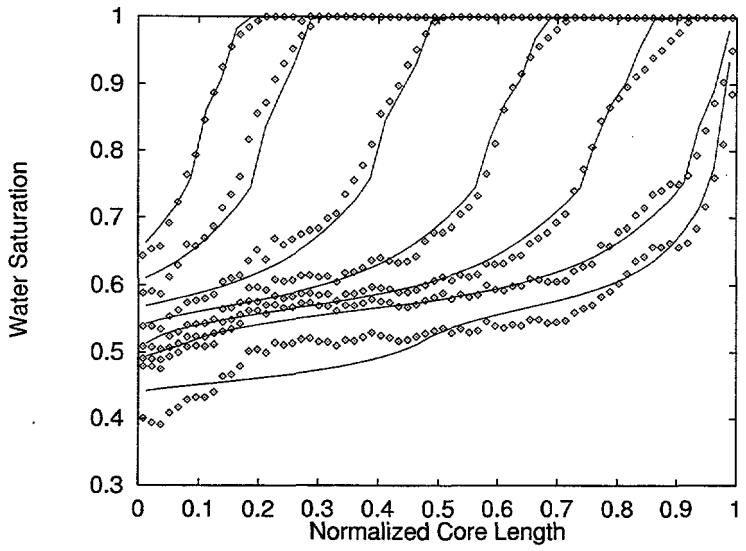

Figure 4: Estimated and measured water saturation profiles for single-rate primary drainage experiment. Curves are simulated values; diamonds are measurements.

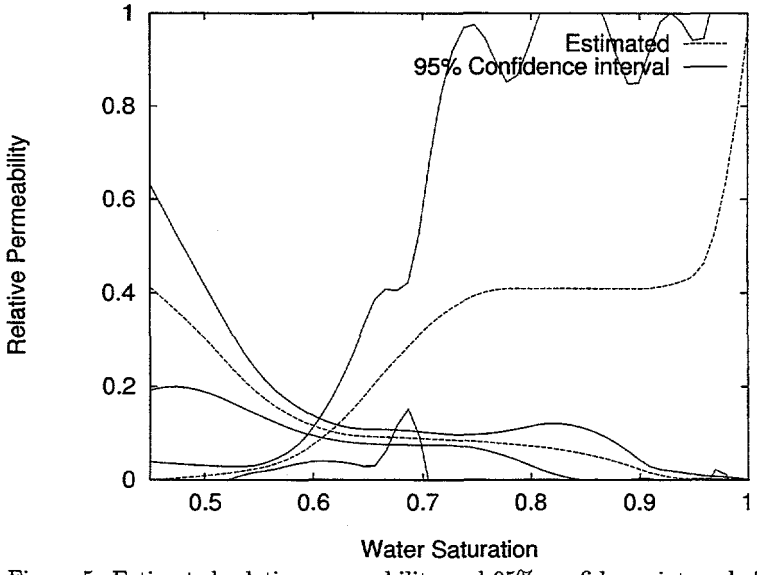

Figure 5: Estimated relative permeability and 95% confidence intervals for single-rate primary drainage experiment.

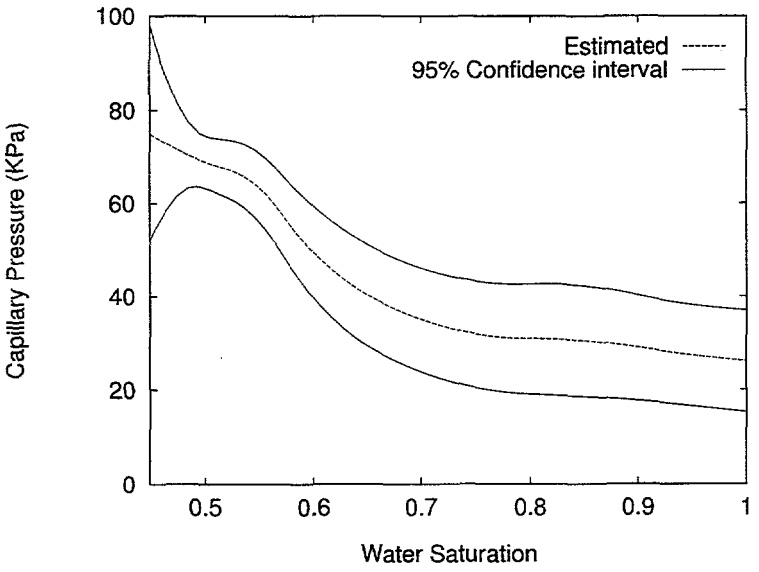

Figure 6: Estimated capillary pressure and 95% confidence intervals for single-rate primary drainage experiment.

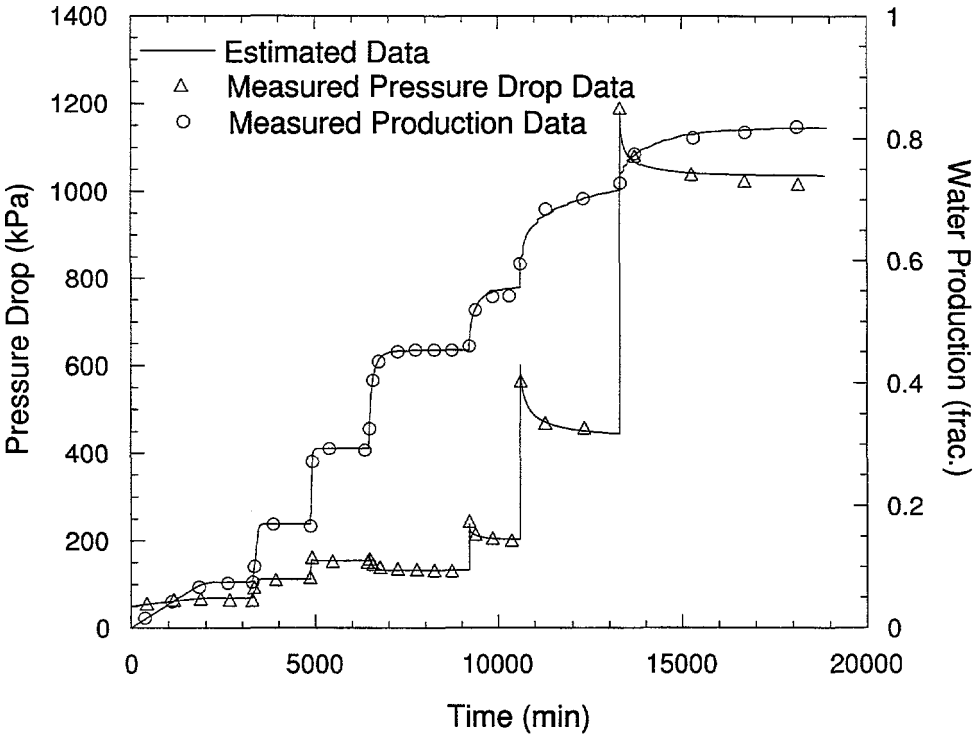

Figure 7: Simulated and measured data in multirate primary drainage experiment.

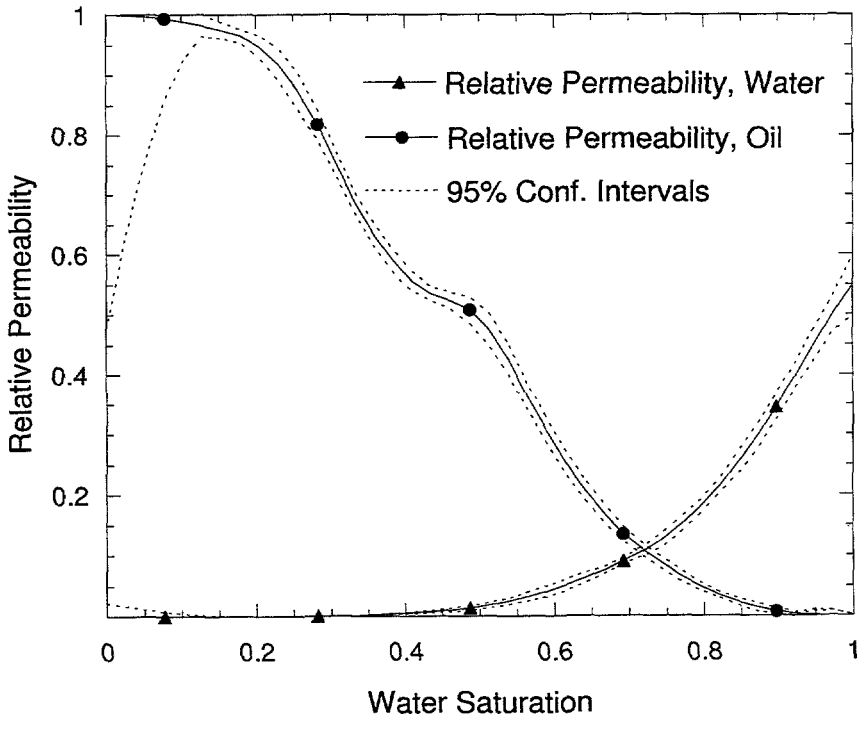

Figure 8: Estimated relative permeability functions with 95% confidence intervals for multirate primary drainage experiment.

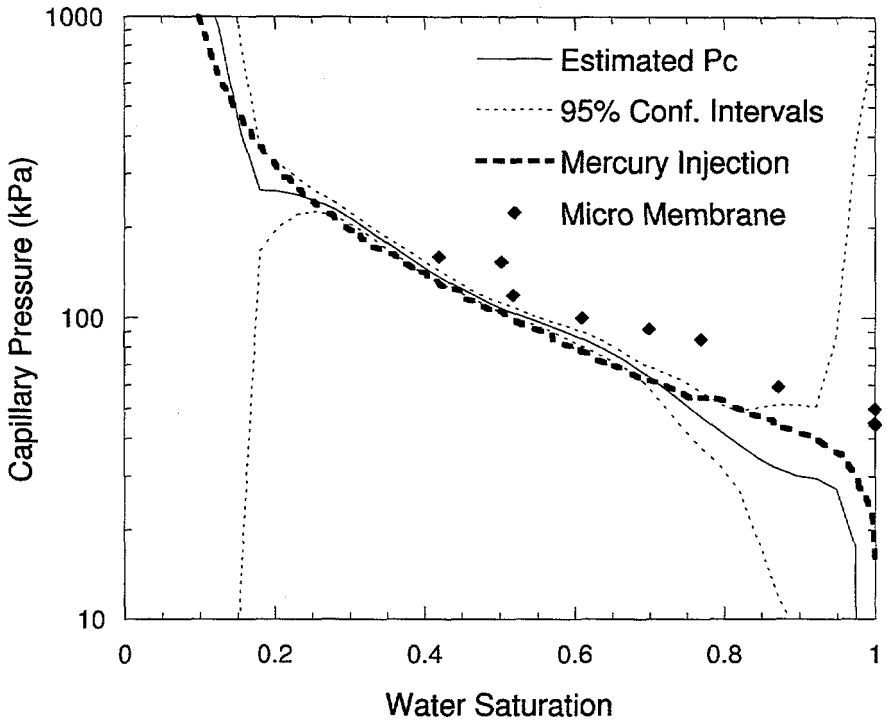

Figure 9: Estimated capillary pressure function with 95% confidence intervals for multirate primary drainage experiment.